TRANSMEMBRANE ELECTRON TRANSFER IN ARTIFICIAL BILAYERS

Lester Y. C. Lee
B.S., University of Washington, 1977

A dissertation submitted to the faculty
of the Oregon Graduate Center
in partial fulfillment of the
requirements for the degree
Doctor of Philosophy
in
Chemistry

July, 1985

The dissertation "Transmembrane Electron Transfer in Artificial Bilayers" by Lester Y. C. Lee has been examined and approved by the following Examination Committee:

James K. Hurst, Thesis Advisor
Professor

William L. Pengelly
Associate Professor

Joann Sanders-Loehr
Professor

Pavel Smejtek, External Examiner
Professor, Department of Physics
Portland State University

TABLE OF CONTENTS

LIST OF TABLES

LIST OF FIGURES

ABSTRACT

Transmembrane Electron Transfer in Artificial Bilayers

Lester Y. C. Lee, Ph.D.
Oregon Graduate Center, 1985

Supervising Professor: James K. Hurst

Electron transfer reactions in artificial vesicle solutions were
studied. Binding of various redox active molecules to vesicles was
demonstrated by gel exclusion chromatography, optical absorption spec-
troscopy, and ultrafiltration techniques. Photoexcitation of (5,10,
15,20-tetrakis(N-methylpyridinium-4-yl)porphinato)zinc(II) ion
($ZnTMPyP^{4+}$) or tris(2,2'-bipyridyl)ruthenium(II) ion ($Ru(bpy)_3^{2+}$)
adsorbed onto the external surface of dihexadecyl phosphate (DHP)
vesicles containing internally bound methyl viologen dications (MV^{2+})
leads to enhanced diffusion of viologens across the bilayer. The
observed temperature dependence of both thermal (in the absence of
sensitizer) and photoenhanced viologen diffusion suggests the
photostimulated mechanism involves localized heating arising from
nonradiative deactivation of the bound excited sensitizer.

Oxidative quenching of unbound $ZnTMPyP^{4+}$ by alkylviologens (C_nMV^{2+})
bound to phosphatidylcholine (PC) vesicles shows Stern-Volmer kinetics.
Similarly, 5,10,15,20-tetrakis(4-sulfonatopyridyl)porphinato zinc(II)
($ZnTPPS^{4-}$) ion undergoes bimolecular quenching with DHP-bound viologens
and in steady-state photolysis gives rise to efficient net formation of

reduced viologens. When ferricyanide ion is incorporated into the
internal aqueous phase of DHP vesicles containing viologens bound to
both surfaces, accumulation of reduced viologen is retarded, suggesting
that the viologens are capable of transmembrane electron transfer.

Reduction of $(NH_3)_5Ru-4-(11'-dodecenyl)$ pyridine(III) ions bound to
inner and outer surfaces of PC vesicles by external reductant is
described. Addition of membrane impermeable reductants in
stoichiometric excess resulted in biphasic ruthenium reduction. The
fast component $(<10^{-3}$ sec) is followed by a slow first-order component
$(t_{1/2} \doteq 500$ s at 23°C) which is independent of both the identity and
concentration of the reductant. The slow component comprises ~30% of
the total reaction, which corresponds to the inner surface to total
vesicle surface area ratio. No transmembrane diffusion of the bound
ruthenium ions on the time scale of the slow redox step could be found.

These results suggest that the rate-limiting step in slow reduction
is transmembrane electron exchange between ruthenium ions bound to
opposite vesicle surfaces. The transfer rate and distance are treated
by an electron tunneling model in which electrons hop to the inter-
mediary trapping sites in the hydrocarbon phase of the bilayer. The
temperature dependence of transmembrane redox is explained in terms of
bilayer thinning at elevated temperatures, giving rise to shorter trans-
ferring distances.

CHAPTER 1

INTRODUCTION

An essential requirement for facile electron transfer between
complex ions in homogeneous solutions is their close approach to form a
precursor or transition complex followed by nuclear activation. The
rate of the reaction is critically dependent on the extent of the
electron orbital overlap of the donor and acceptor. In heterogeneous
systems containing multiphase regions, however, factors controlling
reactivity are more complex. The distribution of solutes, interfacial
diffusion and/or bulk diffusion in the microphases, and interfacial
forces can become the dominant factors in determining reaction
kinetics.[1] Hence, an understanding of various interfacial phenomena is
prerequisite to studying redox reactions in phase-separated media.

1.1 Biological electron transfer

Electron transfer reactions are essential to biological systems.
Energy-linked redox reactions have been an area of intensive study since
the initial discoveries of respiratory and photosynthetic oxidative
phosphorylation.[2] Adenosine triphosphate (ATP), the energy currency in
cells, is synthesized through an intricate mechanism coupled to the
electron transport chain. Other energy-linked cellular processes, such
as active transport of metabolites, also derive energy from the oxida-
tive processes to maintain cell viability. Three general models have
been proposed to account for the energy transduction process: the

chemical intermediate,[3] conformation,[4] and chemiosmotic hypotheses.[5] Of the three, the chemiosmotic view, which has the support of a substantial body of experimental evidence, seems most correct. In essence, the theory states that ATP synthesis is driven by electrostatic and hydrogen ion gradients that develop across the mitochondrial membrane during respiration. It also implies that net charge separation occurs across the mitochondrial membrane during respiration. Although the pathway of electron flow and the general sites of ATP formation in the transport chain have been identified,[6-8] the molecular details of electron transport across the membrane remain obscure. It is not clear whether electron transfer between redox centers that are localized on opposite sides of the membrane[9] is achieved by long-range electron tunneling or by transmembrane diffusion of the electron carrier. Study of electron transfer reactions in organized molecular assemblies that mimic properties of biological membranes can yield insight in understanding biological redox processes.

I.2 Micelles in solar energy conversion schemes

Another primary interest in heterogeneous electron transfer originates from the idea of converting sunlight into useful chemical energy.[10] Many efforts have been directed toward the design of a complex photochemical process capable of efficient water splitting.[11] These solar energy conversion schemes commonly utilize light-absorbing sensitizer compounds (S) whose redox properties in the excited state differ dramatically from that in the ground state to carry out a photoredox reaction. The photoexcited sensitizer reacts with a suitable redox quencher (Q) to form high energy redox products. The photoredox pair can be cycled using a series of electron relays to yield other high

energy species. Ultimately, intermediary redox products are used in catalytic reduction and oxidation of water molecules to yield molecular hydrogen and oxygen. The reaction schemes of such a photochemical process are outlined below:

$$S \xrightarrow{\text{h}\nu} *S \qquad (1)$$

Scheme I

$$*S + Q \rightarrow S^+ \cdot Q^- \qquad\qquad (2)$$

$$S^+ \cdot Q^- \rightarrow S^+ + Q^- \qquad\qquad (3)$$

$$Q^- + A \rightarrow Q + A^- \qquad\qquad (4)$$

$$S^+ + D \rightarrow S + D^+ \qquad\qquad (5)$$

Scheme II

$$*S + Q \rightarrow S^- \cdot Q^+ \qquad (2)$$

$$S^- \cdot Q^+ \rightarrow S^- + Q^+ \qquad (3)$$

$$Q^+ + D \rightarrow Q + D^+ \qquad (4)$$

$$S^- + A \rightarrow S + A^- \qquad (5)$$

$$2D^+ + H_2O \xrightarrow{\text{cat.}} O_2 + 2H^+ + 2D \qquad (6)$$

$$A^- + H_2O \xrightarrow{\text{cat.}} H_2 + OH^- + A \qquad (7)$$
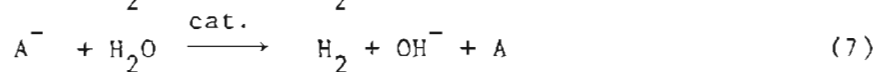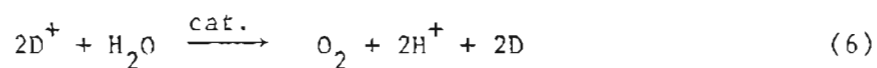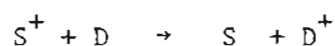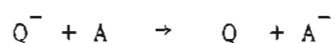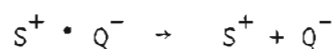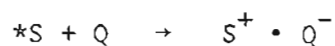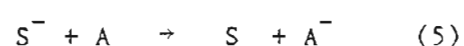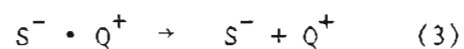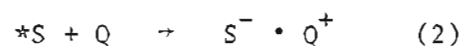
In Scheme I, the initial photoinduced charge separation is achieved by oxidative quenching of the photoexcited sensitizer, *S, whereas Scheme II represents the redox sequence following reductive quenching of *S. In both instances the ground states of the primary redox pair are re-generated by reacting with donor D and acceptor A (Eq. 4 and 5). It is worthwhile to note that oxidation of water (Eq. 6) requires minimally a two-electron transfer process, i.e.,

$$2H_2O \xrightarrow[2H^+]{2e^-} H_2O_2 \xrightarrow{2e^-} O_2 + H_2$$
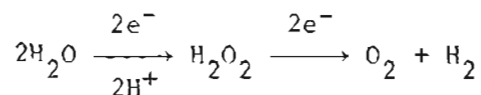
A critical problem frequently encountered in developing photoredox conversion systems is the existence of dissipative back reactions, i.e.,

$$S^- + Q^+ \rightarrow S + Q$$
$$S^+ + Q^- \rightarrow S + Q$$
$$D^+ + A^- \rightarrow D + A$$
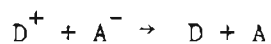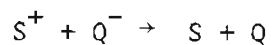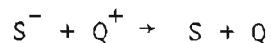
These reactions are generally highly exothermic and occur rapidly in homogeneous solutions; measured rates often approach diffusion-controlled limits.

Attempts have been made to minimize undesirable back reactions by carrying out the photochemical events in phase separated media.[12,13,22,23] The general strategy involved is to selectively solubilize redox species in different phase regions that are separated by electrostatic and/or hydrophobic barriers to attain control of selectivity and specificity in their reactions. In different microenvironments, the course taken by the photoinitiated redox reactions is critically dependent upon the dynamics of various electron transfer, ion adsorption and diffusional processes occurring at the phase boundaries, as well as the reactant molecular organization in the phases.

An excellent example of modified reactivity and pathways in heterogeneous electron transfer is provided by the micelle, in which reactions can potentially occur in three distinguishable phase regions. Micelles are colloidal aggregates of surfactant molecules that associate in water above a certain critical concentration. One structural model[14] describes it as closely packed polar or charged head groups oriented toward the bulk water with long hydrocarbon chains directed away from the bulk water, forming an oil-like core. Hence three phase regions exist: the bulk aqueous medium, hydrophobic micellar core, and the charged interfacial region called the Stern layer.[15]

A number of micellar redox processes have been studied, primarily by Grätzel and coworkers,[16-21] to investigate the importance of the micellar interface in controlling reaction dynamics. They have found that lifetimes of initially formed high energy photoproducts are generally enhanced in the micelle solution. Specifically:

1. The reaction rates between ions in the bulk solution and hydrophobic molecules solubilized in the micelle are greatly influenced by the micellar surface; a similarly-charged Stern surface inhibits the approach of ions, leading to rate retardation, and the oppositely charged surface attracts the ions, resulting in rate enhancement.[16-21]

2. Reduction of an adsorbed molecule at the micellar surface by a donor in the micellar interior causes its repulsion into the bulk solution.[17-21]

The latter observation is particularly interesting because it suggests long-range electron transfer across an electrostatic barrier has occurred. Recombination rates of photoinduced redox products are greatly reduced when one member of the redox pair is repelled from the micellar surface into the bulk aqueous medium.

The mechanism of electron transfer across micellar phase boundaries cannot be firmly established, however, because the detailed structure of the micelle is not well defined. For example, experimental evidence obtained from critical micellar concentrations[24] and small-angle x-ray scattering studies[25] of straight alkyl-chain ionic surfactants suggests that the hydrophobic interior might be hydrated to a greater extent than has generally been believed.[26] Furthermore, surfactant aggregates are thought to be dynamic in nature; rapid equilibria exist between

surfactant molecules in the aggregates and their monomeric form in solution. This relatively loose structure can allow a greater access of solution components to solubilized reagents in the interior than that of a rigid microphase separation. Therefore, the electron transfer distance between redox pairs that are thought to be in different phases of the micellar system might actually be shorter than their spatial localization would indicate.

A more distinct and better-defined microphase system that contains the salient features of a micelle can be obtained by combining two micellar surfaces to form a bilayer membrane. Bilayers are bimolecular sheets of amphiphilic molecules with their hydrophilic head groups oriented outward and their hydrocarbon chains sequestered from the water, forming a continuous hydrocarbon phase, 40-60 Å in width, separating two aqueous compartments. This sandwich-like molecular organization closely resembles the fluid-mosaic model of biological membranes.[27] The electrical and permeability properties of the hydrocarbon barrier also are very similar to the native membranes. Hence, it has been used extensively in reconstitution studies[28-30] of many membrane-associated biological functions.

There are two general types of bilayer membranes, differing in their geometry and formation techniques, that are amenable to experimentation. A planar bilayer film, usually called black lipid membrane (BLM), can be formed by applying a lipid solution onto a small aperture of a Teflon piece separating two aqueous phases in which desirable conditions can be imposed. Electrical properties such as resistance, capacitance, membrane potential, and ion movement can be directly determined, providing the membrane maintains its stability

during the course of measurement. The major problems with BLMs are their relative small surface area to medium volume ratio, lack of reproducible stability over long periods of time, and contamination of hydrocarbon solvent in the bilayer, making chemical studies generally difficult.

A second type of bilayer which is widely used is the vesicle. When amphiphilic lipids are dispersed in water and subjected to mechanical agitation, ultrasonication, or emulsification through rapid mixing, small liquid crystalline particles are formed. X-ray diffraction, electron microscopy, and quasi-elastic light scattering spectroscopy have shown that these particles have a lamellar structure with lipid bilayers intercalated by a water space of variable thickness.[31,32] Prolonged sonication or controlled emulsification generates homogeneous unilamellar vesicles that can be separated by gel chromatography or selective centrifugation.[33,34] These vesicles, ranging from 250 Å to 1200 Å in diameter, can be either neutral or charged bilayer membranes, depending on the nature of the monomer. A spherical unilamellar vesicle dispersed in an aqueous medium forms a heterogeneous system that contains five distinct microphases. The internal volume enclosed by the hydrocarbon barrier and the external bulk medium are aqueous phases where small ions can be preferentially solubilized. The two membrane surfaces, i.e., the inner and outer vesicle-water interfaces, are Stern-type regions where amphiphilic molecules can be adsorbed, orienting with their hydrophobic moieties extended into the membrane interior and the hydrophilic groups localized at the interface. Finally, there is the hydrocarbon membrane interior which favors solubilization of organic molecules.

With its greater surface area, improved stability in aqueous media and accessibility to various spectroscopic and physical methods, the vesicle provides a more suitable model membrane system than the BLM for studies of chemical dynamics. However, since reactants may have different solubility properties in various phase regions, detailed information about the localization, permeability, and binding properties of the chemical species are critical for correct interpretation of reaction dynamics.

Interactions between substrates and vesicular membranes can be classified into two types: electrostatic and hydrophobic. Oppositely-charged ions are electrostatically attracted to a charged membrane surface, whereas like-charged ions are repelled from it. Molecules that contain a high degree of hydrocarbon character favor solubilization in the hydrophobic bilayer interior. Thus, amphiphilic molecules which contain both alkyl and charged head groups are bound most strongly to an oppositely-charged membrane because the electrostatic and hydrophobic interactions are cumulative. By adjusting the amphiphilicity of a molecule, i.e., changing the charges of the head groups and/or varying the chain length of the hydrocarbon tail, it may be possible to control its distribution in the microphases to achieve the desirable chemical reactivity. This fine-tuning of reactivity in a photoredox process has been demonstrated in a micellar system.[35]

Another physical property of a vesicular membrane pertinent to reaction dynamics is its permeability. Numerous studies have shown that passive diffusion of small ions across neutral lipid bilayers is slow.[36] Permeability coefficients of 10^{-13}-10^{-14} cm/sec for K^+ and Na^+, and

considerably faster rates for Cl^- (10^{-11}-10^{-12} cm/sec) are well documented.[37-39] The penetration of simple monovalent ions through bilayers is unfavorable, presumably because the energy involved in the displacement of ions from an aqueous environment to the low dielectric medium of the hydrocarbon core is extremely high. Activation energies for this process have been estimated to be about 30 kcal/mole.[38] However, relatively large ionic molecules such as transition metal complexes in which the overall charges can be distributed over the ligands, thus decreasing the effective charge density, may possibly diffuse at appreciable rates across a hydrophobic barrier. In studies of membranes which are impermeable to aqueous ions, diffusion rates can be increased many orders of magnitude by addition of ionophores.[40-42] Analogously, metal complexes contain hydrophobic ligands may acquire sufficient ionophoric character to increase their diffusion rates.

1.3 Mechanisms of electron transfer in heterogeneous media

The above discussion serves to illustrate that the vesicle is a favorable system to study heterogeneous electron transfer reactions. Specifically, the use of the vesicle bilayer to demonstrate trans-membrane electron transfer can be illuminating in understanding the fundamental nature of electron transfer processes. The mechanisms by which electron transfer occurs in biological systems and artificial molecular assemblies are presently not well understood.[43,44] Historically, knowledge about electron transfer reactions was obtained mainly from studies of coordinated inorganic complexes in solution. Successful theoretical models originally developed in this regime[45,46] were based on the concepts of close approach of the reactant ions to the point of contact of their primary coordination spheres, and thermal electronic

interaction between donor and acceptor orbitals in the activated complex is thought to be sufficiently great that electron tunneling is not rate limiting. Without π-conjugated ligand mediation between the metal centers, electron transfer was thought not to occur over distances greater than several angstroms with measurable rates. However, recent studies of biological redox particles revealed that redox reactions are generally rapid over a distance of 10 Å or more.[47-52] Furthermore, structural evidence also indicates that redox sites in these particles are separated by distances greater than their "closest approach" during the course of charge redistribution.[51,53] Therefore, despite some earlier skepticism and disapproval, long-range electron transfer now is generally accepted. Recent theoretical developments[54] suggest that tunneling mechanisms are important; vibronic-coupled electron tunneling through the nuclear barrier (Franck-Condon barrier) is thought to be rate-limiting.

1.4 Experimental strategy

In view of its theoretical importance, biological implication, and potential utility in solar energy storage systems, investigations to examine transmembrane electron transfer have been undertaken and the results are presented in this dissertation. The general strategy employed is to immobilize chromophoric electron acceptor molecules on opposite surfaces of the vesicle bilayer, then initiate asymmetric photoinduced or thermal electron transfer on the outer bilayer surface.

Asymmetric photoinduced charge separation is achieved by photo-excitation of light sensitizers that are accessible only to the external vesicular surface, thus allowing only oxidative quenching by externally-bound acceptor molecules. Similarly, asymmetric thermal electron

transfer is accomplished by addition of an external reductant. In both systems, reaction kinetics are followed by spectrophotometric detection of the vesicle-bound reduced chromophore and evidence is sought for transmembrane electron exchange which leads to reduction of internally-bound acceptor.

Two types of vesicles are used in the present study. Phospha-tidylcholine (PC), a natural phospholipid from egg, and dihexadecyl-phosphate (DHP), a synthetic dialkyl phosphate ester, are induced to form neutral and anionic vesicles, respectively. Their sizes and homogeneity are determined by transmission electron microscopy and quasielastic light scattering spectroscopy. Binding and diffusion properties are determined by methods of membrane ultrafiltration, gel chromatography, and absorption difference spectroscopy.

Transition metal complexes and metalloporphyrins are used as electron donors in the transmembrane redox studies. In photoinduced electron transfer reactions, tris(2,2'-bipyridyl)ruthenium(II) $(Ru(bpy)_3^{2+})$, 5,10,15,20-(4'-methylpyridyl)porphinatozinc(II) $(ZnTMPyP^{4+})$, 5,10,15,20-(4'-sulfonatophenyl)porphinatozinc(II) $(ZnTPPS^{4-})$ ions are used as light sensitizers with 1,1'-dimethyl-4,4'-bipyridinium dication (also known as methyl viologen, MV^{2+}) or N-methyl-N'-alkylbipyridinium (C_nMV^{2+}) as the electron acceptor. In thermal electron transfer studies, electron exchange reaction is initiated between the amphiphilic ruthenium complexes, 4-(11'-dodecenyl)pyridine-pentaamineruthenium(III)/(II) $(NH_3)_5Ru$-4-alkenylpyr$^{3+/2+})$.

CHAPTER 2

EXPERIMENTAL

2.1 Materials

2.1.1 Purification of egg lecithin

Phosphatidylcholine (PC) was isolated from commercial eggs accord-
ing to the method of Singleton et al.[55] Five hundred g of hen egg yolks
were homogenized in 1 liter of acetone at room temperature and allowed
to stand for 1 hour. The yellow acetone extract was filtered and
discarded. The solids were washed three times with 200 ml of cold
acetone and resuspended in 1 liter of 95% ethanol for 1 hour. Following
filtration, the washing step with ethanol was repeated and the combined
extracts were concentrated to dryness. The solids were extracted with
two portions of 300 ml of petroleum ether and reduced to 200 ml. Addi-
tion of cold acetone to the ether extract (1:5 v/v) with rapid mixing
yielded white precipitates. The suspension was allowed to settle at
4°C, followed by suction filtration. After washing the solids with cold
acetone and filtration, the ether-acetone extraction step was repeated.
Crude phosphatides were collected, redissolved in 1:9 $CH_3OH/CHCl_3$, and
fractionated on an alumina column.

A 4 cm i.d. x 87 cm long glass column fitted with a perforated
glass disc was packed with 625 g of alumina suspended in 700 ml $CHCl_3$.
The flow rate was adjusted to 10 ml/minute and a sample of the crude
phosphatide (1:25 wt/wt to alumina) was loaded onto the column. Elution

with 1:9 $CH_3OH/CHCl_3$ solvent yielded large white hazy fraction after a small yellow front of impurities had passed. Evaporation of the solvent gave white waxy product. Thin layer chromatography on silica gel using a solvent mixture containing $CHCl_3:CH_3OH:CH_3CO_2H:H_2O$ (25:15:4:2) showed a single spot at R_f = 0.71, which was identical to commercial PC (Sigma). Purified PC was resuspended in distilled H_2O and kept frozen until use.

2.1.2 Potassium hexacyanocobaltate(III) $K_3[Co(CN)_6]$

Twelve g $CoCl_2 \cdot 6H_2O$ dissolved in 125 ml H_2O was heated to boiling and 7.5 g KCN in 50 ml H_2O was added dropwise with stirring. Precipitated $Co(CN)_2$ was filtered, washed with cold H_2O and dissolved in 50 ml hot H_2O. Fifteen g KCN was added and heated to boiling for 15 minutes. The hot solution was filtered; product which precipitated upon cooling was collected and washed. The product was purified by recrystallization from hot H_2O. The IR spectrum obtained using Nujol mull technique showed a characteristic cyanide stretching vibration at 2130 cm^{-1}, Co-CN bending vibration at 565 cm^{-1}, and Co-C stretching vibration at 405 cm^{-1}, which are consistent with literature values (2129, 564, 416 cm^{-1}).[56]

2.1.3 Trinitrotriaminocobalt(III) $Co(NH_3)_3(NO_2)_3$

Cobaltous carbonate was prepared by adding 51.8 g Co(II) nitrate hexahydrate to a hot solution of 30 g anhydrous sodium carbonate in 300 ml H_2O. After boiling for 15 minutes, the product was recovered by cooling and filtration; solids were washed with H_2O and air dried. Cobaltous carbonate (28 g) was redissolved in 100 ml hot diluted glacial acetic acid (1:2) and 0.7 mole of sodium nitrate in 250 ml NH_3 was added. The resulting mixture was cooled and 140 ml of 30% H_2O_2 was

slowly added with stirring. After standing in the ice bath for 20 minutes, 1.5 g of activated charcoal was added and the mixture was heated for 1 hour. The charcoal was removed by filtration and the filtrate was cooled for an hour to induce precipitation. The product was filtered, washed with ethanol and ether, and air dried. The yield was about 40%. The visible absorption spectrum obtained showed λ_{max} (ε) = 430 nm (322 M^{-1} cm^{-1}).[57]

2.1.4 Potassium dinitrodiglycinatocobaltate(III)

$K[Co(NO_2)_2(CH_2CO_2(NH_2)_2]$
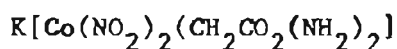
Twenty ml H_2O containing 0.2 mole (15 g) of glycine and 0.1 mole (5.6 g) of KOH was added to 0.2 mole (17 g) of KNO_2 in 20 ml H_2O. The resulting mixture was added to 0.1 mole (17.7 g) of $CoO_2CCH_3 \cdot 3H_2O$ in 20 ml H_2O. Air was bubbled vigorously through the mixture overnight. The brown crystalline product was filtered and washed successively with 50% CH_3CH_2OH, 95% CH_3CH_2OH, and ether. The final product was obtained by recrystallization from hot H_2O and air dried. The visible absorption spectrum obtained was $\lambda_{max}(\varepsilon)$ = 466 nm (209 M^{-1} cm^{-1}) in H_2O.[58]

2.1.5 Alkyl bromides

Alkyl bromides were synthesized from the corresponding alcohols according to the method of Wiley et al.[59] Triphenylphosphine (0.16-0.2 mole) was dissolved in 250 ml of methylene chloride under nitrogen, cooled in an ice bath and a stoichiometric amount of bromine was added dropwise over 20 minutes with stirring. The resulting slightly colored solution was decolorized by back titration with additional triphenyl-phosphine. A stoichiometric amount of pyridine then was added, followed by slow addition of the alkyl alcohol (0.15-0.18 mole) over 45 minutes. The ice bath was removed and the solution was allowed to stand for an

additional 90 minutes. The solvent then was removed by rotary evaporation. The solids were extracted three times with 100 ml pentane. The pentane solution was chilled in a dry ice-acetone bath and the residual white solids (triphenylphosphine oxide) were filtered. The final product was obtained as a liquid by rotary evaporation of the solvent. Yields were generally quantitative (94-100%). Purity was determined by proton NMR spectroscopy;[60] proton signals corresponding to a terminal bromide (3.28-3.32 ppm) on methylene were found, whereas proton signals attributable to the alcohol (3.45 ppm) of the starting materials were absent.

2.1.6 4-Alkylpyridine ligands

Alkylpyridine compounds were synthesized by reacting the C_{n-1} alkyl bromide with 4-methylpyridine according to the method of Brown and Murphy.[61] A 10% excess of 4-methylpyridine (0.17 mole) was added to 200 ml of liquid ammonia under nitrogen, followed by addition of 0.15 mole of $NaNH_2$. The mixture was stirred for 30 minutes and the alkyl bromide (0.15 mole) was slowly added over 90 minutes. The solution was stirred until ammonia was no longer detected. Fifteen ml of H_2O was carefully added to the organic phase and the mixture was extracted with diethyl ether. The ether extract was dried over CaO, decolorized by activated charcoal, and suction filtered. The crude product was obtained by rotary evaporation of the solvent. Distillation under reduced pressure yielded a minor fraction (~1 ml) at low temperatures (30-35°C, 0.2-0.8 mm) and a major component (~20 ml) at high temperatures (60-135°C, 0.12-0.5 mm) depending on the chain length of the alkyl group. Boiling points for individual ligands $NC_5H_4(CH_2)_nCH=CH_2$ are: n = 2, 60°C, 1.5 mm; n = 5, 92°C, 0.4 mm; n = 7, 94°C, 0.14 mm: n = 9, 125°C, 0.2 mm;

n = 10, 132–135°C, 0.5 mm. Proton shifts from ^{1}H NMR analysis of the final products were identical to those previously reported for pyridine and vinyl groups.[60] For the longer chain ligands (n = 7–10), silica gel chromatography was necessary to further purify the product following distillation. Silica gel 60 (70–230 mesh) was packed onto glass columns (5 cm x 50 cm) and chloroform-ethyl acetate mixture (9:1, v/v) was used as eluent. Colorless liquids were obtained, with slightly yellow impurities retained on the column.

2.1.7 Chloropentaammineruthenium(III) dichloride

$[(NH_3)_5Ru(III)Cl]Cl_2$ was prepared according to a modified method of Basolo et al.[62] 7.0 g of $(NH_3)_5Ru(III)Cl_3$ was refluxed in 150 ml 6N HCl solution for 3.5 h. After cooling, yellow solids were recovered by suction filtration, followed by washing with 6N HCl, ethanol, and ether. The crude product then was redissolved in 6 l of hot 3N HCl; residual red unsoluble material was removed by filtration and discarded. Overnight storage of the solution at 4°C yielded yellow crystals. The product was recovered by filtration, washed successively with 6N HCl, ethanol, and H_2O, and dried in vacuum. The electronic spectrum obtained showed $\lambda_{max}(\epsilon)$ = 325 nm (1.87 x 10^3 M^{-1} cm^{-1}) which is consistent with literature values[62] $\{\lambda(\epsilon)$ = 328 nm (1.8 x 10^3 M^{-1} cm^{-1})\}.

2.1.8 4-Alkenylpyridinepentaammineruthenium(III) complexes

Attempted synthesis of the amphiphilic ruthenium(II) complex by a previously reported method[63] met with considerable difficulty. Specifically, extensive hydrolysis was observed during complexation in the initial reaction mixture as indicated by pronounced optical absorption at 298 nm.[64] Furthermore, ether extraction following complexation did not yield clean separation of unreacted ligand from the complex, as

evident from formation of emulsified solvent layers. Introduction of water in the recrystallization step with ammonium hexafluorophosphate also caused significant formation of hydrolyzed product. Overall, these difficulties arose due to the hydrophobic nature of the ligand. These problems were eliminated by minimizing the water content in the synthesis, thereby slowing hydrolytic processes, and by using a less polar solvent to achieve better separation of the product from the reaction mixture. An explicit procedure for the complete synthesis of the pentaammineruthenium(II) complexes is described below.

Approximately 250 mg $[Ru(NH_3)_5Cl]Cl_2$ in 5 ml dilute trifluoroacetic acid (HTFA), pH 3.5, was reduced by amalgamated zinc for 40 minutes under argon. The deoxygenated solution was transferred to an argon-flushed solution containing 2.5 ml of ligand and 10 ml 100% ethanol. The resulting bright orange solution was cooled in an ice bath and allowed to react for 20 minutes, then was transferred to a 25 ml separatory funnel. An optical spectrum taken at this juncture showed a shoulder at 298 nm and undefined intense uv absorption. Addition of a few ml of ethanol gave a white precipitate. Following suction filtration, the solution was extracted with 10 ml pentane. Small amounts of white precipitate could also be seen in the lower phase. The optical spectrum obtained following filtration still showed a small shoulder at 298 nm but well-defined bands at 247 and 261 nm appeared. The pentane extract was discarded and to the remaining solution was added, with stirring, a saturated ethanolic solution of ammonium hexafluorophosphate. The precipitate was stored several hours in the cold; filtration yielded bright yellow solids. The complexes were recrystallized from warm ethanol, washed with pentane, and freeze-dried in a lyophilizer.

The electronic spectrum obtained in ethanol was $\lambda_1(\epsilon_\lambda) = 408$ nm (7180 M^{-1} cm^{-1}) and $\lambda_2(\epsilon_\lambda) = 245$ (4170 M^{-1} cm^{-1}), which are similar to previously reported values for the shorter $(NH_3)_5Ru$-4-alkenylpyridine analogs.[63]

Oxidation of the Ru(II) complex to Ru(III) was accomplished with silver ion. Approximately 100 mg Ru(II) complex was added to 5 ml of dilute HTFA in which had been dissolved stoichiometric amounts of Ag_2O. The resulting mixture was cooled in an ice bath and filtered through celite to remove the black Ag precipitate. Solid sodium perchlorate was added to the cooled filtrate until precipitation occurred. The product was recrystallized from warm water and dried under vacuum over anhydrous $CaSO_4$. Yields were generally 20-50 mg. The electronic spectrum obtained in 0.1 M HTFA was $\lambda(\epsilon_\lambda) = 251$ nm (5750 M^{-1} cm^{-1}) which is consistent with reported values[61] for $(NH_3)_5Ru(III)$-4-alkenylpyridine complexes.

2.1.9 (4-Alkenylpyridine)pentaamminecobalt complexes

The synthesis of pentaamminecobalt(III) complexes of the 4-alkenylpyridine derivatives followed explicitly previously reported procedures.[60] Prolonged heating of an appropriate amount of dimethylsulfoxidepentaamminecobalt(III) perchlorate and the 4-alkenylpyridine ligand in dimethylsulfoxide (DMSO) or dimethylformamide (DMF) yielded a deep-orange product solution. Moisture was excluded by adding 4 Å molecular sieve. The reaction was carried out in an N_2 atmosphere. These procedures minimize hydrolysis and oxidation of the ligand during the reaction. The product complex was extracted into water, followed by ether extraction to achieve separation from unreacted ligand, which was in excess. The final product was obtained by

precipitation with diluted perchloric acid. The electronic and proton NMR spectral features were consistent with the previously reported values.[60]

2.1.10 Vanadous Ion

Vanadous ion was prepared according to a previously reported method.[65] Vanadium(V) oxide in sulfuric acid (40 g V_2O_5, 25 ml H_2SO_4, 20 ml H_2O) was reduced by SO_2 to form vanadyl sulfate. The sulfate ion was precipitated as barium sulfate by addition of barium perchlorate, and vanadyl perchlorate was separated by filtration. The vanadium content of the vanadyl perchlorate solution was determined by oxidation to vanadium(V) using $KMnO_4$ followed by titration of vanadium(V) by standard Fe^{2+} solution, with diphenylaminesulfonic acid as the indicator.[66] Vanadous ion was prepared by amalgamated zinc reduction of the standard vanadyl perchlorate solution under argon.

2.1.11 Other reagents

Dihexadecylphosphate (DHP) and methylviologen dichloride ($MVCl_2$) were purchased from Sigma and recrystallized from acetone before use. N-alkylviologen (C_nMV^{2+}) dichlorides and Zn(II) porphyrin ($ZnTMPyP^{4+}$ and $ZnTPPS^{4-}$) tetrachlorides were supplied by Drs. A. M. Braun and K. Kalyanasundaram at EPFL, Lausanne, Switzerland. Cupric ion solutions were prepared by dissolving $Cu(ClO_4)_2$ in dilute trifluoroacetatic acid, followed by precipitation of perchlorate ion by adding a stoichiometric amount of potassium hydroxide. Cu(II) concentrations were determined by the method of Kitson.[67] Cuprous ion solutions were generated by anaerobic (Ar) reduction of excess Cu(II) by Cr(II) which was obtained by reduction with zinc amalgam. Chromic perchlorate solutions were prepared by reduction of primary standard potassium dichromate in HTFA

with hydrogen peroxide following addition of perchloric acid to precipitate potassium ion. Ascorbic acid solutions were freshly prepared before use by dissolution in distilled water. Other chemicals were reagent grade and used without further purification. Aqueous solutions were prepared with distilled water that was either doubly-distilled or purified by reverse osmosis in exchange chromatography.

2.2 Vesicle Preparations

2.2.1 Phosphatidylcholine vesicles

(a) _Formation_. Typically, vesicles were formed in 20 ml of 0.1 M sodium acetate or potassium acetate buffer solution, pH 4.0, in a 25 ml round bottom flask containing an appropriate amount of purified PC (80-100 mg). Solutions were deoxygenated by purging with N_2. Sonication was administered with constant flushing of N_2 over the solution surface for 2-3 hours with the flask immersed in an ice bath. Sonicated solutions were centrifuged at 100,000 G for 195 minutes to obtain unilamellar vesicles. The clear supernatant was collected and kept at 4°C until use. Usually the vesicles were used within 24 hours after they were prepared. Incorporation of metal ions, ruthenium or cobalt complexes into the vesicles was accomplished by cosonication of the reagent with the phospholipid suspension.

Formation of nearly monodisperse PC vesicles containing $C_{16}MV^{2+}$ bound to both inner and outer surfaces was achieved by cosonication of phospholipids with the alkylviologen dichloride in 0.05 M phosphate buffer, pH 6.0. For the photolytic experiments, appropriate amounts of $ZnTMPyP^{4+}$ and EDTA were added externally to give final concentrations of 2×10^{-5} M and 1×10^{-3} M, respectively.

(b) <u>Determination of PC content in vesicle solutions</u>. Known amounts of ^{14}C labeled phosphatidylcholine (0.1 μCi, Amersham) were evaporated to dryness by blowing a stream of N_2 into the sonication flask. Phosphatidylcholine suspension was then added and deoxygenated, following the normal procedures for vesicle preparation. Analysis for radioactive carbon was performed by dissolving the PC sample solution into Aquasol scintillation liquid (1:9, v/v). The PC concentration in the sample was calculated from scintillation counts that were recorded on a Beckman LS-3133P instrument. An external standard of ^{14}C-labeled blank solution (2200 cpm) was measured prior to measurement of sample solutions to ensure the accuracy of the instrument. The detection limit of the instrument was about 30-50 cpm.

2.2.2 DHP vesicles

(a) <u>General procedures</u>. Appropriate amounts of DHP (40-50 mg) in 20 ml water or buffer solution was sonicated at elevated temperatures (35-50°C) in air without presonication deaeration. The manipulative procedures were different for various types of vesicle assemblies. Detailed descriptions of the individual systems are given below.

(b) <u>Preparation of asymmetrical MV^{2+}/DHP/sensitizer vesicles</u>. Fifty mg DHP in 20 ml distilled water was preheated at 80°C and sonicated for 5 minutes before addition of 1.8-3.6 mM methylviologen dichloride; 0.1 N NaOH was added dropwise during 30-45 minutes of sonication at maximum power for the microtip to obtain clarification. The final pH was adjusted to 8.4. The slightly hazy solution was either filtered successively through 0.45 and 0.22 μm Millipore membranes or centrifuged at 100,000 G for 1 h to remove particulate matter. The filtered or centrifuged solution was passed down a 2 x 15 cm Bio-Rad

AG 50W-X8 column in the hydrogen ion form. Vesicles were recovered in 2.0 ml fractions immediately following the column void volume. Internal methyl viologen concentrations were determined spectrophotometrically both as MV^{2+} at 256 nm ($\varepsilon = 1.88 \times 10^4$ M^{-1} cm^{-1}) and as MV^+ at 600 nm ($\varepsilon = 1.24 \times 10^4$ M^{-1} cm^{-1})[68] by sodium dithionite reduction in the presence of methanol. Sodium dithionite solutions were freshly prepared in aqueous buffer (0.05 M Tris, pH 7.8); all solutions were purged of oxygen by bubbling with argon before viologen reduction with dithionite. Sufficient EDTA (0.1 M, pH 7.8) and 0.1 N NaOH were added to the chromatographed vesicle fractions (pH 2.8) to give a final concentration of 1 mM EDTA, pH 8.4. Appropriate amounts of $Ru(bpy)_3^{2+}$ or $ZnTMPyP^{4+}$ ions were added to give formal concentrations of 3×10^{-5} M and 1.6×10^{-5} M, respectively.

The preparation of DHP-bound methylviologen in buffer solutions was similar to that in water. DHP and methylviologen were cosonicated in 0.05 M Tris-HCl, pH 7.8, at 50°C for 45 minutes. Filtered or centrifuged vesicle solutions were passed down a 2 x 20 cm Sephadex G-50 column to remove external methylviologen. Subsequent manipulations and analysis of the chromatographed vesicles were the same as in preparation of DHP vesicles in water except addition of NaOH was unnecessary.

(c) <u>Preparation of symmetrically-bound $C_{16}MV^{2+}$-DHP-sensitizer vesicle assemblies.</u> 5×10^{-4} M $C_{16}MV^{2+}$ in 0.02 M Tris, pH 7.8 was cosonicated with 4×10^{-3} M DHP at 50°C for 45 minutes. The sonicated solution was centrifuged to give nearly monodisperse viologen-containing vesicles free of titanium particles. In vesicles containing internal ferricyanide, 0.02 M of potassium ferricyanide was included in the sonication solution. External ferricyanide was then removed by Sephadex

G-50 chromatography similar to the preparative procedure for DHP vesicle
assemblies in buffer solutions. Occluded ferricyanide concentration
levels were determined either by difference absorption spectral
measurements of ferricyanide-viologen-DHP vesicles against DHP vesicles,
using a molar absorptivity $\epsilon_{420} = 1040$ M^{-1} cm^{-1} for ferricyanide, which
was determined spectrophotometrically, or atomic absorption measurements
using $Fe(CN)_6^{3-}$ standard solutions containing DHP vesicles. In the
photolytic experiments, appropriate amounts of external donor tricine
and photosensitizer $ZnTPPS^{4-}$ were added externally to give final concen-
trations of 0.1 M and 4×10^{-5} M, respectively.

(d) <u>Preparation of externally-bound $C_{16}MV^{2+}$-DHP-sensitizer</u>
<u>vesicle assemblies.</u> Adsorption of $C_{16}MV^{2+}$ ions to the external surfaces
of DHP vesicles which carried internal ferricyanide ions was achieved by
either solution mixing or sonication pulses. In the former method, 3 ml
of $C_{16}MV^{2+}$ (5×10^{-4} M) in 0.02 M Tris, pH 7.8 was added dropwise in 50
μl fractions to 3 ml of gel-chromatographed DHP vesicles (8×10^{-3} M)
containing internal ferricyanide. The mixing required 1 hour with
constant slow stirring. The resulting solution was further chromato-
graphed on a Sephadex G-50 column. The latter method involved short
bursts of sonication (15 seconds) to obtain clarification of the vesicle
solution after each viologen addition followed by gel chromatography to
remove any residual viologen or $Fe(CN)_6^{3-}$ ion in the external medium.
Ferricyanide concentration levels were determined both before and after
the viologen addition to vesicles prepared by both methods.

2.3 Other Methods

2.3.1 Gel exclusion chromatography

Sephadex G-50 beads were presoaked in distilled water overnight prior to loading into the glass column, which was 2 x 40 cm and equipped with two reversible flow adaptors. The column void volume was determined by applying 2 ml samples of blue dextran (2 mg) onto the packed column, and measuring the eluted solvent volume until blue dextran appeared in the eluant. Column void volumes were about 12 ml. The column was preequilibrated with buffer prior to loading of vesicle samples. Eluted vesicle solutions were collected in 2 ml fractions using a Gilson Model FC-80E fractionator operated in the drop-counting mode. The flow rate was adjusted to 1 ml/minute.

2.3.2 Passive diffusion of MV^{2+} from DHP vesicles

The leakage of methylviologen bound to inner surfaces of DHP vesicles in 0.05 M Tris, pH 7.8 was studied from 10-35°C. The vesicle solution was incubated in a temperature bath. At various time intervals, 20 µl of freshly prepared sodium dithionite solution was added to 2.0 ml aliquots taken from the solution and absorbance changes at 600 nm were recorded.

Hydroxylic amine-induced viologen diffusion was measured in a similar manner. 20 µl of 0.5 M Tris-HCl, triethanolamine, or tricine, pH 7.8, was added to 2.0 ml aliquots of MV^{2+}//DHP//$Ru(bpy)_3^{2+}$ vesicles[69] in aqueous solutions at 23°C followed by a 15-20 minute incubation period. Then freshly prepared sodium dithionite (20 µl) was added and the absorbance changes were recorded.

2.3.3 Investigation of possible photodamage of DHP vesicles

A 2 ml aliquot of DHP vesicle solution prepared in 0.05 M Tris, pH 7.8, which contained internally bound MV^{2+} (0.1 M), externally bound $Ru(bpy)_3^{2+}$ (2 x 10^{-5} M), and external EDTA (1 mM) was tested for external viologen by adding 0.2 ml deoxygenated sodium dithionite. The residual external methylviologen radical cation concentration detected was 3.4 x 10^{-6} M. Another 2 ml aliquot was photolysed by continuous illumination at 15°C for 30 min and again subjected to the dithionite test. The detected MV^+ concentration was 6.5 x 10^{-6} M. Similarly, another 2 ml aliquot of vesicle solution was photolysed in identical condition and allowed to stand in the dark for an additional 30 minutes. The dithionite test gave identical external MV^+ concentrations before and after ageing.

2.3.4 Thermal diffusion of ferricyanide across DHP vesicles

DHP vesicles containing internal ferricyanide were prepared as usual by cosonicating 20 mM $K_3Fe(CN)_6$ with 4 mM DHP in 0.02 M Tris, pH 7.8. External $Fe(CN)_6^{3-}$ was removed by Sephadex G-50 chromatography. Seventy-six ml of the chromatographed sample solution was subjected to ultrafiltration in a 47 mm stirred cell using a 10,000 nominal molecular weight cutoff Pellicon membrane. Three successive filtrations were performed with a time interval of 2 hours between each filtration without replacing lost solvent from the retained vesicle solution. The combined filtrates were 68 ml. Iron contents in the filtrates and retained vesicle solutions were analyzed by atomic absorption spectroscopy.

2.3.5 Photoinduced diffusion of $Fe(CN)_6^{3-}$ ion across DHP vesicles containing $C_{16}MV^{2+}$

An asymmetrically organized vesicle solution (0.02 M Tris, pH 7.8) comprising DHP vesicles (4 mM) with $C_{16}MV^{2+}$ bound to both surfaces (0.5 mM), $Fe(CN)_6^{3-}$ within the inner aqueous phase (0.02 M) and both $ZnTPPS^{4-}$ (2×10^{-5} M) and tricine (0.1 M) in the external medium was prepared by the usual procedures. Fifteen ml of this sample solution was subjected to membrane ultrafiltration and subsequent atomic absorption spectroscopy as described above to examine leakage of $Fe(CN)_6^{3-}$. Another 10 ml aliquot was illuminated with visible light ($\lambda > 500$ nm) under conditions described in the photolytic experiments to form viologen radical cations (See Section 2.4.4). After 60 minutes, the distribution of $Fe(CN)_6^{3-}$ in the aqueous phase was again determined by membrane ultrafiltration and atomic absorption analysis.

2.3.6 Membrane ultrafiltration

The vesicle solution containing either encapsulated or bound species was placed in a 47 mm filtration cell containing a prewetted Pellicon PSED semipermeable membrane, nominal molecular weight cutoff 2.5×10^4 amu, with a Teflon stirring bar. The cell was connected to a Pellicon Carousel Manifold equipped with a magnetic stirring motor in the central column, then was pressurized with N_2 gas to 20-25 psi. The flow rate of the filtering solution was about 0.2 ml/minute.

2.3.7 Encapsulation of transition metal complexes in phosphatidylcholine vesicles

The species to be entrapped was cosonicated with phosphatidylcholine suspension to achieve clarification of the solution. Nearly monodisperse vesicles were collected by ultracentrifugation at

100,000 G. The metal ions in the external aqueous phase of vesicle solutions were removed in an ultrafiltration cell using Pellicon membrane. Typically, 20 ml filtrate was collected from a 40 ml sample, and 20 ml buffer was added to the retained vesicle solution after each filtration step. Completion of the entire washing process consisted of 9-14 filtration steps and usually required 3-4 hours. The metal content in the filtrates, initial vesicle solution, and final vesicle solution were analyzed by atomic absorption spectroscopy. The integrity of the vesicles was checked by analysis for ^{14}C radioactivity in the filtrates obtained from vesicle solutions containing ^{14}C-phosphatidylcholine.

2.3.8 External binding of cobalt complexes to phosphatidylcholine vesicles

Standard solutions of 4-alkenylpyridinepentaamminecobalt(III) complexes (~1 x 10^{-4} M) were prepared in 0.1 M acetate buffer, pH 4.0. The cobalt content was determined either spectrophotometrically using previously reported molar absorptivities[58] or by atomic absorption spectroscopy. One ml increments of the standard cobalt solutions were added to 20 ml of preformed PC vesicle solution contained in an ultrafiltration cell. One ml filtrates were collected following each addition of complex solution. The cobalt contents in the filtrates and final vesicle solution were analyzed by atomic absorption spectroscopy. Vesicle integrity was checked by ^{14}C-radioisotopic analysis.

The cobalt content in the retained vesicle solution before each filtration step (n) was determined from the following equation:

$$Co^n_{total} = Co^{n-1}_{total} - C^{n-1}_{out} + Co^n_{add} \qquad (8)$$

The retained cobalt concentration Co^n_{total} (mg) in step n is obtained by subtraction of the filtrate cobalt concentration C^{n-1}_{out} (mg) which was determined by atomic absorption spectroscopy in the previous step (n-1), from the previous total cobalt concentration Co^{n-1}_{total} (mg), then combined with the added cobalt concentration Co^n_{add} (mg). In the inital step, n=1, $Co^1_{total} = Co_{add}$. The cobalt concentration in the vesicle solution is obtained by dividing Co^n_{total} (mg) by the vesicle solution volume, $V^n(1)$. The bound cobalt concentration Co^n_{bound} is obtained by subtracting the filtrate cobalt concentration Co^n_{out} from the total concentration, i,e.,

$$Co^n_{bound} = Co^n_{total} - Co^n_{out} \tag{9}$$

Because the cobalt complexes contain a hydrophobic alkyl group, substantial adsorption onto the filter membrane in the absence of vesicles was observed. Correction factors were obtained in vesicle-free solutions by taking the ratio of retained concentration to filtrate concentration. Figure 18 shows results indicating that retention by the filter is nearly linear over the concentration range investigated; ratio values of 1.8 and 1.4 (retained Co concentration to filtrate Co concentration) were obtained for $(NH_3)_5Co-4-(10'-undecenyl)pyridine^{3+}$ and $(NH_3)_5Co-4-(8'-nonenyl)pyridine^{3+}$ ions.

2.4 Instrumentation

2.4.1 Atomic absorption spectroscopy

Analysis of metal contents of solutions containing ferricyanide, pentaamminecobaltalkenylpyridine complexes, and other transition metal complexes were made on an Instrumentation Laboratories Model 551

spectrometer operated in the absorption mode. An air/acetylene flame
was used to atomize the samples. Lamp currents were adjusted to 70-80%
of the maximum allowed values to obtain maximum sensitivity. The detec-
tion wavelengths for iron, cobalt, copper and ruthenium were 372.6,
346.4, 218.3, and 349.9 nm, respectively. For each metal analysis,
standard solutions of the metal complex in the appropriate concentration
levels (1-30 ppm) were freshly prepared to obtain calibration curves; in
all instances, the curves were linear. Sample solutions were also ad-
justed to the appropriate concentration range before measurement.
Chemical interference was not found in PC vesicle solutions for iron and
cobalt, i.e., addition of PC vesicles to standard solutions did not
change the measured absorbancies, but for ruthenium analysis, added
phospholipid vesicles caused the measured ruthenium concentration levels
to increase two-fold over the original concentrations. Calibration
curves obtained with vesicles included gave erratic results; hence,
ruthenium contents in PC vesicles containing 4-alkenylpyridinepenta-
ammineruthenium(III) ions could not be determined by this method.

2.4.2 Transmission electron microscopy

Two to four drops of sample solution containing approximately
10^{-3} M phospholipid were deposited on a 200 mesh copper grid which was
supported by carbon or Formvar films. An absorbing filter paper was
placed beneath the copper grid to facilitate sample dispersion on the
surface. Immediately after deposition of the sample, 1-2 drops of
staining solution containing 70% phosphotungstic acid in 70% ethanol was
added to the grid surface in the same manner. It was found that
allowing the sample to dry completely before the staining step gave
fictitiously large vesicle sizes (~800 Å diameter), presumably due to

evaporating action of the solvent causing the vesicles to become

flattened. Fixation by the stain before the complete evaporation of the

vesicle internal solvent eliminated this error.

Electron micrographs were obtained on a Hitachi HU 11-BB transmis-

sion electron microscope operating at 100 kV with the No. 2 polepiece

inserted. Magnification factors were obtained from the corresponding

intermediate lens current calibration curve.

2.4.3 Low angle laser scattering spectroscopy

The determination of vesicle size by quasielastic light scattering

spectroscopy is based on the measurements of time-averaged light

intensities of the scattered light due to the thermal diffusion of the

scattering particles in the solution.[70] These measurements can generate

a power spectrum which can be transformed into the autocorrelation

function, $C(t)$, which is an exponential function of the general form:

$$C(t) = e^{-2K^2 Dt} \tag{10}$$

where K is the scattering vector given by

$$K = \frac{4\pi n}{\lambda_0} \sin \theta/2 \tag{11}$$

and D represents the diffusion coefficient of the particles. In

equation 11, n is the solution refractive index, λ_0 is the wavelength of

the incident light in vacuum, and θ is the angle of scattered light.

For a monodisperse solution of noninteracting particles, the time

constant τ_c of $C(t)$ is directly related to D, i.e.,

$$\tau_c = [2K^2D]^{-1} \tag{12}$$

For a polydisperse solution, the decay is non-exponential and the deviation can be represented by Koppel's equation,[71] a cubic polynomial fit to the logarithm of the time dependent part of the correlation function:

$$\ln [C(t) - C(\infty)] = 2(x_o - x_1t + x_2t^2 - x_3t^3) \tag{13}$$

If deviation from exponential decay is positive (positive curvature) the x_2t^2 term is greater than x_3t^3, thus:

$$\ln [C(t) - C(\infty)] \approx 2(x_o - x_1t + x_2t^2) \tag{14}$$

The deviation from exponential decay is

$$\Delta\ln [C(t) - C(\infty)]$$
$$= \ln [C(t) - C(\infty)] - \ln [C(t) - C(\infty)]_{exponential} \tag{15}$$

Since $\ln [C(t) - C(\infty)]_{exponential} = -2K^2Dt$, $x_1 = K^2D$, and

$$\Delta\ln [C(t) - C(\infty)] = 2x_o + 2x_2t^2 \tag{16}$$

Also, $2x_2 = K^4D^2v$, where v is the variance; hence,

$$\ln [C(t) - C(\infty)] = 2x_o + K^4D^2vt^2 \tag{17}$$

Plotting $\ln [C(t) - C(\infty)]$ vs. t^2 would yield a straight line with slope equal to $K^4 D^2 v$. From equation (12), the variance is obtained:

$$v = (4 \tau_c^2)(\text{slope}) \tag{18}$$

Assuming the particles to be spherical, the diffusion coefficient, D, in a medium of viscosity η is related to the hydrodynamic radius, R_H, of the scattered particle by the Stokes-Einstein equation:

$$D = kT/6 \pi \eta R_H \tag{19}$$

where T is the temperature (°K) and k is the Boltzmann constant. Combining equations (12) and (19) eliminates D, and the hydrodynamic radius is obtained:

$$R_H = \left(\frac{2kTK^2}{6\pi\eta} \right) \tau_c \tag{20}$$

Quasielastic light scattering measurements were made on a Chromatix KMX-6 photometer interfaced to a Langley-Ford autocorrelator. Experimentally determined τ_c values were used in equation (20) to calculate R_H values using $k = 1.358 \times 10^{-16}$ g-cm^2/s^2, $T = 298$ K, $\eta = 8.904 \times 10^{-3}$ poise, and for calculation of K in equation (11), $n = 1.332$, $\lambda_o = 632.8$ nm, and $\theta = 4.5°$ were used.

2.4.4 Photochemical methods

(a) <u>Steady-state photolysis</u>. Six to ten ml sample solutions containing viologen-DHP vesicles which had been manipulated into their

proper configurations (symmetrically or asymmetrically bound) were purged of O_2 by bubbling with argon in a glass vessel in the dark for one hour. Traces of oxygen were removed by passing the argon stream through a BASF R3-11 activated copper column before entering the vessel. The gas delivery line was made entirely of copper and glass tubing. Transfers of deoxygenated solutions were made via a special V-bore 4-way stopcock[72] to a cylindrical optical cell (1 cm pathlength) which was fitted to the purging vessel using all-glass connections. This assembly allows solution transfer with minimum risk of O_2 contamination. The optical cell was immersed in a beaker-shaped glass vessel (~500 ml) through which water was circulated from a Lauda K-2/R temperature bath. The vessel was fitted with a Pyrex optical flat to allow entrance of photostimulating light. During illumination, the bath temperature was maintained constant to 0.1°C. An iron-constantan thermocouple immersed in the optical cell was used to measure temperature changes in the reaction solution during illumination of sensitizer-bound vesicles. Solution temperatures were found to increase only a few tenths of a degree (maximum 0.8°C/hour) during the illumination period.

The illumination source was a Hanovia 200 W high-pressure mercury-xenon compact arc lamp mounted in a Bauch & Lomb mercury light source housing powered by a Kepco Model KS 60-20(M) regulated DC power supply. Emitted light was passed through an achromatic condenser lens and appropriate optical cutoff filters to remove high energy radiation before impinging on the sample. Corning 410 nm, 515 nm, and 495 nm cutoff filters were used for experiments with $Ru(bpy)_3^{2+}$, $ZnTMPyP^{4+}$, and $ZnTPPS^{4-}$ ions as photosensitizers, respectively. Incident light intensities were estimated by ferrioxalate actinometry[73] to be 6.4×10^{-8}

einstein/second for the 410 nm filtered light; calculations were based upon the assumption that $\Phi_{Fe}2+ = 1.0$. Because the spectral envelopes of $Ru(bpy)_3^{2+}$ and ferrioxalate are similar under these conditions, the method gives a rough estimate of the photons absorbed by sensitizer during continuous photolysis. Solution transmittances in the near uv (340-400 nm) and visible regions (550-680 nm) where the viologen radical cation is the principal chromophore, were recorded before illumination and at various time intervals during illumination.

Individual determinations were generally repeated three times. External viologen was measured immediately before and after illumination by dithionite. In photostimulated methyl viologen diffusion experiments where the viologen radical cation had accumulated as a consequence of photolysis, it was reoxidized by pulsing the solution with O_2, then repurging of residual oxygen before dithionite addition.

(b) <u>Laser flash photolysis</u>. Laser flash photolysis was performed with a JK-2000 frequency doubled (532 nm) Q-switched neodynium laser with a pulse width of 15 nanoseconds. The optical detection in kinetic spectroscopy was essentially as previously described.[74] For 610 nm detection wavelength, an RCA 1P28 photomultiplier and 630 nm optical cutoff filters were used to attenuate incident light beam, while for 890 nm detection, a photodiode and 810 nm cutoff filters were used. Slit widths were adjusted to obtain $I_o = 100$ mv in both detection wavelengths. Transient curves were recorded using a Tektronix WP-2221 data acquisition system equipped with two R-7912 transient digitizers. Sample solutions were contained in 1 cm pathlength rectangular optical quartz cells fitted with long necks to allow rigorous deoxygenation.

Anaerobic conditions were achieved by bubbling with N_2 purified by passing through an Oxiclear oxygen purifier.

2.4.5 Kinetic methods

Rapid kinetic measurements were made on a stopped-flow instrument of conventional design.[63] Sample solutions were prepared in argon-purged anaerobic reservoirs and loaded directly into the drive syringes without exposure to air in the mixing block, which was thermostatted. Transmittance changes were recorded on a Tektronix 549 storage oscilloscope.

Kinetic measurements of slow-phase reduction of vesicle-bound 4-alkenylpyridinepentaammineruthenium(III) complexes in phosphatidyl-choline vesicles were made on a Cary 16 spectrophotometer. Typically, deoxygenated ruthenium-vesicle solutions (2.3 ml) which had been bubbled under chromous-scrubbed argon at 4°C for 45 minutes were syringe-transferred into an argon-flushed 1.0 cm pathlength cylindrical optical cell capped with a rubber serum, then were allowed a few minutes to attain thermal equilibrium with the thermostatted cell compartment in the spectrophotometer. Reaction was initiated by syringe-transfer of the anaerobic reductant solution (0.2 ml) into the optical cell containing the sample solution. Absorbance changes at 415 nm were followed within 30 seconds after mixing. Complete visible spectra were recorded 5-10 minutes after reaction started and at different time intervals.

The procedure for reduction of pentaammineruthenium(III) complexes in homogeneous solutions was similar as described above except phosphatidylcholine vesicles were absent from the sample solutions and the monitored wavelength for absorbance changes was 400 nm.

2.4.6 Other instrumentation

Ultracentrifugation was performed using a Beckman Ty65 fixed-angle rotor on a Model LS-65 instrument. Polycarbonate tubes (13 ml) were used to hold sample solutions. The temperature was maintained at 4°C for phosphatidylcholine and 23°C for DHP vesicle solutions. Electronic absorption and optical difference absorption spectra were obtained on Cary 16 or Varian 219 instruments. Sonication was performed on an Ultrasonic Model W185 F sonicator equipped with a microtip probe run at 70 W power. Turbidity measurements were made on Hach 2100 A turbidimeter. Infrared absorption spectra were obtained on a Perkin-Elmer 621 spectrophotometer. Proton magnetic resonance spectra were obtained on a Varian Model H-100 spectrometer using tetramethylsilane as an internal standard.

CHAPTER 3

RESULTS

3.1 Formation of vesicle solutions

Continuous sonication of phosphatidylcholine (PC) suspensions for 2
hours at 4°C produced slightly hazy solutions which showed no further
visual change upon prolonged sonication (up to 3 hours). Incorporation
of pentaammineruthenium and pentaamminecobaltalkyenlpyridine complexes,
or alkylviologen ions into PC vesicles by cosonication required less
sonication time (1.5 hour) than formation of PC vesicle alone. Trans-
mission electron microscopy showed the sonicated solution contained both
large multilamellar and small vesicles (Figure. 1). Ultracentrifugation
of the sonicated solution yielded a clear supernatant and a small
pellet. Analysis of PC preparations by incorporating ^{14}C-labeled PC
showed that the supernatant contained 30-40% of the phospholipid used.

Usually, PC samples containing 100-120 mg of the starting material
gave 30-40 mg in the supernatant fraction. The centrifuged solution
contained nearly monodisperse unilamellar vesicles with radii of 130 $\pm$
15 Å and a small fraction of large vesicles with radii of 353 $\pm$ 18 Å as
determined by electron microscopy (Figure 2). Autocorrelation decay
curves from light scattering spectroscopy performed on centrifugated
solutions gave average hydrodynamic radii (R_H) of 230 Å. Incorporation
of $(NH_3)_5$Ru-4-(11'-dodecenylpyridine) complexes into vesicles produced
slightly smaller R_H values and increasing variance with increasing
concentration of the complex. Light scattering data are summarized in

Table 1. Representative decay curves are given in Figure 3. Changing medium conditions did not appear to affect the physical parameters; sodium or potassium acetate buffers from 0.01 to 0.1 M, pH 4.0, or 0.05 M phosphate, pH 6.5, all allowed formation of single bilayer vesicles. Inclusion of various transition metal complexes in PC suspensions also did not appreciably alter the macroscopic formation characteristics. In general, the colored vesicle solutions reflected the chromophoric metal ions that were contained within them.

Dihexadecylphosphate (DHP) vesicles formed more readily than PC at elevated temperatures (50-60°C) in either neutral or basic media. Sonication of 4 mM DHP suspended in hydroxylic amine buffers (Tris, tricine, triethanolamine) ranging from 0.02 to 0.5 M, pH 7.8, produced clear solutions that passed easily through 0.2 μm Millipore membranes. However, attempts to form DHP vesicles in water without addition of base failed. Prolonged sonication (>2 hours) of DHP suspensions at 80°C did not yield clear solutions; i.e., large undispersed particles remained in solutions. Clarification was obtained only after addition of sodium hydroxide (~1 mM). Other researchers have found that formation of DHP vesicles in acidic aqueous media (pH 3.5) requires melting of the DHP solids or films prior to sonication,[75,76] and vesicles prepared from NaOH solutions have a slightly different size[75] and head-group structure.[76] These results suggest that interaction between the head groups with the bulk medium is important in promoting vesicle formation. Presumably, protonation of the phosphate head group retards solubilization of monomers in aqueous solution, thus preventing bilayer formation. In addition, prolonged sonication in the presence of polyanions such as $EDTA^{4-}$ (0.3 M), $Fe(CN)_6^{3-}$ (0.05 M), or acetate (0.1 M) ions, and high

concentrations of glycine (0.1 M), tetramethylammonium (0.5 M), or methyl viologen dications (>3 mM), also did not produce clarification of solutions. Addition of MV^{2+} up to 80%, or alkyl viologen ($C_{16}MV^{2+}$, $C_{14}MV^{2+}$) up to 30% of the molar concentration of DHP still allowed formation of stable vesicles. Data obtained from light scattering spectroscopy are summarized in Table 2.

3.2 Solute binding by vesicles

Binding of a variety of compounds to vesicle surfaces was demonstrated by three general methods. Adsorption of chromophoric dyes to the vesicle surface, which is a different microenvironment from the bulk aqueous phase, gives rise to spectral shifts in their optical spectra that are easily detected by difference spectroscopy. Strong binding can further be demonstrated by membrane ultrafiltration. When the chromophores are added to solutions containing vesicles that are unable to pass through the semipermeable membrane, the added chromophores remain with the vesicles; when the vesicles are absent, the chromophore passes freely through the membrane. Finally, comigration of the bound chromophore with vesicle fractions occurs when chromophore-vesicle solutions are passed down dextran gel columns, indicating binding, while free chromophores are retarded by the sieving action of the gel. The binding of four types of compounds to PC and DHP vesicles is summarized in Table 3.

Optical difference spectra obtained by addition of photosensitizers $ZnTMPyP^{4+}$ and $Ru(bpy)_3^{2+}$ (1:120, sensitizer to DHP ratio) in 0.05 M Tris solutions show bathochromic shifts of 15-18 nm in their visible bands as presented in Figure 4. For $ZnTMPyP^{4+}$, strong binding was also confirmed by ultrafiltration in which 90% of the added porphyrin was retained in

DHP vesicle solutions (a few percent loss was attributable to minor adsorption onto the semipermeable membrane surface), and by gel chromatography experiments in which the sensitizer comigrated with the vesicles under conditions where unbound $ZnTMPyP^{4+}$ ions showed a significantly longer retention time (Figure 5). However, when increasing concentrations of TEOA were added to the medium, the bound $ZnTMPyP^{4+}$ ions were gradually displaced from the DHP vesicle surface. At 0.25 M TEOA, the binding properties were completely lost: spectral shifts disappeared, $ZnTMPyP^{4+}$ ions became diffusible through semipermeable membranes and were retarded on gel columns. This displacement was not due to simple salt effects since tetramethylammonium chloride at comparable ionic strength ($\mu = 0.5$ M) had no detectable effect on binding.

In contrast to $ZnTMPyP^{4+}$, $ZnTPPS^{4-}$ ions do not bind to DHP vesicles by the above-mentioned criteria. Likewise, when DHP was replaced by PC (in 0.05 M phosphate, pH 6.5), no evidence of binding of the three sensitizers was detected.

Binding of MV^{2+} ion and its alkyl derivatives to vesicle surfaces was also studied in asymmetrically organized vesicle assemblies. Since viologen dications do not absorb in the visible region ($\lambda_{max} = 256$ nm), the use of optical difference spectroscopy to obtain directly the spectral perturbation due to binding is hindered. However, viologen radical monocations formed by one electron reduction are intensely colored in the visible region, providing a means to obtain indirect evidence of dication adsorption if one can assume that MV^{2+} binds more strongly to the vesicle surface than MV^{+}. This assumption is reasonable on the basis of electrostatics; an anionic surface should display a

higher affinity for dipositive species than its monopositive counterpart. Reduction of MV^{2+} by dithionite in anaerobic DHP vesicle solution generated a spectrum which is slightly different from that of MV^+ in homogeneous solution (Figure 6). Similarly, reduction of the alkylviologen, $C_{16}MV^{2+}$, under the same conditions, also produced the same type of perturbation in its electronic spectra (Figure 7). Close examination of the spectral changes reveals a lack of broad absorption at 382 nm with the appearance of a strong sharp band at 395 nm, and in the visible region, a broad absorption envelope centered around 602 nm, which are diagnostic of the presence of predominantly monomeric species. In contrast, alkylviologen monocation radicals are known to form aggregates in homogeneous solutions,[77] exhibiting broad absorption bands at 382 nm and 545 nm. In the present DHP system, alkylviologen radical cations appear to be solubilized as monomers on the vesicle surface. This conclusion is supported by the observation that in the absence of vesicles, $C_{16}MV^+$ ions slowly precipitated out of solution, while in the presence of DHP, they remained solubilized.

Gel chromatography performed on MV^{2+}-DHP solutions also gave evidence of viologen binding. Association of MV^{2+} ions to vesicle surfaces appears weaker than that of $ZnTMPyP^{4+}$ ions as illustrated in the elution profile presented in Figure 8. Only partial binding was observed, while a substantial portion of MV^{2+} ions lagged behind the vesicle band. Binding of alkylviologens to DHP vesicles, on the contrary, was complete, as shown in Figure 9; essentially all the viologens co-chromatographed with vesicles, as detected by dithionite reduction.

Binding of amphiphilic charged species to PC vesicle surfaces was also demonstrated by gel chromatography. Phosphatidylcholine vesicles formed in the presence of $C_{16}MV^{2+}$ or $C_{14}MV^{2+}$ ions incorporated the viologens as shown by their elution profiles on dextran gel columns (Figure 10). With $C_{16}MV^{2+}$, no lagging was observed; in the case of $C_{14}MV^{2+}$, however, about 10% of the viologen was retarded. Partial binding was also observed when $C_{16}MV^{2+}$ ions were added externally to preformed vesicles (Figure 11).

Similar results were obtained in studies of binding of penta-ammineruthenium(III) alkenylpyridine complexes to PC vesicles. The degree of binding increases with the length of the alkyl chain on the substituted pyridine. Figures 12 and 13 show the elution behavior of the complexes on Sephadex G-50 columns. The $(NH_3)_5Ru-4-(11'-$ dodecenyl$)py^{3+}$ ions, which contain the longest alkyl group used, show complete comigration with the vesicles, while the other three complexes show increasing amounts of retarded free ions as the number of carbon atoms in the alkyl chain decreases from 9, 7, to 4, respectively. Optical difference spectroscopy performed on $(NH_3)_5Ru-4-(11'-$ dodecenyl$)py^{2+}$-PC vesicle solutions generated by either dithionite or ascorbate reduction, also gave differing degrees of spectral shifts for the various ions in the 396-420 nm region where 4-alkenylpyridine pentaammineruthenium(II) ions absorb strongly. Again, the $(NH_3)_5Ru-4-(11'-dodecenyl)py^{2+}$ ion shows the largest bathochromic shift, from 396 to 418 nm (Figure 14), while $(NH_3)_5Ru-4-(8'-nonenyl)py^{2+}$ and $(NH_3)_5Ru-4-(6'-heptenyl)py^{2+}$ show correspondingly smaller shifts (Figures 15, 16). The $(NH_3)_5Ru-4-(3'-butenyl)py^{2+}$ ion, which contains only a four-carbon chain, shows an almost undetectable shift (<2 nm).

Binding of two amphiphilic Co(III) complexes, $(NH_3)_5Co-4-(10'-undecenyl)py^{3+}$ and $(NH_3)_5Co-4-(8'-nonenyl)py^{3+}$, to external PC vesicle surfaces was demonstrated by membrane ultrafiltration. Incremental addition of the Co complexes to solutions containing PC vesicles resulted in significant retention. Figure 17 shows the measured cobalt concentration in the filtrates was less than that in the retained solution before filtration, which is indicative of binding. However, due to the hydrophobic alkyl group which the complexes contain, substantial adsorption onto the filter membrane in the absence of vesicles was also observed. Correction factors were obtained in vesicle-free solutions by taking the ratio of retained concentration to filtrate concentration (Figure 18). Curves of bound Co concentrations corrected for binding to the semipermeable membrane versus free Co concentrations show saturation binding as shown in Figures 19 and 20, the $(NH_3)_5Co-4-(10'-undecenyl)py^{3+}$ complex exhibits stronger binding. An adsorption density value σ(number of adsorbed Co/$Å^2$) was calculated by the following equation:[78]

$$\sigma = \bar{v}n/4\pi r_o^2 \qquad (21)$$

where n = number of PC monomers in a vesicle, r_o = vesicle outer radius, and $\bar{v}$ = number of adsorbed ions per vesicle. Taking n = 2700 and r_o = 130 Å,

$$\sigma = \bar{v}/78.7 \ Å^2 \qquad (22)$$

To describe the binding of charged molecules to a neutral vesicle membrane surface, one has to take into account the surface potential generated. Three basic relations to describe the binding of ions to the surface, the statistical distribution of the electrolytes in the solution volume near the charge interface, and the electrostatic effects of the potential on the ions can be incorporated to give what is called the Stern model.[78] Equation (23),

$$\sigma = 1/K(\sigma^m - \sigma)[B]_{x=0}$$ (23)

is a form of the Langmuir adsorption isotherm which relates σ, the number of molecules adsorbed per unit area to σ^m, the maximum number of adsorbed molecules per unit area, K, is the dissociation constant, and $[B]_{x=0}$ is the aqueous concentration of the adsorbing species at the membrane-solvent interface. Equation 24,

$$[B^{n+}]_{x=0} = [B^{n+}] \exp[nF\psi_0/RT]$$ (24)

relates $[B^{n+}]_{x=0}$ to $[B^{n+}]$, the aqueous concentration of B^{n+} in the bulk phase using the electrostatic potential ψ_0 at the membrane surface in a Boltzmann form. Finally, equation 25,

$$\sinh(F\psi_0/2RT) = A\sigma_s/C^{1/2}$$ (25)

which is based on the Gouy-Chapman theory of diffuse double layer, describes the electrostatic potential produced by σ_s, the charge density on the surface due to adsorbed ions. In this equation, C is the

concentration of monovalent ions in the bulk phase, and A is a constant
which depends on temperature and dielectric constant. At 25°C,
$A = 136.6 \ M^{1/2} \ \text{Å}^2$/electric charge. For n = 1, i.e., adsorption of
monopositive ions, combination of equations 23-25 results in a
transcendental expression relating σ and $[B^+]$ (equation 26, derivation
given in Appendix II),

$$\frac{\sigma K}{(\sigma^m - \sigma)[B^+]} + \frac{(\sigma^m - \sigma)[B^+]}{\sigma K} = \frac{4A^2\sigma^2 n^2}{C} + 2 \qquad (26)$$

For n > 1 cases, however, the exponential form contained in equation 24,
$\exp[nF\psi_0/RT]$, cannot be easily transformed into a hyperbolical function
in the form of equation 25 which is not dependent on n. Therefore, for
adsorption of multicharged ions, the Stern equation is not obtained.
Nonetheless, a treatment of the experimental data obtained in binding
studies of amphiphilic pentaamminecoblat complexes using the Stern
equation is attempted. Experimentally determined values of σ and
$[Co]_{out}$, the concentration of Co complexes in the bulk phase, were fitted
into equation 26 by choosing appropriate values of σ^m and K. Values for
σ^m were estimated from Figures 21 and 22, and K values were selected by
minimizing the mean deviation of c^m in equation 23. Figure 22 is a
representation of the calculated ideal Stern curves and their comparison
with experimental data points.

Considerable deviation from the ideal curves can be seen in both Co
complexes. Poor fitting is clearly observed for the $(NH_3)_5Co-4-(8'-$
nonenylpy^{3+} ion; the experimental values exhibit a smaller curvature than
the calculated curve predicts. Varying σ changes the curvature, but it

also causes a vertical shift of the curve, and changing K values only shifts the curve horizontally. Therefore, better fitting cannot be achieved by altering these parameters. Best-fit values for σ^m of 1/285 $\mathring{A}^2$ and 1/167 $\mathring{A}^2$, and K values of 1.2 x 10^{-3} M and 3.0 x 10^{-3} M were estimated for the $(NH_3)_5Co-4-(8'-nonenyl)py^{3+}$ and $(NH_3)_5Co-4-(10'-undecenyl)py^{3+}$ complexes, respectively.

3.3 Retention of entrapped transition metal complexes by PC vesicles

Retention of transition metal complexes of different charges within their inner aqueous phase of PC vesicles was studied using a successive ultrafiltration method. For each aliquot taken, the volume of PC vesicle solutions formed in the presence of the complex was reduced to one-half by filtration through a semipermeable membrane. Fresh solvent was then added to return the filtered solution to its original volume. This method allows the gradual removal of metal complexes in the external aqueous phase. Metal concentrations in the filtrates and in both initial and final vesicle solutions were analyzed by atomic absorption spectroscopy. Data obtained are presented in Table 4. The ratio of final to initial metal concentration in the vesicle solution is represented as a retention factor. It is a measure of the ability of vesicles to retain the complex after filtrations. Removal of the external metal complex causes the distribution equilibrium between the internal and external metal complex to shift to the right, i.e.,

$$M_{(in)} \overset{K}{\rightleftharpoons} M_{(out)}$$
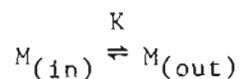
If transmembrane diffusion occurs on the timescale of the dilution experiments, only a few of the internally trapped ions will remain;

otherwise the system will not approach equilibrium and significant retention will occur. Prior to filtration, the complex concentration measured in the vesicle solution is assumed to be equal to the external concentration, while the final complex concentration measured is the amount of complex entrapped, assuming the concentration of external complex at the final dilution is negligible. Thus, the retention factor reflects the ability of entrapped complex to diffuse across the vesicle bilayer.

Phosphatidylcholine (PC) concentrations were determined by ^{14}C analysis. Only trace amounts of PC were detected in the filtrates, whereas about 90% were recovered in the final filtered vesicle solutions. From Table 4, the retention factor decreases as either positive or negative charge on the complex decreases. The neutral complex $Co(NH_3)_3(NO)_3$ showed almost no retention after nine washes, inferring that all occluded complex had diffused across the bilayer and had become dialyzable. On the contrary, the tripositive ions, $(NH_3)_5CoOH_2^{3+}$, $Co(bpy)_3^{3+}$, Cr^{3+}, and trinegative ions, $Fe(CN)_6^{3-}$ and $Co(CN)_6^{3-}$, all showed strong retention (~3% of the original metal concentration in vesicle solution), while the dipositive $(NH_3)_5CoN_3^{2+}$ and mononegative $Co(NO_2)_2(glycinate)_2^{-}$ ions were moderately retained. The percentage of total solution volume entrapped by the vesicles was calculated based on an internal volume of 0.3 µl/µmol PC.[79] The entrapped complex concentration levels were obtained by dividing the total complex concentration (mg) by the internal volume. Under the present experimental conditions, the internal aqueous phase comprises less than 1% of the total solution volume.

3.4 Asymmetric MV^{2+}-DHP-sensitizer assemblies

3.4.1 Preparation and properties

Similar to the preparation of DHP vesicles in water, basification facilitates formation of stable vesicles in the presence of MV^{2+}. The amount of NaOH added approximates the concentration of the ionizable hydrogen of the DHP head group (~2 mM). Slow addition of aqueous MV^{2+} to preformed DHP vesicles causes immediate cloudiness, indicating instability occurs when the anionic membrane surface is neutralized by the positively charged viologen. Cosonication of DHP and MV^{2+} in water with base at 80°C produces clarified vesicle solution containing MV^{2+} ions bound to both inner and outer vesicle surfaces.

External MV^{2+} ions are removed by strong-acid cation exchange chromatography. A large pH drop is usually observed (8.4 to 2.8) in the chromatographed solution. Addition of electron donors (EDTA, tricine, TEOA) and photosensitizers (Ru(bpy)$_3^{2+}$, ZnTMPyP^{4+}) to asymmetrically labeled MV^{2+}-DHP vesicles that are restored to basic pH (8.4) does not cause any visual change in the solution turbidity.

Entrapped MV^{2+} determined by spectrophotometric measurement of MV^{2+} agrees with the amount of MV$^+$ radicals formed by application of the dithionite test. Internally bound MV^{2+} ions which cannot be reduced by external dithionite are immediately reduced when methanol is added. DHP vesicles are ruptured by the alcohol and internalized MV^{2+} ions become accessible to dithionite reduction. Generally, about 50-80% of the entrapped MV^{2+} ions are reduced instantly, approaching 100% upon standing two hours.

Formation of MV^{2+}-DHP vesicles in buffered solutions does not require addition of NaOH. Passage of sonicated solutions down amine buffer

equilibrated Sephadex G-50 columns gave clear separation of vesicles and external MV^{2+} ions when buffer concentration levels were greater than 0.02 M (Figure 23). At lower buffer concentration levels, a significant amount of MV^{2+} ions comigrates with the vesicles (Figure 8). Of the three amine buffers, Tris offers the most efficient separation, less than 5 μM external MV^{2+} being detected by dithionite in the chromatographed solutions. Addition of donors and sensitizers did not cause any observable change in the solutions. Hydrodynamic radii derived from light scattering measurements (400-500 Å) are slightly smaller than reported values for DHP in water and in buffer (600 Å).[80,81]

3.4.2 Transmembrane diffusion of viologen

Passive diffusion of internally bound MV^{2+} across DHP bilayers was studied. Temperature dependent leakage of internalized MV^{2+} in the presence of external dithionite was monitored in MV^{2+}-DHP (0.05 M Tris, pH 7.8) by measuring the optical change at 600 nm. The absorbance changes vs. time plots are given in Figure 24. Initial rates obtained from these curves are given in Table 5. An apparent activation energy was calculated from the ln R_i vs. T^{-1} plot (Figure 25), $\Delta H = 21.2$ Kcal/mol. Similarly, leakage of viologens in the presence of external hydroxylic amines in DHP solutions containing internally bound MV^{2+} and externally bound $Ru(bpy)_3^{3+}$ ions at 23°C was measured by dithionite reduction. The viologen leakage data are summarized in Table 6.

3.5 Preparation and properties of $Fe(CN)_6^{3-}$-$C_{16}MV$-DHP vesicle assemblies

Sonication of DHP in buffered solutions in the presence of the alkylviologens $C_{16}MV^{2+}$ and $C_{14}MV^{2+}$ at a ratio of 1:8 viologen:DHP led to formation of symmetrically bound viologen-DHP vesicles (see Section 2.2.2). Addition of $C_{16}MV^{2+}$ solution to preformed DHP vesicles, however,

caused an immediate increase in turbidity. Asymmetrical binding of $C_{16}MV^{2+}$ ions to the outer vesicle surface was accomplished by either slow addition or short bursts of sonication, followed by Sephadex G-50 chromatography. Cosonication of DHP with 0.02 M $Fe(CN)_6^{3-}$ gave clear yellow solutions. Gel chromatography of the sonicated solution removed $Fe(CN)_6^{3-}$ ions from external medium as indicated by the retardation of an intense yellow band. The slightly tinted vesicle fraction obtained contained $Fe(CN)_6^{3-}$. Optical difference spectral curves of these vesicles against similar vesicles prepared in the absence of $Fe(CN)_6^{3-}$ gave a broad absorption band at 390-420 nm ascribable to the ion (Figure 26). Using a molar absorptivity of 1040 M^{-1} cm^{-1} at 420 nm, the apparent $Fe(CN)_6^{3-}$ concentration was calculated to be 3.8 µM; this value agreed with $Fe(CN)_6^{3-}$ concentration determined by atomic absorption spectroscopy (3.5 µM). The absence of $Fe(CN)_6^{3-}$ ions in the external solution was confirmed by analyzing eluate fractions from membrane ultrafiltration by atomic absorption spectroscopy. Whether analysis was made immediately or hours after separation, the iron content measured in the external solution was below the limit of detection (0.3 µM). In contrast, vesicle solutions retained by impermeable membrane gave apparent $Fe(CN)_6^{3-}$ solution concentration levels of 4-40 µM, depending upon the vesicle concentrations. Vesicles that contained $Fe(CN)_6^{3-}$ showed instability over extended periods, as evidenced by increasing turbidity after 24 hours at room temperature.

In addition to possible passive diffusion of occluded $Fe(CN)_6^{3-}$ across DHP bilayers, possible leakage due to photostimulation was also examined. Illumination of DHP vesicle solutions (60 minutes, I_o = 6.4 x 10^{-8} einstein/sec) which contained $ZnTPPS^{4-}$, an unbound sensitizer in

external medium, symmetrically bound $C_{16}MV^{2+}$, and internalized $Fe(CN)_6^{3-}$ [$Fe(CN)_6^{3-}$, $C_{16}MV^{2+}//DHP//C_{16}MV^{2+}$, $ZnTPPS^{4-}$],[69] did not give detectable iron in vesicle-free eluate fractions by membrane ultrafiltration as measured by atomic absorption spectroscopy, and the iron concentration level determined in the vesicle-containing solution was unchanged from the value measured before illumination (34 μM).

3.6 Photochemical kinetic studies

3.6.1 Photoinduced MV^{2+} diffusion across DHP bilayers

Steady-state illumination of aqueous DHP vesicle suspensions containing internally bound MV^{2+}, externally bound sensitizer, $ZnTMPyP^{4+}$, and external sacrificial donor, EDTA, or TEOA, below 5°C led to formation of trace quantities of viologen radicals after 120 minutes (Figure 27). When $Ru(bpy)_3^{2+}$ was substituted for $ZnTMPyP^{4+}$ ion, a slightly greater accumulation of reduced viologen was observed (Figure 28). Illumination of similar vesicle assemblies prepared in buffered solutions (0.05 M Tris, pH 7.5) gave higher yields for both sensitizers (Figures 29, 30). After illumination, a significant fraction of the originally entrapped viologen had become accessible to dithionite reduction. Typically about 25% of the viologen was reducible after 40 minutes of illumination. Data are summarized in Table 7. Viologen leakage was found to be both wavelength and temperature dependent. Figure 31 shows illumination of both Soret and visible metalloporphyrin bands gave more extensive diffusion than illumination of only visible bands over an equivalent time period. Initial rates of absorbance changes in temperature-controlled illumination are given in Table 8. Figure 32 represents the Eyring plot for 10-40°C; an apparent activation energy of 19.5 Kcal/mole was calculated.

Possible damage to bilayers induced by photoexcitation of bound sensitizer which might lead to viologen diffusion was also examined. A buffered solution of DHP vesicles containing external $Ru(bpy)_3^{2+}$ and internal MV^{2+} was illuminated for 30 minutes at 15°C, followed by a 30 minute dark period. External dithionite tests given both immediately after illumination and dark periods gave identical reduced viologen concentrations (6.5 µM), which were about two-fold greater than the residual external viologen concentration (3.4 µM) in the vesicle preparation after gel chromatography.

3.6.2 $Fe(CN)_6^{3-}-C_{16}MV^{2+}-DHP-ZnTPPS^{4-}$ vesicle assemblies

Continuous illumination of DHP vesicles containing $C_{16}MV^{2+}$ ions bound to both inner and outer surfaces in the presence of externally added photosensitizer $ZnTPPS^{4-}$ and the sacrificial donor, tricine, resulted in prompt formation of monomeric viologen radical cations, as detected by the appearance of bands at 396 and 600 nm in the visible spectrum (Figure 33). Accumulation of $C_{16}MV^+$ radicals usually ceased after 60-80 minutes of illumination, by which time extensive bleaching of sensitizer had occurred. The rate of reduced viologen formation of $C_{16}MV^{2+}-DHP$ vesicles was not appreciably altered by prior passage down G-50 gel columns. However, when 0.1 M tricine was replaced by 1 mM EDTA as donor, no spectral change was observed after 45 minutes of illumination. In solutions of DHP vesicles containing externally bound $C_{16}MV^{2+}$ formed by slow mixing of $C_{16}MV^{2+}$ with preformed vesicles, followed by gel chromatography, initial rates of radical formation were similar to viologen bound to both surfaces with a slight decrease in the net formation of reduced product. However, when $C_{16}MV^{2+}$ was added by the method of short bursts of sonication, the initial rates were reduced

2- to 3-fold under the same conditions. In vesicles containing occluded $Fe(CN)_6^{3-}$ within their internal aqueous phase, a slower rate of radical formation preceded by a pronounced induction period was observed (Figure 34). The lack of $C_{16}MV^+$ accumulation during the induction period can be attributed to its rapid reoxidation by internalized $Fe(CN)_6^{3-}$. The amount of viologen radical reoxidized can be approximated using initial rates obtained in other systems where $Fe(CN)_6^{3-}$ was absent. A comparison of these values with the amount of internalized $Fe(CN)_6^{3-}$ is given in Table 9. In solutions containing 5-50 μM $Fe(CN)_6^{3-}$ ion in the external medium, no radical formed within 60 minutes of illumination. Asymmetrically organized vesicles with $C_{16}MV^{2+}$ bound only to their outer surfaces and carrying internalized $Fe(CN)_6^{3-}$ showed immediate formation of viologen radical with a 5-fold enhancement of the initial rate. Rate data obtained for reduction of $C_{16}MV^{2+}$ in various vesicle configurations are summarized in Table 10. Eyring plots are given in Figure 35. Evaluated activation parameters are given in Table 10.

3.6.3 $C_{16}MV^{2+}$-PC-ZnTMPyP^{4+} vesicle assemblies

Continuous illumination of deoxygenated PC vesicle solutions containing either $C_{16}MV^{2+}$ bound to the outer surface or both surfaces in the presence of externally added unbound ZnTMPyP^{4+} and donor EDTA resulted in prompt development of reduced viologen. Figure 36 shows typical absorbance changes during a 20 minute period of illumination. Loss of absorption at 468 nm indicated significant porphyrin bleaching; about 80% of original ZnTMPyP^{4+} ions were bleached. The initial rate of radical formation was also dependent on the adsorbed viologen concentration. Initial rates obtained from viologen buildup are given in Table 11. Increase in $C_{16}MV^{2+}$/PC from 1:10 to 1:3 gave a proportionate

increase in the initial rate. In the absence of PC, the rate of $C_{16}MV^+$ formation was about 10 times greater than that in vesicle solutions.

3.6.4 Flash photolysis

The triplet photoexcited $ZnTMPyP^{4+}$ ion underwent exponential decay following laser flash excitation in buffer solutions containing PC vesicles; the reaction was monitored at 600 and 890 nm.[82] Observed first order relaxation curves are reproduced in Figure 37, with a rate constant of 3.9×10^3 s^{-1} obtained by averaging the values at both detection wavelengths. Deactivation of the porphyrin triplet ion in the presence of donor EDTA in PC vesicles also yielded well-resolved first order decay curves with 4-fold increase in rate constant (1.9×10^4 s^{-1}) (Figure 38). This is attributable to reductive quenching by EDTA.[83] In contrast, the quenching behavior of excited Zn(II) porphyrin appeared more complex in the presence of PC vesicles containing $C_{16}MV^{2+}$ ions bound to both inner and outer vesicle surfaces. Rapid buildup of viologen radical formation was observed at 600 nm, followed by a slow decay ($k = 2-7 \times 10^2$ s^{-1}) in the absence of donor. Figures 39 and 40 represent typical kinetic curves obtained. Overall, oxidative quenching of porphyrin triplet state by PC-bound $C_{16}MV^{2+}$ did not follow strictly first order decay; considerable curvature is seen in the first order curves. Rate constants derived from best-fit plots of the integrated rate laws also varied randomly from preparation to preparation. The rate data are summarized in Table 12. The Stern-Volmer plot of the first order deactivation rates measured at 840 nm versus viologen concentration gave a bimolecular constant, $k_Q = 1.2 \times 10^6$ M^{-1} s^{-1} in 0.05 M phosphate, pH 6.5, 23°C, with correlation coefficient obtained from linear regression analysis, $r = 0.96$ (Figure 41). We ascribe the slow decay observed at 600 nm (Figure 40) to the

back electron transfer between the reduced viologen and $ZnTMPyP^{5+}$ π-cation.[82] Using a molar extinction coefficient of 1.24×10^4 M^{-1} cm^{-1} for viologen radical,[68] the second order rate constant for the recombination of the redox pair is calculated to be within the range $1.5\text{-}15 \times 10^8$ M^{-1} s^{-1} (Table 13).

3.7. Thermal redox reactions

3.7.1 Reduction of $(NH_3)_5Ru\text{-}4\text{-}(11'\text{-}dodecenyl)py^{3+}$ ion bound to phosphatidylcholine vesicles

Anaerobic addition of 3- to 7-fold excess of reducing agents (Cr^{2+}, V^{2+}, Cu^+ and ascorbate) to acetate buffer solutions (0.01-0.1 M), pH 4.0, containing $(NH_3)_5Ru\text{-}4\text{-}(11'\text{-}dodecenyl)py^{3+}$ ions bound to both inner and outer surfaces of PC vesicles caused immediate formation of the reduced ruthenium complex as indicated by the appearance of an intense absorption band at 415 nm. This fast reaction was generally over within time of mixing, as measured by the stopped flow method. Figure 42 shows the kinetic trace obtained upon mixing of sample solution with V^{2+} as the reductant. As can be seen, the lack of measurable decay indicates the reaction was faster than the detection limit. Therefore a lower limit of 10^{-3} second is estimated for the fast reduction. Slow continuous reduction was observed when reductant concentration levels were kept above 1:1 stoichiometric equivalence of reductant to $(NH_3)_5Ru\text{-}4\text{-}(11'\text{-}dodecenyl)py^{3+}$ ion. When the reductant concentration was below this level, the rapid appearance of the 415 nm band was followed by slow bleaching. The reduced ruthenium complex generated in the slow step was also vesicle-bound, as was apparent in the bathochromic shift from 396 to 418 nm in the absorbance of the $Ru(d) \rightarrow py(\pi^*)$ charge transfer band

maximum relative to homogeneous solution. Optical changes due to the slow reduction by V^{2+}, Cr^{2+}, ascorbate, and Cu^+ ions are reproduced in Figures 43, 44, 45 and 46, respectively. Inclusions of valinomycin (7 µM) or carbonyl cyanide m-chlorophenylhydrazone (CCCP) (5 µM) in $(NH_3)_5Ru-4-(11'-dodecenyl)py^{3+}$ PC vesicles prepared in 0.1 M potassium acetate buffer solutions did not alter the kinetic features of reduction by Cr^{2+}. Complex behavior was observed in Cu^+ reduction in which the slow increase was followed by bleaching of the $(NH_3)_5Ru-4-(11'-dodecenyl)py^{2+}$ ion (Figure 46).

The amount of $(NH_3)_5Ru-4-(11'-dodecenyl)py^{2+}$ formed in the slow reaction, represented as per cent of the total optical change, was calculated by dividing the optical change due to the slow phase by the total optical change. In kinetic plots which showed curvature, the initial optical changes were obtained by extrapolation of the best straight line drawn. Apparent first order rate constants determined for different reductant concentrations and at different temperatures are listed in Tables 14-19. Since considerable scatter was observed from preparation to preparation for each reductant, the derived rate constants are likely to contain large uncertainty; no systematic dependence of rate constants upon reductant concentrations or identities was evident in the studies. Activation parameters evaluated from the $\ln(k/T)$ vs. T^{-1} plots (Figures 47-51) are summarized in Table 20. Except for Cu^+, for which only 12-20% of the total reduction is attributable to the slow phase, slow reduction by other reductants generally comprised 30-40% of the total reaction.

3.7.2 Reduction of $(NH_3)_5Ru-4-(6'-heptenyl)py^{3+}$ ion bound to phosphatidylcholine vesicles

Addition of excess Cr^{2+} to $(NH_3)_5RuNC_5H_5(CH_2)_5CH=CH_2^{3+}$-PC vesicles prepared by cosonication also resulted in biphasic formation of the ruthenium(II) complex. Data obtained for the slow reaction at 10°C are presented in Figure 52. The apparent first order rate constant (5.8×10^{-4} s^{-1}) is similar to the rate of the C_{12}-ruthenium complex, but its relative amplitude is less (15% total change).

3.7.3 Reduction of Externally Bound $(NH_3)_5Ru-4-(11'-dodecenyl)py^{3+}$ Ion in phosphatidylcholine Vesicles

One possible interpretation of the slow reaction observed in PC-bound $(NH_3)_5Ru-4-(11'-dodecenyl)py^{3+}$ reduction is transmembrane exchange of ruthenium complexes that are localized on opposite vesicle surfaces, i.e., diffusion of the Ru(II) complexes from the external surface to the internal surface and Ru(III) complexes from the opposite surface. Furthermore, the bleaching reaction observed when external reductant becomes limiting indicates degradation of the Ru(II) ions formed. For these reasons, ruthenium diffusion and $(NH_3)_5Ru-4-(11'-dodecenyl)py^{2+}$ bleaching were examined. The method involves addition of $(NH_3)_5Ru-4-(11'-dodecenyl)py^{3+}$ ions to preformed PC vesicles, followed by external reduction. The amount of ruthenium(II) formed was monitored spectrophotometrically.

Externally bound $(NH_3)_5Ru-4-(11'-dodecenyl)py^{3+}$ ions ([Ru] = 0.1 mM) in PC vesicle solutions ([PC] = 7 mM) were reduced by excess Cr^{2+} ([Cr^{2+}] = 0.6 mM) at 5°C and 25°C. Immediate formation of bound Ru(II) complexes was detected at 415 nm. No slow reduction was observed; the absorbance remained constant for at least 30 minutes. Similar results

were obtained by reduction of externally bound $(NH_3)_5Ru-4-(11'-$

dodecenyl)py^{3+} complex with excess ascorbate at 5°C. In this experiment,

the Ru(III) complex was added to preformed PC vesicles and allowed to

incubate. At various incubation times, aliquots of the solution were

reduced by ascorbate and the absorbance changes were recorded. Again, no

slow absorbance change was observed up to several hours of incubation.

This result indicates the lack of appreciable diffusion of externally

bound $(NH_3)_5Ru-4-(11'-dodecenyl)py^{3+}$ ions to the internal surface after

mixing with vesicles.

In order to investigate the possibility of transmembrane diffusion

of $(NH_3)_5Ru-4-(11'-dodecenyl)py^{2+}$ ion after it is formed, reversible

reduction-oxidation of the Ru(III) ion by Cr^{2+} and $Fe(CN)_6^{3-}$ was studied

in PC vesicle solutions at ambient temperature. The redox sequence is

illustrated by Scheme III. Initially the Ru^{2+} complex was generated by

Cr^{2+} ($[Cr^{2+}]$ = 0.3 mM) reduction. After an incubation period of
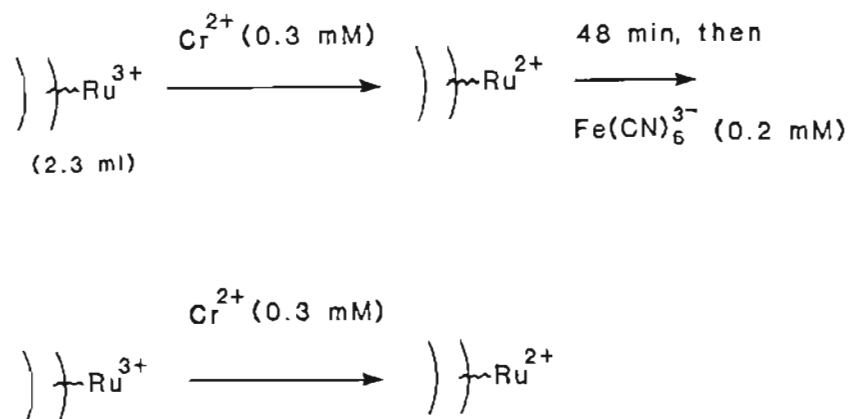
Scheme III

48 minutes, the Ru^{2+} complex ion was reoxidized by $Fe(CN)_6^{3-}$ ($[Fe(CN)_6^{3-}]$ = 0.2 mM), then immediately reduced again by Cr^{2+} ion. The amount of Ru^{2+} complex that formed immediately ($[Ru^{2+}]$ = 0.2 mM) was 90% of the initial concentration (2.2 mM) corrected by a dilution factor of 2.5/2.7. No slow-phase reduction was detected. This result indicates that diffusion of Ru(II) complex across vesicle bilayers is negligible in 48 minutes. In conjunction with the previous external Ru(III) reduction study, this cyclic oxidation-reduction of the externally bound Ru(III) complex demonstrated that the diffusion of both Ru(II) and Ru(III) complex ions across the bilayer appears to be negligible on the timescale of the slow-phase reduction step under our experimental conditions.

Slow reduction was also not observed when reductant concentrations (V^{2+}, Cr^{2+} ascorbate, $2-4 \times 10^{-5}$ M) were less than the total concentration of the Ru(III) used. Instead a reversible slow bleaching was observed after the prompt formation of the Ru(II) ions. Following bleaching, the ruthenium(II) complex could be regenerated by addition of more reductant. The Ru(II) complex reformed in this manner was also detected as the bound form from its spectral properties. This bleaching process was further investigated in a set of kinetic runs where $(NH_3)_5Ru-4-(11'-dodecenyl)py^{3+}$ ions were reduced in the absence of PC vesicles. Complex bleaching was observed: rates and reaction order varied from the identity of reductant and to a lesser extent, from run to run. Data obtained are given in Table 21. Representative kinetic curves are shown in Figure 53. From crude estimation, bleaching rates ranging from 10^{-4} to 10^{-5} s^{-1} were obtained in the following order of reductant, V^{2+} > Cr^{2+} > ascorbate. Since $(NH_3)_5Ru-4-(11'-dodecenyl)py^{3+}$ ion was isolated as its perchlorate salt, and pentaamminepyridineruthenium(II)

ions are known to undergo complex catalytic oxidation by perchlorate ion,[84] the potential role of perchlorate counterions was examined. Use of V^{2+} reagent prepared from stock solutions containing 0.1 M ClO_4^- resulted in a 100-fold increase in the bleaching rate of $(NH_3)_5Ru-4-(11'-dodecenyl)py^{2+}$ in homogeneous solution. Similarly, Cr^{2+} prepared in ClO_4^--containing solutions also enhanced bleaching; however, the increase was only 2-fold. Perchlorate catalyzed bleaching was also evident from the reduction behavior of the Ru^{3+} ion by amalgamated zinc. Only minute amounts of the reduced ion were generated by Zn(Hg) in deoxygenated solutions containing 0.1 M ClO_4^-, as evident from the yellow color developed in the vicinity surrounding the zinc surface after 30 minutes. Once the solution was removed from the zinc particles, the color disappeared quickly. In contrast, in 0.1 M sodium trifluoroacetate, reduction was efficient and the ruthenium(II) complex formed was more stable. Since the ruthenium(II) complexes contained perchlorate counterions, the ClO_4^- concentration was three-fold greater than the metal concentration in the reaction solutions. For the kinetic runs in which perchlorate was not added to the medium, the perchlorate counterion concentration was about 1 mM. The bleaching of Ru(II) complex observed in the presence of limiting concentrations of reducing agents is therefore probably due to oxidation by perchlorate although catalysis by the reductant, e.g., V^{2+}, may be involved.

The bleaching rate was greatly reduced when PC vesicles ([PC] = 7 mM) were present. With V^{2+} as reductant ($[V^{2+}]$ = 17 μM) in 0.1 M ClO_4^-), a bleaching rate of 1.6×10^{-4} s^{-1} was obtained, which is an order of magnitude smaller than the rate (1.3×10^{-3} s^{-1}) in the absence of vesicles with the same V^{2+} ion concentration. Based on this experiment,

bleaching rates for other reductants in the presence of PC vesicles were also assumed to be retarded from values in homogeneous solution. Under conditions where reductants were in excess (3-7-fold), no net bleaching occurred over an extended period of time (7.3 hours). The $(NH_3)_5Ru-4-(11'-dodecenyl)py^{2+}$ ions formed by reduction in excess Cr^{2+} in both homogeneous solution and externally bound to PC vesicles remained stable over the observed time span. Hydrolytic processes[84,85] and displacement of the chromophore from the vesicle surface were also undetectable in this time frame as confirmed by its unchanged spectral properties. A lower limit of the rate of hydrolysis is estimated to be 10^{-7} s^{-1}, which is much smaller than the reported values[84] for hydrolysis of the 4-pyridinepentaamineruthenium(II) ions in homogeneous solution ($k \approx 3 \times 10^{-5}$ s^{-1}, $\mu = 2.0$ M, 25°C, extrapolated to pH 4.0). The conclusion drawn from these observations is that vesicle-bound ruthenium complex is less susceptible to oxidative bleaching and aquation than in homogeneous solution, and remains in the reduced form in the presence of excess reductant.

3.8 Mechanism for Reduction of Vesicle—Bound 4-(11'-dodecenyl)pyridinepentaammineruthenium(III) Ions

The overall results can be fitted to Scheme IV. Step 1 depicts the fast reduction of externally bound $(NH_3)_5Ru-4-(11'-dodecenyl)py^{3+}$ by added reductant. Step 2 depicts the transmembrane redox process involving net reduction of internal Ru(III) by external Ru(II), which is immediately reduced again by the external reductant as shown in Step 3. Step 4 represents a pseudo-first order oxidation reaction of internal Ru^{2+} to Ru^{3+}. This process is inducible by exogenous agents such as perchlorate. Combination of Steps 1, 2, and 3 results in the net

reductant + $\xrightarrow{k_1}$ oxid. +

 $\xrightarrow{k_2}$

reductant + $\xrightarrow{k_1'}$ oxid. +

 $\xrightarrow{k_3}$
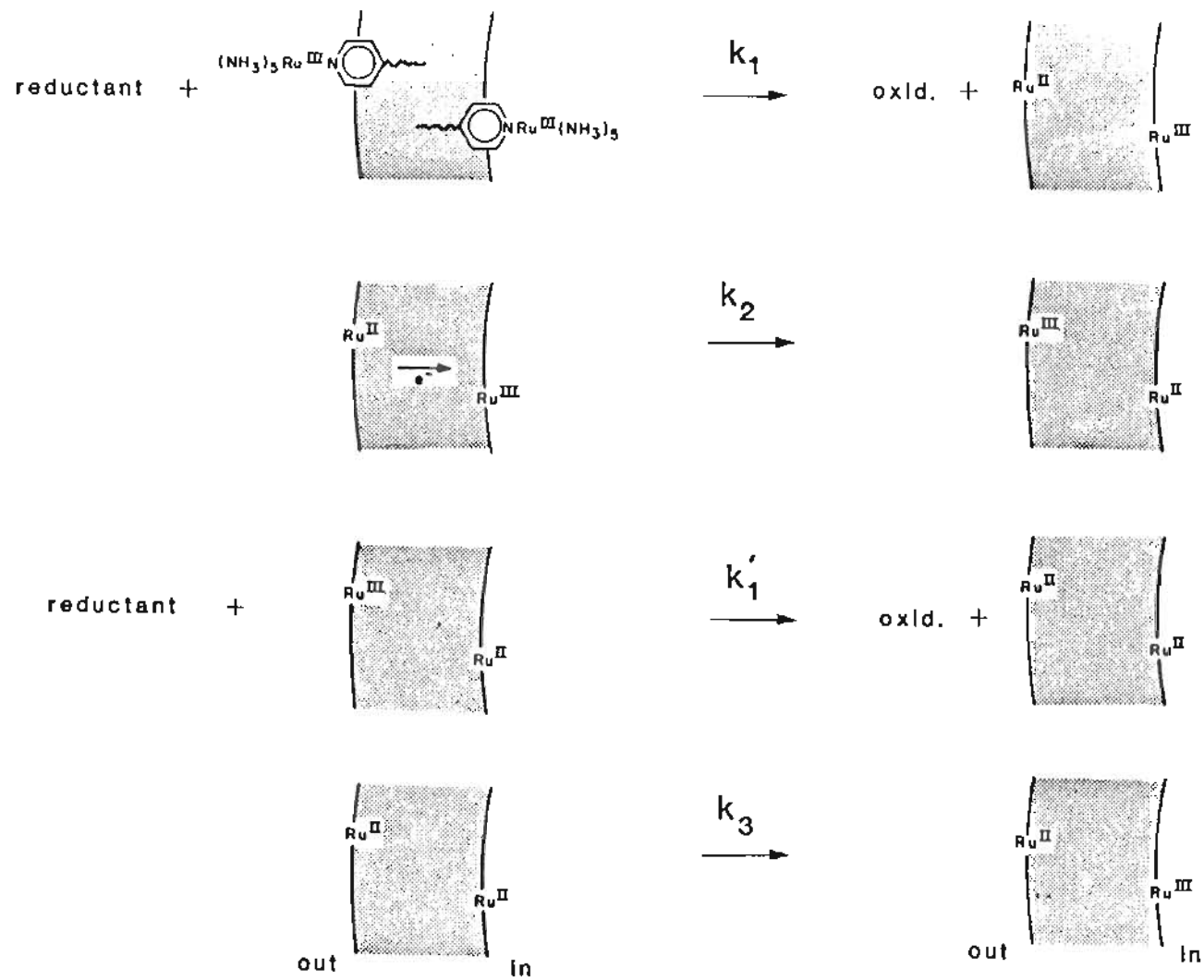
Scheme IV

oxidation of the external reductant. Under conditions where $k_1 \gg k_2$, $k_2 > k_3$, and reductant is in excess, the overall reaction results in the steady accumulation of internal Ru^{2+} ions. A quasi-equilibrium can be approached where there is no net change in Ru_{in}^{2+} and Ru_{in}^{3+} concentrations, i.e., $[Ru_{in}^{2+}] + [Ru_{in}^{3+}] = [Ru_{in}^T] = $ constant, before depletion of the external reductant. Three assumptions have to be made to achieve this state:

(1) There is no transmembrane diffusion of ruthenium species.

(2) $[Ru_{out}^{2+}]$ remains unchanged relative to concentrations of internal ruthenium species.

(3) Ru_{in}^{3+} is inaccessible to external reductant.

Assumption (2) is established by the observation of biphasic kinetics, i.e., $k_1 \gg k_2$; the other assumptions, (1) and (3), are established by experiments described in Section 3.7.3 and 3.3, respectively. Under these conditions, a rate expression for Ru_{in}^{2+} analogous to a reversible first order reaction can be written (Appendix I):

$$\frac{d[Ru_{in}^{2+}]}{dt} = k_2[Ru_{out}^{2+}][Ru_{in}^{3+}] + k_3[Ru_{in}^{2+}]$$

This is a pseudo-first order rate expression in $[Ru_{in}^{2+}]$, i.e., plot of $\ln[Ru_{in}^{2+}]$ vs. time yields a straight line with negative slope equal to $(k_2' + k_3)$, where $k_2' = k_2[Ru_{out}^{2+}]$ is a constant under assumption (2). The apparent first-order rate constant determined in the slow reduction, therefore, is the sum of the transmembrane electron transfer rate and the bleaching rate. Based on the 10-fold decrease in the bleaching rate of PC-bound $(NH_3)_5Ru-4-(11'-dodecenyl)py^{2+}$ for vanadous reduction in perchlorate media relative to homogeneous solutions, k_3 values are

estimated to be 10^{-5} s^{-1} for Cr^{2+}, and 10^{-4} s^{-1} for V^{2+} and ascorbate. These bleaching rates are about an order of magnitude smaller than the experimentally obtained apparent first-order rates for the slow reduction, $k_0 = 5-9 \times 10^{-4}$ s^{-1}; hence, the contribution of k_3 to the overall transmembrane transfer rate is small.

CHAPTER 4

DISCUSSION

4.1 Formation Characteristics of Vesicles

Phospholipids are amphiphilic molecules consisting of well differentiated head groups and hydrophobic tails. The approximately cylindrical shape of the molecules favors aggregation in the form of stacked bilayers.[86] The molecular structures of phosphatidylcholine (PC) and dihexadecylphosphate (DHP) are presented below.

Phosphatidylcholine

$$H_3C-(CH_2)_{16}-\overset{\overset{\displaystyle O}{\|}}{C}-O-CH_2$$

$$H_3C-(CH_2)_7-CH=CH-(CH_2)_7-\underset{\underset{\displaystyle O}{\|}}{C}-O-CH$$

$$CH_2-O-\overset{\overset{\displaystyle O}{\|}}{\underset{\underset{\displaystyle O^-}{|}}{P}}-O-CH_2-CH_2-\overset{+}{N}\begin{matrix}CH_3\\CH_3\\CH_3\end{matrix}$$

Dihexadecyl Phosphate

$$H_3C-(CH_2)_{15}-O\diagdownO$$
$$P$$
$$H_3C-(CH_2)_{15}-O\diagupO^-$$

Natural egg PC contains various degrees of unsaturation in the diacyl ester,[55] and a cis- double bond in one of the acyl chains. Under

appropriate conditions, PC and DHP molecules can be induced to form metastable unilamellar vesicles. In the present study, the physical dimensions of vesicles formed by sonication are generally consistent with literature values.[76,80,81] However, unilamellar PC vesicle radii determined by electron microscopy (130 Å) are smaller than those measured by dynamic light scattering spectroscopy (230 Å). This discrepancy can be resolved by recognition of the inherent error contained in the photocorrelation data analysis in the light scattering technique. It has been shown[87] that in solutions of polydispersed particles, a small fraction of strong scatters can weight the average radii much greater than their actual population distribution, resulting in larger apparent hydrodynamic radii for the major fraction of the smaller particles. For example, in a study of unilamellar dipalmitoyl-phosphatidylcholine (DPPC) vesicle stability, Chang and coworkers have found that addition of less than one percent of larger fused vesicles (384 Å) to small unilamellar vesicles (104 Å) produced an apparent measured radius of 250 Å.[88] This result is very similar to the data obtained from electron microscopy and light scattering spectroscopy in the present system, thus providing a self-consistent rationalization of the data. The small number of larger PC vesicles observed in electron micrographs also suggests that a few percent of unilamellar vesicles may have undergone aggregation or fusion after their formation.

The inability of DHP to form vesicles in a number of different media indicates that the vesicles are stable only over a relatively narrow range of medium condition. In general, high salt concentrations, presence of oxyanions or polyanions, and high concentrations of adsorbed cations lead to destabilization. Since the behavior of amphiphilic

molecules in water is determined by the balance of energies of three types of interaction (water with head groups, water with hydrophobic groups, and hydrophobic groups with each other), it could be argued that in DHP, Coulombic forces between the head groups and ionic species can become significantly large such that formation of the bilayer is disrupted. In the presence of high concentrations of anions, charge-charge repulsive forces between the monomers and ions tend to disperse the monomers, thus preventing proper aggregation, while cations tend to adhere to the negatively charged membrane surface during bilayer formation, promoting fusion by aggregation of the vesicles. The intricate interplay between head groups and the bulk medium is further demonstrated by the use of hydroxylic amine buffers. Tris, tricine, and triethanolamine (TEOA) at neutral pH not only facilitate DHP vesicle formation, but also improve their longevity. Polyalcohols are known to act as stabilizing co-surfactants in micelles.[89] Similar effects can be inferred here, i.e., adsorption of hydroxylic amines at the DHP vesicle interface enhances their stability.

Although DHP vesicles are easier to form and more stable than PC vesicles, as indicated by the shorter sonication time required to achieve clarification of solutions and the greater homogeneity obtained in light scattering measurements, they are highly sensitive to medium conditions and are only formed at elevated temperatures. This is attributable to the differences in their head groups and acyl ester chains. The phase transition temperature (T_c) of phospholipids, which is defined as the melting point of the acyl chains in H_2O, is characterized primarily by the configuration and length of the chain and the degree of hydration of the head group. Although PC contains slightly

longer chains (C_{18}) than DHP (C_{16}), the presence of double bonds and zwitterionic head groups as opposed to the saturated chains and anionic head groups in DHP, gives rise to greater disorder in the lattice, thus resulting in a much lower T_c[90] (-4°C) than that of DHP[76] (60°C). The larger diameter (~500 Å) of the DHP vesicle is also attributable to the anionic head group. Since vesicle size is probably limited by the constraint of the radius of curvature on the packing of monomers, greater electrostatic repulsion between DHP head groups would dictate a looser packing than the neutral head groups of PC in their bilayer configuration. The negative charges on the DHP bilayer surface also allow greater dispersion of the vesicles in H_2O, i.e., less fusion or aggregation, thus increasing their stability.

4.2 Binding Properties of Vesicles

Binding of water-soluble cationic photosensitizers ($ZnTMPyP^{4+}$, $Ru(bpy)_3^{2+}$) to anionic vesicle surfaces, demonstrable by their spectral shifts in the visible spectrum, is predominantly electrostatic in nature. This is supported by the observations that $ZnTPPS^{4-}$, a metalloporphyrin similar to $ZnTMPyP^{4+}$ except for its negative charges, is excluded from DHP vesicle surfaces and that of $ZnTMPyP^{4+}$ binding to neutral PC vesicles is undetectable. Binding of $ZnTMPyP^{4+}$ to DHP vesicles has been studied by Hurst and coworkers.[91] They have shown that Beer's law was obeyed over a metalloporphyrin concentration range greater than 100-fold; difference spectra obtained by increasing ratios of $ZnTMPyP^{4+}$ to DHP showed isosbestic points at 433, 540, and 566 nm and the bandshapes remained constant. This result suggests homogeneous binding to the vesicle surface. Furthermore, they have also shown that bathochromic shifts in $ZNTMPyP^{4+}$ dissolved in organic solvents increased

with decreasing solvent polarity. The spectrum of DHP-bound $ZnTMPyP^{4+}$ is very similar to that obtained in isopropanol. This is consistent with binding of the chromophore in the region of the charged head groups on the vesicle surface. This claim is further supported by the displacement of bound $ZnTMPyP^{4+}$ in media containing high TEOA concentrations where the number of available binding sites is diminished by the competitive binding of TEOA. This suggests that labile equilibria exist between bound and free chromophores, e.g., $ZnTMPyP^{4+} + DHP^{n-} \underset{\rightleftharpoons}{K}$ $ZnTMPyP^{4+}:DHP^{4-n}$, which are media sensitive. The inhibitory effect on external binding caused by hydroxylic amine adsorption is also observed in the removal of MV^{2+} ions from outer vesicle surfaces in a high concentration of Tris buffer (0.05 M) by gel columns, although in this case, the influence of nonspecific salt effects has not been evaluated. Similarly, other researchers have found that $Ru(bpy)_3^{2+}$ ions adsorb only weakly to DHP vesicles in 0.05 M Tris.[75] Thus, it can be concluded that binding of hydrophilic adsorptive cations to external DHP bilayer surfaces is attained by strong electrostatic attraction to the head groups.

Binding of methyl viologen and its alkyl derivatives to vesicles was demonstrated by gel chromatography. Dihexadecylphosphate-bound MV^{2+} ions were detected in the vesicle fraction by dithionite at lower buffer concentration (0.02 M Tris). Clean separation from the vesicles was achieved in higher buffer concentration (0.05 M Tris); presumably, externally bound viologen was removed by continuous shifting of the binding equilibrium to the left as the sample passed down the column. This binding equilibrium is greatly affected by increasing the hydrophobicity of the viologen. With $C_{16}MV^{2+}$, for which the methyl group at the 4 position of one of the pyridinium groups is replaced by a

saturated 16-carbon chain, nearly complete binding to DHP vesicles was observed. Presence of the long alkyl tail increases the affinity between the viologen and the vesicle to the extent that they are no longer separable on the dextran gel. Hydrophobic binding is clearly evident in alkylviologen binding to PC vesicles where $C_{16}MV^{2+}$ exhibits stronger binding than $C_{14}MV^{2+}$. The degree of binding is not only dependent on the chain length of the viologen, but also dependent on the method of incorporation. Cosonicated viologen-PC solutions showed stronger binding than that obtained from mixing with preformed vesicles. These observations suggest that interaction between alkyl tails of the ions and the hydrophobic bilayer is important. Presumably, incorporation of viologen during bilayer formation produces a more ordered binding configuration than the one obtained by external addition. Since $C_{16}MV^{2+}$ has the same number of carbon atoms in the alkyl chain as in DHP, one could speculate that the viologen has become an integral part of the bilayer. It is also interesting to note that reduced viologens bound to vesicles are monomeric, in contrast to the aggregated form in solution. Apparently, the greater affinity between viologens and vesicles precludes self-association of the viologens.

Similar conclusions can be drawn from the binding studies of $(NH_3)_5Ru$-4-alkenylpyridine^{3+} complexes to PC vesicles. The results obtained from difference spectroscopy and gel chromatography support the notion that binding of amphiphilic ruthenium complexes is also predominantly hydrophobic in nature, which is determined primarily by the chain length of the alkyl tail. A recent study[92] on binding of alkylviologens of varying chain length ($C_{12}MV^{2+}$-$C_{18}MV^{2+}$) to cationic micelles has shown that the free energy change associated with displacement of the

alkylviologen from the aqueous phase to the micellar phase ($\Delta G^{\ddagger}$) is 0.43 kcal/mol per methylene group of the viologen.

Hydrophobic adsorption of amphiphilic cobalt(III) complexes to PC vesicles was studied using membrane ultrafiltration techniques and atomic absorption spectroscopy. Due to the inherent adsorptive nature of the semipermeable filter membrane used, accurate measurement of vesicle-bound Co(III) complex concentrations was not possible. Correction factors obtained from vesicle-free solutions were required to calculate the true vesicle-bound Co concentration, assuming adsorption to the filter membrane is independent of binding to vesicles. Hence, substantial scattering is seen in the experimentally determined σ values (Figures 19, 20). Nonetheless, a quantitative treatment of the data was attempted by fitting to a simplified Stern model.

The derivation of the Stern equation is based on the recognition that adsorption of charged molecules to initially neutral membrane surfaces produces an electrostatic potential at the interface. Two simple theoretical approaches are possible to describe this adsorption process. The Langmuir model principally describes the hydrophobic binding of molecules to spatially fixed sites as a function of the adsorbing molecule concentration at the interface. Electrical effects produced are completely ignored, and the adsorbing ion concentration at the interface is set equivalent to the molecule concentration in the bulk phase. The other simple, more appropriate approach is to consider that the charges on the membrane are smeared uniformly over the surface giving rise to an average surface potential. The behavior of monovalent ions near the electrical interface is adequately described by the Gouy-Chapman theory of diffuse double layer, which states there is a

region near the interface where distribution of ions is determined by the balance between electrical and thermal forces. Oppositely charged ions tend to adhere to the interface, while ions of same charge are repelled. The surface potential therefore tends to lower the concentration of the adsorbing ions in the aqueous phase immediately adjacent to the surface according to the Boltzmann relation. If the adsorbing ion and the electrolyties in the solution are monovalent, the Gouy-Chapman model can be easily incorporated into the Langmuir adsorption isotherm to give a modified Stern expression that embodies the assumptions contained in the theories: (a) adsorbing ions are point charges; (b) adsorption sites are spatially fixed; (c) charge density is uniform over the surface; and (d) image effects which arise from insertion of ions from high dielectric medium (water) to low dielectric medium (membrane) are ignored. However, for adsorption of multivalent ions, the incorporation of these charge effects into the Langmuir model is not easily attainable. Binding of the multivalent ion to the surface not only increases the surface density (σ_s) at a greater rate than the surface ion concentration, the resulting surface potential (ψ_o) also increases faster, i.e., the adsorbing ion in the solution near the itnerface would experience a greater electrostatic repulsion. Since the Gouy-Chapman equation only describes the statistical distribution of the monovalent electrolytes near the interface, the description of the adsorbing ion near the interface requires a different Boltzmann relation than the electrolytes. The Stern model for multivalent ion adsorption to neutral membrane surfaces has not yet been developed.

Application of the Stern model has met with considerable success for monovalent ion adsorption.[78,93,94] In particular, binding of an

anionic fluorescent molecule, 2,6-toluidinylnaphthalenesulfonate (TNS) to PC vesicles was studied by gel chromatography[95] and was found to fit the Stern equation.[78] A dissociation constant of 2×10^{-4} M and a maximum number of binding sites of 1/70 Å^2 were reported. Surface potentials determined by two independent techniques were also found to agree with the Stern prediction. In general, the theory describes remarkably well the hydrophobic adsorption of monovalent ions to uncharged bilayer membranes.

Qualitatively, the results obtained from binding studies of tripositive amphiphilic cobalt complexes indicate hydrophobic binding (Figure 17) since $(NH_3)_5CoOH_2^{3+}$ ions which lack the alkyl chain do not bind to PC vesicles (Section 3.3). The binding parameters determined from fitting to the Stern equation assuming monopositive ion, $\sigma^m = 1/285 \, \text{Å}^2$ for the shorter chain complex, $(NH_3)_5Co-4-(8'-nonenyl)py^{3+}$, and $\sigma^m = 1/167 \, \text{Å}^2$ for $(NH_3)_5Co-4-(10'-undecenyl)py^{3+}$, are consistent with the notion that binding is attained by insertion of the hydrophobic alkyl chain into the bilayer. The dissociation constants obtained, $\sim 10^{-3}$ M, are one order of magnitude greater than TNS, which suggests binding is relatively weaker. This is also consistent with the notion that charge-charge repulsion between the tripositive cobalt ions on the membrane surface is greater than for TNS.

The assumption of monopositive ion binding in the present study to fit the Stern equation is incorrect since the adsorbing cobalt complexes are formally tripositive ions. However, the overall surface charge density might be lower than the valence of the ion indicates. The headgroup of PC is a zwitterion; the choline group being a positive quarternary ammonium ion and the phosphate group being a negative ion.

Hence the vesicle membrane surface formed from PC contains strong

dipoles. Binding of charged molecules onto the surface would result in

alignment of these dipoles according to the magnitude and the sign of

the charged ions adsorbed. The oriented dipoles around the adsorbed ion

would lower the charge of the ion, thus decreasing the overall effective

surface charge density. Furthermore, the cobalt complexes are fairly

"soft" ions; the charge at the metal center is somewhat delocalized

around the ligands contributing to the diffusion of charges of the

adsorbed ion. The reasonable fits of the binding data to the Stern

equation assuming monopositive ion adsorption tend to support this

argument.

4.3 Permeabilities of Vesicle Bilayers

The general belief that phospholipid bilayer membranes have low

ionic permeability is supported by a large body of experimental evi-

dence. Numerous studies using vesicles and black lipid membranes have

shown that in the absence of lipophilic carriers or ionophores, the

transport of charged molecules across bilayers is slow.[39,96,97] This

unfavorable process is mostly attributable to the high electrical

resistance of the hydrocarbon layer (10^8-10^{10} Ω cm^2) stabilized by polar

headgroups. Activation energies reported for ion diffusion are in the

order of 15-30 kcal/mole.[38] Permeabilities of vesicles generally in-

crease with increasing unsaturation and decreasing chain length. The

presence of cis- double bonds and shorter acyl chains allows less or-

dered packing in the interior of the bilayer, thus increasing membrane

fluidity. Fixed charges and the dielectric constant also play an

important role in determining bilayer permeability. A number of

studies[97-100] have shown that the presence of acidic groups on the

membrane surface increases cation diffusion and decreases anion diffu-
sion, while the presence of excess positive charges has the opposite
effect. It was also found that increasing the dielectric constant of an
artificial bilayer increases its permeability to perchlorate and
thiocyanate by a factor of 1000.[101] This enhancement of diffusion was
ascribed to a large decrease in the Born charging energy, the
electrostatic energy required to transfer ions from the aqueous phase
into the center of the bilayer, which is directly dependent on the
dielectric constants of the media and the width of the bilayer.

The results obtained from the entrapment experiments of various
metal complexes by PC vesicles are in accord with the general observa-
tion that bilayers are impermeable to small ions. The entrapped
molecules are trivalent transition metal ions coordinated in octahedral
environments provided by various charged ligands. The overall charge of
the complex can be regarded as fairly evenly distributed over the entire
molecule. This is in contrast to amphiphiles, where ionicity is
concentrated in the vicinity of the headgroups. Transport of hydro-
philic complexes from one aqueous phase to the other aqueous phase,
therefore, requires movement of the entire charged species across the
water-lipid interface and the hydrocarbon interior.

In the entrapment studies, metal complexes in the external aqueous
bulk medium were removed stepwise by successive filtrations. Each wash
constituted a two-fold dilution in the external metal concentration,
with the final dilution factor equal to 2^n, n being the number of
washes. It can be seen that under this experimental constraint, the
metal concentration in the retained vesicle solution should be reduced
(10^3-10^8-fold) to an undetectable level after extensive washing

($>$ 9 washes) if the metal complexes were freely permeable to the vesicles. However, atomic absorption measurements of the final vesicle solutions showed that the metal concentrations were reduced only 10-100-fold, which indicates retention by vesicles. Quantitatively, the percentage of retention increased as the charge of the complex increased. Since the PC concentration used (1-2 mM) was relatively constant for all the complexes except for Cr^{3+} ions ($[Cr^{3+}]$ = 7mM), the retention percentages are reflective of the amount of complexes entrapped relative to each other. The PC concentration dependence of entrapment was not pursued in the present study.

The internal volume of a PC vesicle has been estimated to be 0.3 $\mu l/\mu mole$ of phospholipid by electron microscopy.[79] Using this value, the apparent concentrations of entrapped metal complexes in the aqueous phase of the vesicle were calculated (Table 4, column 8). The values obtained are 10-15-fold greater than the initial solution concentrations of the complexes. The origin of this apparent concentration effect is not known. Since the washing experiment with externally added Cr^{3+} to preformed PC vesicles showed all the Cr^{3+} ions were removed by filtration, binding of small ions to the vesicle surface was not observed by this technique. However, interaction of multivalent ions with vesicles is detected by more sensitive physical methods. Using deuterium and phosphorus magnetic resonance,[102] Akutsu and Seelig found that Ca^{2+} and La^{3+} ions adsorb to synthetic dipalmitoylphosphatidyl-choline (DPPC) vesicles, giving apparent binding constants of 19 M^{-1} and 120 M^{-1}, respectively. A similar type of moderate interaction between the metal complexes and PC vesicles might exist here. It is conceivable that metal complex adsorption at the inner vesicle membrane surface is

significant, thus giving rise to an apparent higher entrapped concentration. Using a modified form of the Adair equation[103] by assuming the ions, A, are bound to independent sites on the vesicle,

$$\bar{\nu} = n - \bar{\nu}/K[A] \tag{27}$$

where $\bar{\nu}$ is the binding fraction, $\bar{\nu} = [A]_{bound}/[PC]_{total}$, n is the number of binding sites per vesicle, [A] is the ion concentration in the aqueous solution, and K is the binding constant, the binding ion concentration is calculated. Substituting values of $n = 10^3$, [A] = 10^{-2} M, $K = 10^2$ M^{-1}, and $[PC]_{total} = 10^{-3}$ M, $[A]_{bound} = 0.5$ M, which is similar to the calculated internal metal concentrations in the entrapment studies (Table 4).

Incorporation of $Fe(CN)_6^{3-}$ ions within anionic DHP vesicles was conclusively demonstrated by a combination of chromatographic, spectral, and filtra- tion techniques. Clean separation of external $Fe(CN)_6^{3-}$ ions from DHP vesicles was achieved by gel chromatography. Both optical difference spectroscopy and atomic absorption spectroscopy showed the vesicles contained $Fe(CN)_6^{3-}$; ultrafiltration experiments demonstrated that diffusion of occluded $Fe(CN)_6^{3-}$ across the bilayer did not occur over a period of hours. Assuming spherical symmetry, the internal volume of a DHP vesicle is calculated to be 2.3 μl/μM of DHP using 250 Å as the internal radius. Under the present experimental condition, the maximal ferricyanide incorporation should give an apparent solution concentration of 0.12-0.6 mM, which is an order of magnitude greater than the experimentally determined value (4-40 μM). This discrepancy suggests that vesicle size might be smaller than the measured hydrodynamic

radii indicate. A recent study of DHP vesicles by light scattering spectroscopy[104] strongly suggests that a small fraction (1-2%) of large scatterers in the size distribution could give a fictitiously large hydrodynamic radius for the major component. Alternatively, the low apparent entrapped $Fe(CN)_6^{3-}$ concentrations could be due to its partial exclusion from the vesicle interior during formation of the enclosed bilayer arising from charge repulsion from the bilayer.

In contrast to $Fe(CN)_6^{3-}$, MV^{2+} ions bound to inner DHP vesicle surfaces diffuse slowly across the bilayer, as can be detected by external dithionite reduction. Methyl viologen translocated to the external surface is also surface-bound as indicated by its spectral properties, i.e., monomeric viologen radical cation forms upon one-electron reduction. The results obtained from the temperature-dependent study of MV^{2+} reduction by dithionite show that passive transmembrane diffusion does not occur at an appreciable rate below 25°C (Figure 24), but becomes rapid at higher temperatures, suggesting that movement of adsorbed MV^{2+} into the hydrocarbon phase has a high energy barrier. The apparent activation energy from initial rate data obtained at 25°C and 35°C is 30 kcal/mole. It has been proposed that Arrhenius activation energies for transmembrane ion diffusion are generally high because temperature-dependent changes in the membrane increase membrane fluidity in this temperature range (25-35°C).[38] Although the major phase transition temperature for DHP has been estimated to be 60°C,[76] localized changes in the bilayer structure could occur at lower temperatures which give rise to increased membrane fluidity. Further-more, external addition of hydroxylic amines to asymmetric MV^{2+}-DHP vesicle assemblies also increases internal MV^{2+} diffusion. This implies

that major changes at the interface due to the adsorption of amines, probably in the headgroup orientation and the electrostatic potential, can lower the energy barrier for viologen transport.

These results, in addition to photostimulated MV^{2+} diffusion which will be discussed in detail, suggest that enhancement of viologen movement is probably due to increase in the bilayer fluidity. This hypothesis can probably be tested by incorporating cholesterol in the bilayer. Physical studies have shown that when cholesterol is present in bilayer membranes, thermal molecular motion in the region of the first 8-10 carbon atoms of the acyl chain from the lipid-water interface is more restricted and the headgroups are more closely packed, producing a more perpendicular orientation and a thicker membrane.[105] This effect tends to lower the membrane permeability. Moreover, activation energies for MV^{2+} diffusion in membranes with varying composition should provide insight into the diffusion mechanism. Comparative studies on diffusion of electrolytes and nonelectrolytes gave evidence that ions diffuse via a different pathway than that of nonelectrolytes;[38] incorporation of cholesterol decreased the activation energies for ions drastically (from 30 to 15 kcal/mole), while it had only a small effect on nonelectrolyte diffusion.

4.4 Photoinduced Diffusion of Methyl Viologen Across
DHP Vesicle Bilayers

Photostimulated diffusion of methyl viologen across membrane bilayers in asymmetrically organized DHP vesicles is enhanced by binding photosensitizer to the opposite vesicle surface. Continuous illumination of either $Ru(bpy)_3^{2+}$ or $ZnTMPyP^{4+}$ ions electrostatically bound to the outer surface causes migration of internally bound MV^{2+} ions to the

outer surface as detected by external dithionite reduction. This

enhancement does not occur in the absence of light or in illuminated

vesicles that contain entrapped MV^{2+} but lack vesicle-bound photo-

sensitizer. Since the physical properties of the asymmetrically

organized DHP vesicles appear to be unchanged by illumination, and

diffusion ceases when illuminated vesicles are removed from the light,

diffusion is not due to photodegradative damage of the vesicle membrane.

The requirement for vesicle-bound sensitizer is demonstrated by the

absence of detectable enhancement of viologen diffusion in illuminating

asymmetrically labeled vesicle solution containing $ZnTPPS^{4-}$, an unbound

sensitizer. The wavelength dependence of diffusion rates on the light

source suggests that the driving force is directly related to the

photoenergy captured by the bound sensitizer. The relatively large

apparent activation energy (19.5 kcal/mole) is also comparable to the

activation energy estimated for the passive thermal diffusion (21.2

kcal/mole). Hence, collectively, these results strongly suggest the

mechanism(s) of photoinduced viologen diffusion involves localized

heating arising from nonradiative deactivation of the photoexcited bound

sensitizer. Although the molecular details are not delineated, one

could speculate that the heat dissipation by the photoexcited sensitizer

to the microenvironment in the bilayer structure causes significant

increase in the membrane fluidity which leads to enhancement of viologen

movement. A recent study[76] of phase transition temperatures in DHP

vesicles has found that the quenching rates of vesicle-incorporated

fluorescence probes in the cooling cycle were different from that in the

initial heating cycle. This hysteresis suggests that the bilayer

structure was significantly altered by heat which might account for its

enhanced fluidity. The diffusion mechanism also appears to be sensitive to the aqueous bulk medium. Vesicles prepared in hydroxylic amine buffers exhibit slightly higher MV^{2+} diffusion rates than vesicles prepared in water (Table 7). Light scattering spectroscopy[81] has shown that DHP vesicles formed in water are slightly larger than those formed in buffers. Apparently, adsorption of cosurfactant amine molecules in the bilayer-water interface not only stabilizes the headgroups, but also alters the bilayer structure to the extent that its fluidity is promoted.

Photoinduced electron transfer has been reported between donor and acceptor molecules separated by bilayer membranes.[22,68,106] Transmembrane electron exchange between amphiphilic derivatives of $Ru(bpy)_3^{2+/3+}$ has been proposed to account for photosensitized reduction of externally bound N-methyl-N'-heptylbipyridium ion (C_7MV^{2+}) by encapsulated EDTA in PC vesicles.[107] Similarly, photoreduction of internally bound MV^{2+} by externally bound $Ru(bpy)_3^{2+}$ in DHP vesicles was interpreted as direct transmembrane electron transfer from photoexcited ruthenium to acceptor.[68] These studies, however, did not demonstrate unambiguously transmembrane electron transfer because the possibility of photostimulated diffusion of the redox species across the bilayer was not investigated. Furthermore, to account for the measured overall redox rates in these two systems, it is necessary that electron transfer occur with apparent first-order rates in the order of 10^5 s^{-1}. From studies of electron transfer through fatty acid monolayers and multilayers, Kuhn has developed a tunneling model to describe the transfer mechanisms.[108] The electron is allowed to hop to intermediate interlayer sites located at the interface between hydrocarbon chains. Here, the transfer rate

from photoexcited $Ru(bpy)_3^{2+}$ at the outer surface to MV^{2+} at the inner

surface of the DHP vesicle can be calculated using the following

equation: $\tau = Ae^{2\alpha d}$. The tunneling relaxation time, τ, which is the

inverse of the first-order transfer rate constant, k, is related by A, a

constant term that contains the encounter frequency, orientation factor,

and densities of states: d, the transfer distance, and α, a barrier

height term that corresponds to the difference of energy between the

height of a square barrier and the linear momentum of the impinging

electron perpendicular to the barrier, i.e.,

$$\alpha = \sqrt{2m\varphi}/\hbar \tag{28}$$

where m is the mass of electron, $\hbar$ is the Planck's constant divided by

2π, and φ is the difference between the potential barrier height and the

electron's kinetic energy, $p^2/2m$ in the direction perpendicular to the

barrier. Using experimentally determined barrier heights for photo-

excited $Ru(bpy)_3^{2+}$ (1.6 eV,[109] which corresponds to $\alpha = 0.6 \, \text{Å}^{-1}$), a

transfer distance of 20 Å (the distance from the vesicle surface to an

intermediate sites in the hydrocarbon interface), and a pre-exponential

factor of 10^{-13} s, the electron transfer rate constant calculated, $k \leq$

$10^2 \, s^{-1}$, is several orders of magnitude smaller than the required rate.

Hence, earlier observations that were taken as indicative of trans-

membrane electron transfer are inconsistent with theoretical expecta-

tions. Hurst and coworkers[91] have studied the transient kinetics of

asymmetrically organized MV^{2+}-DHP vesicles in buffer solutions using

either $Ru(bpy)_3^{2+}$ or $ZnTMPyP^{4+}$ as sensitizer. No evidence for photo-

induced transmembrane electron transfer was found; no detectable buildup

of MV^+ or quenching of ruthenium luminescence could be observed in the

first several laser pulses in $MV^{2+}//DHP//Ru(bpy)_3^{2+}$ vesicle assemblies[69] although repeated pulsing or aging of the samples resulted in measurable electron transfer products.[68] Likewise, the complex triplet state deactivation of photoexcited vesicle-bound $ZnTMPyP^{4+}$, which can be resolved by three concurrent first-order processes, is unaffected by incorporation of MV^{2+} bound to the opposite surface, although photoexcited $ZnTMPyP^{4+}$ is quenched by viologens when bound to the same surface.[91] An alternative explanation to account for the photoreduction of viologen in illumination of vesicle-bound sensitizer, therefore, is transmembrane diffusion of MV^{2+}, followed by oxidative quenching of photoexcited sensitizer bound to the same surface.

Photostimulated diffusional processes in bilayer membranes can be further studied by using membrane-bound sensitizers that are incapable of redox quenching or energy transfer when photoexcited. This require-ment should limit the deactivation of the photoexcited sensitizer to pathways that are more likely to give rise to localized heating effects. Binding of the chromophore to different regions in the membrane bilayer, i.e., hydrophobic interior or hydrophilic interface, should provide insight into the nature of enhanced membrane fluidity. Conversely, restriction of molecular motion in the hydrocarbon chains can be achieved by incorporation of cholesterol, which should have a pronounced effect on molecular diffusion. In addition, the photoenergy requirement can be more accurately assessed by comparison of sensitizers that have vastly different light-capturing capabilities, i.e., that have different optical absorption spectra. These proposed studies, therefore, should be useful in understanding the mechanism(s) of photoinduced diffusion, which has potentially important implications in photobiological systems.

4.5 Deactivation of Zn(II) Porphyrin Excited States

Photoexcited $ZnTMPyP^{4+}$ ion undergoes exponential decay in PC vesicle solutions. The lifetime obtained (254 μsec) is similar to values reported for excited triplet deactivation in homogeneous buffer solutions[82,83] (t = 100-222 μsec). The lack of appreciable adsorption of the highly charged porphyrin molecule to neutral PC vesicle surfaces shown by various binding techniques indicates that deactivation of the excited Zn(II) porphyrin ion in PC vesicle suspensions is very similar to that in homogeneous solutions. Likewise, the non-binding Zn(II) porphyrin, $ZnTPPS^{4-}$, in anionic DHP vesicle solutions also exhibits simple first-order relaxation when photoexcited (t = 71 μsec).[91] The conclusion drawn from these results, then, is that in the absence of redox quenchers, spontaneous decay, which is due mostly to impurity quenching of the triplet state, is the predominant pathway for deactivation of photoexcited Zn(II) porphyrins in solutions where binding to vesicles is negligible.

Complex deactivation has been shown to occur following photoexcitation of DHP vesicle-bound $ZnTMPyP^{4+}$ ion by laser flash photolysis.[91] There appear to be three distinct independent relaxation processes on timescales that are separable by about an order of magnitude (2 μsec-200 μsec). This claim is supported by three pieces of experimental evidence. First, the minimal kinetic scheme that can account quantitatively for the decay curves requires use of three concurrent first-order relaxation processes (Figure 54). The resolved rate constants are reproduced in Table 22. Secondly, transient spectra of photochemical intermediates formed at various times after laser pulse show three absorbing species (Figure 55); the rapidly (t = 2 μsec) and

slowly (t = 200 μsec) decaying components have broad absorption in the near-infrared region of the optical spectrum which is attributable to porphyrin triplet ions,[110] whereas the intermediate component (t = 20 μsec) which has an absorption maxima around 740 nm, is indicative of porphyrin π-cation and π-anion formation.[111,112] The existence of three decaying components is also confirmed from the different quenching behavior of the photoexcited intermediates by $C_{14}MV^{2+}$ bound to the same vesicle surface. This aspect will be discussed later (Section 4.6.2).

We have proposed mechanisms for the three photoexcited Zn(II) porphyrin deactivation pathways.[91] The rapidly decaying pathway of vesicle-bound $ZnTMPyP^{4+}$ triplet ion is attributed to concentration quenching in which the photoexcited porphyrin is deactivated by reacting with one of its neighboring ground state molecules, i.e.,

$$^{*}ZnTMPyP^{4+} + ZnTMPyP^{4+} \rightarrow 2\ ZnTMPyP^{4+} \tag{29}$$
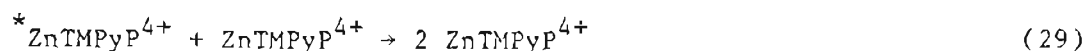
The intermediate pathway is ascribable to ionogenesis in which charge transfer between a photoexcited and a ground state porphyrin yields its π ion pair, i.e.,

$$^{*}ZnTMPyP^{4+} + ZnTMPyP^{4+} \rightarrow ZnTMPyP^{5+} + ZnTMPyP^{3+} \tag{30}$$
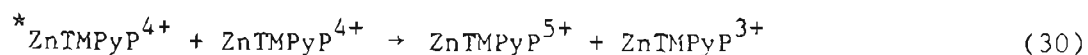
The slowly decaying component which has first-order deactivation rates $(1.9-5.6 \times 10^{3}\ s^{-1})$ similar to its decay in homogeneous solutions, suggests it is spontaneous decay of the triplet state, i.e.,

$$^{*}ZnTMPyP^{4+} \rightarrow ZnTMPyP^{4+} \tag{31}$$

The multiplicity of deactivation mechanisms in DHP-bound Zn(II) porphyrin is attributable to the immobilization of the sensitizer on the vesicle surface. The mobility of the excited triplet ion on the vesicle surface has been estimated[83] based on its diffusion kinetics on micellar surfaces.[113,114] Assuming a surface viscosity, η = 15 cp,[113] and molecule radius, γ = 10 Å, the diffusion coefficient, D, is calculated to be 5×10^{-7} cm^2 sec^{-1} using the following equation:[115]

$$D = RT/2\pi\eta\gamma N \tag{32}$$

where R = 8.3×10^7 erg-deg^{-1} mole^{-1}, T = 293 K, and N = 6×10^{23} mole^{-1}. Based on its normal triplet lifetime, t = 2×10^{-4}, a mean square displacement for Zn(II) porphyrin during its triplet lifetime, $(\overline{\Delta x^2})^{1/2}$ = 1.1×10^3 Å, is calculated using

$$(\overline{\Delta x^2})^{1/2} = (2Dt)^{1/2} \tag{33}$$

This displacement is far greater than the average separation of Zn(II) porphyrin under the reported experimental conditions (Table 22). If the porphyrin molecules are randomly distributed on the vesicle surface, and their surface diffusion rates are normal, multiple collisions should occur within its triplet lifetime, yet a substantial fraction of the triplet ion is observed to decay by simple first-order kinetics and the measured rate constant (k_3) is nearly independent of the surface concentration of Zn(II) porphyrin, indicating that collisional quenching cannot be encounter-controlled. This suggests either surface diffusion

of the ZnTMPyP^{4+} is anomalously slow or the metalloporphyrin forms

aggregates on the vesicle surface. The existence of optically

undetectable aggregates has been proposed by Cellarius and Mauzerall to

explain fluorescence quenching in pheophytin bound to polystyrene

particles.[116] The presence of similar types of aggregates that have an

identical absorption spectrum to the monomer could account for the rapid

deactivation pathway (k_1) observed in vesicle-bound porphyrin ions.

Photoionization of Zn(II) porphyrins in homogeneous solution has

been studied.[117] Employing transient conductimetry, Ballard and

Mauzerall have observed π-ion pair formation from photoexcited

Zn(II)octaethylporphyrin (ZnOEP) (Eq. 30). Based on the electrochemical

potentials of ZnOEP and its photoexcitation energies obtained from

emission spectra, they estimated the ZnOEP triplet state as 460 mv below

the ion pair, while the singlet state is almost isoenergetic (90 mv).

These values suggest the singlet state is more likely to produce the ion

pair. However, the authors argued that correlation of electrochemical

redox potentials to spectroscopic energies is poor because entropy

effects are ignored, and furthermore, general application of pseudo-

thermodynamic treatments to irreversible processes such as tunneling,

relaxation, and multistep encounter-controlled reactions is inappropri-

ate. Therefore, porphyrin excited state reactivities cannot be properly

assessed using redox potentials. A similar situation exists in the

ionogenesis pathway of DHP-bound photoexcited ZnTMPyP^{4+} deactivation.

The formation of the ion pair from two ZnTMPyP^{4+} ground state molecules

requires 2.03 eV[110] while the excited singlet and triplet states lie 2.0

and 1.6 eV above the ground state, respectively.[83,110] Again, these

values seem to favor electron transfer from the singlet state, but as

discussed above, conclusions drawn from energetic considerations could be incorrect. This problem can only be resolved by direct examination of the porphyrin singlet state lifetimes and kinetic behavior.

4.6 Photoreduction of Viologen Dications in Vesicle Assemblies

4.6.1. General Observations

One of the key elements of light-driven charge separation in organized media is the production of relatively long-lived high energy intermediates capable of useful chemical work. Viologens in the reduced free radical form have suitable reduction potentials (MV^{2+}/MV^+ = -0.46 v, pH 7.4) to meet the thermodynamic requirement for reduction of water to molecular hydrogen in neutral or acidic media, i.e., $H^+ + e^- \rightarrow 1/2$ H_2, E^o = -0.41 v, pH 7. For this reason, methyl viologen and its amphiphilic derivatives have been employed extensively as charge relays in photolytic redox processes.

Oxidative quenching of photoexcited sensitizers by viologens in homogeneous solutions and microphase systems has been investigated.[22,82,83,91,106,118,119] In particular, triplet-excited $ZnTMPyP^{4+}$ ion has been shown to undergo one-electron oxidation by MV^{2+}, with k_Q = 1.8×10^7 M^{-1} s^{-1} at 23°C in phthalate buffer, pH 5.0, μ = 0.05 M (NaCl).[83] A similar quenching rate was obtained (k_Q = 5.3×10^7 M^{-1} s^{-1} by $C_{14}MV^{2+}$ in 0.05 M TEOA, pH 7.8 at 23°C.[91] In homogeneous solutions, photoreduced viologen formation is generally detectable by the appearance of an absorbing species below 700 nm in the optical spectrum which forms at a rate identical to the deactivation of the excited sensitizer.

4.6.2 Quenching of photoexcited $ZnTMPyP^{4+}$ ions in DHP vesicles

The redox quenching behavior of photoexcited Zn(II) porphyrins is drastically altered in the presence of anionic DHP vesicles.[91] The

various photochemical intermediates formed by photoexcitation of
DHP-bound ZnTMPyP^{4+} (Section 4.5) exhibit vastly different quenching
behavior by bound viologen. Deactivation rates corresponding to the
intermediate and slow pathways were found to increase upon addition of
$C_{14}MV^{2+}$ to DHP vesicle solutions, while the rate of the fast decaying
component was unaffected. Bimolecular quenching was observed for the
intermediate component, with $k_Q = 1.7 \times 10^9$ M^{-1} s^{-1}, obtained from the
Stern-Volmer plot (Figure 56a). Reaction of the slowly-decaying
component, however, appears to be more complex. Saturation was observed
in the Stern-Volmer plot (Figure 56b) which has a limiting first order
rate constant of about 10^3 s^{-1}, suggesting that the quenching might be
controlled by diffusional processes on the vesicle surface. This is
consistent with the notion that reactions in micelles and vesicles are
often limited by the free diffusion of the reacting species along the
surface.

The intermediate pathway in DHP-bound ZnTMPyP^{4+} deactivation has
been ascribed to ionogenesis (Section 4.5). The quenching reaction can
therefore be described as donation of an electron from the ZnTMPyP^{3+}
π-anion to the acceptor molecule, $C_{14}MV^{2+}$, i.e.,

$$ZnTMPyP^{3+} + C_{14}MV^{2+} \rightarrow ZnTMPyP^{4+} + C_{14}MV^+ \tag{34}$$
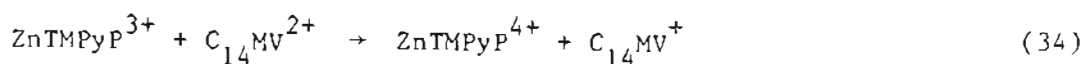
The rate constant measured ($k_1 = 1.7 \times 10^9$ M^{-1} s^{-1}) is several orders of
magnitude larger than the estimated upper limit (10^6 M^{-1} s^{-1}) for
diffusive reaction rates on vesicle surfaces[91] suggesting that the
quenching reaction is not surface-encounter controlled. This implies
that at least one of the reactants is no longer vesicle bound. Since

the alkylviologen is strongly bound by all criteria, formation of the
π-anion must be followed by its release from the vesicle surface. This
claim is supported by the similar fast quenching rates observed in other
vesicle systems where the sensitizer does not adhere to the vesicle
surface. Oxidative quenching data of unbound $ZnTPPS^{4-}$ excited triplet
ions by DHP-bound viologens are given in Table 23. Both quenching
constants, 2.5×10^9 M^{-1} s^{-1} for MV^{2+}, and 2.4×10^8 M^{-1} s^{-1} for
$C_{14}MV^{2+}$, are comparable to the π-anion quenching by $C_{14}MV^{2+}$, but are in
direct contrast with the slow quenching of the bound $ZnTMPyP^{4+}$ triplet
ion by bound $C_{14}MV^{2+}$. These results strongly suggest that formation of
charge-separated species will be effective only if one member of the
redox pair is excluded from the surface.

Reduced viologen radical cation is not detected in the transient
spectra of the oxidatively quenched Zn(II) porphyrin (Figure 57) as
indicated by the absence of appreciable growth at 610 nm, suggesting
that it is rapidly consumed. One plausible explanation is its
reoxidization by the π-cation, i.e.,

$$ZnTMPyP^{5+} + C_{14}MV^+ \rightarrow ZnTMPyP^{4+} + C_{14}MV^{2+} \qquad (35)$$
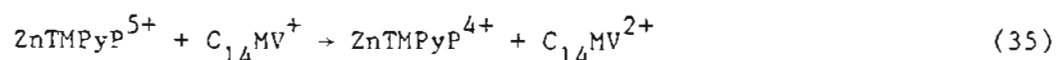
Since both reactants are probably vesicle-bound, their recombination is
also expected to be surface-encounter controlled, $k \leq 10^6$ M^{-1} s^{-1}.
However, the lack of detectable $C_{14}MV^+$ formation following laser pulse
suggests it is a very efficient reaction. It has been suggested that
the apparent unusual fast reaction is due to its high exothermicity[91];
ΔE° for Eq. 35 is estimated to be 1.64 eV.[110] More detailed information
on the effective charges and dielectric strength of the vesicle

interface is required to understand the kinetic nature of this recombination reaction.

Mobilities of the ionogenic and redox products along the vesicle surface must be important in determining their fate. The porphyrin π-anion, with its added electron residing primarily on the porphyrin periphery, should increase the negative character of the ring where it will encounter charge repulsion by the anionic vesicle head groups, thus promoting its expulsion from the surface. Similarly, the reduced viologen should also have a greater surface diffusion rate than its oxidized form. Presumably, electrostatic forces are considerably less, although the hydrophobic character of amphiphilic viologen binding should not be affected. On the contrary, the porphyrin π-cation should exhibit stronger binding since porphyrin binding is primarily electrostatic in nature.

It can be seen that combining reactions (34) and (35) results in very effective charge recombination of the porphyrin π-ion pair using viologen as the relay. Thus the only viable pathway to photogenerate net viologen free radical in vesicles containing both bound sensitizer and acceptor is by slow quenching of the bound porphyrin triplet ion, i.e.,

$$^{*}ZnTMPyP^{4+} + C_{14}MV^{2+} \rightarrow ZnTMPyP^{5+} + C_{14}MV^{+} \tag{36}$$
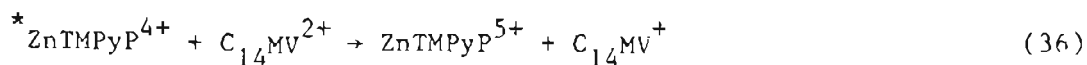
This reaction, however, is relatively slow compared to the rapid cyclic back reactions (34 and 35); therefore the net yield of reduced viologen should be low. Consistent with this expectation, inefficient formation of redox products by oxidative quenching was observed in steady-state

photolysis experiments when both sensitizer and acceptor molecules were adsorbed to the vesicle.[91] In homogeneous buffer solutions, production of radical was fast and efficient for $ZnTMPyP^{4+}$ photosensitized reduction of both MV^{2+} and $C_{14}MV^{2+}$, but in the presence of DHP vesicles, both the rate and extent of radical production were reduced (Figure 58). Net photoproduction of viologen radical was possible in these experiments because a sacrificial donor was included to cycle the sensitizer.

4.6.3 Quenching of photoexcited $ZnTMPyP^{4+}$ ions in PC vesicles

Oxidative quenching of photoexcited $ZnTMPyP^{4+}$ ions by $C_{16}MV^{2+}$ ions adsorbed onto PC vesicles has been investigated by laser flash photolysis. Viologen radical formation was shown to occur concomitantly with Zn(II) porphyrin triplet deactivation, followed by slow recombination with $ZnTMPyP^{5+}$ π-cation in the absence of donor (Figure 40). Kinetic complexity was indicated from the rate data; triplet decay caused by viologen quenching did not follow strictly first-order kinetics, and deviation from strictly second-order kinetics was observed in the back electron reaction. Furthermore, triplet deactivation also increased with surface concentration of viologen. The origin of this rate behavior is not known. Non-linear behavior in oxidative quenching of $ZnTMPyP^{4+}$ in homogeneous solutions has previously been observed and was attributed to instability of the $ZnTMPyP^{5+}$ ion.[120] Non-exponential decay in oxidative quenching of PC vesicle-bound chlorophyll was also observed and has been suggested to be caused by diffusive effects arising from the high apparent viscosity of the vesicle.[121] These rationalizations, however, do not appear to be pertinent to the present study since deactivation of the $ZnTMPyP^{4+}$ triplet state in PC vesicle suspensions and oxidative quenching of $ZnTPPS^{4-}$ triplet ions by

DHP-bound $C_{14}MV^{2+}$ (discussed later) appear well behaved, and the Zn(II) porphyrins are not vesicle-bound. Alternatively, the kinetic anomalies observed in this Zn(II) porphyrin-viologen-PC vesicle system could be due to heterogeneous binding of viologen. Light scattering measurements reveal that PC vesicles are less homogeneous than DHP vesicles (Figure 3), suggesting that the curvature might be a consequence of different reactivities of viologens located in different microenvironments.

The experimentally obtained bimolecular quenching constant for $ZnTMPyP^{4+}$ by PC-bound $C_{16}MV^{2+}$, $k_Q = 1.2 \times 10^6$ M^{-1} s^{-1}, is similar to that reported for MV^{2+} (2×10^6 M^{-1} s^{-1}),[83] and about ten-fold smaller than $C_{14}MV^{2+}$ (1.8×10^7 M^{-1} s^{-1})[35] in buffer solutions. This result is consistent with the notion that quenching of an unbound photoexcited sensitizer in vesicle systems is similar to that in homogeneous solution. The slightly smaller observed quenching rate might be due to slower diffusion of PC vesicles in solution because of their larger size, which would give rise to a lower encounter-controlled frequency. Calculations of the encounter-controlled rate constant based on the Debye equation,[122]

$$k_D = \left(\frac{\delta}{\frac{\delta}{e-1}} \right) \frac{4\pi N^\circ a (D_A + D_B)}{10^3} \tag{37}$$

however, indicate that the quenching reaction is probably not encounter-controlled.

In the above equation, D_A and D_B are diffusion coefficients of the reactant ions, a is the internuclear distance, N° is the Avogadro number

and $\delta/(e^{\delta} - 1)$ is an interionic factor; δ is obtained based on the charges Z_A and Z_B of the ions,

$$\delta = \frac{Z_A Z_B e^2}{a \varepsilon k T} \tag{38}$$

where ε is the medium dielectric constant (78 for water), e is the unit charge (4.8×10^{-10} esu), k is the Boltzmann constant (1.38×10^{-16} erg° K^{-1}), and T is the Kelvin temperature.

Using a diffusion coefficient, $D = 2 \times 10^{-6}$ cm^2 s^{-1}, for ZnTMPyP^{4+} and $C_{16}MV^{2+}$, an interionic factor of 0.085 based on the positive charges of the ions, an internuclear distance of 15 Å, and at 298 K, the encounter-controlled rate constant calculated is 3.8×10^8 M^{-1} s^{-1}. Similarly, assuming the same internuclear distance between ZnTMPyP^{4+} and vesicle-bound $C_{16}MV^{2+}$, k = 2.8×10^7 M^{-1} s^{-1}, is calculated for PC-bound viologen using the same parameters except that the diffusion coefficient for $C_{16}MV^{2+}$ is replaced by $D_{PC} = 1.87 \times 10^{-7}$ cm^2 s^{-1}.[33] These rate constants are about an order of magnitude greater than the experimental values which suggest that orientation effects might exist. This is also consistent with the observation that the quenching rate constant increases with surface viologen concentration (Table 12). Although this is a small dependence, nonetheless it suggests that quenching not only depends on the favorable collision between excited porphyrin and vesicle, but also the localized concentration of MV^{2+} bound to the outer vesicle surface. The rate constant for back electron transfer between the PC-bound viologen radical and ZnTMPyP^{5+} π-cation ($1.5 \times 10^8 - 1.5 \times 10^9$ M^{-1} s^{-1}) is only slightly slower than that observed in homogeneous solution (10^9–10^{11} M^{-1} s^{-1}). Since the viologen radical cation is

bound, this suggests that the PC-vesicle surface does not appreciably inhibit approach of the $ZnTMPyP^{5+}$ π-cations. Lifetime enhancements of charge-separated ions have been observed in ionic micelles in which the reduced violgen is rapidly solubilized in the surfactant assembly while the sensitizer cation is expelled from the charged interface.[20,35] The recombination rates are retarded by several orders of magnitude ($k \leq 10^7$ M^{-1} s^{-1}). In the present vesicle system, however, repulsion of the porphyrin π-cation from the vesicle surface should be small because the vesicle surface is only slightly positively charged due to the adsorption of $C_{16}MV^{2+}$ ions, and less cationic when the viologen is reduced. Recombination of the geminate redox pair, $C_{16}MV^+$ and $ZnTMPyP5^+$, therefore, should be relatively rapid.

Qualitatively, results from continuous illumination studies of $C_{16}MV^{2+}$ substantiate the claim that photoreduction of viologen will be less efficient in the presence of PC vesicles. Initial rates of net viologen radical formation obtained in the presence of externally added donor EDTA in PC vesicles (R_i = 0.29-0.90 x 10^{-6} M s^{-1}) are about an order of magnitude slower than that obtained in buffer solutions only under otherwise identical conditions (R_i = 8 x 10^{-6} M s^{-1}). Although the physical parameters were not completely assessed in these experiments, i.e., there were no systematic studies of the viologen concentration and viologen/PC dependence on the rate of net viologen radical formation, the apparent scatter seen in the rate data in different preparations (Table 11) suggests substantial heterogeneity in the system. Furthermore, the oxidative quenching and back electron transfer constants obtained are very similar to those in homogeneous solution, suggesting that the primary cause of lower net yield of

viologen radical in PC vesicles is proably due to the relatively inefficient reduction of ZnTMPyP^{5+} by the sacrificial donor (Section 4.7, eq. 43). This implies that EDTA is excluded from the vesicle surface where back reaction competes with net reduction of the viologen.

4.6.4 Quenching of photoexcited ZnTPPS^{4-} ions in DHP vesicles

Oxidative quenching of the tetraanionic Zn(II) porphyrin triplet ions, ^{3}ZnTPPS^{4-}, by DHP vesicle-bound viologens is kinetically well-behaved. Transitory viologen radical cation formation is clearly visible at 600 nm concurrent with triplet decay at 890 nm (Figure 59) in the absence of electron donors. Stern-Volmer rate laws are observed for both MV^{2+} and C$_{14}$MV^{2+} (Table 23). The back electron transfer reaction also appears to proceed by a second-order pathway.[91] These reactions are remarkable because photoinitiated electron transfer products for this reaction are not generally observed in homogeneous solution[82,119] where ion association between porphyrin and viologen gives rise to static quenching of the photoexcited porphyrin. At sufficiently high concentration levels (1 mM), methyl viologen dications have been shown to form ion pairs with ZnTPPS^{4-} and PdTPPS^{4-} porphyrin ion in sodium chloride solution, as detected by bathochromic shifts in the optical absorption spectra of the chromophores.[119] Photoexcitation of the sensitizer leads to efficient electron displacement from the porphyrin periphery to the viologen. However, the inability of the redox pair to separate during their lifetimes results in rapid recombination of the transfer products. Also, in very dilute viologen solutions in which association with ground state porphyrin is negligible (< 7%), transient species are not detectable by flash photolysis following oxidative quenching.[119] This observation is attributed to the formation of an

encounter complex during the quenching process. Thus, regardless of the origin of complexation, very rapid back transfer competes with separation of the ions, preventing escape of photoreduced viologen into the bulk solution.

In contrast, the DHP vesicle, by preferentially binding the viologen while excluding the $ZnTPPS^{4-}$ ion from its anionic surface, prevents ion complexation and thereby enables the separation of the electron transfer products. The measured quenching rates of $ZnTPPS^{4-}$ triplet by MV^{2+} and $C_{14}MV^{2+}$ (Table 23) indicate that the quenching process is retarded by increasing the hydrophobicity of the quencher. This suggests that $C_{14}MV^{2+}$ binds to a region on the vesicle surface that is less accessible to the sensitizer. Presumably, insertion of the alkyl chain into the bilayer could orient the viologen head group more deeply within the interfacial layer; as a result, close approach by the porphyrin is hindered. Examination of the initial porphyrin triplet formation in the presence of quenchers also revealed that degree of binding to the vesicle and the sensitizer is different for MV^{2+}.[91] The amplitudinal decrease in initially formed triplet ion upon addition of viologen is a measure of the amount of triplet that is statically quenched by complexation. It was found that complexation with MV^{2+} was only 10% at the highest concentration studied (0.2 mM), whereas $C_{14}MV^{2+}$ gave 50% at the same concentration, and reached 75% up to 0.6 mM viologen. This result is somewhat intriguing since alkyl substituents were found to strengthen association with micelles.[35] In this case, increasing the hydrophobicity of the viologen not only enhances vesicle binding, but also appears to promote the complexation with $ZnTPPS^{4-}$ to a greater extent. This observation suggests that ion association between

viologen and ZnTPPS^{4-} involves hydrophobic forces in addition to electrostatic attraction.

Facile photoproduction of viologen radical sensitized by ZnTPPS^{4-} in DHP vesicles is also confirmed by steady-state photolysis. Under continuous illumination in the presence of sacrificial donors, prompt formation of viologen radical is detected spectrophotometrically. As discussed above, the lifetimes of charge-separated ions are enhanced by the negatively charged interfacial boundary provided by the vesicle. This molecular organization, hence, offers a tractable system to study photoinitiated transmembrane redox processes. By utilizing viologens that are bound to both inner and outer vesicle surfaces as charge relays, oxidative and reductive reactions can be selectively carried out in different vesicle microphase regions and evidence of electron transport across the bilayer can be sought. A system using Fe(CN)$_6^{3-}$ occluded within the internal aqueous compartment of the vesicle as an electron scavenger was investigated and will be discussed later (Section 4.8).

4.7 Photochemical Side Reactions

The principal deactivation pathway of unbound photoexcited Zn(II) porphyrins (ZnP) in vesicle systems containing viologens and electron donors is oxidative quenching, as shown by the formation of net viologen radical under continuous illumination. However significant irreversible bleaching of the sensitizer was also observed, specifically with ZnTMPyP^{4+} in PC vesicle solutions (0.05 M PO$_4^{2-}$, pH 6.5) containing bound C$_{14}$MV^{2+} and EDTA, and ZnTPPS^{4-} in DHP vesicle solutions (0.02 M Tris, pH 7.8) containing C$_{16}$MV^{2+} and tricine. The substantial loss of Soret band intensities indicates that the π-conjugated electron system of the

porphyrin is no longer intact. Photobleaching of Zn(II) porphyrins has been reported in both homogeneous and vesicle solutions.[83,91] The destruction of the chromophore during illumination in the absence of oxidative quencher but in the presence of electron donor has been attributed to extensive reduction of the porphyrin giving rise to dihydro- and tetrahydroporphyrin derivatives.[83] The photochemical pathways to form these reduction products have been ascribed to the disproportionation of the reduced porphyrin π-anion in the presence of hydrogen ions, i.e.,

$$2H^+ + ZnP^- + ZnP^- \rightarrow H_2ZnP + ZnP \qquad (39)$$

and further reduction by the donor, D,

$$2H^+ + ZnP^- + D \rightarrow H_2ZnP + D^+ \qquad (40)$$

following reductive quenching of the photoexcited porphyrin triplet by the donor, i.e.,

$$ZnP^* + D \rightarrow ZnP^- + D^+ \qquad (41)$$

Bimolecular reductive quenching of ZnTMPyP^{4+} triplet ion in solution by TEOA and EDTA has been observed, with $k_Q = 4 \times 10^3$ M^{-1} s^{-1} (TEOA = 0.05-1.0 M, pH 7.8, $\mu = 0.5((CH_3)_4NCl)$, 23°C) for TEOA,[83] and $k_Q = 1.7 \times 10^5$ M^{-1} s^{-1} at 23°C, $\mu = 0.05$ M for EDTA.[83] These rates are several orders of magnitude slower than the oxidative quenching by viologens, suggesting that in the presence of both viologen and donor the oxidative

process should be more favorable. This is confirmed by retardation of bleaching in solutions containing MV^{2+}, EDTA and $ZnTMPyP^{4+}$.[82,83] Hence, in a three-component system that contains excited sensitizer S^*, acceptor A, and donor D, the major reaction sequence is

$$S^* + A \rightarrow S^+ + A^- \tag{42}$$

$$S^+ + D \rightarrow S + D^+ \tag{43}$$

As can be seen, the role of the donor in systems in which oxidative quenching is efficient is to regenerate the ground state sensitizer.

The observed bleaching of $ZnTMPyP^{4+}$ and $ZnTPPS^{4-}$ in vesicle solutions containing viologens and donors suggest that the protective action of viologen must be less than that in homogeneous solution. Reductive quenching of the $ZnTMPyP^{4+}$ triplet in PC vesicles is confirmed by the four-fold increase in the decay rate in the presence of 1 mM EDTA (Figure 39). This rate increase is higher than previously reported values under other conditions, and can account for the enhanced bleaching of $ZnTMPyP^{4+}$ in the illumination experiments. Presumably this enhancement of bleaching is due to the higher rate of porphyrin π-anion production in the presence of EDTA.

4.8 Photoinitiated Transmembrane Electron Transfer

A common feature found in several reports of photoinduced oxidation-reduction across vesicle bilayers is that the photosensitizer is vesicle-bound.[22,68,106] Net redox between donor and acceptor molecules that are adsorbed onto opposite vesicle surfaces that follows photoexcitation in systems lacking lipid-soluble mobile redox carriers has been interpreted as the consequence of electron tunneling across the

hydrocarbon barrier. However, since photostimulated diffusion of viologen dications across the bilayer is shown to be caused by the presence of bound zinc porphyrin (Section 4.4), similar photophysical processes leading to mixing of initially compartmentalized reactants could not be excluded in these studies. Hence, by using the nonbinding Zn(II) porphyrin, $ZnTPPS^{4-}$ in the sensitized reduction of DHP-bound viologen, this ambiguity is removed.

Initial rates of $C_{16}MV^{+}$ radical formation in DHP vesicle suspensions containing internalized $Fe(CN)_6^{3-}$, unbound $ZnTPPS^{4-}$, and the electron donor tricine in the external medium show substantial decrease compared to systems containing no $Fe(CN)_6^{3-}$ (Table 10), and the viologen radical appearance was also preceded by a pronounced induction period (10-20 minutes). Ferricyanide oxidation of reduced methyl viologen in homogeneous solution has been observed to be encounter-controlled ($k = 7.6 \times 10^9 \ M^{-1} \ s^{-1}$)[123]; therefore the rate decrease may be attributable to $Fe(CN)_6^{3-}$ reoxidation of $C_{16}MV^{+}$ initially formed by oxidative quenching of photoexcited $ZnTPPS^{4-}$. Since transmembrane diffusion of $Fe(CN)_6^{3-}$ has been demonstrated to be absent over the time course of illumination by the membrane ultrafiltration method, i.e., iron was not detected in the external solution medium, the reaction between $Fe(CN)_6^{3-}$ and reduced viologen must have occurred on the inner vesicle surface. This claim gains support from the magnitude of observed induction preceding net violgen radical formation.

Assuming that the absence of detectable violgen radical in this time span is due to the rapid scavenging action of $Fe(CN)_6^{3-}$, the amount of $Fe(CN)_6^{3-}$ incorporated should correspond to the total reduced violgen concentration formed on the inner surface that is not optically

detected. Estimates of viologen radical that would be formed if $Fe(CN)_6^{3-}$ were absent can be made from the maximal rate measured immediately following the induction period or from initial rates for vesicle systems lacking internal $Fe(CN)_6^{3-}$. Since the latter rate is greater than the former, calculations based upon the two measurements approximate the upper and lower limits for viologen radical cation formation during the induction period. Calculated scavenged $C_{16}MV^+$ concentration levels and their corresponding $Fe(CN)_6^{3-}$ concentration levels measured either spectrophotometrically or by atomic absorption spectroscopy are given in Table 9. The values are in good agreement. Since viologen radical does not accumulate during the induction period, $Fe(CN)_6^{3-}$ reduction is not rate-limiting. When solutions contained comparable concentration levels of $Fe(CN)_6^{3-}$ in the external bulk solution, radical formation was greatly suppressed and followed an extensive induction period (~60 min). This observation is consistent with $Fe(CN)_6^{3-}$ oxidation of reduced viologen and/or direct competitive quenching of the $ZnTPPS^{4-}$ triplet ion. The quenching pathways of photoexcited $ZnTPPS^{4-}$ ions of both viologen and $Fe(CN)_6^{3-}$ in homogeneous solution were not examined in the present study.

The above rate behavior suggests net transmembrane redox involving the bound viologens. The overall photoredox process and the spatial organization of various reactants are illustrated in Scheme V. Photo-excitation of the unbound $ZnTPPS^{4-}$ in the external solution medium generates the porphyrin triplet ion which is rapidly quenched by $C_{16}MV^{2+}$ bound to the outer surface ($k_Q = 10^8-10^9$ M^{-1} s^{-1}). Subsequent slow diffusion of $C_{16}MV^+$ from the outer to inner surface or transmembrane electron exchange between external $C_{16}MV^+$ and internal $C_{16}MV^{2+}$ occurs, followed by rapid reoxidation by $Fe(CN)_6^{3-}$ entrapped within the internal

Scheme V
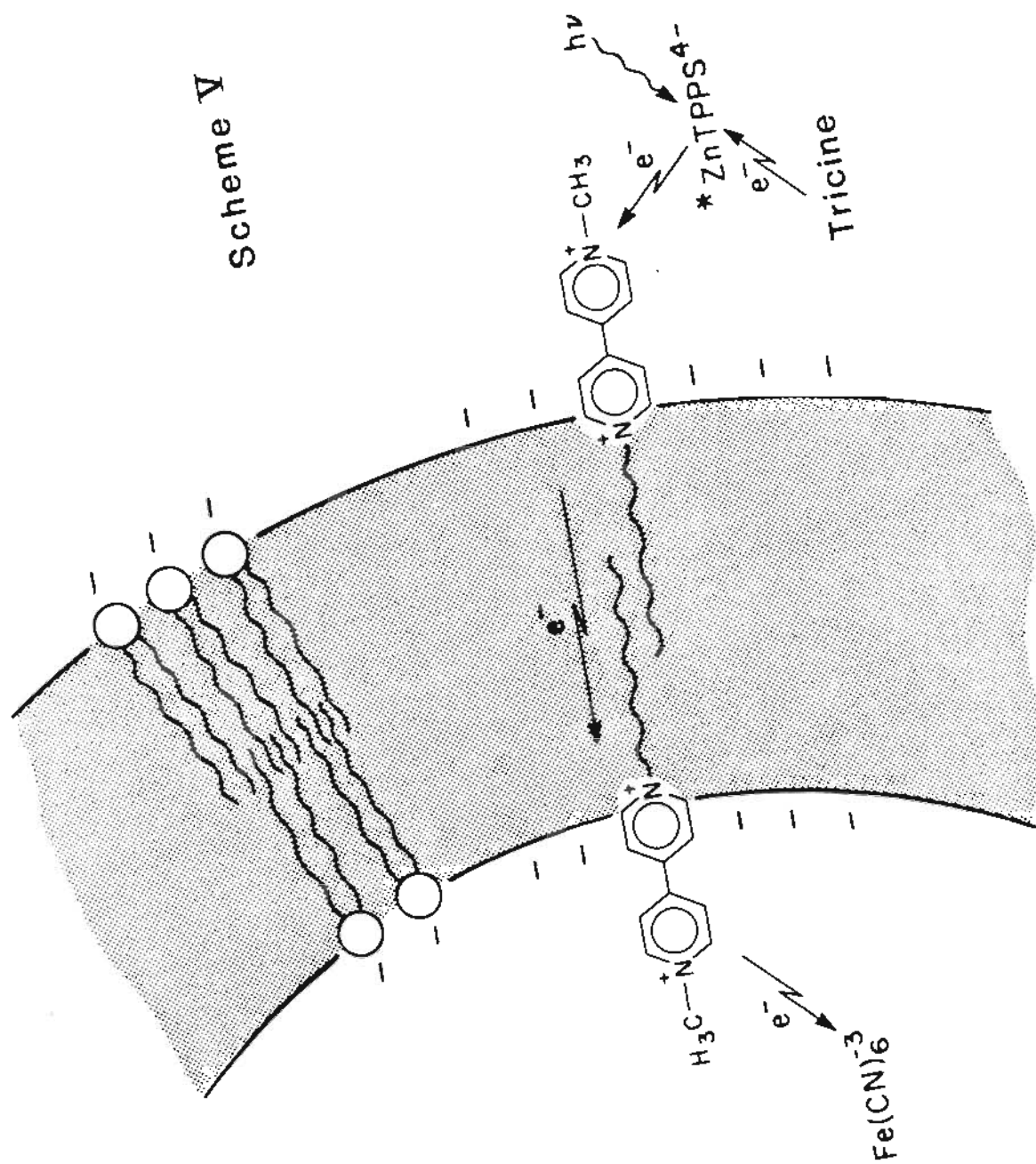
aqueous phase. The addition of tricine in the external medium replenishes the electron to the porphyrin π-cation, completing the redox cycle.

The requirement of symmetrically bound viologens as charge relays to reduce internal $Fe(CN)_6^{3-}$ is demonstrated by carrying out the photoreaction in asymmetrically organized vesicles. Illumination of $Fe(CN)_6^{3-}$-incorporated DHP vesicles with $C_{16}MV^{2+}$ bound only to the external surface gave immediate formation of viologen radical, i.e., no induction, with a 5-fold rate enhancement over the photosensitized reaction in absence of $Fe(CN)_6^{3-}$ (Table 10). If transmembrane diffusion of the viologen species occurred, the rate of net radical formation would have been retarded due to internal ferricyanide reduction. However, the contrary was observed. Although the origin of the rate enhancement is uncertain, it is clear that illumination does not cause transmembrane viologen radical diffusion that would lead to reaction with $Fe(CN)_6^{3-}$ on the inner surface. Therefore, transmembrane redox occurs only when viologens are bound to both surfaces.

The rate parameters determined from temperature-dependent illumination studies of $C_{16}MV^{2+}$ reduction in various vesicle configurations (Table 10) also lend support to the claim that the photoinitiated redox process is not diffusional in nature. Based on diffusion studies of ions in bilayer membranes[37-39] and photoinduced viologen diffusion in DHP vesicles (Section 4.4), transmembrane diffusion enthalpies are expected to be high (15-30 kcal/mole). However, the relatively small activation enthalpy values obtained and their insensitivity to the molecular structure of the reactants indicate that transmembrane diffusion is probably insignificant.

4.9 Reduction of $(NH_3)_5Ru$-4-$(11'$-dodecenyl$)py^{3+}$ ion in phosphatidylcholine vesicle solution

Biphasic kinetics are observed when reductants are added to PC vesicles containing $(NH_3)_5Ru$-4-$(11'$-dodecenyl$)py^{3+}$ ions bound to both surfaces (Figures 44-47). Rapid bimolecular reaction of the shorter $(NH_3)_5Ru$-4-alkenylpy^{3+} analogs by cuprous ion has been observed in homogeneous solution with reported rate constants, $3-9 \times 10^3$ s^{-1}.[63] The fast component of the reduction step thus can be ascribed to the reduction of the Ru^{3+} complex bound to the outer vesicle surface. Reduction potentials for $(NH_3)_5Ru$-4-$(11'$-dodecenyl$)py^{3+}$ and various reducing reagents are listed in Table 24. As can be seen, the net driving force for Ru(III) reduction is sufficiently large to ensure complete Ru(II) formation in homogeneous solution for all the reductants used. The slow continued amplitudinal rise in the presence of excess external reductant comprises about 25-40% of the total optical change and is indicative of the net reduction of the ruthenium complexes bound to the inner vesicle surface. This claim is supported by a comparison of the inner surface area to the total surface area of the vesicle. Assuming the vesicle is spherical, the fraction of the inner surface area to the total surface area can be calculated with known radius and bilayer width. The surface area of a sphere is given by $S = 4r^2$, where r is the radius. The fraction of inner surface area to the total surface area of a spherical vesicle hence is:

$$S_i/S_i + S_o = r_i^2/(r_i^2 + r_o^2) \qquad (44)$$

where r_i and r_o are the inner and outer radius, respectively. The inner surface area of a vesicle having an outer radius of 145 Å and bilayer width of 45 Å comprises about 32% of the total area. Thus vesicle radii

of 135-150 Å and bilayer widths of 40-50 Å give the best agreement with the kinetics data. These values are also consistent with the results obtained from electron microscopy.

Kinetic analysis shows that, within a relatively large experimental error, the slow component of the biphasic kinetics is a first-order process and, except for Cu^+ ion, appears to be independent of both the concentration and identity of reductants used. This indicates that involvement of the external reductant in the slow-phase kinetics must be inconsequential. Diffusion of multivalent ions across neutral vesicle bilayers is slow. Presumably, the hydrophobic interior constitutes a high energy barrier that disfavors ion penetration. Furthermore, since the phospholipid vesicle membrane is doped with positively charged ruthenium ions, its permeability to the reductant ion should depend on the charge of the ion. Both Cr^{2+} and V^{2+} are small divalent cations and therefore should not penetrate through the cationic vesicle interface; hence, diffusion to the inner surface is highly unlikely. Conversely, ascorbic acid in pH 4.0 solution exists partially as a mononegative ion ($pK_a = 4.17$) and thereby should exhibit a greater diffusion rate. However, first-order rate constants of the slow reaction measured for these reductants are almost identical, suggesting that their diffusion to the inner surface is not rate determining.

The anomalously faster rate of slow-phase reduction by Cu^+ ion can possibly be attributed to its capacity to bind olefins. Cuprous ion has been shown to complex with the terminal double bond of $(NH_3)_5Ru$-4-alkenylpy ions.[63] Since the hydrocarbon bilayer of PC vesicles also contains unsaturation, complexation by Cu^+ ion might also occur. As a result, the accessibility of Cu^+ ion to the ruthenium ions on the inner

surface might be enhanced through both its binding to olefin bonds in the vesicle interior and binuclear ion formation with the ruthenium complex on the surfaces.

Complex bleaching of PC-bound reduced $(NH_3)_5Ru-4-(11'-$ dodecenyl)py^{2+} complex is observed when the external reductant concentration becomes limiting. Results obtained from bleaching experiments of Ru(II) ions in homogeneous solutions for various reductants show that the disappearance of the Ru(II) chromophore deviated markedly from first-order kinetics for the reductants with rate constants in the range of 10^{-4} to 10^{-5} s^{-1}, but increased linearly with perchlorate ion concentration. These results are attributable to perchlorate oxidation of Ru(II) ions. In PC vesicle solutions, however, the stability of reduced Ru(II) complex appears to be enhanced both toward bleaching and hydrolytic processes.

The absence of transmembrane diffusion of PC-bound $(NH_3)_5Ru-4-(11'-$ dodecenyl)py$^{3+/2+}$ ion is demonstrated in the studies of time-dependent redox behavior of externally-bound ruthenium complexes (Section 3.7.3). The method involves incubation of PC vesicles initially containing only ruthenium ions bound to the external surface, then followed by cyclic redox reactions with external reagents. Implicit in this method is the assumption that the fast and slow reduction measure the ion on the external and internal surfaces, respectively. The absence of measurable slow-phase reduction of externally-bound Ru(III)-vesicle suspensions that were incubated for several hours at 25°C by either Cr^{2+} or ascorbate ion indicates that Ru(III) did not diffuse appreciably to the inner surface during the incubation period. If transmembrane Ru(III) diffusion were significant in this time span, the slow-phase reduction

should have been detected with an amplitudinal increase corresponding to the amount of diffused ions. Similarly, externally-bound Ru(II)-vesicle solution formed by Cr^{2+} reduction was incubated for 1 hour, then oxidized with $Fe(CN)^{3-}$, and reduced again with Cr^{2+} ion. No biphasic kinetics in the reduction was observed and greater than 90% of the original Ru(II) complex absorbance was recovered in the oxidation-reduction cycle. Again, if diffusion of the reduced complex were significant, the amount of Ru(II) recovered in the final reduction step would be substantially less than the original concentration, with the corresponding growth of the slow-phase reduction component reflecting the formation of internalized Ru(II). Therefore, these results indicate that the slow component in reduction of ruthenium complexes by external reductant cannot be due to transmembrane diffusion of either the oxidized or reduced ruthenium species.

The most straightforward interpretation of the overall kinetic behavior observed in the reduction of $(NH_3)_5Ru-4-(11'-dodecenyl)py^{3+}$ in PC vesicles is that fast reduction of Ru(III) complex ion occurs on the outer vesicle surface followed by slow transmembrane electron exchange between Ru(II) and Ru(III) ions bound to the opposite surfaces. A plausible reaction sequence of this redox process is depicted in Scheme IV. The assumptions embodied in the kinetic scheme (Section 3.7.4) are substantiated by the lack of observable transmembrane diffusion of ruthenium species and external reductant. The quasi-equilibrium condition attained following slow reduction is also verified by the observed plateau in the optical absorption at 415 nm, which indicates the total concentration level of reduced ruthenium complex ion, both externally and internally bound, is maintained constant by the external reductant.

The apparent first-order rate constant obtained for the slow reduction, k_o, is the sum of k_2' and k_3, the pseudo first-order transmembrane electron transfer and bleaching rate constant, respectively. Results from bleaching studies indicate that contribution of k_3 could be as much as 10% of the overall observed rate; therefore, k_o ($5-9 \times 10^{-4}$ s^{-1}) sets an upper limit for the transmembrane transfer rate.

Electron transfer reactions between two ions in homogeneous solution in general exhibit second-order kinetics, i.e., first-order in each reactant. Assuming independent binding sites (Langmuir binding) for the amphiphilic ruthenium complex ions on PC vesicle surfaces, transmembrane electron transfer should also be a second-order process. The rate constant for the slow reduction step should increase with increasing surface ruthenium concentration. However, within experimental error, measured transmembrane rate constants did not vary appreciably when ruthenium/PC ratios were increased five-fold (Table 20) and the relative amplitudes of both fast and slow reduction also were not affected. These results suggest that the slow reaction on the vesicle surface is a first-order process. Bimolecular reactions in geometrically restricted systems such as micelles have been studied and pseudo-first-order behaviors were observed.[74,113,114] Based on theories of reaction-diffusion kinetics, models to account for the reduction of reaction order have been developed.[113,124] In particular, micellar surface diffusion kinetics has been shown to explain both enhancement of reaction rates and reduction of dimensionality of dismutation reactions of Br_2^- ion radicals in aqueous cetyltrimethylammonium bromide (CTAB) micelles.[113] Similarly, in the present vesicle system, if lateral diffusion of bound ruthenium ions within the membrane plane and exchange

of bound ions among the vesicles were slow relative to transmembrane electron transfer, the reaction would be intramolecular and gives rise to first-order kinetics. Alternatively, other mechanisms could also give rise to first-order behavior. The binding site of ruthenium ions might not be totally independent, i.e., ions bound to opposite surfaces might preferentially align in a configuration that minimizes the charge repulsion on the surface imposed by the bound ions. Without a detailed knowledge of the ruthenium ion microscopic binding properties and its diffusion kinetics on the vesicle surface, it is difficult to assess the reaction order of the slow redox step.

4.10 Energetics of transmembrane electron transfer

Thermodynamically, the overall reduction of $(NH_3)_5Ru-4-(11'-$ dodecenyl)py^{3+} ions bound to opposite surfaces in PC vesicles by external reductant can be separated into two distinct steps (Scheme IV), the initial rapid reduction of external Ru(III) (k_1 pathway) and the subsequent slow transmembrane reduction of internal Ru(III) (k_2 pathway). Reduction of the external Ru(III) ions generates a transient potential gradient across the vesicle bilayer as a consequence of the decreased positive charge density on the outer vesicle membrane. However, electroneutrality is still maintained because there is no net charge translocation across the bilayer. Addition of external reductant causes only electron exchange between the externally bound ruthenium and the reductant ion. The free energy change associated with the added negative charges on the external surface is analogous to the electrostatic energy required to charge up a spherical surface from the external bulk medium; hence, it contributes to the net free energy change of external reduction:

$$\Delta E = \Delta E^{\circ} - RT/F \ \ln \ \left(\frac{[Ru_o^{2+}][ox.]}{[Ru_o^{3+}][red.]} \right) - E_{charge} \tag{45}$$

where $\Delta E^{\circ} = E_{1/2} \ (Ru^{3+/2+}) - E_{1/2} \ (ox./red.)$

and $E_{charge} = Q^2/C$ (46)

In equation 46, Q is the total charges deposited on the extenral vesicle surface per mole of external ruthenium reduced and C is the capacitance of the outer vesicle surface. Under the experimental conditions, E_{charge} is calculated to be 0.1 v (Appendix III). Except for Cu^+ ion, the ΔE° calculated is much greater than zero for all reductants used (Table 24). Since the external reductant is in excess, external reduction of the ruthenium complex is essentially complete; i.e., at equilibrium, 97% of the external ruthenium is reduced for cuprous reduction. Values of $\Delta E^{\circ} - E_{charge}$ ranges from 0.049 to 0.612 v depending on the reductant (Table 24).

The slow reduction of vesicle-bound Ru(III) ions following the initial fast reaction can be viewed as rate-determining transmembrane electron exchange between external Ru(II) and internal Ru(III), followed by rapid reduction of external Ru(III) by the reductant, i.e.,

$$Ru_i^{3+} + Ru_o^{2+} \rightarrow Ru_i^{2+} + Ru_o^{3+} \tag{47}$$

$$Ru_o^{3+} + red. \rightarrow Ru_o^{2+} + ox. \tag{48}$$
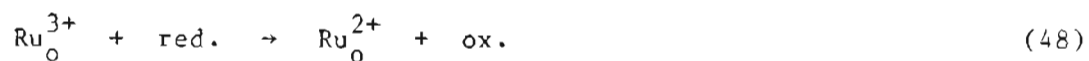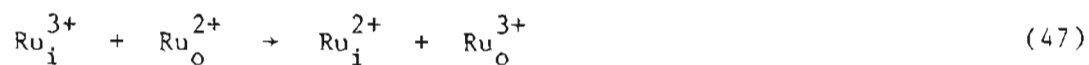
The net result hence is the conversion of internal Ru(III) to Ru(II) by external reductant,

$$Ru_i^{3+} + red. \rightarrow Ru_i^{2+} + ox. \tag{49}$$

Assuming transmembrane electron transfer between $Ru^{3+/2+}$ ions is thermodynamically reversible, the net free energy change for the reaction can be represented as:

$$\Delta E_t = \Delta E^\circ - RT/F \ln\left(\frac{[Ru_o^{2+}]\ [ox.]}{[Ru_{in}^{3+}]\ [red.]}\right) \tag{50}$$

However, transmembrane reduction of internal ruthenium by external Ru(II) is electrogenic. As shown in step 2 of Scheme IV, the inward movement of electrons causes the external phase of the bilayer to be more positive and the internal phase more negative if there is no compensating ion diffusion across the bilayer, thereby disfavoring further charge influx. This opposing force is analogous to the electrostatic force involved in removing charges from the outer terminal to the inner terminal of a concentric plate capacitor. For the highest ruthenium/PC ratios used in the present study (1:11), the potential energy developed across the vesicle bilayer due to transmembrane electron transfer, E_{cap}, is calculated to be 1.12 volt (Appendix III) if all internal Ru(III) ions are reduced. Since the net chemical driving force, ΔE°, is only 0.149-0.712 volt for the various reductants (Table 24), without compensating ion diffusion the electrical polarization of the bilayer that develops as transmembrane electron transfer proceeds

would increasingly oppose the further reduction of internal Ru(III) ions. Taking this capacitor effect into the driving force, $\Delta E_t' = \Delta E_t - E_{cap}$, the extent of transmembrane electron transfer limited by membrane polarization can be calculated (Table 24); e.g., at equilibrium, only 33% of the internal ruthenium would be reduced using ascorbate ion as external reductant. Since reduction of internal ruthenium is essentially complete regardless of the reductants used, charge-compensating ion diffusion must occur.

Symport of oppositely charged ions in ion transport across both biological and artificial membranes has been observed.[125-127] Conceivably, cation diffusion might be rate-limiting in the slow transmembrane redox step. Although phospholipid bilayers in general are relatively impermeable to small ions, i.e., diffusion coefficients are in the order of $10^{-9}-10^{-11}$ cm/s, passive proton diffusion across vesicle bilayers has been observed with half-times in the order of minutes,[128,129] which is in the same time span for transmembrane electron transfer. However, kinetic data obtained for the slow reduction in vesicle systems containing a lipid-soluble proton carrier, carbonyl cyanide m-chlorophenylhydrazone (CCCP), were almost identical to that without the proton translocator (Table 20). Similarly, addition of valinomycin, a potassium ionophore in K^+ media also did not accelerate the slow-phase redox rate. These observations suggest that transmembrane electron transfer is rate-limiting and membrane polarization during redox is minimal because charge-compensating ion diffusion is relatively fast.

4.11 An electron-tunneling model

The ruthenium ions remain vesicle-bound during redox as indicated by the bathochromic shift of the Ru(II)-to-pyridine charge transfer band at 415 nm. This shift is greater than that observed when the ion is transferred from water to ethanol ($\lambda_{max}(H_2O)$ = 398 nm, $\lambda_{max}(EtOH)$ = 408 nm), which suggests it is localized in a more hydrophobic environment than alcohol. Hence, it is reasonable to assume that the ions are relatively constrained in the lipid region near the hydrocarbon-water interface which should give rise to relatively deep potential energy wells for electron transfer across the hydrophobic bilayer. Since ruthenium ions are bound to opposite vesicle surfaces, electron exchange between them would require a transfer distance of almost the total width of the bilayer, i.e., about 40 Å. Long-range electron transfer between two rigid redox centers has been observed in several instances; the reaction mechanism is thought to involve rate-limiting electron tunneling.[52,130-132] Inasmuch as transmembrane diffusion of both the ruthenium ions and external reductant is precluded in the present work, the transmembrane electron transfer step could be treated in terms of an electron tunneling model.

Photoelectric conduction in monolayer assemblies has been studied.[133-135] In this type of experiment, layered Langmuir-Blodgett films which contain linear organic dyes with their C-axis normal to the layer plane are sandwiched between insulating fatty acid monolayers. Photocurrents could be generated between two metal electrodes separated by the multilayer assembly upon light excitation. At low temperatures, this phenomenon is adequately explained by an electron tunneling model[108] in which electrons hop to interlayer trapping sites in the

hydrocarbons of the fatty-acid layers and proceed to the anode. The hopping relaxation time constant, τ^{-1}, is represented as

$$\tau^{-1} = \tau_o^{-1} \ (2\alpha\ell)^{3/2} \ \exp[-2\alpha\ell - (4\alpha/\pi N(E_F)\ell kT)^{1/2}] \tag{51}$$

where α is an energy barrier term assuming a square-shape potential barrier imposed by the hydrocarbon layer, i.e., $\alpha = (2m\varphi)^{1/2}/\hbar$; ℓ is the hopping distance, and the exponential term $(-2\alpha\ell - (4\alpha/\pi N(E_F)\ell kT)^{1/2})$ is the minimal hopping energy obtained by optimizing the number of available transfer sites and the shortest hopping distance. Based on this model, an electron near the Fermi level E_F hops into one of the localized states distributed with a density $N(E_F)$ on the adjacent interface.

Since the morphologies of unilamellar vesicles and monolayers are similar, the vesicle bilayer could be viewed as stacking two opposite monolayers together. Assuming the transfer sites are located in the hydrocarbon phase in the vesicle, the hopping distance would be approximately the half-width of the bilayer. Using the experimental parameters obtained in the monolayer studies, $\tau_o = 10^{-12}$ s, $N(E_F) = 10^{15}$ V^{-1} cm^{-2},[135] a barrier height $\varphi = 2.5$ V estimated from the Fermi energy of the Ru(II) ion in aqueous solution (-4.8 V),[136] and a transfer distance of 22 Å, the electron tunneling relaxation rate constant (τ^{-1}) is calculated to be 1.0×10^{-3} s^{-1} at 23°C. This value is in accord with the experimentally measured transmembrane redox rate constants (Table 20).

4.12 Temperature dependence of the reaction

According to equation 51, the electron tunneling relaxation rate constant $(_{\tau}^{-1})$ has a small temperature dependence. In the range of 5-30°C, the rate increase is calculated to be about 20%. However, the experimental rate constants obtained in this temperature range show a 6- to 7-fold increase (Table 16). This suggests that either there exists a substantial activation barrier (Franck-Condon factor) other than the electron hopping energy barrier or some parameters in the tunneling relaxation rate expression are temperature-dependent.

Phospholipid bilayers undergo dimensional changes with increasing temperatures, e.g., lateral expansion of the bilayers, increase of internal volume, and decrease of the bilayer thickness.[137-139] These changes occur both above and below the gel to liquid crystalline phase-transition temperature but are most pronounced in the phase-transition region, presumably due to the higher degree of rotational freedom of the polar head groups and increased fluidity of the hydrocarbon chains. Watts and coworkers[137] have found that in unilamellar dimyristoyl-phosphatidylcholine vesicles which consist of C_{14} monomer chains, the bilayer width decreases approximately 0.1 Å/degree and 0.3 Å/degree below and above the phase-transition temperature $(T_c = 22°C)$, respectively. Similarly, the linear expansion coefficient (α) determined for dipalmitoyllecithin bilayers in the fluid phase, where $\alpha = dr/adT$, r is the bilayer width and a is the lipid lattice constant, is 3.4 x 10^{-3} °C^{-1}.[138] Since egg phosphatidylcholine has a relatively low phase-transition temperature (-12 to 5°C), the vesicles in the kinetic studies are in the fluid phase. Assuming a similar linear expansion coefficient, the temperature dependence of the slow-phase reduction can be

ascribed to decreases in the bilayer width, i.e., the electron hopping distance (ℓ) in equation 51. A decrease of 0.6 Å over the range of 5-30°C would give rise to an order of magnitude decrease in the tunneling relaxation rate which is consistent with the rate data obtained (Table 16).

Alternatively, the temperature dependence of isoenergetic trans-membrane electron transfer could be rationalized in terms of a nuclear energy barrier in vibronically coupled electron tunneling theories. One essential feature of these theories is that the electron tunneling probabilities are controled by vibronic coupling to low-frequency polarization modes of the solvent and high-frequency modes comprising the intramolecular vibrations of the donor and acceptor molecules. Based on the Franck-Condon principle, which states that there is no change in the nuclear geometry during electron transfer between two centers, the reorganization energies from these vibrational modes contribute to the preexponential factor (v) in the tunneling rate expression,[140] i.e.,

$$k(r) \propto v \exp (-r/a) \tag{52}$$

This Franck-Condon factor has an exponential temperature dependence, except in the special case of activationless electron transfer,[54b,140] i.e., when the product potential energy surface intersects the reactant surface at its minimum.

Activation enthalpies obtained for transmembrane redox are 8-14 kcal/mol (Table 20), similar to values observed in intramolecular reduction of pentaamminepyridineruthenium(III) complex by Cu(I) in the

binuclear ion.[63] Vibronically coupled electron tunneling could
therefore account for the rate behavior in the absence of other effects.
Since bilayer thinning is known to occur with increasing temperatures,
however, it appears more favorable to ascribe the temperature dependence
to decreased tunneling distances in the electron conduction model. The
dominant effect of varying ℓ in equation 51 is in the exponential term,
$\exp(-2\alpha\ell)$; if ℓ varies linearly with temperature, the rate constant
would exhibit an Arrhenius-type temperature dependence.

CHAPTER 5

SUMMARY

Several photoinduced redox reactions between light sensitizers and
viologens and thermal electron transfer reactions have been carried out
in vesicle systems. Transmembrane electron transfer is observed in
symmetrically bound $C_{16}MV^{2+}$-DHP vesicles in which $C_{16}MV^{+}$ monocation
radicals are generated by oxidative quenching of unbound photoexcited
$ZnTPPS^{4-}$ in the external bulk medium. Kinetic data obtained from
steady-state illumination studies indicate that transmembrane redox
between external $C_{16}MV^{+}$ and internal $C_{16}MV^{2+}$ has occurred, since incor-
poration of an internal electron scavenger, $Fe(CN)_6^{3-}$, retards the rate
of net viologen radical formation. Comparison of data obtained from
other DHP vesicle systems of different configurations suggests that
transmembrane redox occurs via a mechanism in which electrons tunnel
across the vesicle bilayer. This claim is further supported by the lack
of detectable photostimulated diffusion of initially compartmented
reactants as demonstrated by binding and diffusion studies.

Diffusion of MV^{2+} across DHP bilayers is enhanced by photoexcita-
tion of vesicle-bound sensitizers. Translocation of internally bound
viologen to the external surface leads to oxidative quenching of the
sensitizer on the same surface. The activation enthalpy of this process
is similar to that for passive thermal viologen diffusion. It suggests
that the enhanced membrane fluidity might be attributable to localized

heating of the bilayer structure produced by nonradiative deactivation of the excited bound sensitizer. This phenomenon is potentially important to designing efficient solar conversion systems where photoexcitation of phase-separated reactants are used.

Reduction of symmetrically bound $(NH_3)_5Ru-4-(11'-$ dodecenyl)pyridine^{3+} ions in PC vesicles by excess external reductant exhibits biphasic kinetics. Kinetic analysis of the slow phase reaction indicates that the rates are best fitted by first-order kinetics, and within a relatively large experimental error, they are independent of both the identity and concentration of the reductant. The simplest interpretation for this observation is the net reduction of internal ruthenium complexes. It has also been demonstrated by binding and diffusion studies that diffusion of ruthenium(II)/(III) complexes and external reductants are insignificant in the time frame of slow-phase reduction. These overall results, therefore, strongly suggest that reduction of internal ruthenium complex in PC vesicles occurs by transmembrane electron transfer.

REFERENCES

(1)   Holt, S. L., "Inorganic Reactions in Organized Media," ACS
Symposium Series 177, Washington, D.C.; 1982, pp. 37-71, 113-139.

(2)   Boyer, P. D.; Chance, B.; Ernster, L.; Mitchell, P.; Racker, E.;
Slater, E. C. Annu. Rev. Biochem. 1977, 46, 955-1026.

(3)   Slater, E. C. Nature 1953, 172, 975-978.

(4)   Boyer, P. D. "Oxidase and Related Redox Systems," King, T. E.;
Mason, H. S., Morrison, M., eds. Wiley, New York, 1965, pp. 994-
1008.

(5)   Mitchell, P. Nature, 1961, 191, 144-148.

(6)   Haddock, B. A.; Jones, C. W. Bacteriol. Rev. 1977, 41, 47-99.

(7)   Racker, E. "A New Look at Mechanisms in Bioenergetics," Academic
Press, New York, 1976, pp. 90-106.

(8)   Nicholls, D. G. "Bioenergetics," Academic Press, New York, 1982,
pp. 99-127.

(9)   Sanadi, D. R. "Chemical Mechanisms in Bioenergetics," ACS
Monograph No. 172, Washington D.C., 1976, pp. 123-220.

(10) Grätzel, M. Acc. Chem. Res. 1981, 14, 376-384.

(11) Connolly, J. S. "Photochemical Conversion and Storage of Solar
Energy," Academic Press, New York, 1981.

(12) Kirch, M.; Lehn, J.-M.; Sauvage, J.-P. Helv. Chim. Acta 1979, 62,
1345-1384.

(13) Delaive, P. J.; Sullivan, B. P.; Mayer, T. J.; Whitten, D. G. J. Am. Chem. Soc. 1979, 101, 4007-4008.

(14) Fendler, J. H.; Fendler, E. J. "Catalysis in Micellar and Macro-molecular Systems," Academic Press, New York, 1975.

(15) Bockris, J. O'M.; Reddy, A. K. N. "Modern Electrochemistry," Vol. 2, Academic Press, New York, 1970, pp. 733-737.

(16) Moroi, Y.; Braun, A. M.; Grätzel, M. J. Am. Chem. Soc. 1979, 101, 567-572.

(17) Grätzel, M.; Thomas, J. K. J. Phys. Chem. 1974, 78, 2248-2254.

(18) Grätzel, M.; Kozak, J. J.; Thomas, J. K. J. Chem. Phys. 1975, 62, 1632-1640.

(19) Scheerer, R.; Grätzel, M. J. Am. Chem. Soc. 1977, 99, 865-871.

(20) Kiwi, J.; Grätzel, M. J. Am. Chem. Soc. 1978, 100, 6314-6319.

(21) Moroi, Y.; Infelta, P. P.; Grätzel, M. J. Am. Chem. Soc. 1979, 101, 573-579.

(22) Ford, W. E.; Otvos, J. W.; Calvin, M. Proc. Natl. Acad. Sci. USA 1979, 76, 3590-3593.

(23) Alkaitis, S. A.; Grätzel, M. J. Am. Chem. Soc. 1976, 98, 3549-3554.

(24) Svens, B.; Rosenholm, B. J. Colloid. Interface Sci. 1973, 44, 495-504.

(25) Stigter, D. J. Phys. Chem. 1974, 78, 2480-2485.

(26) Menger, F. M. Acc. Chem. Res. 1979, 12, 111-117.

(27) Sanger, S. J.; Nicolson, G. L. Science 1972, 175, 720-731.

(28) Racker, E.; Kandrach, A. J. Biol. Chem. 1973, 248, 5841-5847.

(29) Hinkle, P. Biochem. Biophys. Res. Commun. 1970, 41, 1375-1381.

(30) Gerber, G. E.; Gray, C. P.; Wildenauer, D.; Khorara, H. G. Proc. Natl. Acad. Sci. USA 1977, 74, 5426-5430.

(31) Luzzati, V.; Husson, F. J. Cell Biol. 1962, 12, 207-219.

(32) Bangham, A. D.; Horne, R. W. J. Molec. Biol. 1964, 8, 660-668.

(33) Huang, C. Biochemistry 1969, 8, 344-352.

(34) Barenholz, Y.; Gibbs, D.; Litnan, B. J.; Goll, J.; Thompson, T. E.; Carlson, F. D. Biochemistry 1977, 16, 2806-2810.

(35) Brugger, P.; Infelta, P. P.; Braun, A. M.; Gratzel, M. J. Am. Chem. Soc. 1981, 103, 320-326.

(36) Papahadjopoulos, D.; Kimelberg, H. K. Prog. Surf. Sci. 1974, 4, 164-177.

(37) Johnson, S. M.; Bangham, A. D. Biochim. Biophys. Acta 1969, 193, 82-91.

(38) Papahadjopoulos, D.; Nir, S.; Ohki, S. Biochim. Biophys. Acta 1972, 266, 561-583.

(39) Hauser, H. O.; Phillips, M. C.; Stubbs, M. Nature 1972, 239, 342-344.

(40) Pressman, B. C.; de Guzman, N. T. Ann. N.Y. Acad. Sci. 1974, 227, 380-391.

(41) Pressman, B. C. Fed. Proc. Am. Soc. Exp. Biol. 1968, 27, 1283-1288.

(42) Haydon, D. A.; Hladky, S. B. Q. Rev. Biophys. 1972, 5, 187-282.

(43) Chance, B.; DeVault, D. C.; Frauenfelder, H.; Marcus, R. A.; Schrieffer, J. R.; Sutin, N. "Tunneling in Biological Systems," Academic Press, New York, 1979.

(44) Gerisher, H.; Katz, J. J. "Light-Induced Charge Separation in Biology and Chemistry," Verlag Chemie Weinheim, New York, 1979.

(45) Marcus, R. A. Annu. Rev. Phys. Chem. **1964**, 15, 155-196.

(46) Sutin, N. Acc. Chem. Res. **1968**, 1, 225-231.

(47) Hurst, J. K. Biochemistry **1979**, 18, 1504-1510, and references therein.

(48) Caughey, W. S.; Smythe, G. A.; O'Keeffe, D. H.; Maskosky, J. E.; Smith, M. L. J. Biol. Chem. **1975**, 250, 7602-7622.

(49) Paeker, E. L.; Sternlicht, H.; Rabinowitz, J. C. Proc. Natl. Acad. Sci. USA **1972**, 69, 3278-3282.

(50) DeVault, D.; Chance, B. Biophys. J. **1966**, 6, 825-847.

(51) Potasek, M. J.; Hopfield, J. J. Proc. Natl. Acad. Sci. USA **1977**, 74, 3817-3820.

(52) Winkler, J. R.; Nocera, D. G.; Yocom, K. M.; Bardignon, E.; Gray, H. B. J. Am. Chem. Soc. **1982**, 104, 5798-5800.

(53) Dockter, M. E.; Steinemann, A.; Schatz, G. J. Biol. Chem, **1978**, 253, 311-317.

(54) (a) Hopfield, J. J. Proc. Natl. Acad. Sci USA **1974**, 71, 3640-3644; (b) Jortner, J. J. Chem. Phys. **1976**, 64, 4860-4867.

(55) Singleton, W. S.; Gray, M. S.; Brown, M. L.; White, J. L. J. Am. Oil Chem. Soc. **1965**, 42, 53-56.

(56) Jones, L. H. Inorg. Chem. **1963**, 2, 777-780.

(57) Schlessinger, G. Inorg. Synth. **1960**, 6, 189-191.

(58) Celap, M. B.; Janjic, T. J., Radanovic, D. J. Inorg. Synth. **1967**, 9, 173-174.

(59) Wiley, G. A.; Hershkowitz, R. L.; Rein, B. M.; Chung, B. C. J. Am. Chem. Soc. **1964**, 86, 964-965.

(60) Norton, K. A., Jr. Ph.D. Dissertation, Oregon Graduate Center, 1980.

(61) Brown, H. C.; Murphy, W. A. J. Am. Chem. Soc. 1951, 73, 3308-3312.

(62) Broomhead, J. A.; Basolo, F.; Pearson, R. G. Inorg. Chem. 1964, 3, 826-832.

(63) Norton, K. A.; Hurst, J. K. J. Am. Chem. Soc. 1978, 100, 7237-7242.

(64) Endicott, J. F.; Taube, H. Inorg. Chem. 1965, 4, 437-445.

(65) Brauer, G. "Handbook of Preparative Inorganic Chemistry," Vol. 2, Academic Press, New York, 1965, pp. 1285-1286.

(66) Price, H. J.; Taube, H. Inorg. Chem. 1968, 7, 1-9.

(67) Kitson, R. E. Anal. Chem. 1950, 22, 664-667.

(68) Tunuli, M. S.; Fendler, J. H. J. Am. Chem. Soc. 1981, 103, 2507-2513.

(69) The notation, (A)//(vesicle)//(B), indicates that A and B are separated by the vesicle bilayer. A is either bound to the inner surface or resides in the inner aqueous phase. B is either bound to the outer surface or resides in the external aqueous phase.

(70) Hiemeuz, P. C. "Principles of Colloid and Surface Chemistry," M. Dekker, New York, 1977, pp. 160-207.

(71) Koppel, D. E. J. Chem. Phys. 1972, 57, 4814-4820.

(72) Zwickel, A. M. Ph.D. Dissertation, University of Chicago, 1959.

(73) Calvert, J. G.; Pitts, J. N, Jr. "Photochemistry," Wiley, New York, 1966, pp. 783-786.

(74) Rothenberger, G.; Infelta, P. P.; Gratzel, M. J. Phys. Chem. 1979, 83, 1871-1876.

(75) Tricot, Y.-M.; Furlong, D. N.; Sasse, W. H. F.; Daivis, P.; Snook, I. Aust. J. Chem. 1983, 36, 609-612.

(76) Lukac, S. Photochem. Photobiol. 1982, 36, 13-20.

(77) Monserrat, K.; Grätzel, M. J. Chem. Soc. Chem. Commun. 1981, 183-184.

(78) McLaughlin, S.; Harary, H. Biochemistry 1976, 15, 1941-1948.

(79) Johnson, S. M.; Bangham, A. D.; Hill, M. W.; Korn, E. D. Biochim. Biophys. Acta. 1971, 233, 820-826.

(80) Hermann, U.; Fendler, J. H. Chem. Phys. Lett. 1979, 64, 270-274.

(81) Lee, L. Y. C.; Hurst, J. K.; Politi, M.; Kurihara, K.; Fendler, J. H. J. Am. Chem. Soc. 1983, 105, 370-373.

(82) Kalyanasundaram, K.; Grätzel, M. Helv. Chim. Acta 1980, 63, 478-485.

(83) Harriman, A.; Porter, G.; Richoux, M.-C. J. Chem. Soc. Faraday Trans. 2 1981, 77, 833-844.

(84) Ford, P. C.; Kuempel, J. R.; Taube, H. Inorg. Chem. 1968, 7, 1976-1983.

(85) Shepherd, R. E.; Taube, H. Inorg. Chem. 1973, 12, 1392-1401.

(86) Tanford, C. "The Hydrophobic Effect," Wiley, New York, 1973, pp. 78-79.

(87) Briggs, J.; Nicoli, D. F. J. Chem. Phys. 1980, 72, 6024-6030.

(88) Chang, E. L.; Gaber, B. P.; Sheridan, J. P. Biophys. J. 1982, 39, 197-201.

(89) Prince, L. M. "Micellization, Solubilization, and Microemulsions," Vol. 1. Mittel, K. L., ed., Plenum Press, New York, 1977, pp. 45-47.

(90) Ladbrooke, B. D.; Chapman, D. Chem. Phys. Lipids 1969, 3, 304-356.

(91) Hurst, J. K.; Lee, L. Y. C.; Grätzel, M. J. Am. Chem. Soc. 1983, 105, 7048-7056.

(92) Brugger, P. Ph.D. Dissertation, EPFL, Lausanne, Switzerland, 1982.

(93) Froherz, P.; Masters, B. Biochim. Biophys. Acta 1974, 356, 270-275.

(94) Hyer, E. J.; Muller, R. U.; Finkelstein, H. J. Gen. Physiol. 1976, 67, 703-729.

(95) Huang, C.; Charlton,J. P. Biochemistry 1972, 11, 735-740.

(96) Papahadjopoulos, D. Biochim. Biophys. Acta 1971, 241, 254-259.

(97) Papahadjopoulos, D.; Watkins, J. C. Biochim. Biophys. Acta 1967, 135, 639-652.

(98) McLaughlin, S. G. A.; Szabo, G.; Eisenman, G.; Ciani, S. M. Proc. Natl. Acad. Sci. USA 1970, 67, 1268-1275.

(99) Bangham, A. D.; Standish, M. M.; Watkins, J. C. J. Molec. Biol. 1965, 13, 238-252.

(100) Haest, C. W. M.; De Gier, J.; Op Der Kemp, J. A. F.; Bartels, P.; Van Deenen, L. L. M. Biochim. Biophys. Acta 1972, 255, 720-733.

(101) Dilger, J. P.; McLaughlin, S. K. A., McIntosh, T. J.; Simon, S. A. Science 1979, 206, 1196-1198.

(102) Akutsu, H.; Seelig, J. Biochemistry 1981, 20, 7366-7373.

(103) Van Holde, K. E. "Physical Biochemistry," Prentice-Hall, New Jersey, 1971, pp. 58-61.

(104) Tricot, Y.-M.; Furlong, D. N.; Sasse, W. H. F.; Daivis, P.; Snook, I.; Van Megan, W. J. Colloid Interface Sci. 1984, 97, 380-391.

(105) Darke, A.; Finer, G.; Flook, A. G.; Phillips, M. C. J. Molec. Biol. **1972**, 63, 265-279.

(106) Ford, W. E.; Tollin, G. Photochem. Photobiol. **1982**, 35, 809-819.

(107) Laane, C.; Ford, W. E.; Otvos, J. W.; Calvin, M. Proc. Natl. Acad. Sci. USA **1981**, 78, 2017-2020.

(108) Kuhn, H. Pure Appl. Chem. **1979**, 51, 341-352.

(109) Seefeld, K. P.; Möbius, D.; Kuhn, H. Helv. Chim. Acta **1977**, 60, 2608-2632.

(110) Kalyanasundaram, K.; Neumann-Spallart, M. J. Phys. Chem. **1982**, 86, 5163-5169.

(111) Neta, P. J. Phys. Chem. **1981**, 85, 3678-3684.

(112) Borgarello, E.; Kalyanasundaram, K.; Okuno, Y.; Grätzel, M. Helv. Chim. Acta **1981**, 64, 1937-1942.

(113) Frank, A. J.; Grätzel, M.; Kozak, J. J. J. Am. Chem. Soc. **1976**, 98, 3317-3321.

(114) Henglin, A.; Proske, T. Ber. Bunsenges. Phys. Chem. **1978**, 82, 471-476.

(115) Frost, A. A.; Pearson, R. G. "Kinetics and Mechanisms," Wiley, New York, **1963**, p. 271.

(116) Cellarius, R. A.; Mauzerall, D. Biochim. Biophys. Acta **1966**, 112, 235-255.

(117) Ballard, S. G.; Mauzerall, D. C. J. Chem. Phys. **1980**, 72, 933-947.

(118) Lever, A. B. P.; Ramaswamy, B. S.; Licoccia, S. J. Photochem. **1982**, 19, 173-182.

(119) Schmehl, R. H.; Whitten, D. G. J. Phys. Chem. **1981**, 85, 3473-3480.

(120) Harriman, A.; Porter, G.; Walters, P. J. Photochem. 1982, 19, 183-187.

(121) Hurley, J. K.; Castelli, F.; Tollin, G. Photochem. Photobiol. 1981, 34, 623-631.

(122) Jordan, P. C. "Chemical Kinetics and Transport," Plenum Press, New York, 1979, p. 311.

(123) Oliveira, L. A. A.; Haim, A. J. Am. Chem. Soc. 1982, 104, 3363-3366.

(124) Hatlee, M. D.; Kozak, J. J.; Rothenberger, G.; Infelta, P. P.; Grätzel, M. J. Phys. Chem. 1980, 84, 1508-1519.

(125) Burnell, J. N.; Whatley, F. R. FEBS Lett. 1975, 58, 215-218.

(126) MacDonald, R. E.; Lanyi, J. K.; Greene, R. V. Proc. Natl. Acad. Sci. USA 1977, 74, 3167-3170.

(127) Forgac, M.; Chin, G. J. Biol. Chem. 1982, 257, 5652-5655.

(128) Nichols, J. W.; Hill, M. W.; Bangham, A. D.; Deamer, D. W. Biochim. Biophys. Acta 1980, 596, 393-403.

(129) Clement, N. R.; Gould, J. M. Biochemistry 1981, 20, 1539-1543.

(130) Harrington, P. C.; Wilkins, R. G. J. Am. Chem. Soc. 1981, 103, 1550-1556.

(131) Isied, S. S.; Worosila, G.; Atherton, S. J. J. Am. Chem. Soc. 1982, 104, 7659-7661.

(132) McGourty, J. L.; Blough, N. V.; Hoffman, B. M. J. Am. Chem. Soc. 1983, 105, 4470-4472.

(133) Polymeropoulos, E. E.; Möbius, D.; Kuhn, H. J. Chem. Phys. 1978, 68, 3918-3931.

(134) Sugi, M.; Fukui, T.; Ilzima, S. Chem. Phys. Lett. 1977, 45, 163-166.

(135) Sugi, M.; Nembach, K.; Möbius, D.; Kuhn, H. Solid State Commun. 1974, 15, 1867-1870.

(136) The Fermi energy (ε) is related to the standard reduction potentials (E_o) by the following equation:

$$\varepsilon = E_o - 4.5 \; V^{142}$$

where -4.5 V is the energy difference between an electron in gas phase and the Fermi level of standard hydrogen electrode.

(137) Watts, A.; Marsh, D.; Knowles, P. F. Biochemistry 1978, 17, 1792-1801.

(138) Marsh, D. Biochim. Biophys. Acta 1974, 363, 373-386.

(139) Träuble, H.; Haynes, D. H. Chem. Phys. Lipids 1971, 7, 324-335.

(140) Miller, J. R.; Beitz, J. V.; Huddleston, R. K. J. Am. Chem. Soc. 1984, 106, 5057-5068.

(141) Manassen, J.; Cahn, D.; Hodes, G.; Sofer, A. Nature 1976, 263, 97-100.

Table 1. Hydrodynamic Radii of PC Vesicles from Light-Scattering

   Spectroscopy

Vesicle[a]	[PC]mM	Ru:PC[b]	$10^{-2} \cdot \tau_c$ (sec)	R_H (Å)	Variance[c]
PC	0.1	----	4.81	254	0.33
	0.1	----	4.75	251	0.32
	0.1	----	4.34	229	0.28
	0.03	----	4.98	263	0.28
$(NH_3)_5Ru-4-(11'-$ dodecenyl)py^{3+}-PC	0.1	1:17	4.35	230	0.36
	0.1	1:17	4.83	255	0.34
	0.1	1:17	4.12	218	0.34
	0.1	1:4.5	4.42	234	0.47
	0.1	1:4.5	3.99	211	0.45
	0.1	1:4.5	4.52	239	0.41

[a]In 0.1 M sodium acetate, pH 4.0.

[b]Molar ratio of ruthenium to phosphatidylcholine monomer.

[c]Calculated from equation 18.

Table 2. Hydrodynamic Radii of DHP Vesicles from Light-Scattering
          Spectroscopy

Vesicle[a]	Medium	R_H(Å)	Variance[b]
DHP	0.1 M tricine, pH 7.2	638	0.21
DHP//ZnTMPyP^{4+}	1 M TEOA, pH 7.8	480	0.19
DHP//ZnTMPyP^{4+}	0.02 M TRIS, pH 7.8	514	0.12
DHP//ZnTMPyP^{4+}, MV^{2+}	0.02 M TEOA, pH 7.8	484	0.13
MV^{2+}//DHP//ZnTMPyP^{4+}	0.05 M TRIS, pH 7.8	400	0.18

[a]Ref. 69.

[b]From equation 18.

Table 3. Summary of Solute Binding by Vesicles

Solute	Vesicle	Method of determination
Photosensitizers		
$ZnTMPyP^{4+}$	DHP	Gel chromatography, optical difference spectroscopy, membrane ultrafiltration
$Ru(bpy)_3^{2+}$	DHP	Optical difference spectroscopy
Viologen		
MV^{2+}	DHP	Optical difference spectroscopy, gel chromatography
$C_{16}MV^{2+}$	DHP	Optical difference spectroscopy, gel chromatography
$C_{16}MV^{2+}$	PC	Gel chromatography
$C_{14}MV^{2+}$	PC	Gel chromatography
$(NH_3)_5RuNC_5H_4(CH_2)_nCH=CH_2^{3+}$ ions		
n = 2, 5, 7, or 10	PC	Gel chromatography, optical difference spectroscopy
$(NH_3)_5CoNC_5H_4(CH_2)_nCH=CH_2^{3+}$ ions		
n = 7, 9	PC	Membrane ultrafiltration

Table 4. Entrapment of Metal Complexes by PC Vesicles

Complex	Charge Type	Metal Content in Vesicle Solution (μmole)		Amount of PC (mg)		Total Vesicle Internal Volume[b] (μl)	Entrapped Metal Concentration[c] (M)	Retention Factor[d] (%)	No. of Filtrations
		Initial	Final	Initial	Final[a]				
$(NH_3)_5CoOH_2^{3+}$	+ 3	80	2.7	25.6	22.4	8.7	0.31	3.4	9
$Co(bpy)_3^{3+}$	+ 3	40	1.4	23.7	21.9	8.5	0.16	3.5	12
Cr^{3+}	+ 3	68	5.7	63.0	62.6	24.4	0.23	8.4	9
$(NH_3)_5CoN_3^{2+}$	+ 2	75	0.85	29.3	26.9	10.5	0.08	1.1	14
$(NH_3)_3Co(NO_2)_3$	0	83	0.51	28.7	23.7	9.2	0.06	0.6	9
$(NO_2)_2Co(glycinate)_2^-$	- 1	49	1.2	24.0	21.5	8.4	0.14	2.5	9
$Fe(CN)_6^{3-}$	- 3	110	7.2	25.2	21.9	8.5	0.85	6.6	28
$Co(CN)_6^{3-}$	- 3	93	2.8	----	----	----	----	3.1	12

[a]Determined by ^{14}C analysis.

[b]Based on a value of 0.3 μl/μmol PC.

[c]Obtained by dividing values from column 4 by values from column 7.

[d]Obtained by dividing values from column 4 by values from column 3.

Table 5. Initial Rates[a] of MV^+ Formation[b] in Passive
Viologen Diffusion Across DHP Vesicle
Bilayers[c]

R_i (nM s^{-1})	Temperature (°C)
7.3	15, 20
35	25
67	30
113	35

[a]From initial slopes of lines obtained from viologen-
DHP vesicle solutions incubated at temperatures
indicated (Figure 24).

[b]Determined from spectral changes at 600 nm upon
reduction by externally added dithionite.

[c]Initial concentrations = [DHP] = 4.8 mM, [MV^{2+}] =
3.6 mM, in 0.05 M Tris, pH 7.8.

136

Table 6. MV^{2+} Diffusion Induced by External Hydroxylic Amines in DHPr
Vesicles[a]

External Amine Added	Time After Amine ΔT (min)	Viologen Leakage[b] (μM)	% of Total Internal Viologen[c]
0.05 M tricine	15	7	4.7
0.05 M TEOA	20	10	6.7
0.05 M Tris	20	27	18

[a] Reaction conditions = 4.8 mM DHP and 3.0 mM MV^{2+} sonicated in H_2O, pH 8.4, followed by cation exchange chromatography; external reagents added to asymmetric vesicles: 30 μM Ru(bpy)$_3^{2+}$, 1 mM EDTA prior to amine addition, at 23°C, pH 8.4.

[b] External viologen was determined as MV$^+$ at 600 nm by dithionite reduction.

[c] Obtained by dividing values from column 3 by 150 μM internal MV^{2+}, whose concentration was determined from the ultraviolet spectrum of MV^{2+}-DHP asymmetric vesicles referenced against DHP vesicles.

Table 7. Photoinduced Viologen Diffusion in Asymmetric MV^{2+}//DHP//Sensitizer Vesicles[a]

$[MV^{2+}]_{in}$[b] (μM)	$[MV^{2+}]_{out}$[c] (μM)	% Leakage	Illumination Time (min)	Sensitizer	Temperature (°C)	Medium Conditions[d]
120	52	43	120	$Ru(bpy)_3^{2+}$ (e)	23	I
195	50	26	155		23	I
95	38	40	90		23	II
96	50	52	100		23	II
60	9	15	100		10	II
100	20	20	100		20	II
80	30	38	80		30	II
60	50	83	20		40	II

(continued)

Table 7, continued:

$[MV^{2+}]_{in}$[b] (μM)	$[MV^{2+}]_{out}$[c] (μM)	% Leakage	Illumination Time (min)	Sensitizer	Temperature (°C)	Medium Conditions[d]
76	30	39	120	$ZnTMPyP^{4+}$ (f)	23	I
120	50	44	120		23	II
100	38	35	80		23	II
120	0	0	60	$ZnTPPS^{4-}$ (g)	20	II

[a]Reference 69.

[b]Determined by optical difference spectroscopy of asymmetric MV^{2+}-DHP vesicles vs. DHP vesicle at 256 nm
 prior to illumination.

[c]Determined as MV^+ by external dithionite reduction after illumination.

[d]I = H_2O, pH 8.4; II = 0.05 M Tris, pH 7.8; all contained 2 mM external EDTA.

[e]30 μM $Ru(bpy)_3^{2+}$, sensitizer:DHP = 1:160.

[f]16 μM $ZnTMPyP^{4+}$, sensitizer:DHP = 1:300.

[g]50 μM $ZnTPPS^{4-}$, sensitizer:DHP = 1:80.

Table 8. Initial Rates of $Ru(bpy)_3^{2+}$ Sensitized MV^+
Formation[a] in Asymmetric MV^{2+}-DHP Vesicles[b]

R_i $(nM\ s^{-1})$[c]	Temperature (°C)
1.2	10
4.1	20
10.8	30
41.4	40

[a] Based on $\varepsilon_{603} = 1.24 \times 10^4\ M^{-1}\ cm^{-1}$ for MV^+ upon external dithionite reduction.[64]

[b] Reaction conditions: 4.8 mM DHP, 3.6 mM MV^{2+} sonicated in 0.05 M Tris, pH 7.8, followed by Sephadex chromatography; external reagents added: 1 mM EDTA, 30 µM $Ru(bpy)_3^{2+}$; illuminated with 410 nm cutoff filter, $I_0 \approx 6 \times 10^{-8}$ einstein/s.

[c] Determined by absorbance increase at 603 nm.

Table 9. $C_{16}MV^+$ Quenched by Internal $Fe(CN)_6^{3-}$, in $Fe(CN)_6^{3-}$, $C_{16}MV^{2+}$//DHP//$C_{16}MV^{2+}$, $ZnTPPS^{4-}$ Vesicles[a]

$[Fe(CN)_6^{-3}]$[b] in (μM)	R_i(nM s^{-1})	Induction (min)	Temp. (°C)	Calculated $[MV^+]$ Generated Using R_i (μM)	Calculated $[MV^+]$ Generated Using R_i from Vesicles not Containing $Fe(CN)_6^{3-}$ (μM)[c]
1.6 – 2.0	1.0	20	10	1.2	3.7
3.8	1.8	15	23	1.6	4.0
1.6 – 2.0	3.7	8	30	1.8	2.9

[a]Reference 69.

[b]Measured by optical difference spectroscopy (ε_{420} = 1040 M^{-1} cm^{-1}) or atomic absorption spectroscopy.

[c]From Table 10, $C_{16}MV^{2+}$//DHP//$C_{16}MV^{2+}$, $ZnTPPS^{4-}$ vesicles.

Table 10. Initial Rates of $ZnTPPS^{4-}$ Sensitized $C_{16}MV^+$ Formation in DHP Vesicle Solutions[a]

Vesicle Configuration[b]	R_i(nM s^{-1})[c]	Temperature (°C)	$-\ln R_i$	$10^{-3} \times 1/T$ (°K^{-1})	E_a (kcal/mol)
$C_{16}MV^{2+}/\!/DHP/\!/C_{16}MV^{2+}$, $ZnTPPS^{4-}$	3.1	10	19.6	3.53	5.8
	4.4	23	19.2	3.38	
	6.1	30	18.9	3.30	
_____ $/\!/DHP/\!/C_{16}MV^{2+}$, $ZnTPPS^{4-}$	3.4	10	19.5	3.53	8.3
	6.7	23	18.8	3.38	
	8.8	30	18.6	3.30	
$Fe(CN)_6^{-3}/\!/DHP/\!/C_{16}MV^{2+}$, $ZnTPPS^{4-}$ (d)	12	10	18.2	3.53	
	46	23	16.9	3.38	
$Fe(CN)_6^{-3}$, $C_{16}MV^{2+}/\!/DHP/\!/C_{16}MV^{2+}$,	1.0	10	20.7	3.53	10.8[f]
	1.8	23	20.1	3.38	
$ZnTPPS^{4-}$ (d)	3.7	30	19.4	3.30	
$C_{16}MV/\!/DHP/\!/C_{16}MV$, $Fe(CN)_6^{-3}$,	0.8	10	21.0	3.53	
	0.8	23	21.0	3.38	
$ZnTPPS^{4-}$ (e)	1.5	30	20.3	3.30	

[a] 0.5 mM $C_{16}MV^{2+}$, 4 mM DHP, sonicated in 0.02 M Tris, pH 7.8, to form symmetrically-bound viologen-DHP vesicles, 0.25 mM $C_{16}MV^{2+}$ added to 4 mM DHP vesicles to form asymmetrically-bound viologen-DHP vesicles; external reagents added: 40 μM $ZnTPPS^{4-}$, 0.1 M tricine.

[b] Reference 69.

[c] Determined by absorbance increases at 600 nm.

[d] Internal $Fe(CN)_6^{3-}$ incorporated by cosonication of 20 mM $Fe(CN)_6^3$ with $C_{16}MV^{2+}$-DHP suspension, followed by Sephadex G-50 chromatography.

[e] 50 μM external $Fe(CN)_6^{3-}$ added.

[f] After 8-20 minute induction period (Table 9).

Table 11. Initial Rates of $ZnTMPyP^{4+}$ Sensitized $C_{16}MV^+$ Formation in PC Vesicles

Vesicle Configuration[a]	$[C_{16}MV^{2+}]$[b] (mM)	$C_{16}MV^{2+}/PC$[c]	$R_1 (\mu M\ s^{-1})$[d]
$C_{16}MV^{2+}/\!/PC/\!/C_{16}MV^{2+}$, $ZnTMPyP^{4+}$	1.6	1:6	0.29^e
	0.53	1:6	0.13^f
	0.23	1:10	0.30^f
$PC/\!/C_{16}MV^{2+}$, $ZnTMPyP^{4+}$	0.20	1:16	0.12^f
	1.0	1:3	0.92^e
$C_{16}MV^{2+}$, $ZnTMPyP^{4+}$	0.53	----	8.3^e

[a]Reference 69, in 0.05 M phosphate, pH 6.5, with 1 mM EDTA as sacrificial donor.

[b]Initial concentration

[c]Initial concentration ratios

[d]Initial slopes of $C_{16}MV^+$ formation determined at 600 nm; illuminated with filtered visible light ($\lambda > 515$ nm), at ambient temperature.

[e]20 μM $ZnTMPyP^{4+}$

[f]10 μM $ZnTMPyP^{4+}$

Table 12. Oxidative Quenching of Photoexcited ZnTMPyP^{4+} [a] by PC-bound C$_{16}$MV^{2+} [b]

[C$_{16}$MV^{2+}]^c (mM)	[PC]^c (mM)	C$_{16}$MV^{2+}/PC	$10^{-3} \cdot k \ (s^{-1})^d$
0	3.0	0	3.9 $\pm$ 0.4
0.11	3.2	1:29	4.7 $\pm$ 0.5
0.33	3.2	1:10	5.6 $\pm$ 1.0
1.6	9.6	1:6	7.6 $\pm$ 0.4
3.3	9.6	1:3	8.0 $\pm$ 0.7
4.3	13	1:3	10.1 $\pm$ 0.9

[a] 20 μM external ZnTMPyP^{4+}

[b] Vesicles formed in 0.05 M phosphate, pH 6.5

[c] Initial concentration

[d] Deactivation rate of excited Zn(II) porphyrin detected at 890 nm, at 23°C, excitation wavelength 532 nm; results are average values of three or more individual determinations.

Table 13. Recombination Rates of $ZnTMPy^{5+}$ and $C_{16}MV^+$ in $C_{16}MV^{2+}$-PC

Vesicles[a]

$[C_{16}MV^{2+}]$[b] (mM)	$[PC]$[b] (mM)	$C_{16}MV^{2+}/PC$	$10^8 \cdot k$ $(M^{-1} s^{-1})$[c]
1.6	9.6	1:6	6.5
4.3	12.8	1:3	1.5
0.11	3.2	1:30	15
1.1	6.0	1:6	1.8
1.6	9.6	1:6	6.8

[a]Vesicles formed in 0.05 M phosphate, pH 6.5; excitation wavelength

$\lambda = 532$ nm, at 23°C.

[b]Initial concentrations determined by ^{14}C analysis.

[c]Determined from slopes of second-order decay curves (1/Absorbance vs.

time) of $C_{16}MV^+$ formation following excitation, i.e., $k = \epsilon \cdot \ell \cdot$ slope,

with $\ell = 1$ cm, $\epsilon_{610} = 1.2 \times 10^4$ M^{-1} cm^{-1} for $C_{16}MV^+$; detection

wavelength $\lambda = 610$ nm.

Table 14. Rate Data for Slow Reduction of PC-Bound $(NH_3)_5Ru-4-(11'-$dodecenyl)py^{3+} Ion by External Reductants[a]

Reductant (mM)		$10^{-4} \cdot k_1$ (s^{-1})	% Total optical change	Experimental conditions
Cr^{2+}	0.8	9.3	32	b
	1.4	7.8	28	b
	1.6	2.8	38	c
	2.9	4.7	35	b
	3.8	7.2	30	b
	4.3	3.5	27	b
	5.1	4.5	34	c
	5.1	6.0	32	c
	7.4	9.3	27	c
V^{2+}	0.07	3.3	31	c
	0.3	7.1	32	c
	0.7	5.5	26	c
Ascorbate	0.1	13.0	49	c
	0.4	18.0	40	c
	1.0	15.0	31	c

[a]At ambient temperature

[b]Initial conditions: 3.4 mM PC, 0.2 mM Ru(III), in 0.1 M sodium acetate, pH 4.0

[c]Initial conditions: 7.5 mM PC, 0.5 mM Ru(III), in 0.1 M sodium acetate, pH 4.0

Table 15. Temperature Dependent Slow Reduction of PC-Bound

$(NH_3)_5Ru-4-(11'-dodecenyl)py^{3+}$ by Cr^{2+} Ion[a]

Temperature (°C)	$10^{-4} \cdot k \ (s^{-1})$	% Total optical change
10	2.3 ± 0.3	28 ± 3
15	7.8 ± 0.1	29 ± 1
20	9.4 ± 0.7	29 ± 1
25	9.7 ± 1.6	35 ± 6
30	14.6 ± 4.5	32 ± 1

[a]Experimental conditions: 7 mM PC, 0.17 mM Ru(III) sonicated

in 0.1 M sodium acetate, pH 4.0; 0.6 mM Cr^{2+} added externally.

Table 16.   Temperature Dependent Slow Reduction of PC-Bound

$(NH_3)_5Ru-4-(11'-dodecenyl)py^{3+}$ by Ascorbate Ion[a]

Temperature (°C)	$10^{-4} \cdot k \ (s^{-1})$	% Total optical change	
5	1.9	22	b
10	3.1	24	
15	4.9	37	
20	6.7	38	
25	10.5	32	
30	13.7	32	
5	3.3	31	c
10	4.3	37	
15	5.3	36	
20	7.2	33	
25	14.3	43	
5	2.0	38	d
10	4.1	43	
15	7.3	43	
20	9.9	36	
30	12.6	39	

[a]0.6 mM ascorbate added externally.

[b]Initial concentrations: 7.5 mM PC, 0.17 mM Ru(III) sonicated in 0.1 M sodium acetate, pH 4.0.

[c]Initial concentrations: 7.5 mM PC, 0.14 mM Ru(III) sonicated in 0.1 M potassium acetate, pH 4.0.

[d]Initial concentrations: 7.5 mM PC, 0.3 mM Ru(III) sonicated in 0.1 M potassium acetate, pH 4.0.

Table 17. Temperature Dependent Reduction of PC-Bound

$(NH_3)_5Ru-4-(11'-dodecenyl)py^{3+}$ by V^{2+} Ion[a,b]

Temperature (°C)	$10^{-4} \cdot k \ (s^{-1})$	% Total optical change
10	6.0	24
15	7.2	23
20	17.0	17
25	12.0	16

[a] 0.6 mM V^{2+} added externally.

[b] Initial concentrations: 3.7 mM PC, 0.4 mM Ru(III) in 0.1 M

sodium acetate, pH 4.0.

Table 18. Temperature Dependent Slow Reduction of PC-Bound

$(NH_3)_5Ru$-4-(11'-dodecenyl)py^{3+} by Cr^{2+} Ion in

CCCP-Incorporated Vesicles[a,b]

Temperature (°C)	$10^{-4} \cdot k$ (s^{-1})	% Total optical change
10	4.5	24
15	5.8	30
20	8.0	32
25	16.2	30

[a]CCCP: carbonyl cyanide m-chlorophenylhydrazone.

[b]Experimental conditions: 5 μM CCCP, 0.17 mM Ru(III), 7 mM PC

sonicated in 0.1 M potassium acetate, pH 4.0; 0.6 mM Cr^{2+} added

externally.

Table 19. Temperature Dependent Slow Reduction of PC-Bound

$(NH_3)_5Ru-4-(11'-dodecenyl)py^{3+}$ by Cr^{2+} Ion in

Valinomycin-Incorporated Vesicles[a]

Temperature (°C)	$10^{-4} \cdot k \ (s^{-1})$	% Total optical change
5	1.1	32
10	4.0 ± 1.0	29 ± 1
15	6.6 ± 0.5	30 ± 3
20	6.9 ± 0.5	30 ± 1
25	9.4 ± 2.0	32 ± 5
30	12.3 ± 6.4	34 ± 4

[a]Experimental conditions: 7 μM valinomycin, 0.17 mM Ru(III), 7 mM
PC sonicated in 0.1 M potassium acetate, pH 4.0; 0.6 mM Cr^{2+}
externally added.

Table 20. Summary of Kinetics of Slow Reduction of PC-Bound $(NH_3)_5Ru-4-(11'-dodecenyl)py^{3+}$ by External Reductants

Reductant	10^{-4} k (s^{-1})	% Total optical change	Activation parameters ($\Delta H^{\ddagger}$, $\Delta S^{\ddagger}$ (23°C)
Cr^{2+} (0.8 – 7.4 mM)[a]	6.9 ($\pm$ 2.4)[e]	30 ($\pm$ 5)[e]	13 kcal/mol, −29 e.u.
V^{2+} (0.07 – 0.70 mM)[a]	5.3 ($\pm$ 2.0)[e]	30 ($\pm$ 3)[e]	8.3 kcal/mol, −43 e.u.
Cu^+ (0.48 – 1.5 mM)[b]	17.4 ($\pm$ 8.8)	17 ($\pm$ 5)	Bleaching side reaction
Ascorbate (0.14–1.0 mM)[a]	13.8[e]	35 ($\pm$ 6)[f]	11.5 kcal/mol, −33 e.u.
Cr^{2+} ([valinomycin] = 7 µM)[c]	6.9 ($\pm$ 0.5)[i]	31 ($\pm$ 4)[g]	11.8 kcal/mol, −32.7 e.u.
Cr^{2+} ([CCCP] = 5 µM)[d]	8.0[i]	30 ($\pm$ 2)[h]	14 kcal/mol, −24 e.u.

[a]Experimental conditions are those given in Table 14.

[b]Initial concentrations: 7.5 mM PC, 0.4 mM Ru(III) in 0.1 M NaOAc, pH 4.0.

[c]Experimental conditions are those given in Table 19.

[d]Experimental conditions are those given in Table 18.

[e]Averaged value of those listed in Table 14.

[f]Averaged value of those listed in Table 16.

[g]Averaged value of those listed in Table 19.

[h]Averaged value of those listed in Table 18.

[i]At 20°C.

Table 21. Bleaching of $(NH_3)_5Ru-4-(11'-$
dodecenyl)py^{2+} in Reactions Where

Reductant is Concentration-Limiting[a]

Reductant (μM)		$10^{-4} \cdot k$ (s^{-1})
Ascorbate	45	2.9
	90	1.2
Cr^{2+} (TFA, 0.1 M)	160	1.1
	40	0.86
Cr^{2+} (ClO_4^-)[d]	40	2.2
	40	2.9[b]
	40	0.6[c]
V^{2+} (ClO_4^-)[e]	35	13
V^{2+} (TFA, 0.1 M)	22	0.14
V^{2+} (ClO_4^-)[e,f]	17	1.6

[a][Ru^{3+}] $\approx$ 0.1–0.3 mM, in 0.1 M NaOAc, pH 4.0,
 at 15°C.

[b]At 25°C.

[c]At 5°C.

[d]Added 0.12 mM $NaClO_4$

[e]Added 1.2 mM $NaClO_4$

[f]Added 3 mM preformed PC vesicles.

Table 22. Physical Characteristics of ZnTMPyP^{4+}-DHP Vesicles[a]

[DHP]/[ZnTMPyP^{4+}][b]	% Surface coverage[c]	Mean P...P distance (Å)[d]	^{3}(ZnTMPyP^{4+}) Deactivation k(s^{-1})	Initial absorbance[e]
600	0.24	300	$k_1 = 1.5 \times 10^5$	$A^1 = .047$
			$k_2 = 3.1 \times 10^4$	$A^2 = .046$
			$k_3 = 5.6 \times 10^3$	$A^3 = .112$
120	1.2	103	$k_1 = 3.4 \times 10^5$	$A^1 = .107$
			$k_2 = 3.5 \times 10^4$	$A^2 = .051$
			$k_3 = 1.9 \times 10^3$	$A^3 = .034$
30	4.8	52	$k_1 = 3.9 \times 10^5$	$A^1 = .154$
			$k_2 = 4.1 \times 10^4$	$A^2 = .071$
			$k_3 = 4.7 \times 10^3$	$A^3 = .047$

[a] In 0.02 M Tris, pH 7.8, 23°C

[b] [ZnTMPyP^{4+}] = 10-40 μM; [DHP] = 1.2-6.0 mM

[c] Calculated by assuming 70 and 100 Å^2 for DHP monomer and ZnTMPyP^{4+} surface areas, respectively.

[d] Center-to-center distance.

[e] Absorbances at 830 nm of transient species decaying by each pathway extrapolated to initial time.

Table 23.   Quenching of Photoexcited Zn(II) Porphyrin by DHP-Bound Viologen[a]

Viologen	Sensitizer		Quenching rate constant
$C_{14}MV^{2+}$	$ZnTMPyP^{3-}$	(π-anion)	1.7×10^9 M^{-1} s^{-1} (b)
C_{14} MV^{2+}	$^3ZnTPPS^{4-}$	(triplet)	2.4×10^8 M^{-1} s^{-1} (c)
MV^{2+}	$^3ZnTPPS^{4-}$	(triplet)	2.5×10^9 M^{-1} s^{-1} (d)
$C_{14}MV^{2+}$	$^3ZnTMPyP^{4+}$	(bound triplet)	$\sim 10^3$ s^{-1} (b)

[a] 532 nm excitation wavelength, 600 and 826 nm detection wavelengths.

[b] Experimental conditions are those given in Figure 56.

[c] 20 µM $ZnTPPS^{4-}$, 3.6 mM DHP, 67-600 µM $C_{14}MV^{2+}$ in 0.02 M Tris, pH 7.8, at 23°C.

[d] 20 µM $ZnTPPS^{4-}$, 3.6 mM DHP, 33-200 µM MV^{2+} in 0.02 M Tris, pH 7.8, at 23°C.

Table 24.   Free-Energy Charge in PC-Bound $(NH_3)_5Ru-4-(11'-dodecenyl)py^{3+}$

Reduction by External Reductant

Ion	$E°_{1/2}(V)^a$	$\Delta E°^b$	$\Delta E°-E_{charge}{}^c$	$\Delta E_t'{}^d$
$Ru^{3+/2+}$	0.302	0	−0.098	−−−−−
Reductant:				
$Cu^{2+/+}$	0.153	0.149	0.051	−0.954
$V^{3+/2+}$	−0.255	0.557	0.459	−0.546
$Cr^{3+/2+}$	−0.410	0.712	0.614	−0.391
Ascorbate	−0.058	0.360	0.262	−0.743

[a] Reduction potentials

[b] $\Delta E° = E°_{1/2}(Ru^{3+/2+}) - E°_{1/2}(reductant)$

[c] $E_{charge} = 0.098$ V (Appendix III)

[d] $\Delta E_t' = \Delta E° - RT/F \ln \{Ru_0^{2+}\}[Ox.]/[^-Ru_{in}^{3+}][red.] - E_{cap}$, with [red.]/[ox.] $= 4$, $[Ru_0^{2+}] = 2[Ru_{in}^{3+}]$; $E_{cap} = 1.12$ V (Appendix III), $RT/F = 0.025$ V, at 23°C.
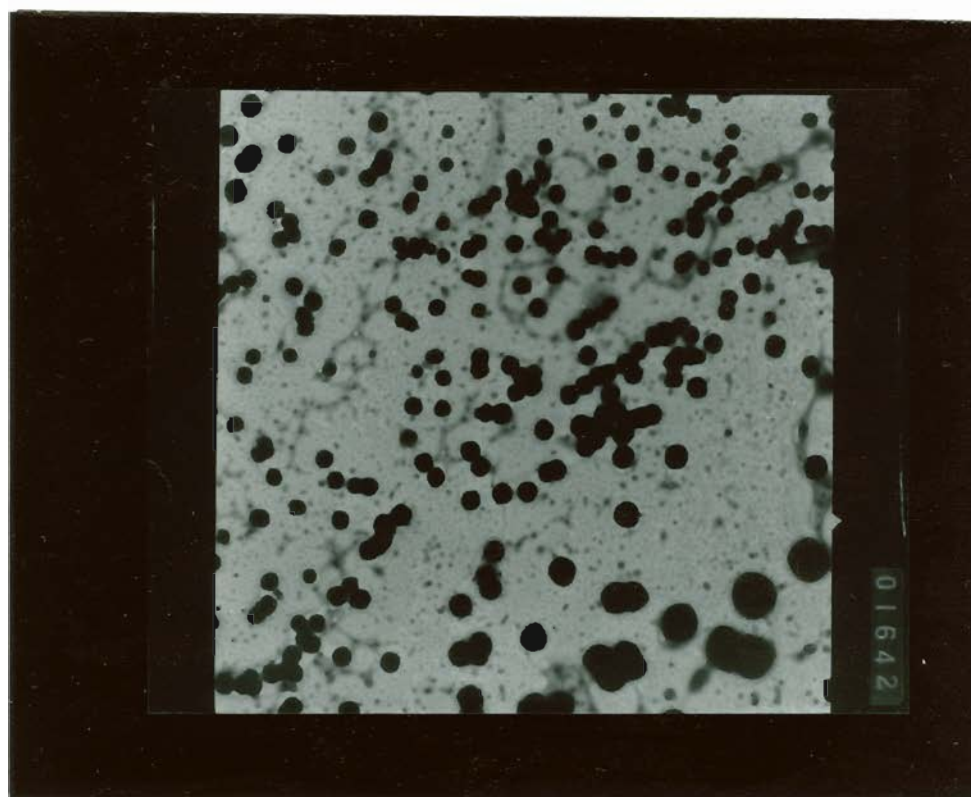
10,000 X   5000 Å

Figure 1. Electron micrograph of polydisperse PC vesicles. PC in 0.01 M sodium acetate, pH 4.0, after 3 hours of sonication; stained with 5% phosphotungstic acid.
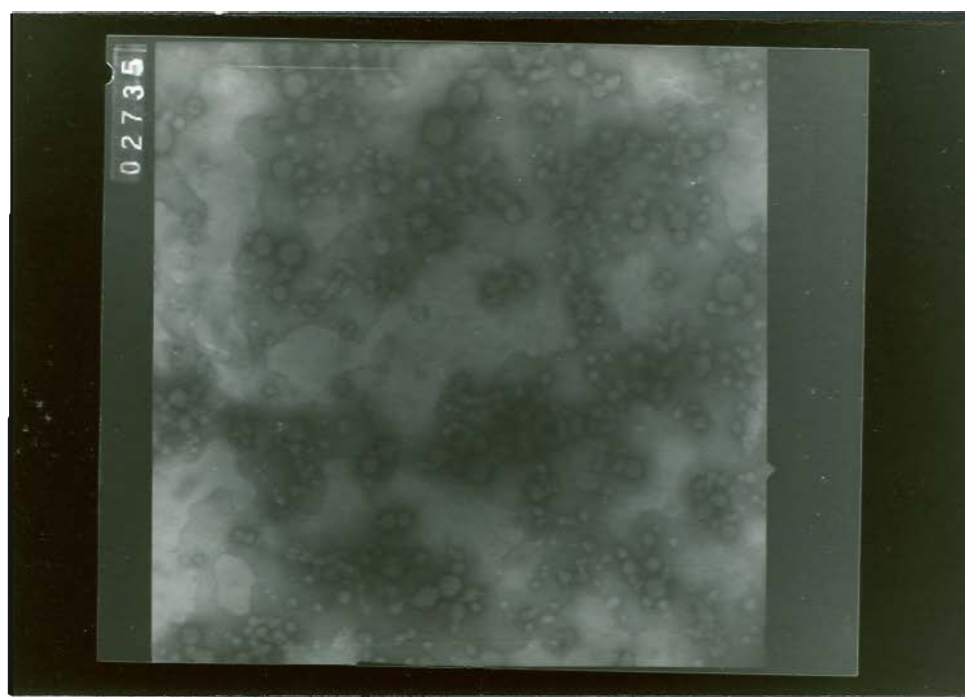
42,000 X   2000 Å

Figure 2. Electron micrograph of PC vesicles. PC vesicles from
the supernatant fraction of sonicated PC suspension after 100,000 G
centrifugation; stained with 5% phosphotungstic acid.

a   b   c
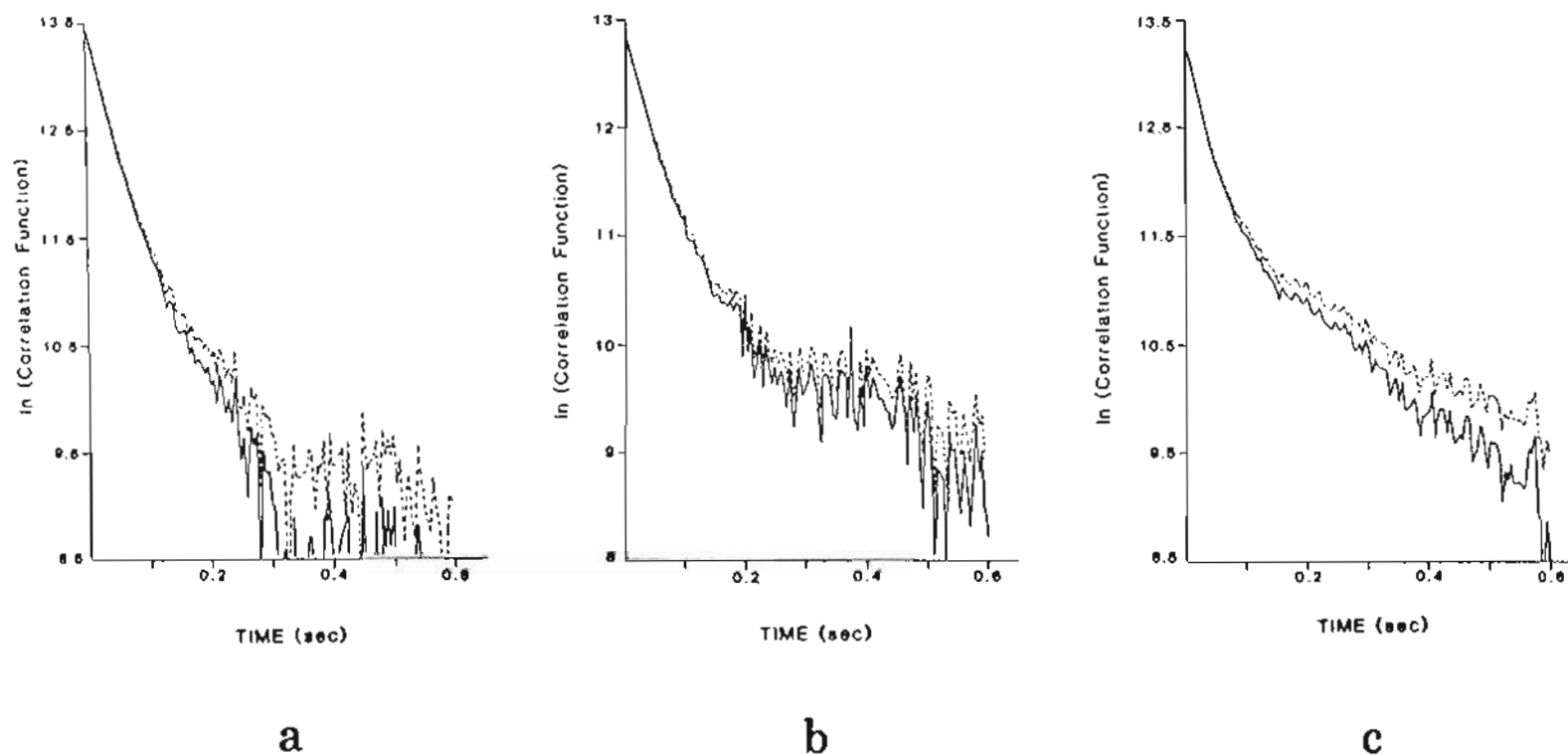
Figure 3. Autocorrelation decay curves of phosphatidylcholine (PC) vesicles.

Curve a: 0.1 mM PC in 0.01 M sodium acetate, pH 4.0.

Curve b: 0.6 µM $(NH_3)_5Ru-4-(11'-dodecenyl)py^{3+}$ with 10 µM PC

             (1:17, Ru:PC) in 0.01 M sodium acetate, pH 4.0.

Curve c: 2.2 µM $(NH_3)_5Ru-4-(11'-dodecenyl)py^{3+}$ with 0.1 mM PC

             (1:4.5, Ru:PC) in 0.01 M sodium acetate, pH 4.0.

a   b
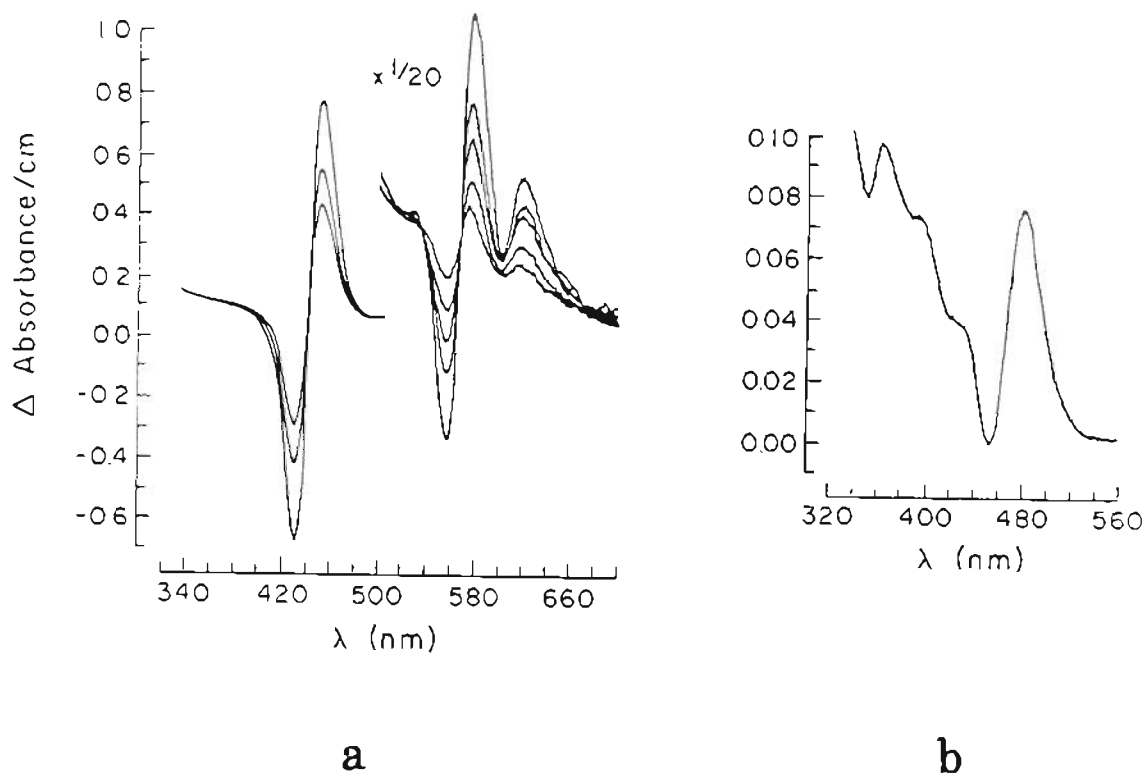
Figure 4. Optical absorption difference spectra of DHP-bound

sensitizers vs. sensitizers in homogeneous solution.

Graph a: 2.4 mM DHP vs 1.6-9.5 µM ZnTMPyP^{4+} in 0.05 M

TEOA, pH 7.8.

Graph b: 0.36 mM Ru(bpy)$_3^{2+}$, 1.8 mM DHP vs. 0.36 mM Ru(bpy)$_3^{2+}$

in 0.1 M tricine, pH 7.2.
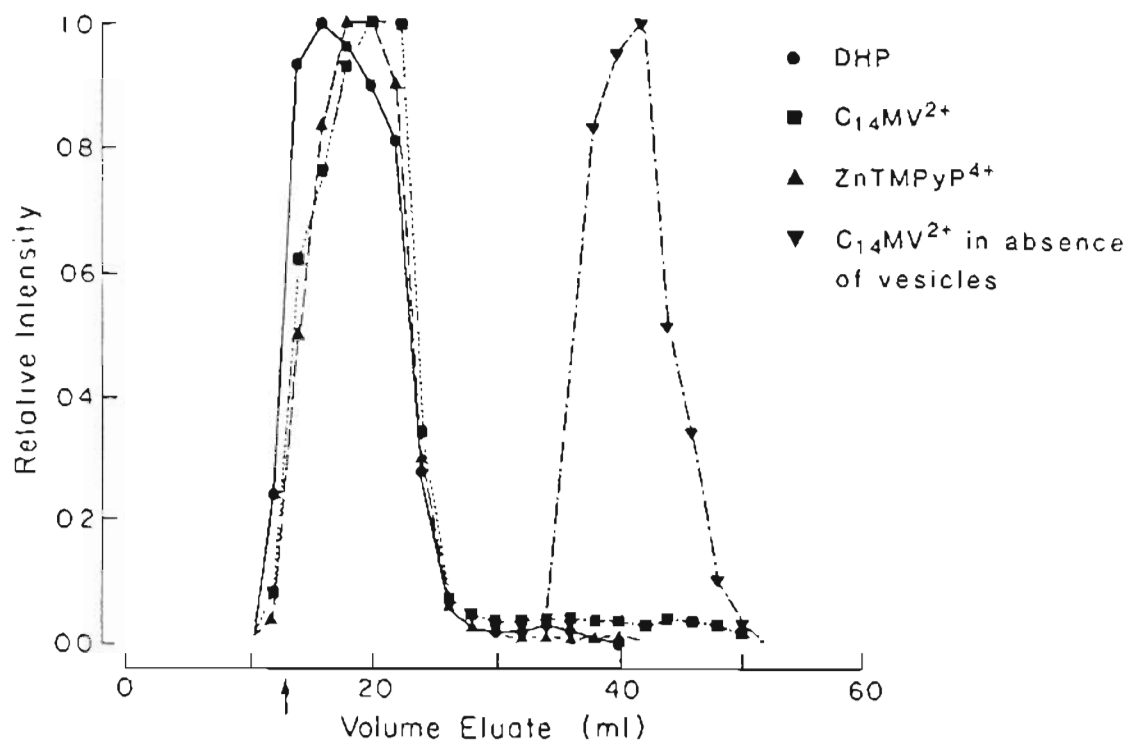
Figure 5. Elution profile of $ZnTMPyP^{4+}$-$C_{14}MV^{2+}$-DHP vesicles on Sephadex G-50. 2.4 mM DHP sonicated in the presence of 0.5 mM $C_{14}MV^{2+}$ and 20 μM $ZnTMPyP^{4+}$ in 0.02 M Tris, pH 7.8. Solid line: relative turbidity. Dashed line: Zn(II) porphyrin absorption, measured at 446 nm. Dotted line: viologen, measured as the $C_{14}MV^{+}$ radical ion at 560 nm by dithionite reduction of eluate fractions. Alternate dash-dotted line: viologen peak obtained in the absence of DHP vesicles. The arrow indicates column void volume determined by elution of blue dextran.
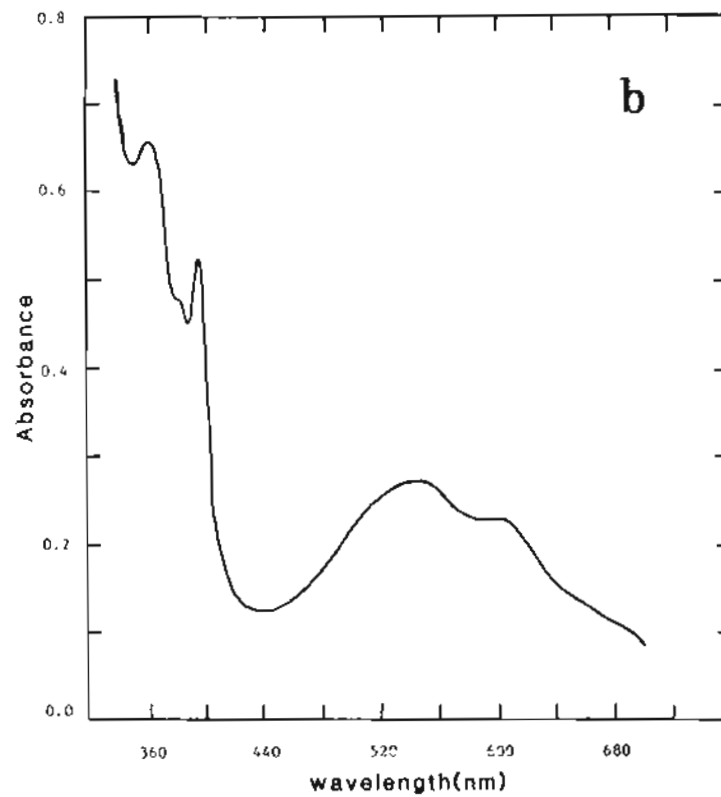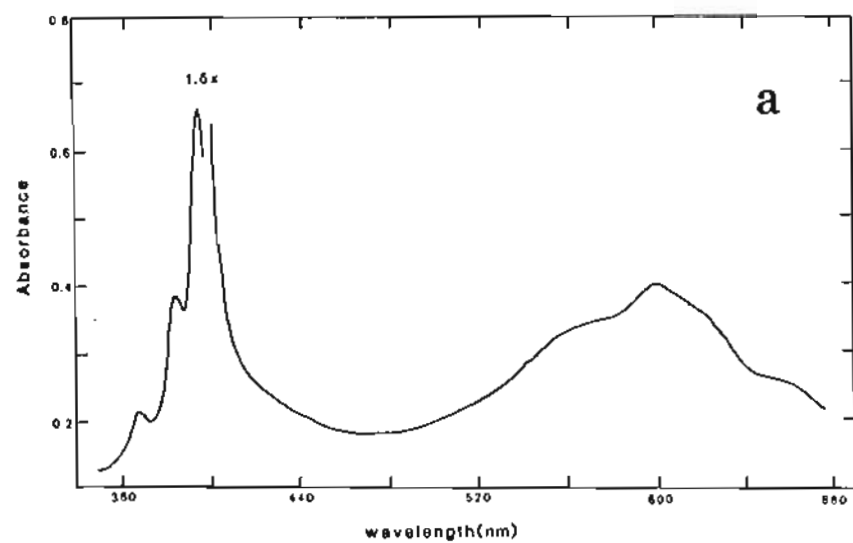
Figure 6. **Optical absorption spectra of methylviologen radical cation (MV⁺).** MV⁺ obtained by dithionite reduction.

a: 3.0 mM DHP and 1.2 mM MV^{2+} sonicated in 0.05 M Tris, pH 7.8.

b: 25 μM MV^{2+} in 0.05 M Tris, pH 7.8.
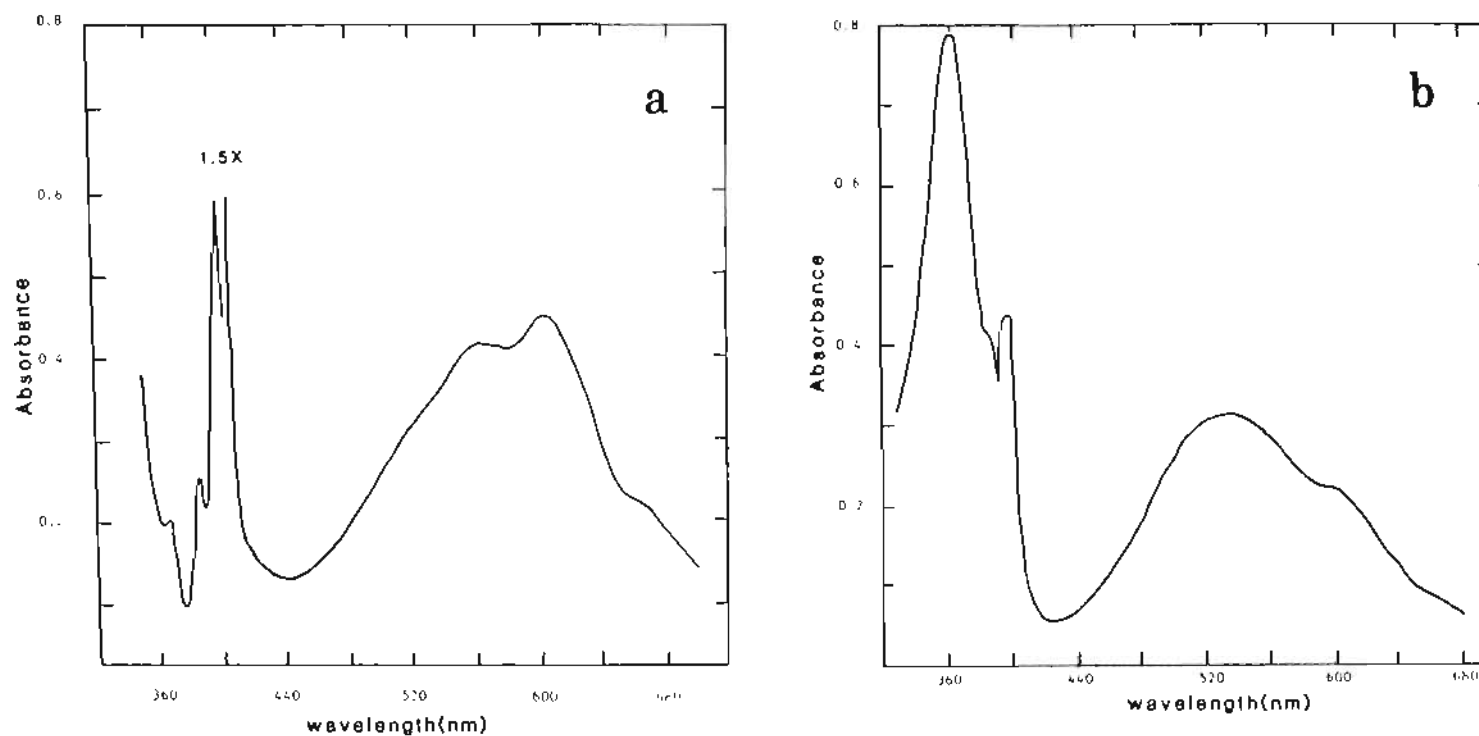
Figure 7. Optical absorption spectra of N-methyl-N'-hexadecylbipyridine radical cation ($C_{16}MV^+$). Initial conditions: 3.0 mM DHP and 1.2 mM $C_{16}MV^{2+}$ sonicated in 0.02 M Tris, pH 7.8, followed by Sephadex G-50 chromatography.

a. DHP-bound $C_{16}MV^+$ obtained by dithionite reduction of viologen-vesicle fractions.

b. $C_{16}MV^+$ obtained by dithionite reduction of viologen fractions (vesicle free).
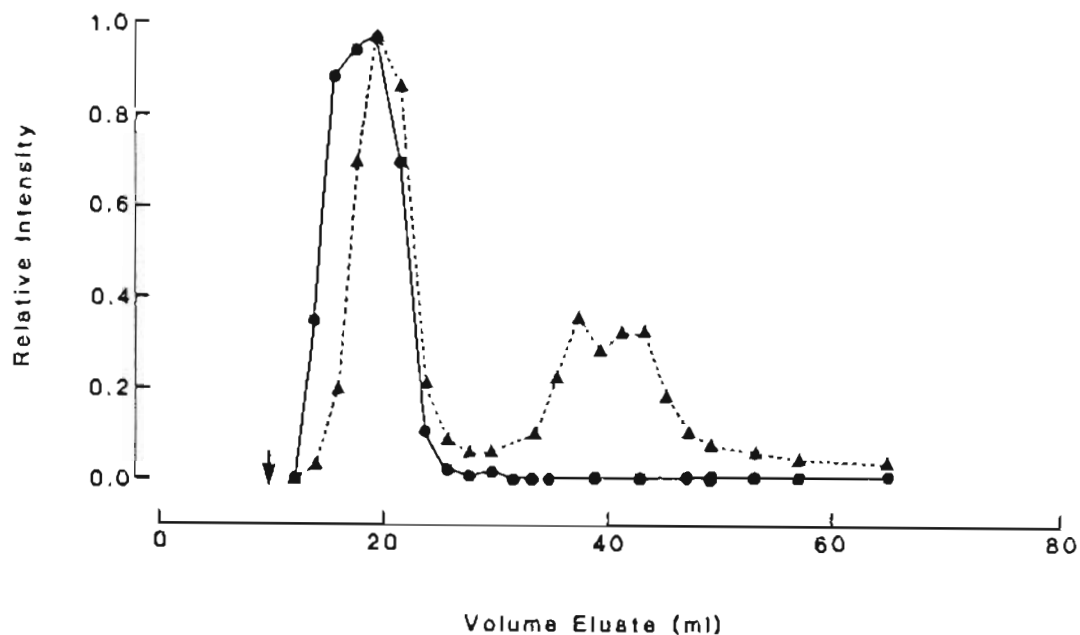
Figure 8. Elution profile of MV^{2+}-DHP vesicles on Sephadex G-50.
4.6 mM DHP and 1.0 mM MV^{2+} sonicated in 0.1 M triethanoamine, pH
7.8. Solid line: relative turbidity. Dashed line: viologen, measured
at 600 nm, as MV^+ by dithionite reduction of eluate fractions. The
arrow indicates the column void volume.
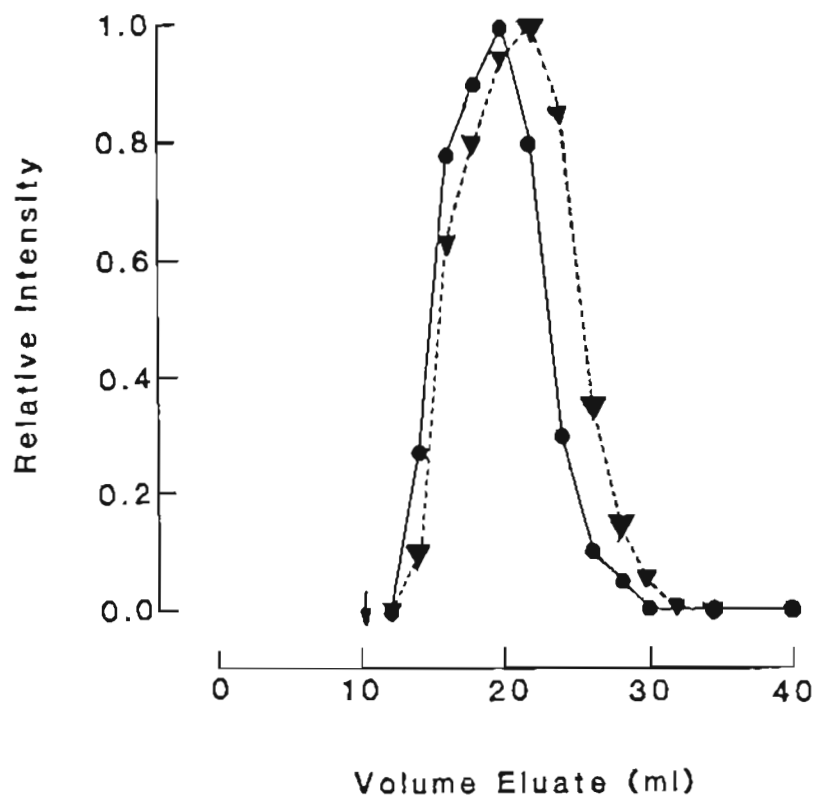
Figure 9. Elution profile of $C_{16}MV^{2+}$-DHP vesicles on Sephadex G-50. 3.0 mM DHP and 0.4 mM $C_{16}MV^{2+}$ sonicated in 0.02 M tris(hydroxymethyl)aminomethane (Tris), pH 7.8. Solid line: relative turbidity. Dashed line: viologen, measured at 600 nm, as $C_{16}MV^+$ by dithionite reduction of eluate fractions. The arrow indicates column void volume.
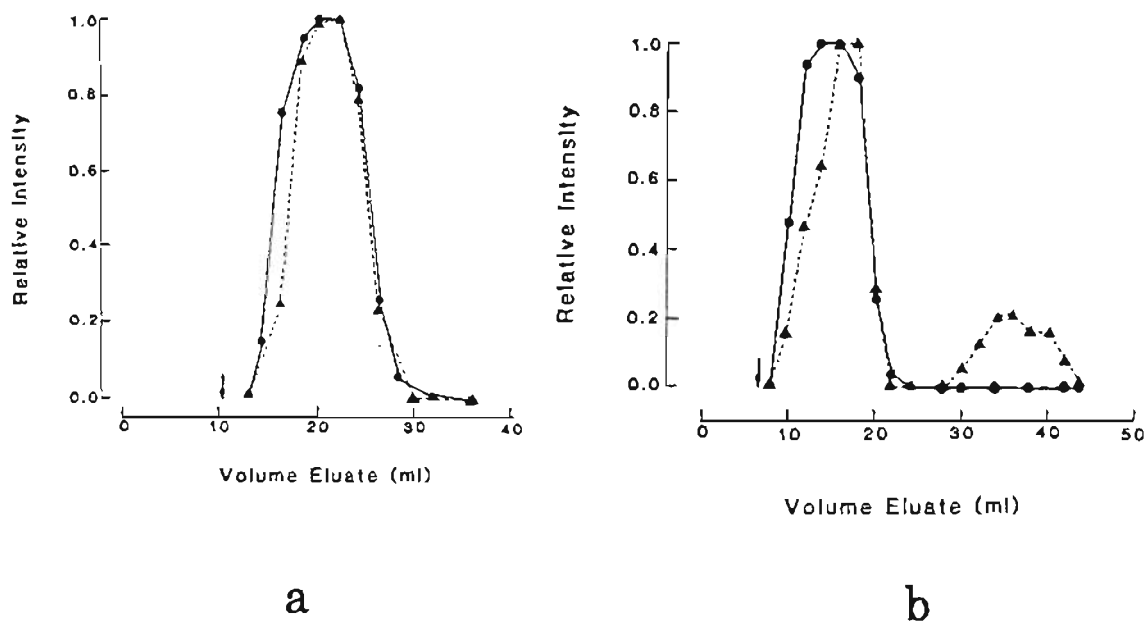
Figure 10.   Elution profile of alkylviologen-PC vesicles on
Sephadex G-50.

Graph a: 2.6 mM PC and 0.16 mM $C_{16}MV^{2+}$ sonicated in 0.05 M

phosphate, pH 6.5.   Solid line: relative turbidity.

Dashed line: viologen, measured at 398 nm, as

$C_{16}MV^+$ by dithionite reduction of eluate fractions.

Graph b: 3.2 mM PC and 0.57 mM $C_{14}MV^{2+}$ sonicated in 0.05 M

phosphate, pH 6.5.   Solid line: relative turbidity.

Dashed line: viologen, measured at 398 nm, as

$C_{14}MV^+$ by dithionite reduction of eluate fractions.

The arrows indicate column void volume.
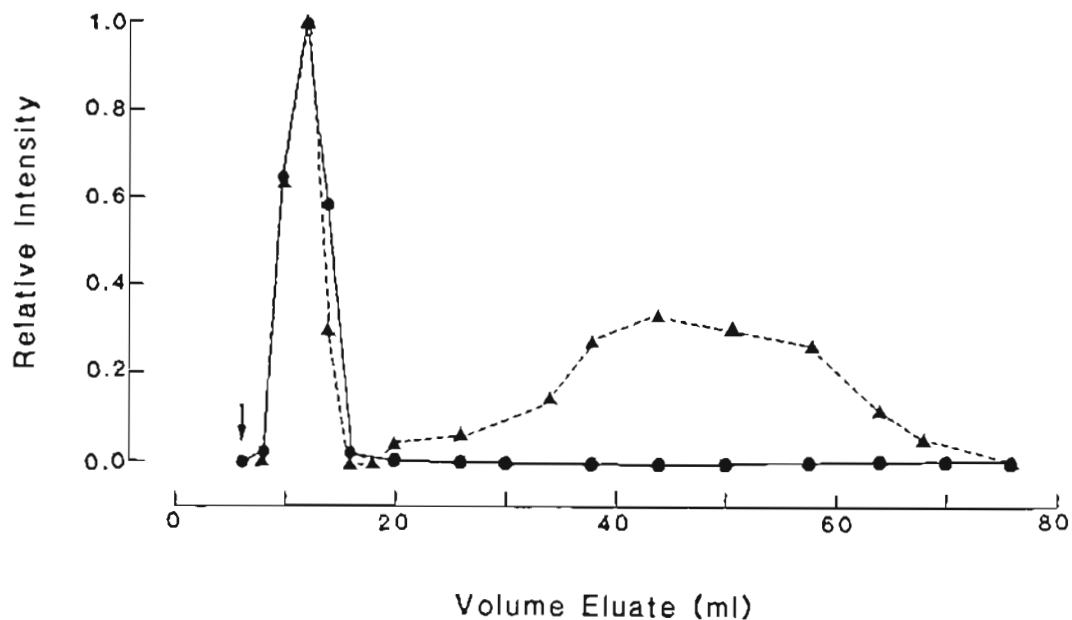
Figure 11. **Elution profile of external $C_{16}MV^{2+}$-PC vesicles on Sephadex G-50.** 0.53 mM $C_{16}MV^{2+}$ added externally to preformed PC (3 mM) vesicles in 0.05 M phosphate, pH 6.5. Solid line: relative turbidity. Dashed line: viologen, measured at 560 nm, as $C_{16}MV^{+}$ by dithionite reduction of eluate fractions. The arrow indicates column void volume.

a

b
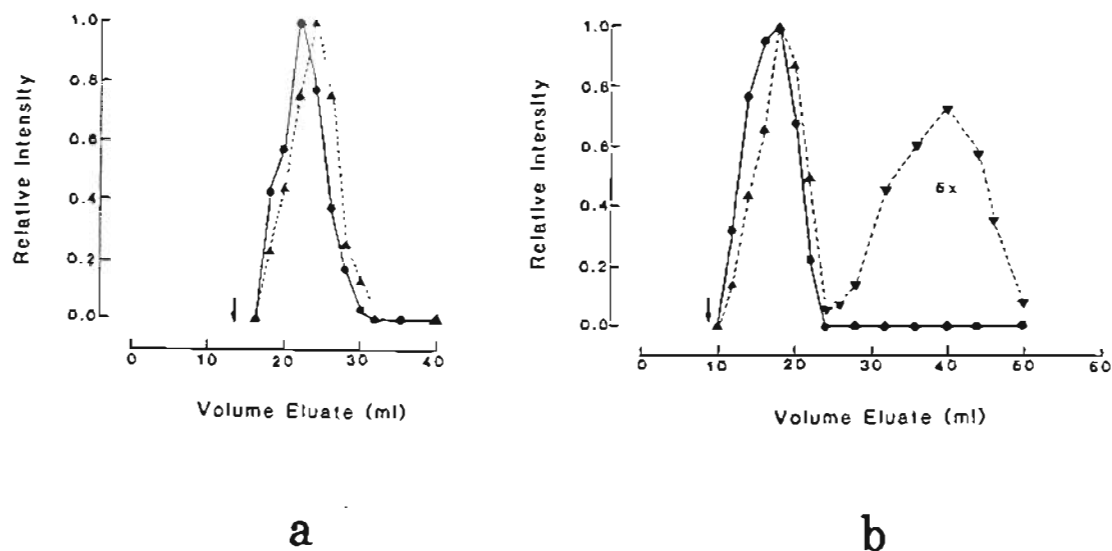
Figure 12. Elution profile of $(NH_3)_5Ru-4-(11'-dodecenyl)py^{3+}-PC$
and $(NH_3)_5Ru-4-(8'-nonenyl)py^{3+}$ on Sephadex G-50.

Graph a: 3 mM PC and 23 µM $(NH_3)_5Ru-4-(11'-dodecenyl)py^{3+}$ sonicated in 0.02 M phosphate, pH 6.0. Solid line: relative turbidity. Dashed line: Ru(II) ion, measured at 415 nm, obtained by ascorbate reduction of eluate fractions.

Graph b: 3 mM PC and 28 µM $(NH_3)_5Ru-4-(8'-nonenyl)py^{3+}$ sonicated in 0.02 M phosphate, pH 6.0. Solid line: relative turbidity. Dashed line: Ru(II) ion, measured at 400 nm, obtained by ascorbate reduction of eluate fractions. The arrows indicate column void volume.

a

b
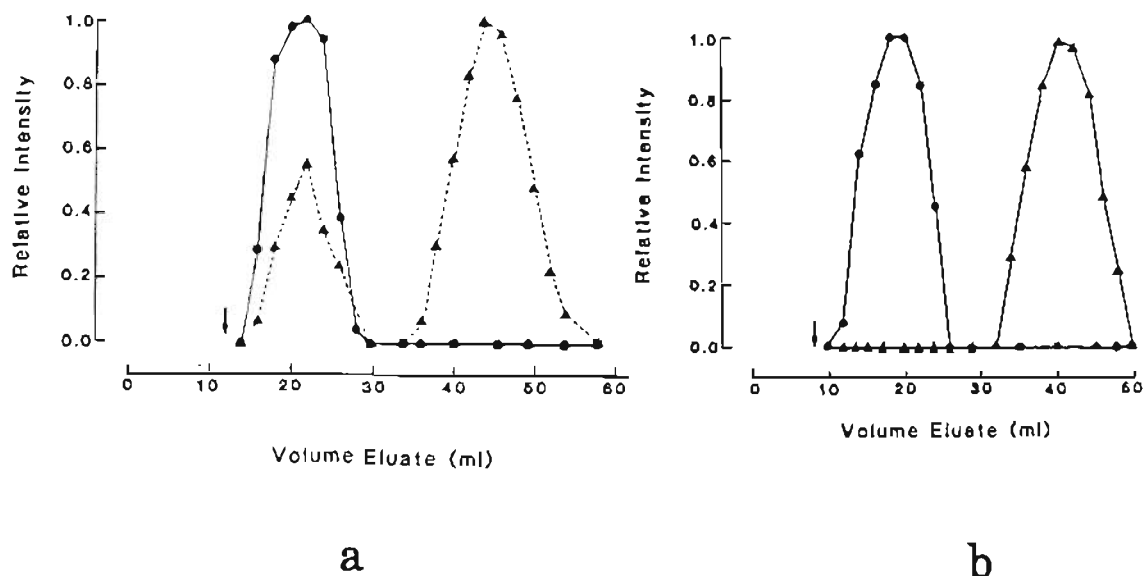
Figure 13. Elution profile of $(NH_3)_5Ru-4-(6'-heptenyl)py^{3+}$-PC and

$(NH_3)_5Ru-4-(3'-butenyl)py^{3+}$-PC vesicles on Sephadex G-50.

Graph a: 3 mM PC and 15 μM $(NH_3)_5Ru-4-(6'-heptenyl)py^{3+}$

sonicated in 0.02 M phosphate, pH 6.0. Solid line:

relative turbidity. Dashed line: Ru(II) ion,

measured at 400 nm, obtained by ascorbate reduction

of eluate fraction.

Graph b: 3 mM PC and 14 μM $(NH_3)_5Ru-4-(3'-butenyl)py^{3+}$

sonicated in 0.02 M phosphate, pH 6.0. Circle:

relative turbidity. Triangle: Ru(II) ion, measured

at 400 nm, obtained by ascorbate reduction of eluate

fractions. The arrows indicate column void volume.

a

b
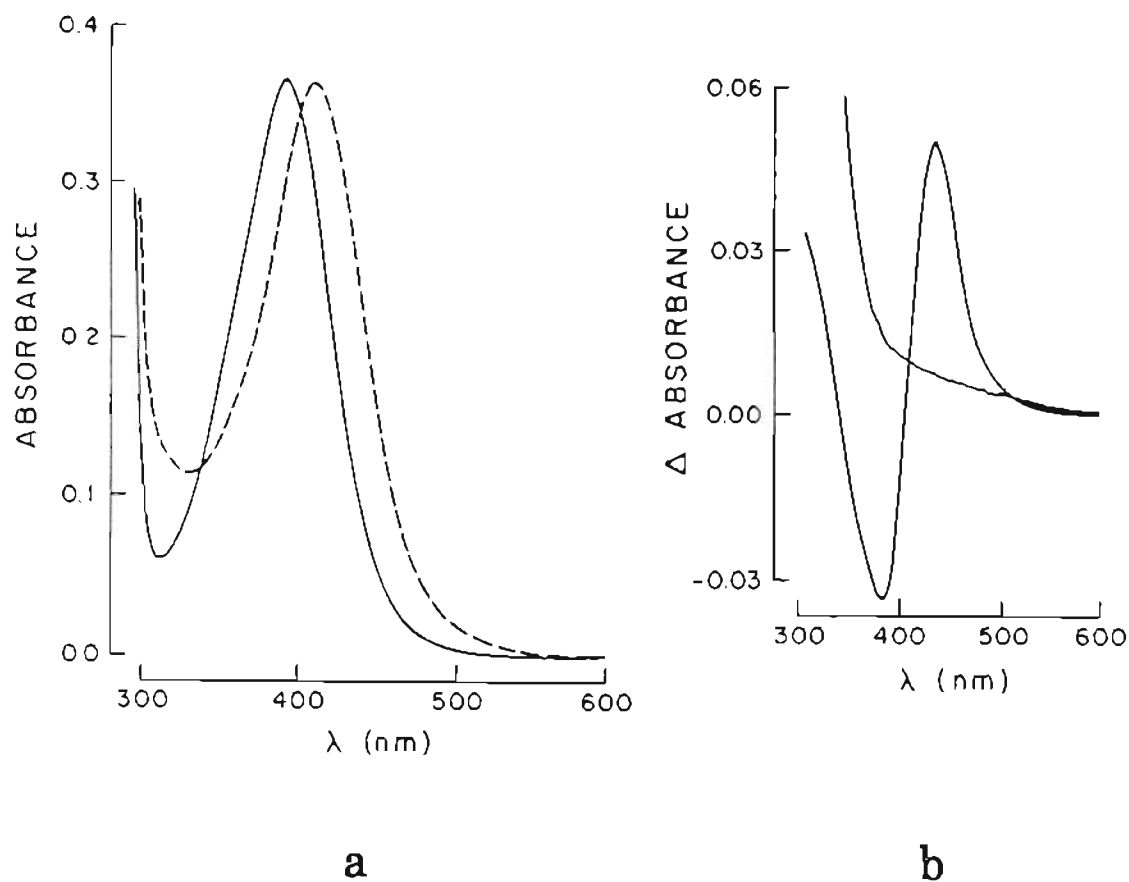
Figure 14. Optical absorption spectra of $(NH_3)_5Ru-4-(11'-$
dodecenyl)py^{2+}-PC vesicles.

a. Solid curve: absorption spectrum of 68 µM Ru(II) ions in

0.02 M phosphate, pH 6.0. Dotted curve: Absorption

spectrum of 68 µM Ru(II) added to preformed PC (3 mM)

vesicles.

b. Difference spectrum of Ru(II)-PC vesicles vs. Ru(II) ions.

Conditions are the same as in a; Ru(II) ions obtained by

ascorbate reduction; baseline is vesicles vs. buffer

solution.

a   b
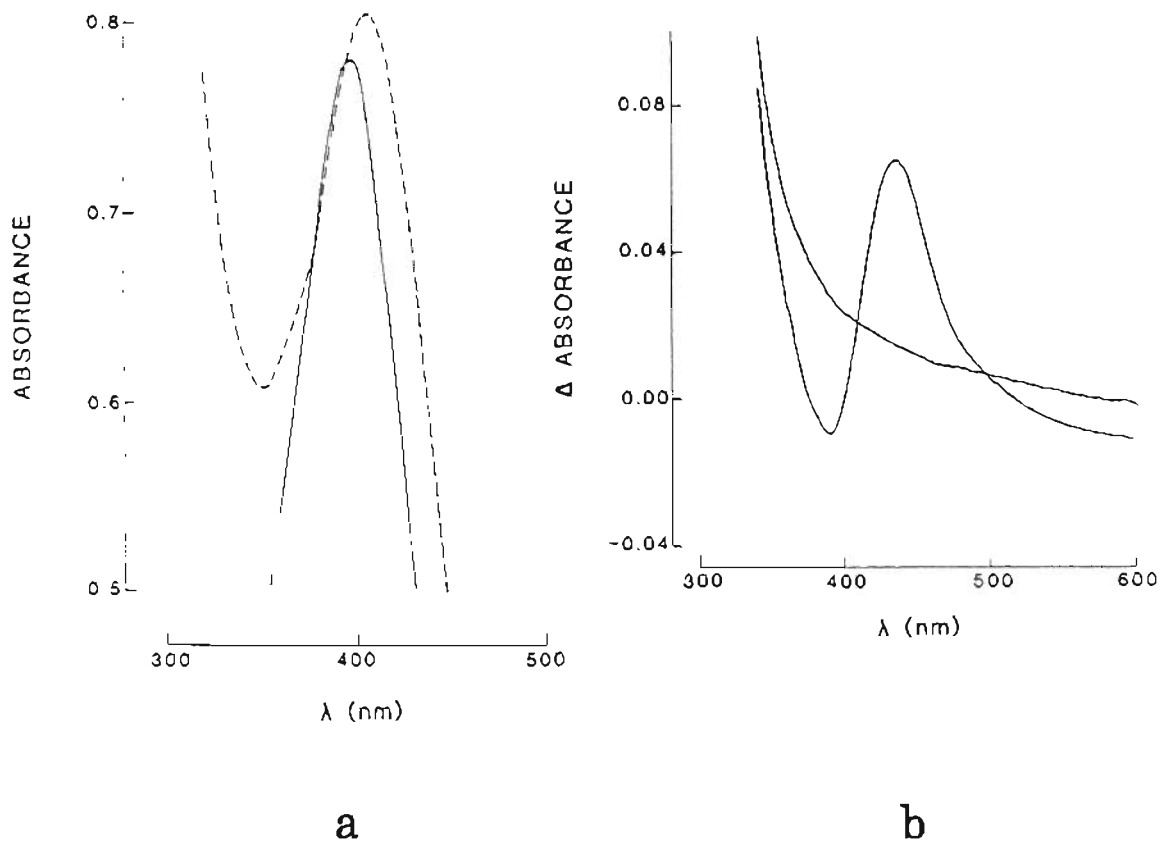
Figure 15. Optical absorption spectra of $(NH_3)_5Ru-4-(8'-$
nonenyl)py^{3+}-PC vesicles.

    a. Solid curve: absorption spectrum of 0.1 mM Ru(II) ions in

        0.02 M phosphate, pH 6.0. Dotted curve: absorption

        spectrum of 0.1 mM Ru(II) added to preformed PC (3 mM)

        vesicles.

    b. Difference spectrum of Ru(II)-PC vesicles vs. Ru(II) ions.

        Conditions are the same as in a; Ru(II) ions obtained by

        ascorbate reduction; baseline is vesicles vs. buffer

        solution.

a   b
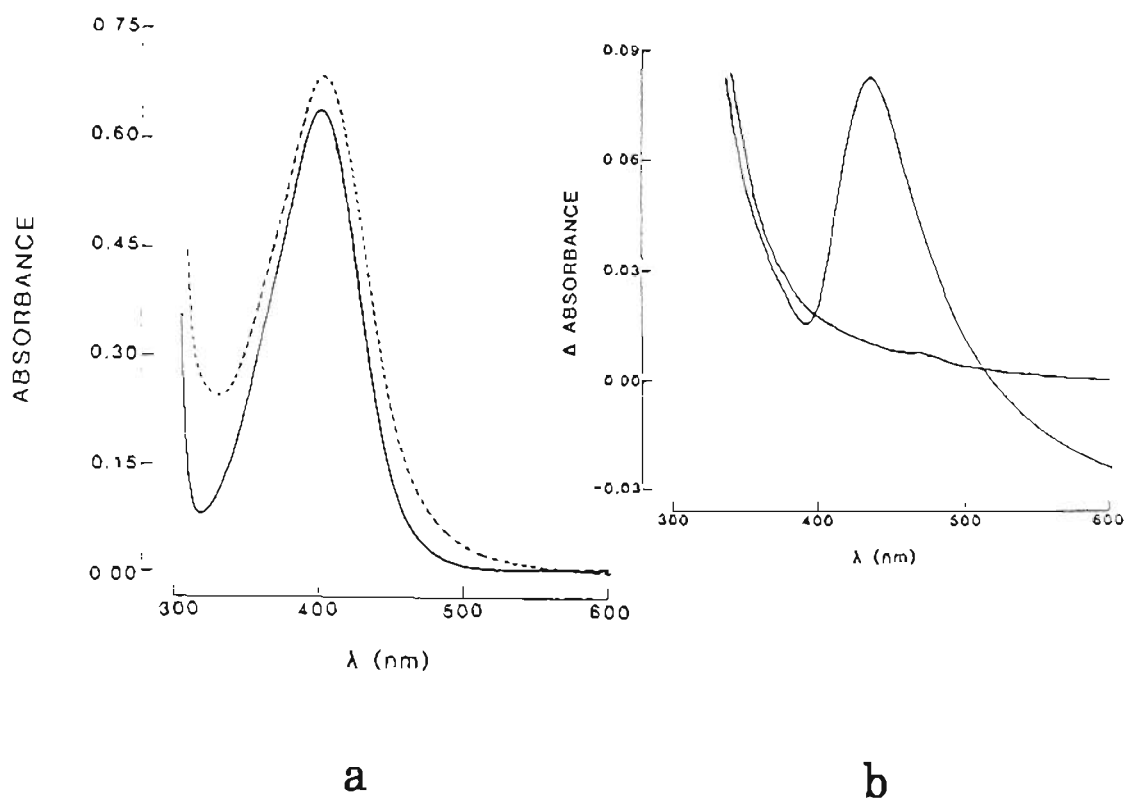
Figure 16. Optical absorption spectra of $(NH_3)_5Ru-4-(3'-$
butenyl)py^{3+}-PC vesicles.

a. Solid curve: absorption spectrum of 90 μM Ru(II) ions in
    0.02 M phosphate, pH 6.0. Dotted curve: absorption
    spectrum of 90 μM Ru(II) added to preformed PC (3 mM)
    vesicles.

b. Difference spectrum of Ru(II)-PC vesicles vs. Ru(II) ions.
    Conditions are the same as in a; Ru(II) ions obtained by
    ascorbate reduction; baseline is vesicles vs. buffer
    solution.
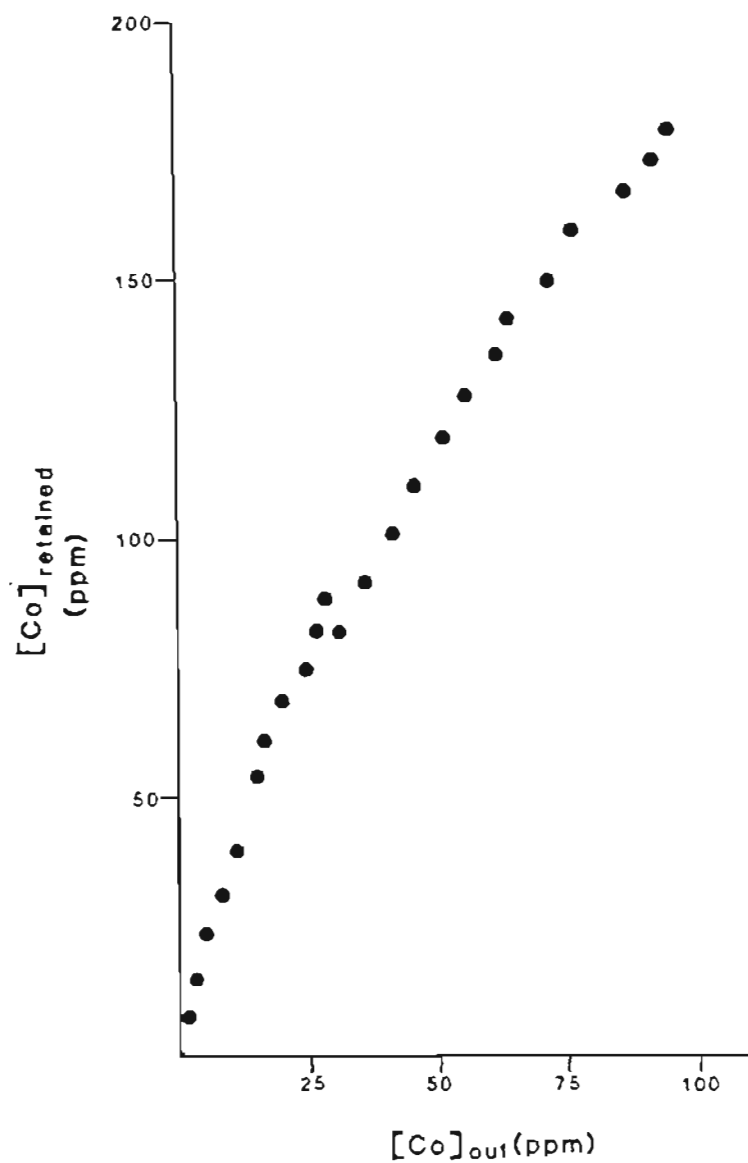
Figure 17. Uncorrected binding curve for $(NH_3)_5Co-4-(8'-$
nonenyl$)py^{3+}$-PC vesicles. The phosphatidylcholine concentration was 4
mM; $[Co]_{out}$ values were determined from atomic absorption measurement,
$[Co]_{retained}$ values determined by subtracting the amount of cobalt in
the filtrates from the total cobalt added (see Section 2.3.8).

a   b
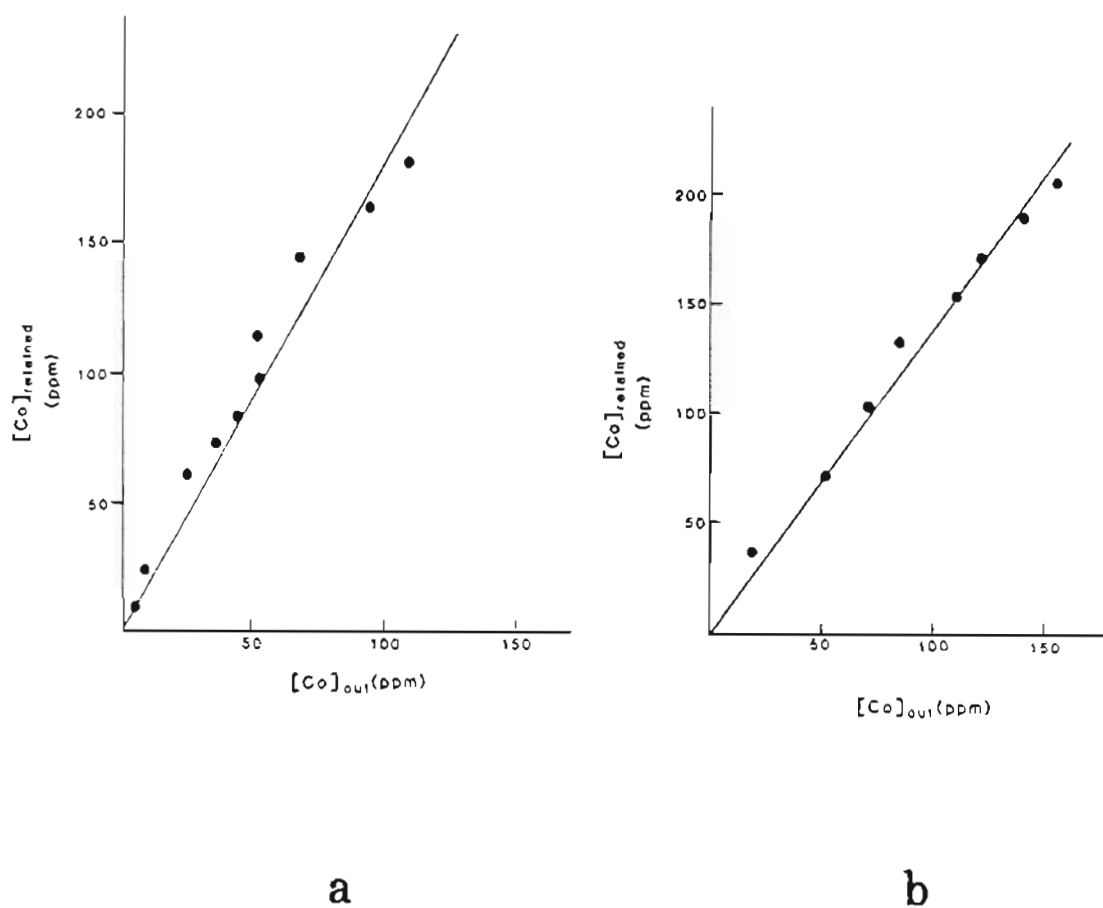
Figure 18. Retention curves for $(NH_3)_5Co-4-(\omega-alkenyl)py^{3+}$ ions by semipermeable membranes.

a. $(NH_3)_5Co-4-(10'-undecenyl)py^{3+}$;

b. $(NH_3)_5Co-4-(8'-nonenyl)py^{3+}$; the lines were drawn from linear regression analysis of data points and constrained to go through the origin; experimental information is given in Section 2.3.8.
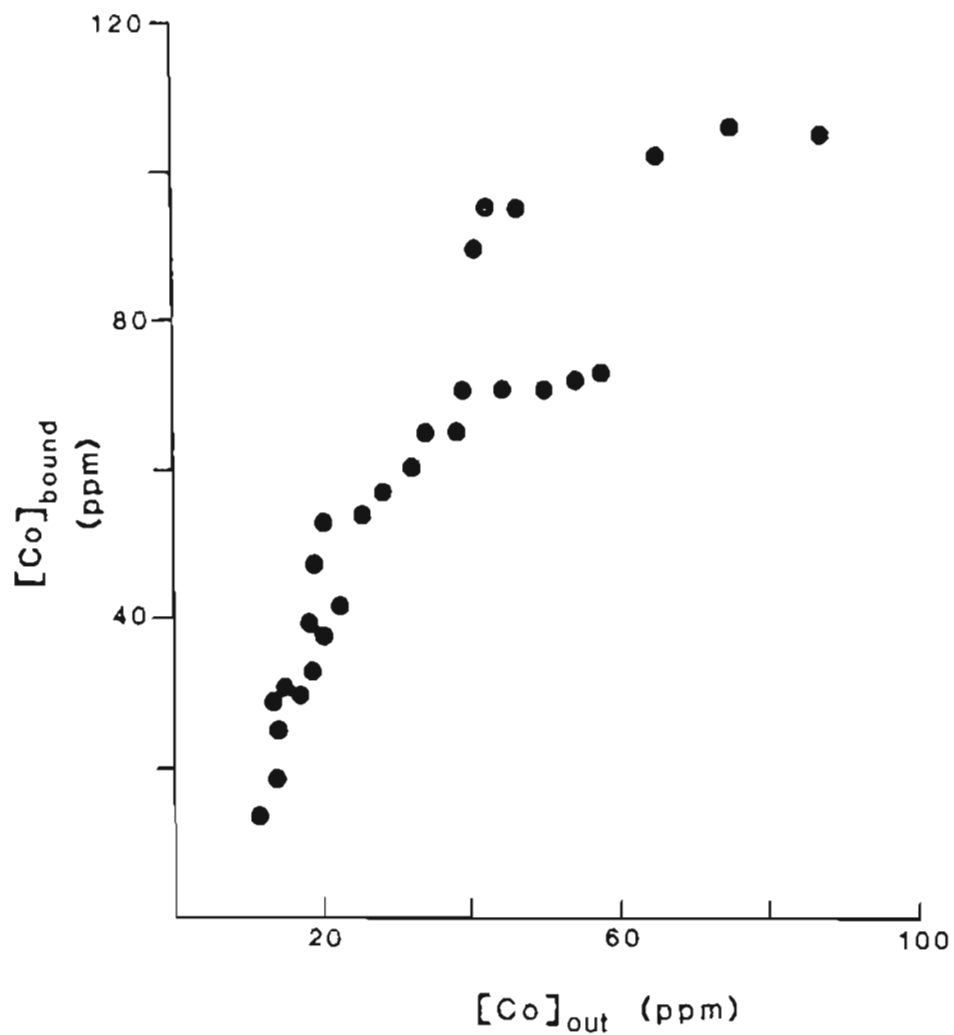
Figure 19. Corrected binding curve for $(NH_3)_5Co-4-(10'-$ undecenyl$)py^{3+}$-PC vesicles. The phosphatidylcholine concentration was 4 mM; $[Co]_{bound}$ values were determined by subtracting the corrected $[Co]_{out}$ values from the calculated retained cobalt concentration. Experimental information is given in Section 2.3.8.
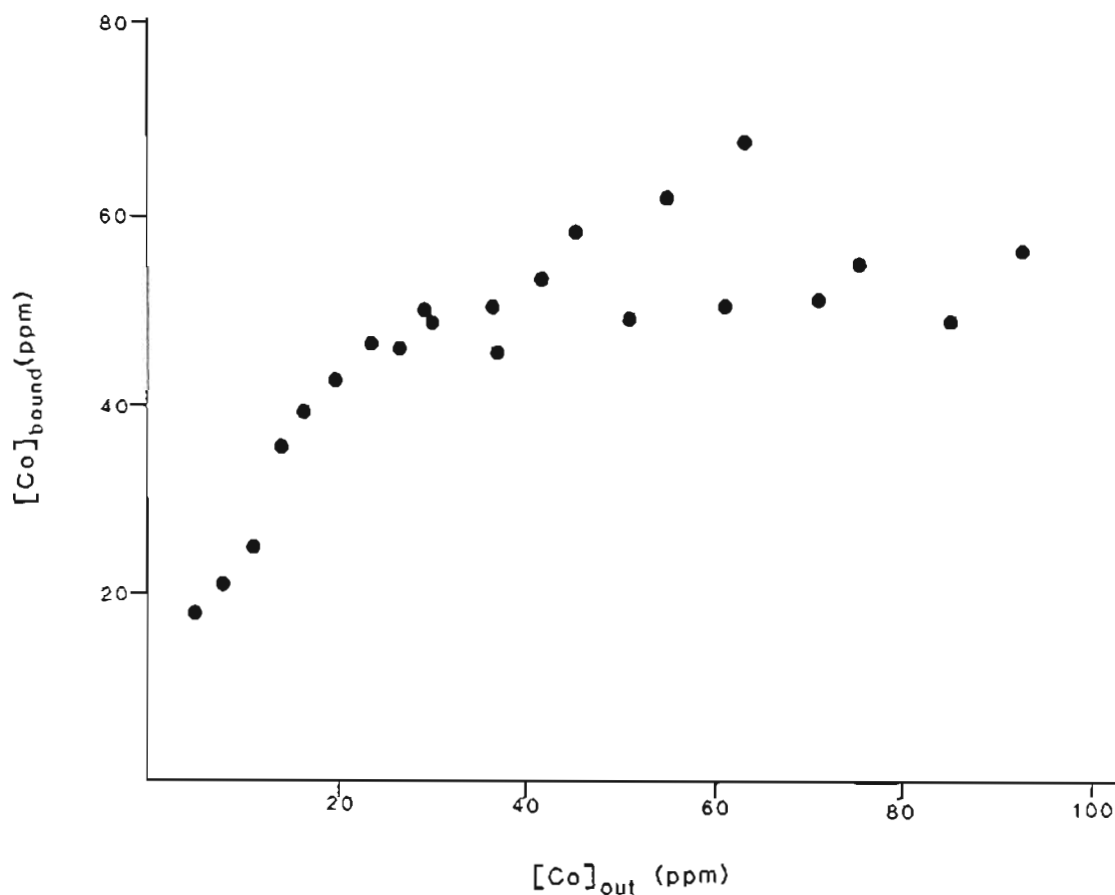
Figure 20. Corrected binding curve for $(NH_3)_5Co-4-(8'-nonenyl)py^{3+}$-PC vesicles. The phosphatidylcholine concentration was 4 mM; $[Co]_{bound}$ values were determined by subtracting the corrected $[Co]_{out}$ values from the calculated retained cobalt concentration. Experimental information is given in Section 2.3.8.
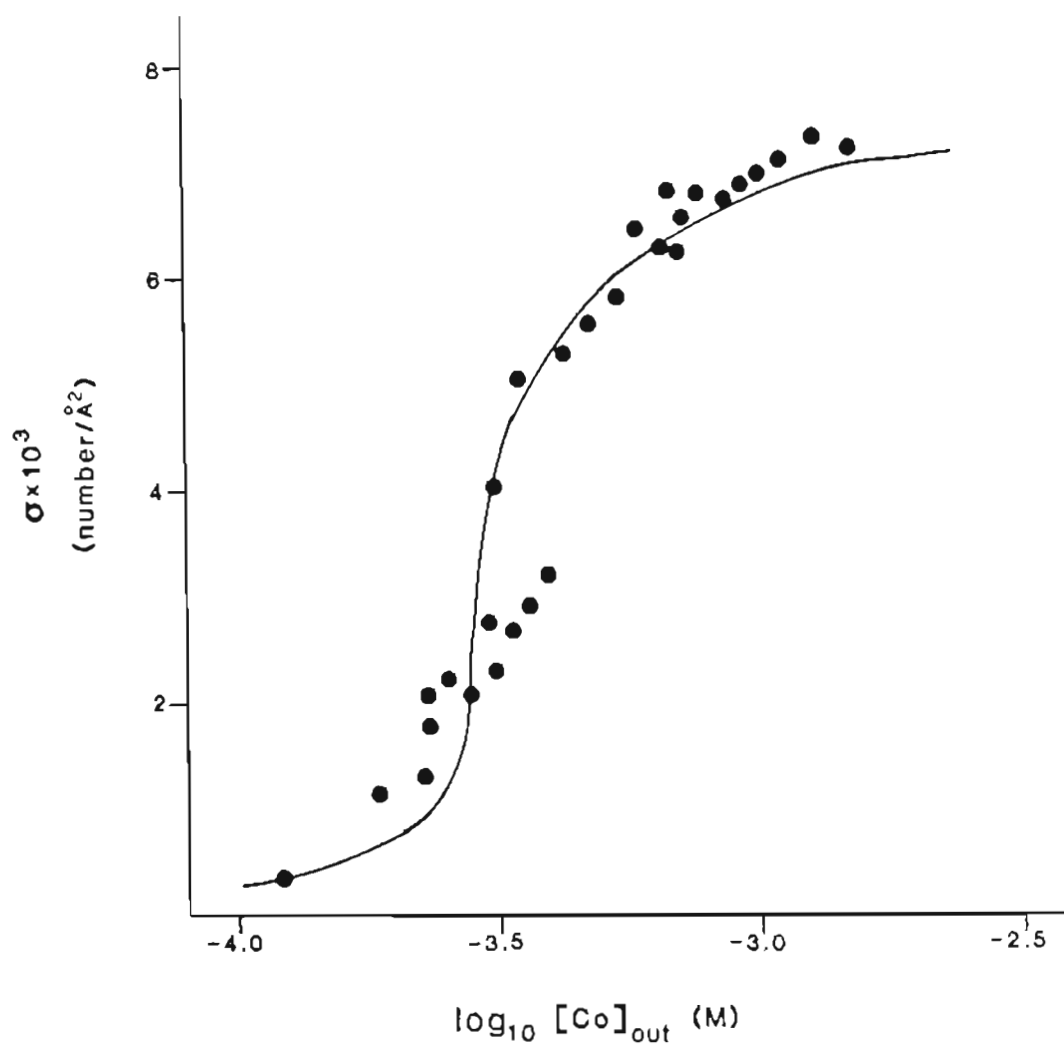
Figure 21. Stern plot for $(NH_3)_5Co-4-(10'-undecenyl)py^{3+}-PC$ vesicles. Solid curve obtained by fitting equation 26 with $\sigma^m = 1/167$ $Å^2$ and $K = 3.0 \times 10^{-3}$ M; σ values obtained by fitting equation 26 with experimentally determined $[Co]_{bound}$ and $[Co]_{out}$ values.
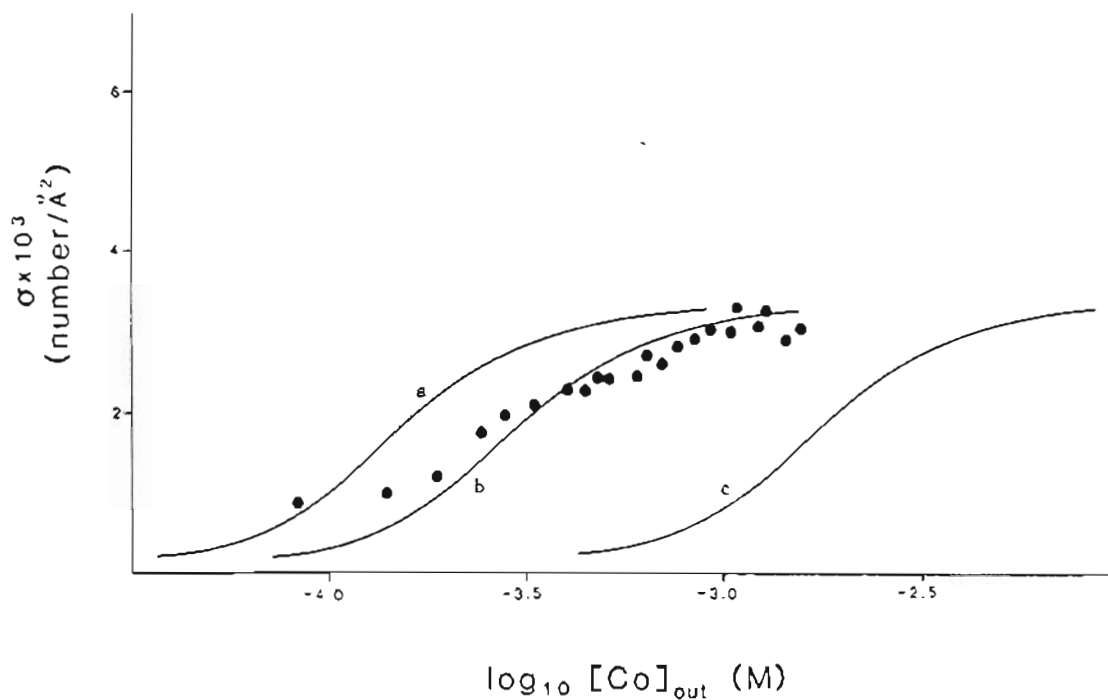
Figure 22. Stern plots for $(NH_3)_5Co-4-(8'-nonenyl)py^{3+}-PC$

vesicles. Curve a: $K = 6 \times 10^{-4}$ M; curve b: $K = 1.2 \times 10^{-3}$ M; curve

c: $K = 7 \times 10^{-3}$ M; $\sigma^m = 1/285$ $Å^2$; values obtained by fitting equation

26 with experimentally determined $[Co]_{bound}$ and $[Co]_{out}$ values.
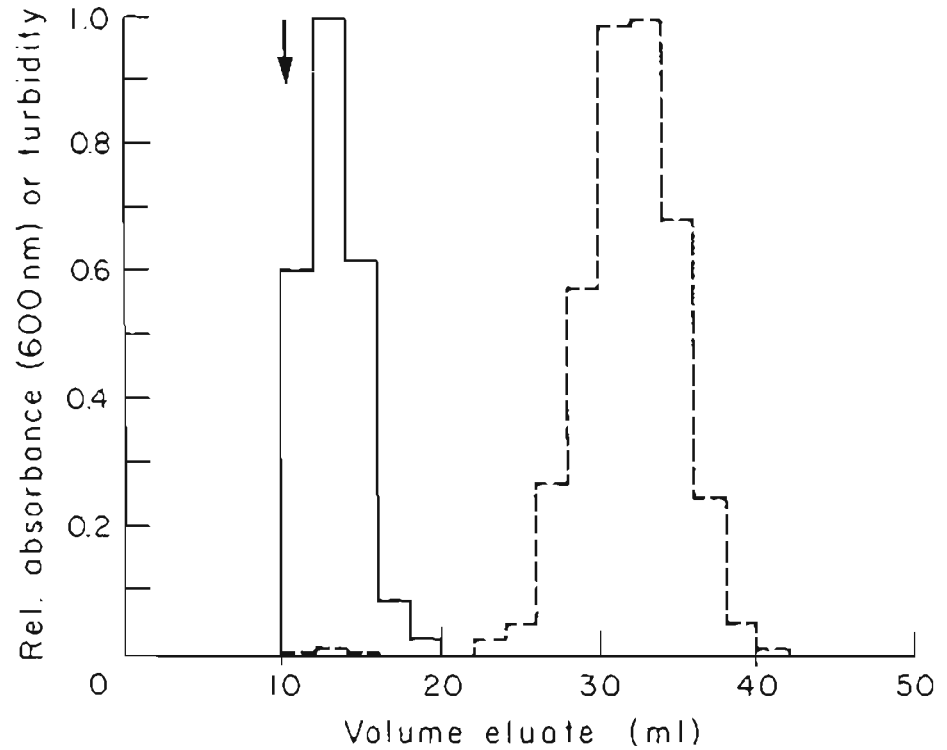
Figure 23. Elution profile of MV^{2+}-DHP vesicles on Sephadex G-50. 4.8 mM DHP, 3.6 mM MV^{2+} sonicated in 0.05 M Tris, pH 7.8. Solid line: relative turbidity. Dotted line: viologen absorption, measured at 600 nm, as MV^+ by dithionite reduction of eluate fractions. The arrow indicates column void volume.
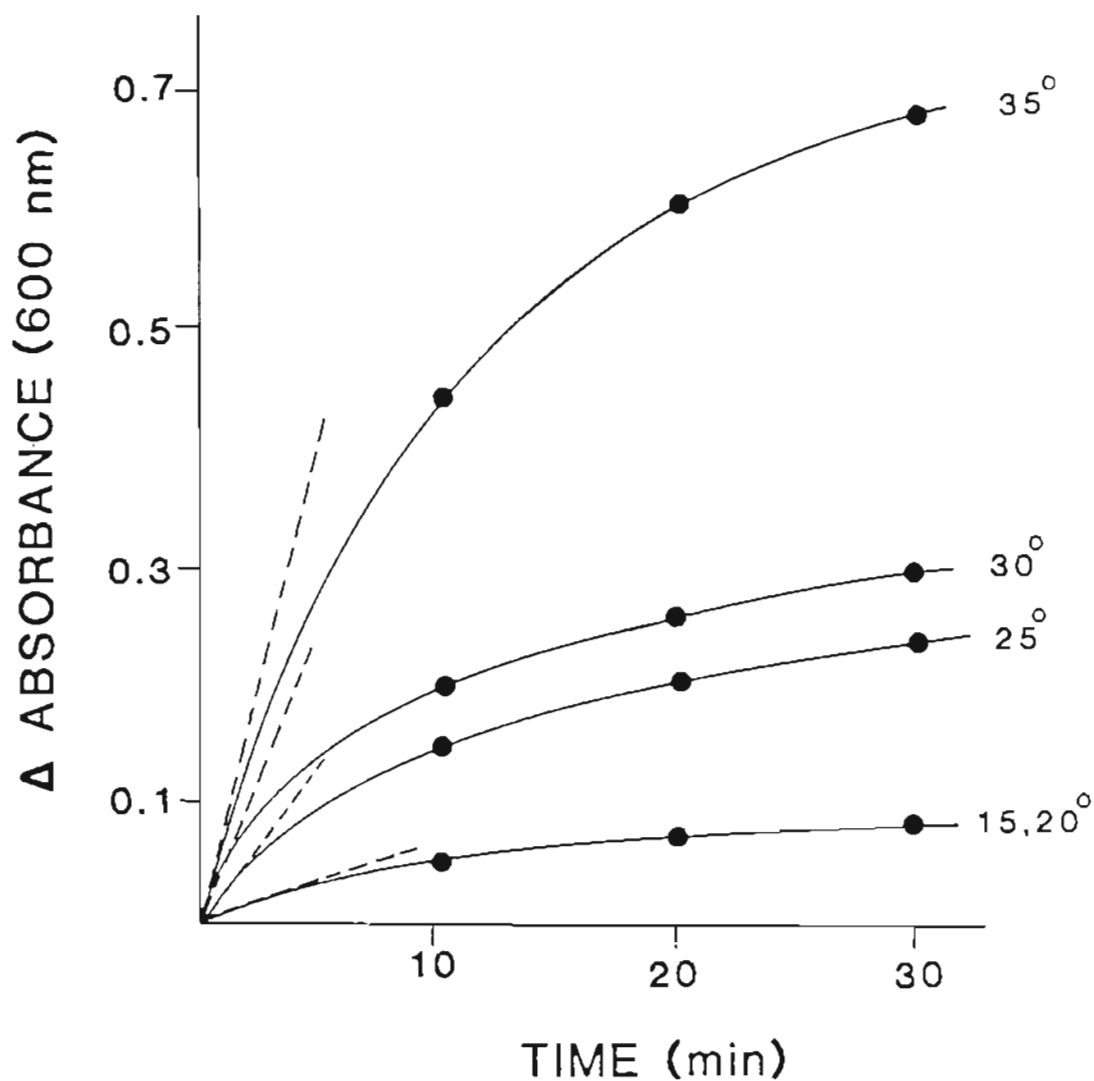
Figure 24. **Temperature dependence of MV^{2+} diffusion across DHP vesicle bilayers.** Asymmetric MV^{2+}-DHP vesicles prepared from 4.8 mM DHP and 3.6 mM MV^{2+}, sonicated in 0.05 M Tris, pH 7.8. Solid curves: external MV^{2+} measured as MV^{+} by dithionite reduction of eluate viologen-DHP fractions. Dotted lines: initial rates of MV^{+} formation. Temeratures are indicated in °C.
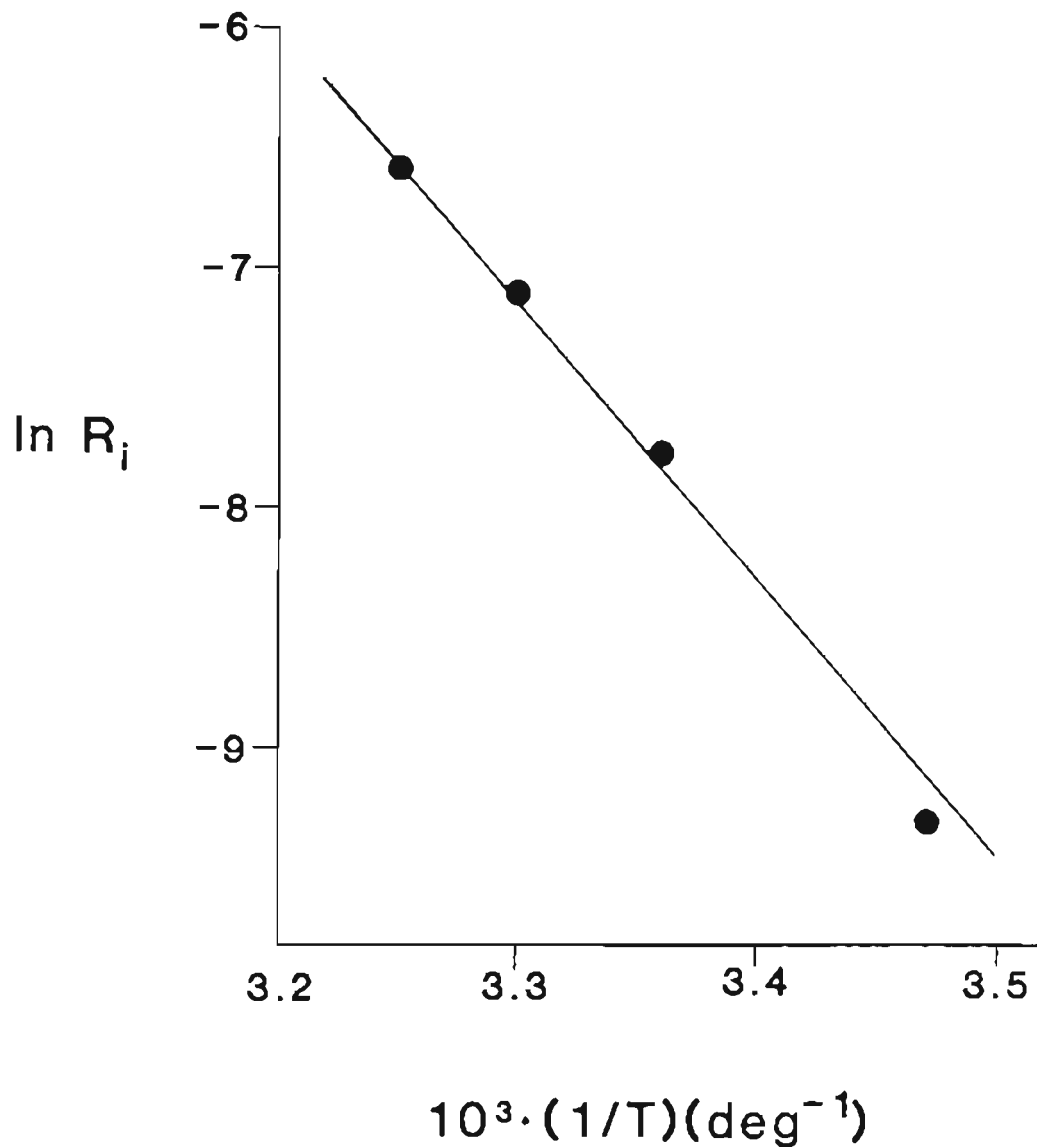
Figure 25. Eyring plot of initial rates of MV+ formation for viologen diffusion in MV^{2+}-DHP vesicles. R_i values are initial rates of MV^+ diffusion obtained from Figure 25. The line was drawn using linear regression of the data points. Experimental conditions are those given in Table 5.
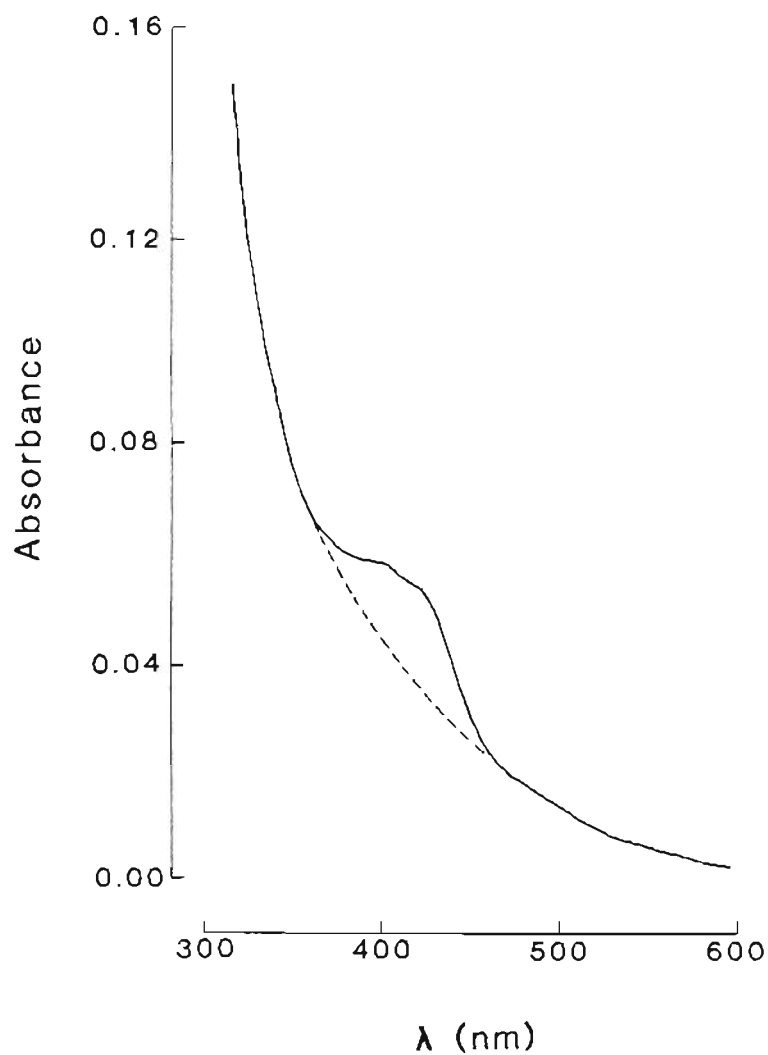
Figure 26. Optical absorption difference spectrum of $Fe(CN)_6^{3-}$, $C_{16}MV^{2+}$-DHP vs. DHP vesicles. $C_{16}MV^{2+}$-DHP vesicles containing internal $Fe(CN)_6^{3-}$ (initial concentrations 200 mM $Fe(CN)_6^{3-}$, 4.8 mM DHP, 1.2 mM $C_{16}MV^{2+}$) vs. DHP vesicles in 0.02 M Tris, pH 7.8. The dotted curve is the extrapolated baseline due to viologen absorption; internal $Fe(CN)_6^{3-}$ concentration is calculated from the peak height of the solid curve to the dotted curve.
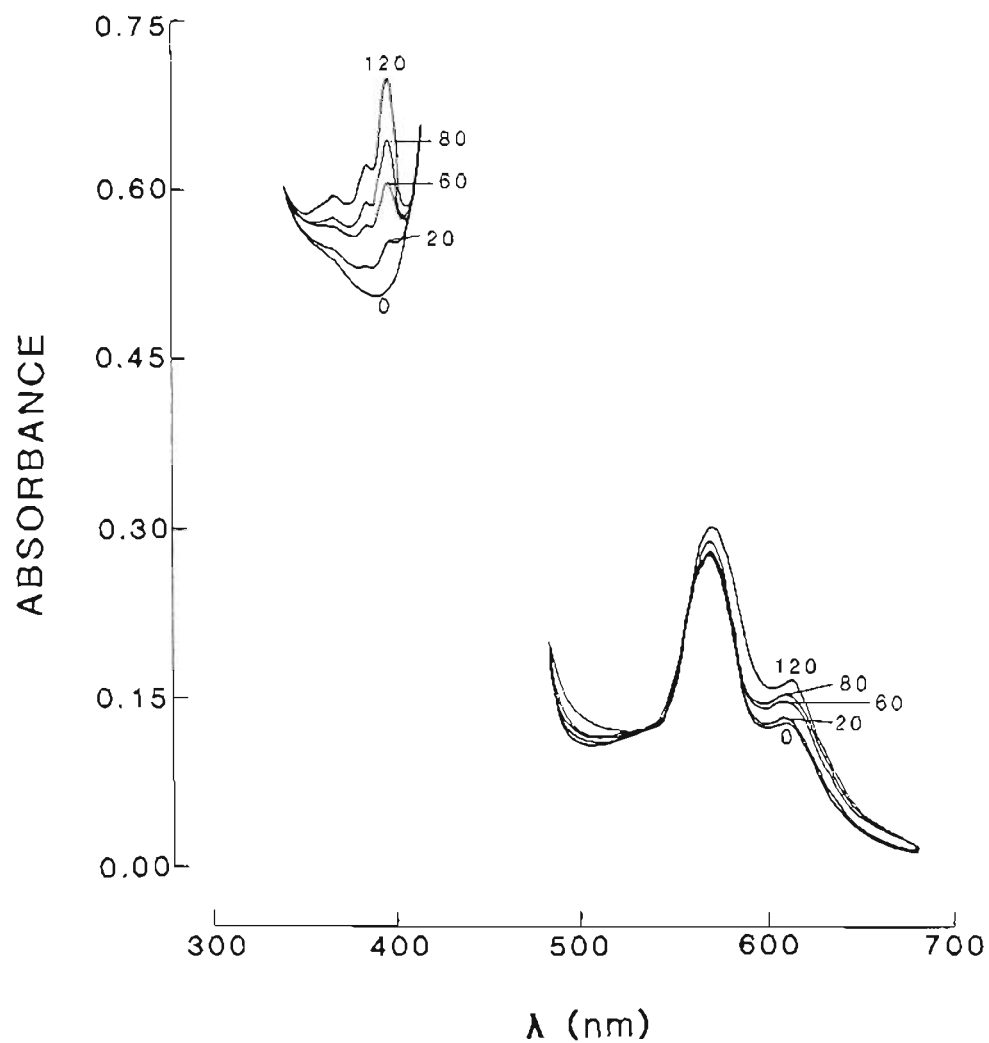
Figure 27. ZnTMPyP^{4+} sensitized MV$^+$ formation in asymmetric MV^{2+}-DHP vesicles in aqueous solutions. 4.8 mM DHP, 3 mM MV^{2+} sonicated in H$_2$O, pH 8.4, followed by cation exchange chromatography, 16 μM ZnTMPyP^{4+}, 1 mM EDTA externally added. Illumination times are indicated in minutes. A 515 nm cutoff filter was used to remove higher energy photons from 0-60 min; a 410 nm cutoff filter was used from 60-120 min. The region from 410 to 480 nm was deleted due to the intense absorption of the porphyrin (A$_{426}$ > 2).
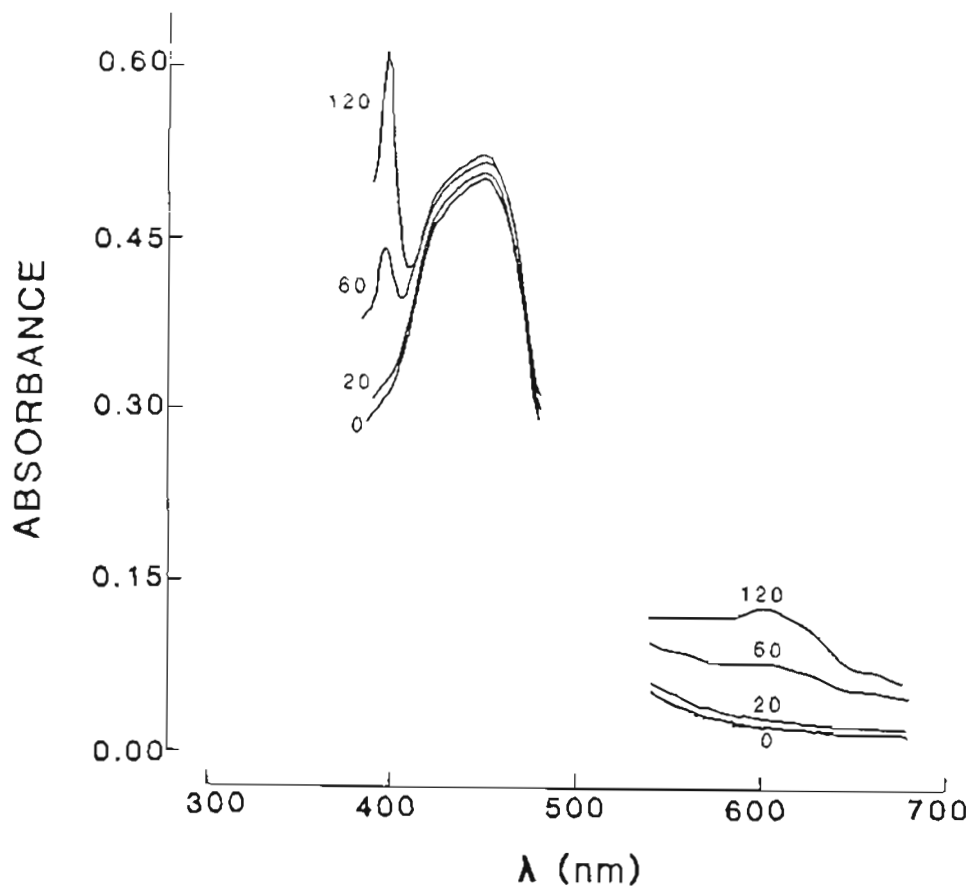
Figure 28. $Ru(bpy)_3^{2+}$ sensitized MV^+ formation in asymmetric MV^{2+}-DHP vesicles in aqueous solutions. 4.8 mM DHP, 3 mM MV^{2+} sonicated in H_2O, pH 8.4, followed by cation exchange chromatography, 30 μM $Ru(bpy)_3^{2+}$, 1 mM EDTA added externally. A 410 cutoff filter was used; illumination times are indicated in minutes. The region from 480-540 nm was not scanned in order to obtain accurate optical changes in the UV region as quickly as possible.
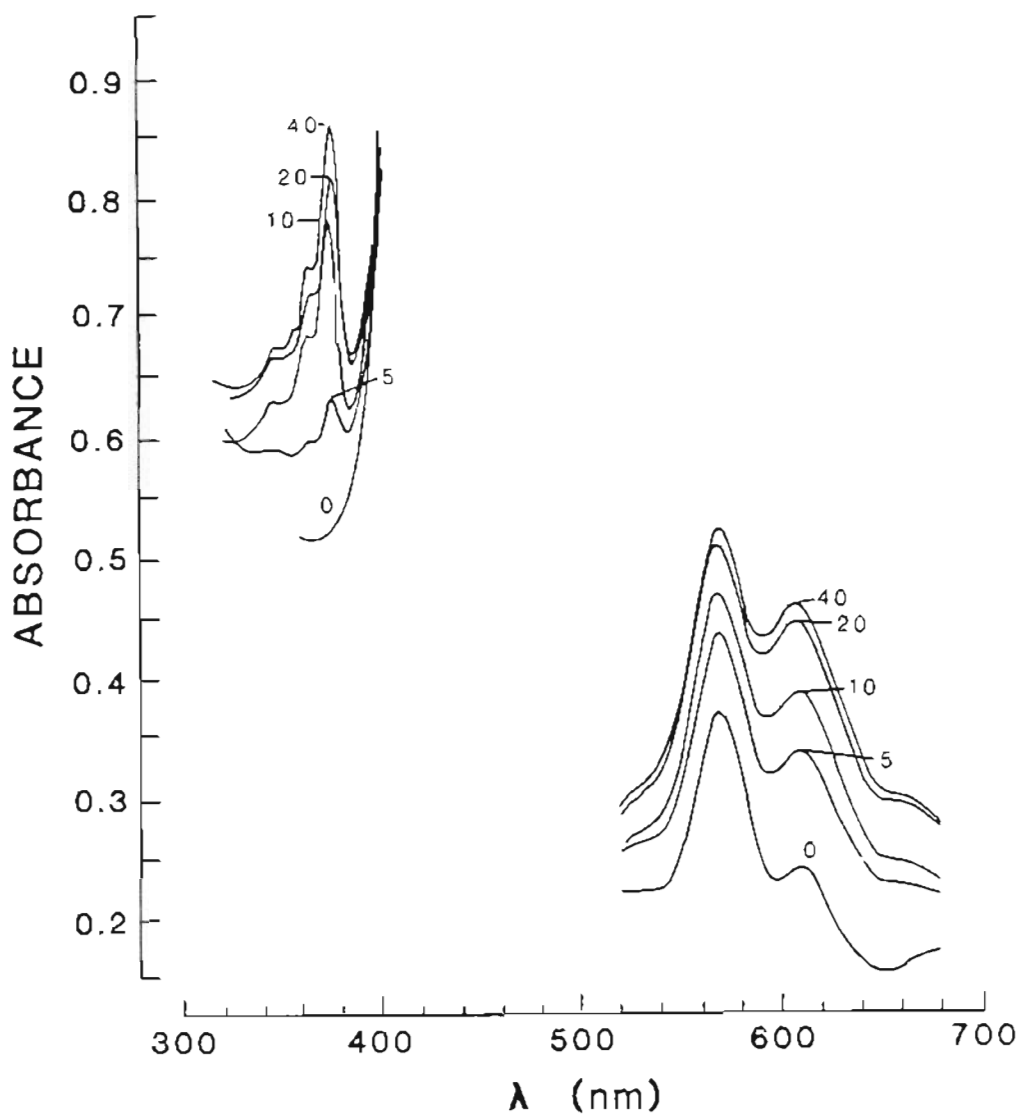
Figure 29. ZnTMPyP^{4+} sensitized MV^{+} formation in asymmetric MV^{2+} vesicles in Tris buffered solutions. 4.8 mM DHP, 1 mM MV^{2+} sonicated in 0.05 M Tris, pH 7.8, followed by Sephadex G-50 chromatography, 16 μM ZnTMPyP^{4+}, 1 mM EDTA added externally. A 515 nm cutoff filter was used; illumination times are indicated in minutes.
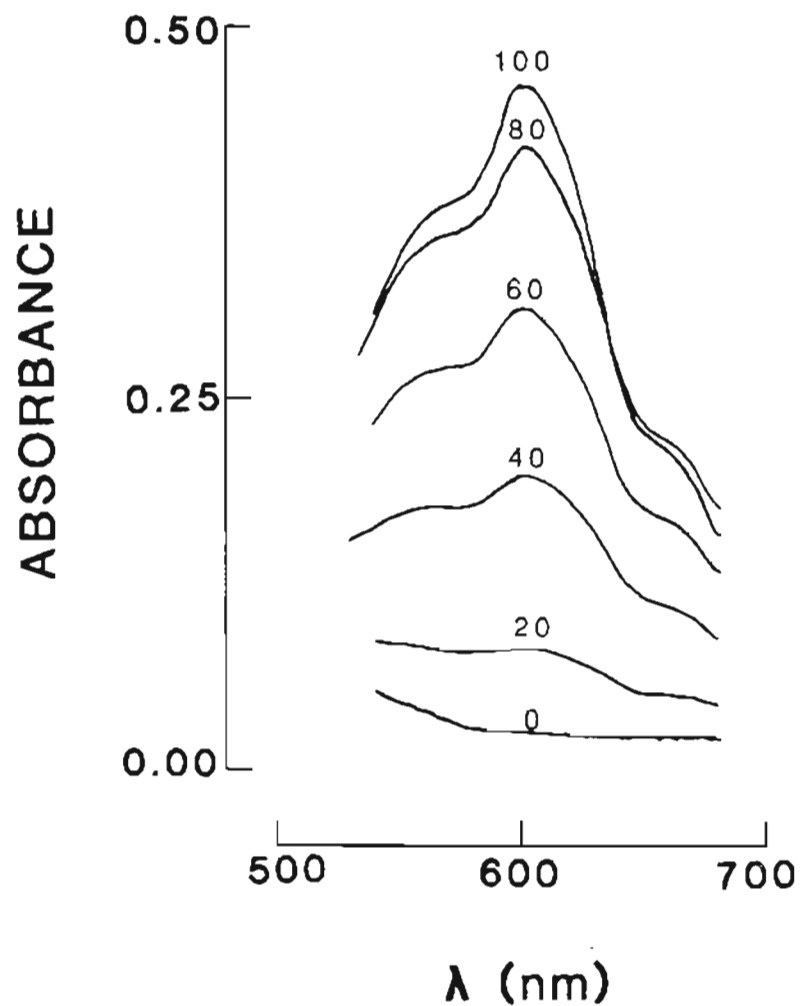
Figure 30. Ru(bpy)$_3^{2+}$ sensitized MV$^+$ formation in asymmetric MV^{2+}-DHP vesicles in Tris buffered solutions. 4.8 mM DHP, 3 mM MV^{2+} sonicated in 0.05 M Tris, pH 7.8, followed by Sephadex G-50 chromatography, 30 μM Ru(bpy)$_3^{2+}$, 1 mM EDTA externally added. A 410 nm cutoff filter was used; illumination times are indicated in minutes.
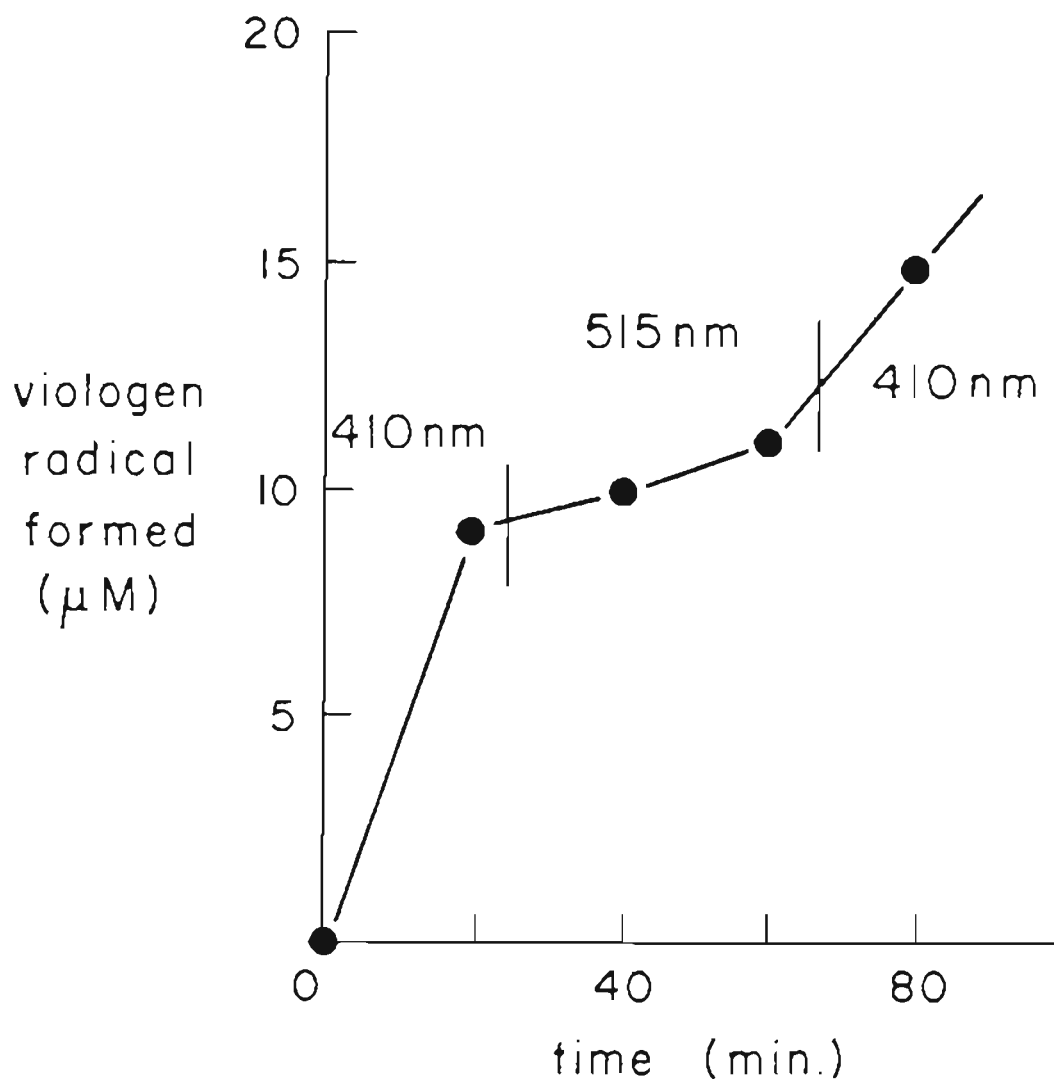
Figure 31. **Wavelengtb dependence of photoinduced viologen
diffusion across DHP vesicle bilayers.** Asymmetric Mv^{2+}-DHP vesicles
(4.8 mM DHP, 3.6 mM MV^{2+}, initial concentrations) in 0.05 M Tris, pH
7.8, 16 μM $ZnTMPyP^{4+}$, 1 mM EDTA externally added; MV^+ determined at 600
nm at 23°C. Optical cutoff filters used during illumination are
indicated.
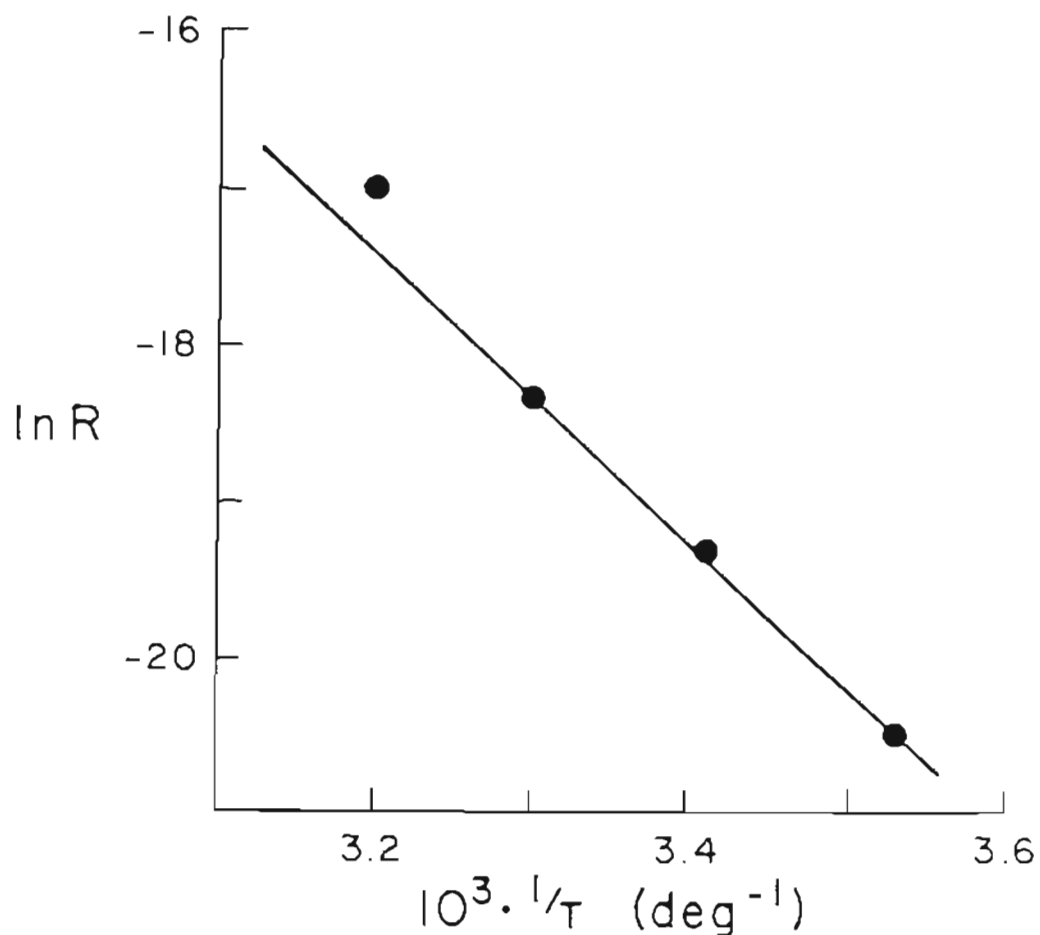
Figure 32. **Eyring plot of initial rates of sensitized MV^+ formation in photoinduced viologen diffusion.** Initial conditions: [DHP] = 4.8 mM, [MV^{2+}] = 3.6 mM, in 0.05 M Tris, pH 7.8, [Ru(bpy)$_3^{2+}$] = 30 µM and [EDTA] = 1 mM added externally; illuminated with filtered visible light (λ > 410 nm, I_o = 6 x 10^{-8} einstein/second); MV^+ was determined from spectral changes at 600 nm. Initial rates (R_i) are given in units of Ms^{-1}.
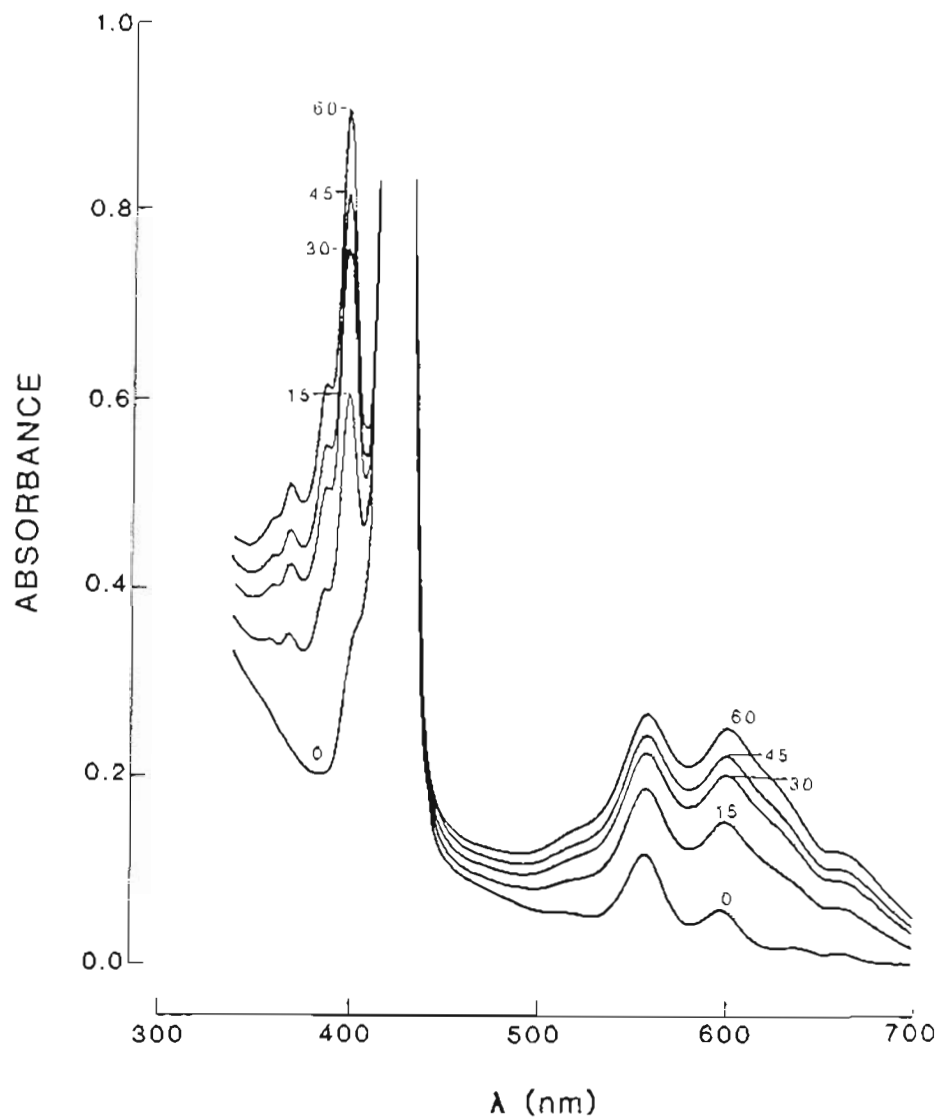
Figure 33. ZnTPPS^{4-} sensitized C$_{16}$MV$^+$ formation in C$_{16}$MV^{2+}-DHP
vesicles. 4 mM DHP, 0.5 mM C$_{16}$MV^{2+} sonicated in 0.02 M Tris, pH 7.8, 40
μM ZnTPPS^{4-}, 0.1 M tricine added externally; illuminated with filtered
visible light (λ > 495 nm). Illumination times are indicated in
minutes.
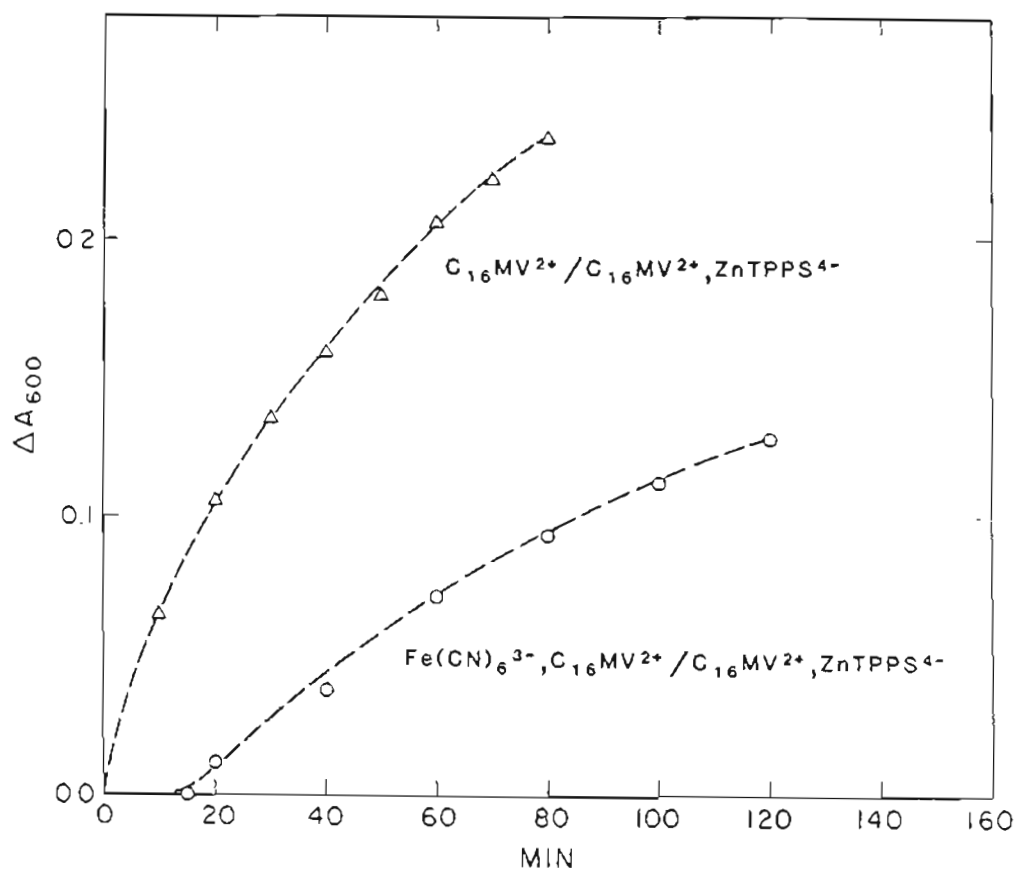
Figure 34. ZnTPPS^{4-} sensitized C$_{16}$MV$^+$ formation in Fe(CN)$_6^{3-}$, C$_{16}$MV^{2+}-DHP vesicles. Triangles: 40 μM ZnTPPS^{4-} and 0.1 M tricine added to DHP vesicles containing Mv^{2+} bound to inner and outer surfaces. Initial concentrations: [C$_{16}$MV^{2+}] = 0.6 mM, [DHP] = 4 mM. Circles: Same conditions except vesicles contain internalized Fe(CN)$_6^{3-}$. Initial concentrations: [C$_{16}$MV^{2+}] = 0.6 mM, [DHP] = 4 mM, [Fe(CN)$_6^{3-}$] = 20 mM. Vesicles were passed down Sephadex G-50 column, illuminated with filtered visible light (λ > 496 nm).
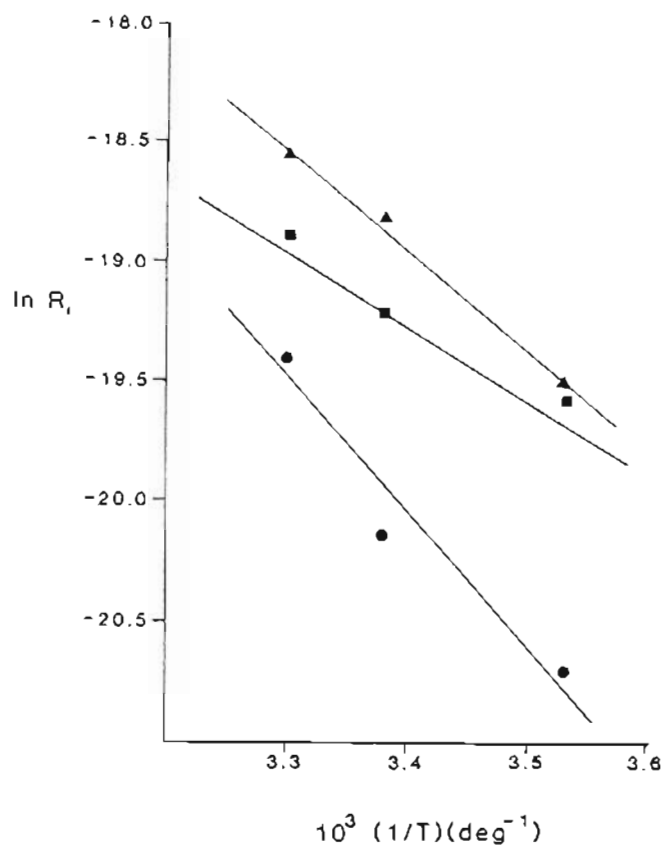
Figure 35. **Eyring plots of ZnTPPS^{4-} sensitized C$_{16}$MV$^+$ formation in C$_{16}$MV^{2+}-DHP vesicles.** R$_i$ is defined in Table 5. Squares: internally and externally bound C$_{16}$MV^{2+}-DHP vesicles with external ZnTPPS^{4-} and tricine in 0.02 M Tris, pH 7.8. Circles: internally and externally bound C$_{16}$MV^{2+}-DHP vesicles containing internalized Fe(CN)$_6^{3-}$, external ZnTPPS^{4-} and tricine in 0.02 M Tris, pH 7.8. Triangles: externally bound C$_{16}$MV^{2+}-DHP vesicles with external ZnTPPS^{4-} and tricine, in 0.02 M Tris, pH 7.8. The lines were drawn using linear regression analysis of the data points; experimental conditions are given in Table 10.
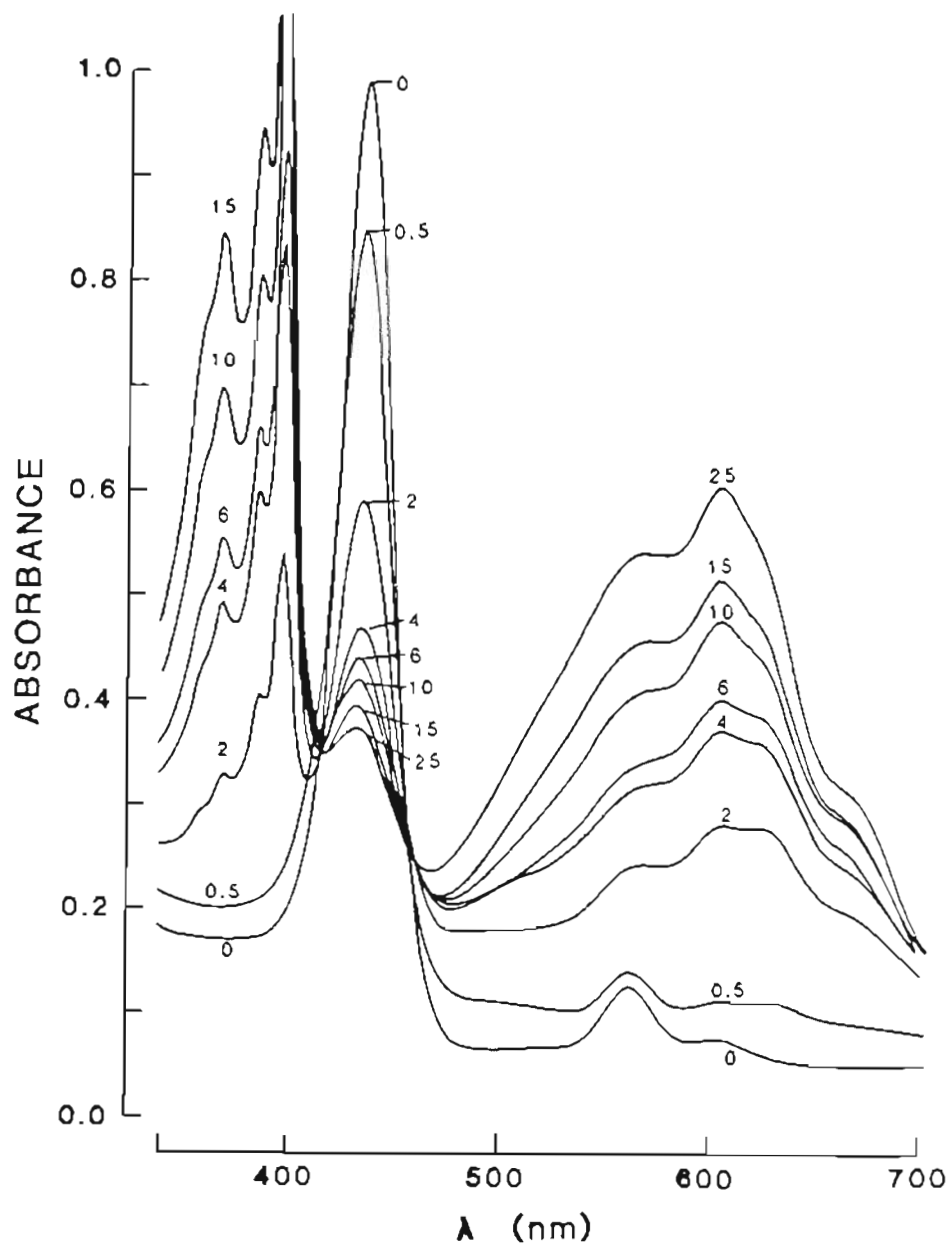
Figure 36. ZnTMPyP^{4+} sensitized C$_{16}$MV^{2+} reduction in C$_{16}$MV^{2+}-PC vesicles. 3 mM PC, 0.3 mM C$_{16}$MV^{2+} sonicated in 0.05 M phosphate, pH 6.5, with 10 µM ZnTMPyP^{4+} and 1 mM EDTA added externally. Illuminated with filtered visible light ($\lambda > 515$ nm); illumination times are indicated in minutes.
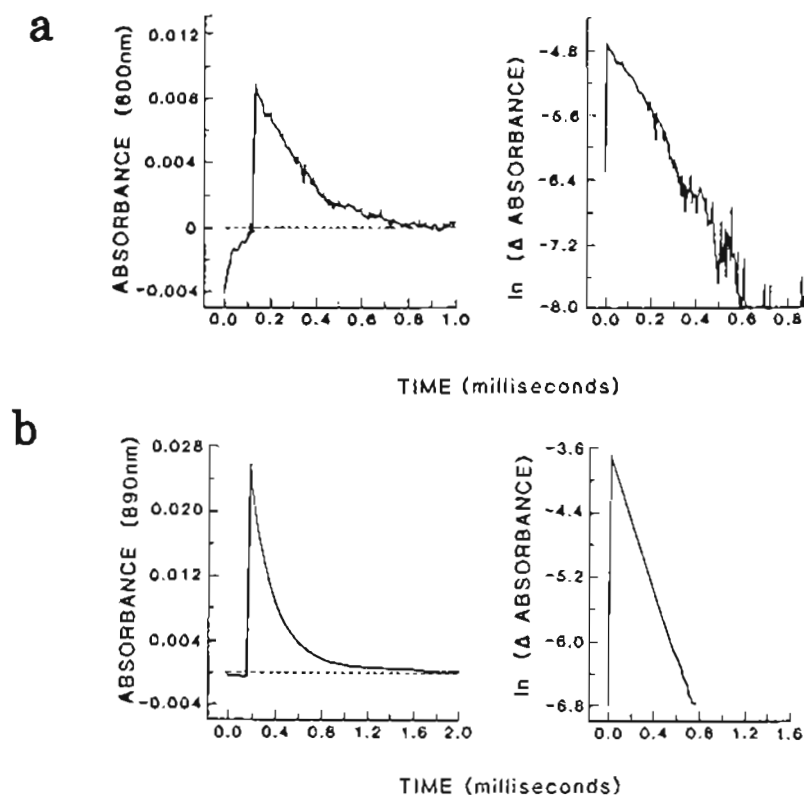
Figure 37. **Deactivation of photoexcited ZnTMPyP^{4+} in PC vesicle solution.**

Left column, curve a: time course of absorbance changes following laser flash excitation detected at 600 nm; curve b: absorbance changes detected at 890 nm. The excitation wavelength was 532 nm; point of initiation of the laser flash is marked with an x.

Right column, curves a, b: first-order kinetic plots based on the baselines drawn in the corresponding curves displayed in the left column. Reaction conditions: 10 μM ZnTMPyP^{4+}, 3 mM PC in 0.05 M phosphate, pH 6.5, at 23°C.
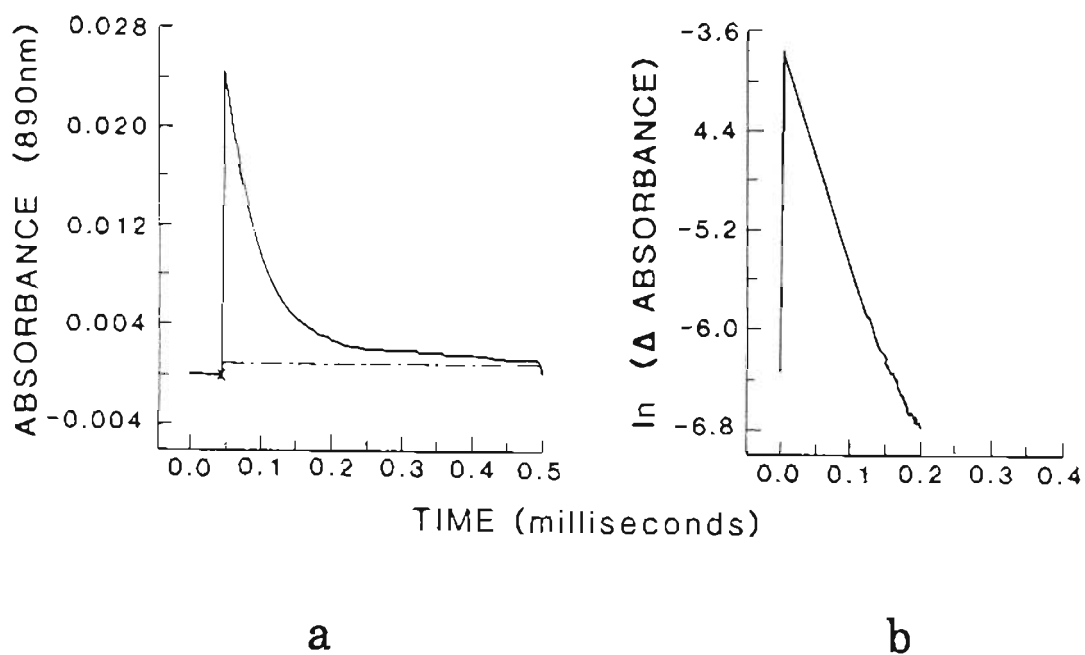
Figure 38. **Reductive quenching of photoexcited ZnTMPyP^{4+} in PC vesicles.**

Curve a: time course of absorbance changes detected at 890 nm

following 532 nm laser flash excitation.

Curve b: first-order kinetic plot based on the baseline drawn

in a. Reaction conditions: 10 µM ZnTMPyP^{4+}, 3 mM PC,

1 mM EDTA, in 0.05 M phosphate, pH 6.5, at 23°C.
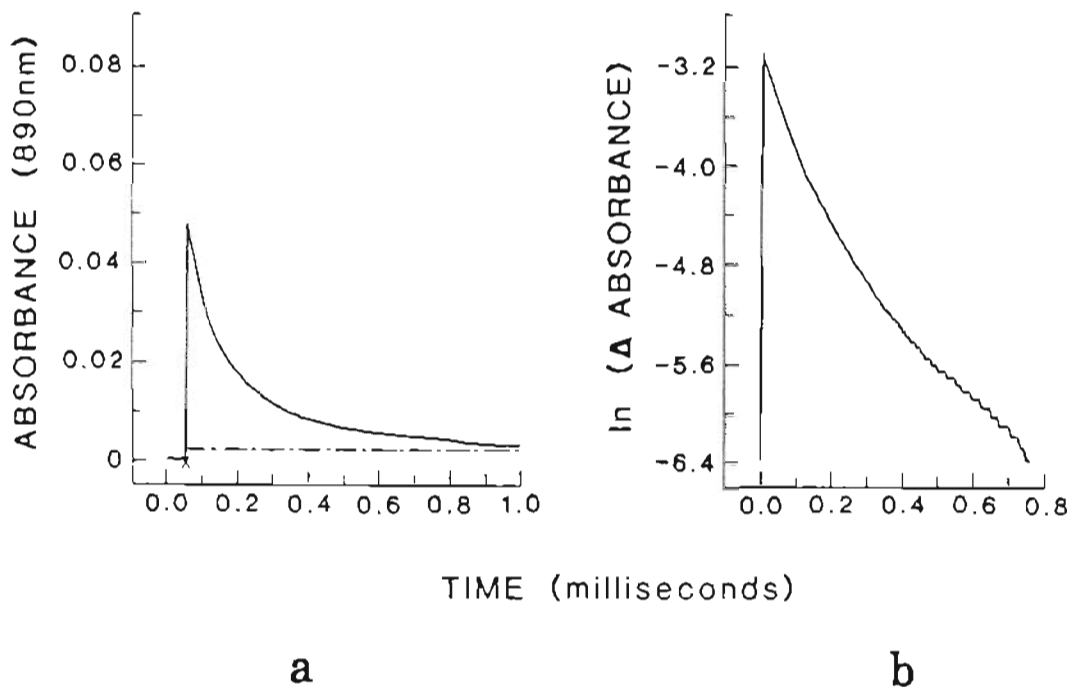
Figure 39. Deactivation of photoexcited $ZnTMPyP^{4+}$ in $C_{16}MV^{2+}$-PC vesicles.

      Curve a: time course of absorbance changes detected at 890 nm following 532 nm laser flash excitation.

      Curve b: first-order kinetic plot based on the baseline drawn in a. Reaction conditions: 1.6 mM $C_{16}MV^{2+}$, 9.6 mM PC, 20 μM $ZnTMPyP^{4+}$, in 0.05 M phosphate, pH 6.5, at 23°C.

a   b
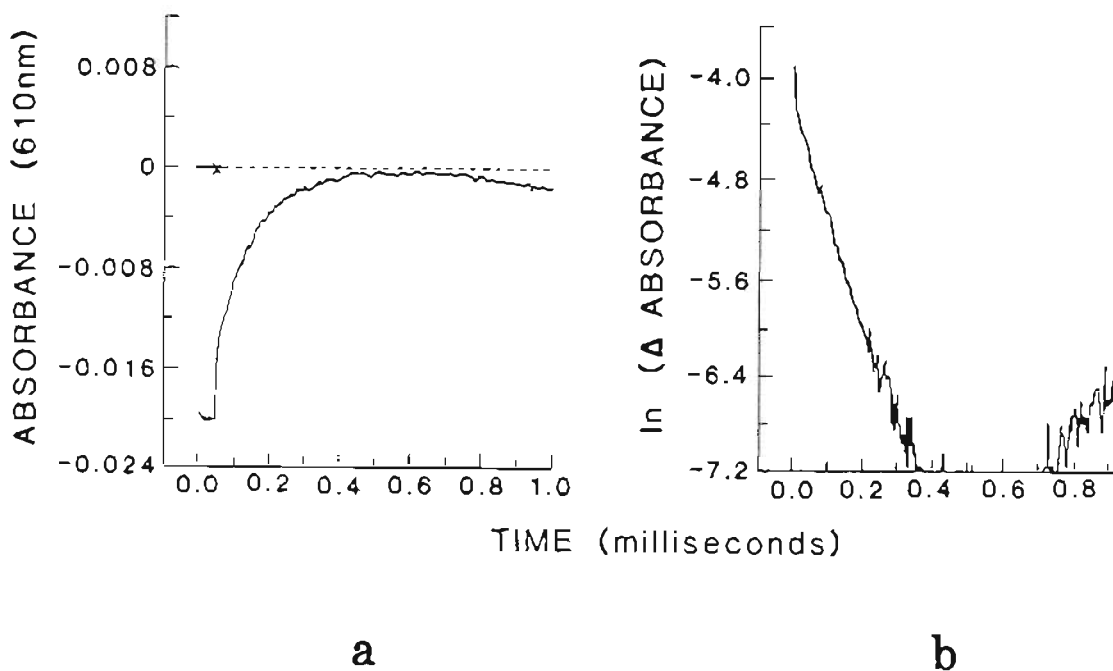
Figure 40. ZnTMPyP^{4+} sensitized C$_{16}$MV^{+} formation in C$_{16}$MV^{2+}-PC

vesicles.

Curve a: Time course of absorbance changes detected at 610 nm

following 532 nm laser flash excitation.

Curve b: first-order kinetic plot based on the baseline drawn

in a. Reaction conditions: 1.6 mM C$_{16}$MV^{2+}, 9.6 mM PC, 20

µM ZnTMPyP^{4+}, in 0.05 M phosphate, pH 6.5, at 23°C.
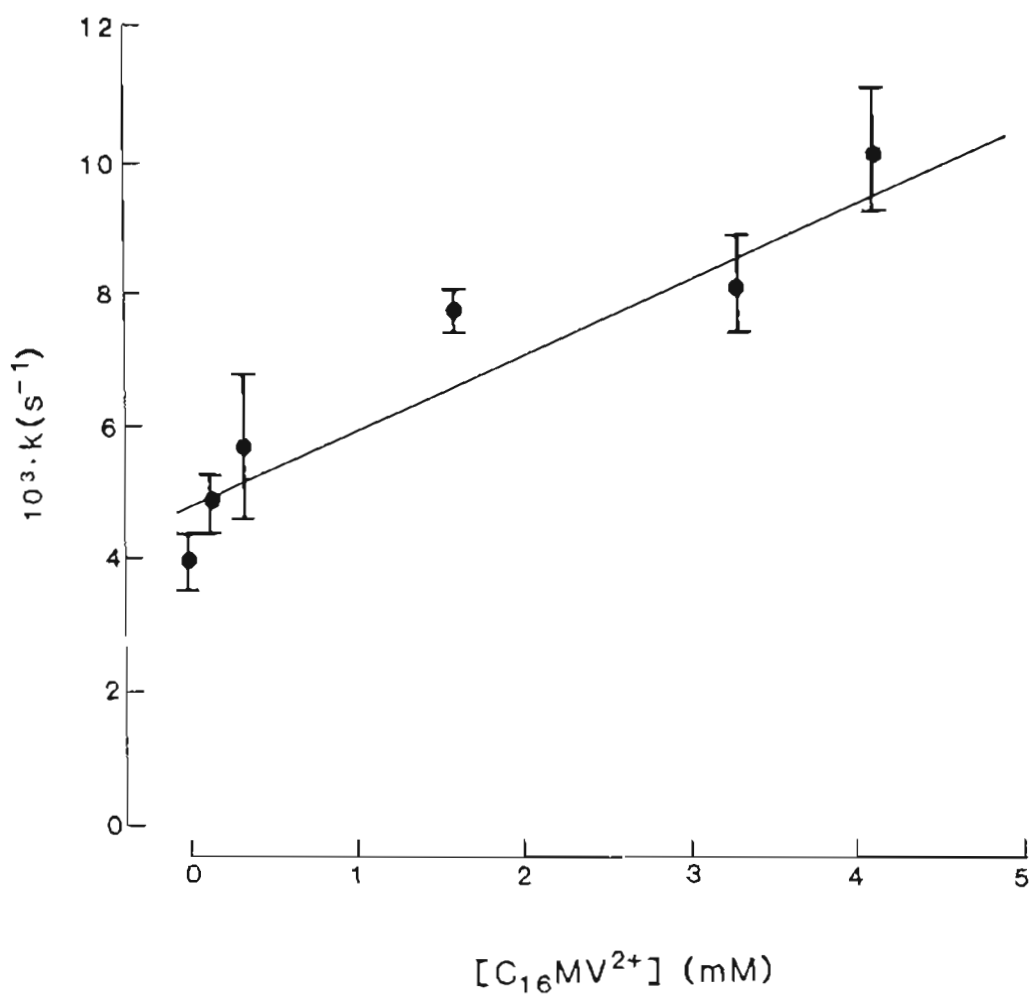
Figure 41. **Stern-Volmer plot of oxidative quenching of photo-excited ZnTMPyP^{4+} by PC-bound C$_{16}$MV^{2+}.** The line was drawn from linear regression analysis of data points; experimental conditions are those given in Table 12.

10 msec

Baseline →
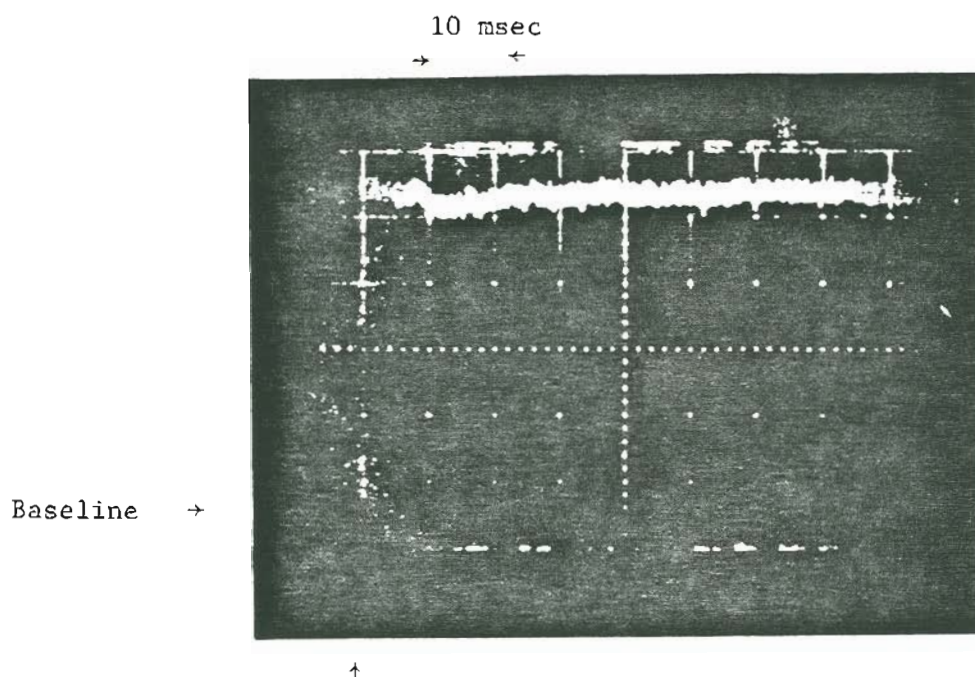
Figure 42. **Fast reduction of PC-bound $(NH_3)_5Ru-4-(11'-$
dodecenyl$)py^{3+}$ ion by V^{2+} ion.** The arrows indicate the point of mixing
of reactants; amplitudes are 10 mV/division. Conditions: 1 mM V^{2+}, 3
mM PC, 0.16 mM Ru^{3+} in 0.01 M acetate, pH 4.0, at 23°C.

a

b
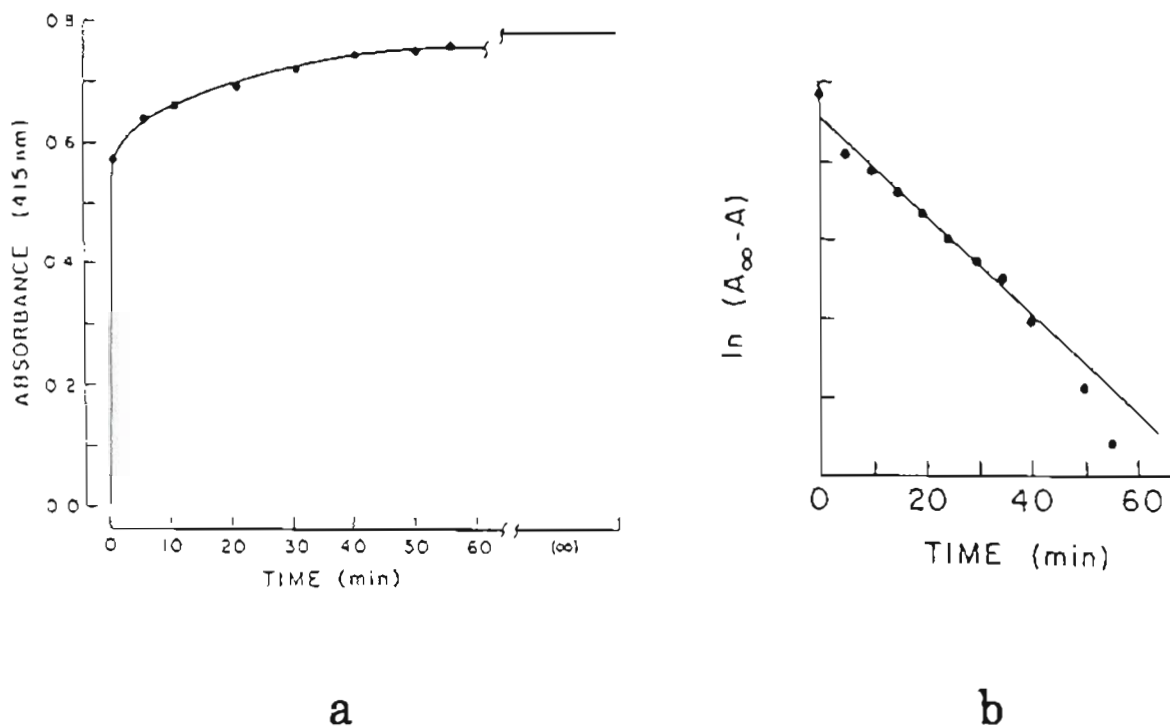
Figure 43. Slow reduction of PC-bound $(NH_3)_5Ru-4-(11'-$

dodecenyl)py^{3+} by V^{2+} ion.

Graph a: 0.7 mM V^{2+} added to $(NH_3)_5Ru-4-(11'-dodecenyl)py^{3+}-$

PC vesicles, at 23°C. Initial concentrations: [PC] = 7.5

mM, [Ru] = 0.4 mM, in 0.1 M sodium acetate, pH 4.0.

Graph b: first-order kinetic plot of data points in b.

a

b
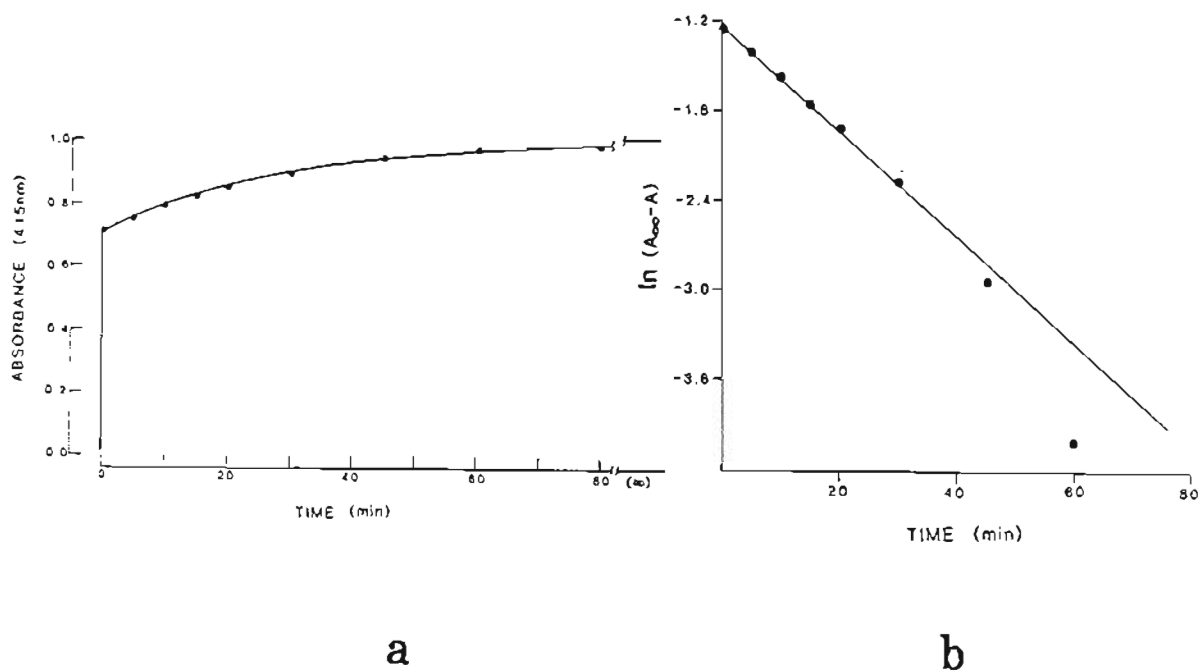
Figure 44. Slow reduction of PC-bound $(NH_3)_5Ru-4-(11'-$
dodecenyl)py^{3+} by Cr^{2+} ion.

Graph a: 5.1 mM Cr^{2+} added to $(NH_3)_5Ru-4-(11'-$dodecenyl)py$^{3+}-$

PC vesicles at 23°C. Initial concentrations: 7.5 mM PC,

0.4 mM Ru(III), in 0.1 M sodium acetate, pH 4.0.

Graph b: First-order kinetic plot of data points in graph a.

a

b
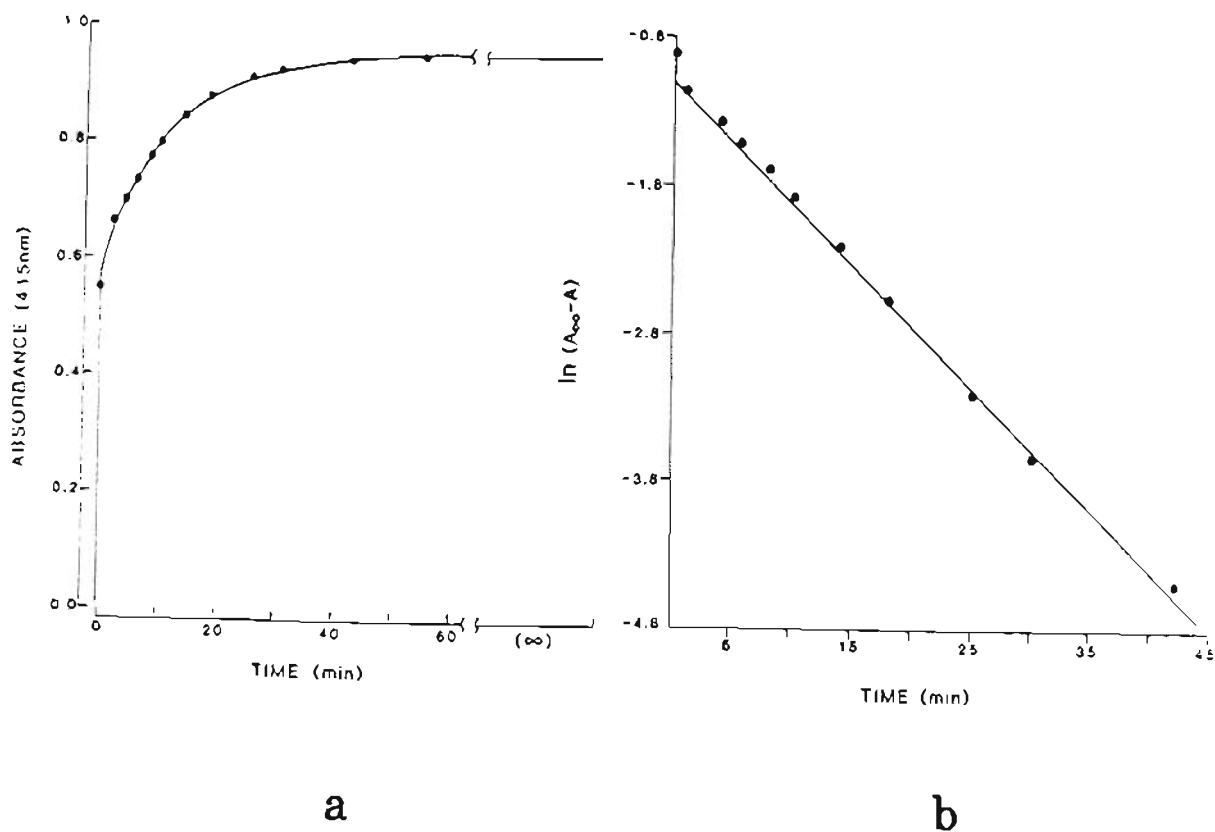
Figure 45. Slow reduction of PC-bound $(NH_3)_5Ru-4-(11'-$
dodecenyl)py^{3+} by ascorbate ion.

Graph a: 0.6 mM ascorbate added to $(NH_3)_5Ru-4-(11'-$
dodecenyl)py^{3+}-PC vesicles at 20°C. Initial concentra-
tions: 7.5 mM PC, 0.17 mM Ru(III), in 0.1 M sodium
acetate, pH 4.0.

Graph b: First-order kinetic plot of data points in graph a.

a   b
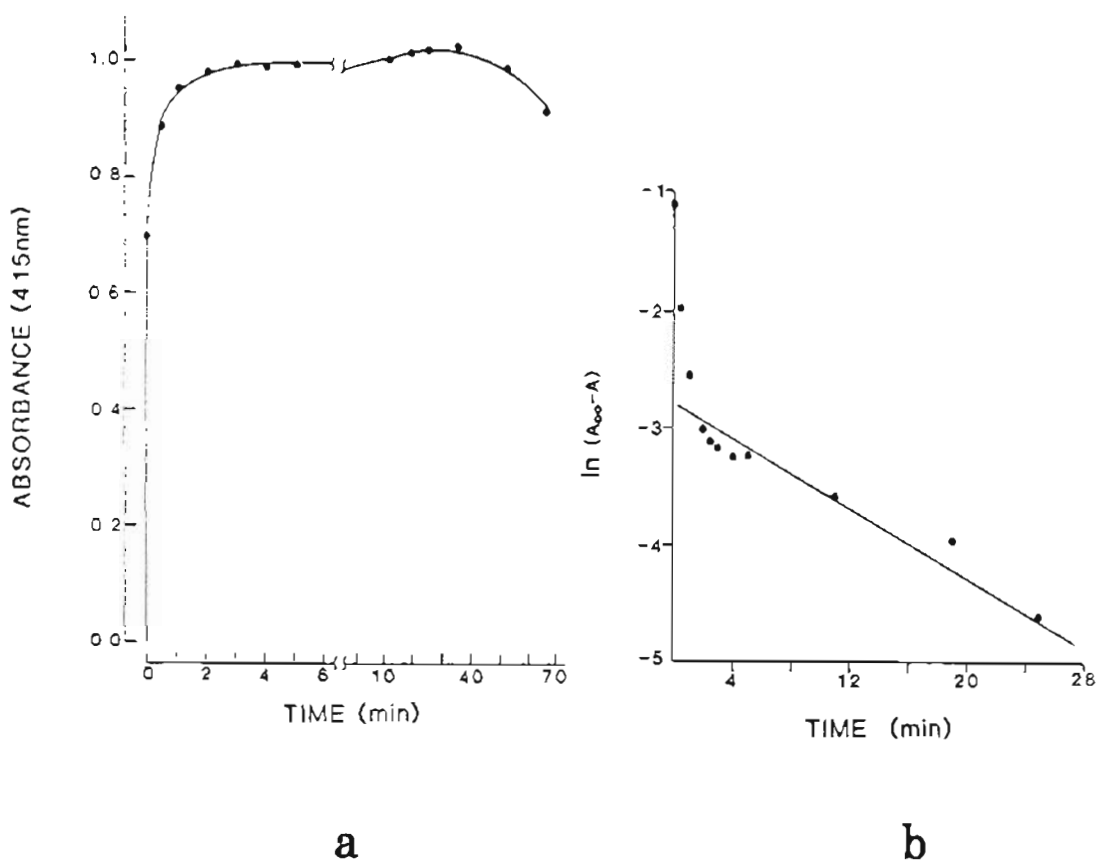
Figure 46. Slow reduction of PC-bound $(NH_3)_5Ru-4-(11'-$
dodecenyl$)py^{3+}$ by Cu^+ ion.

Graph a: 0.48 mM Cu^+ added to $(NH_3)_5Ru-4-(11'-dodecenyl)py^{3+}-$
PC vesicles at 23°C. Initial concentrations: 7.5 mM PC,
0.4 mM Ru(III), in 0.1 M sodium acetate, pH 4.0.

Graph b: First-order kinetic plot of data points in graph a.
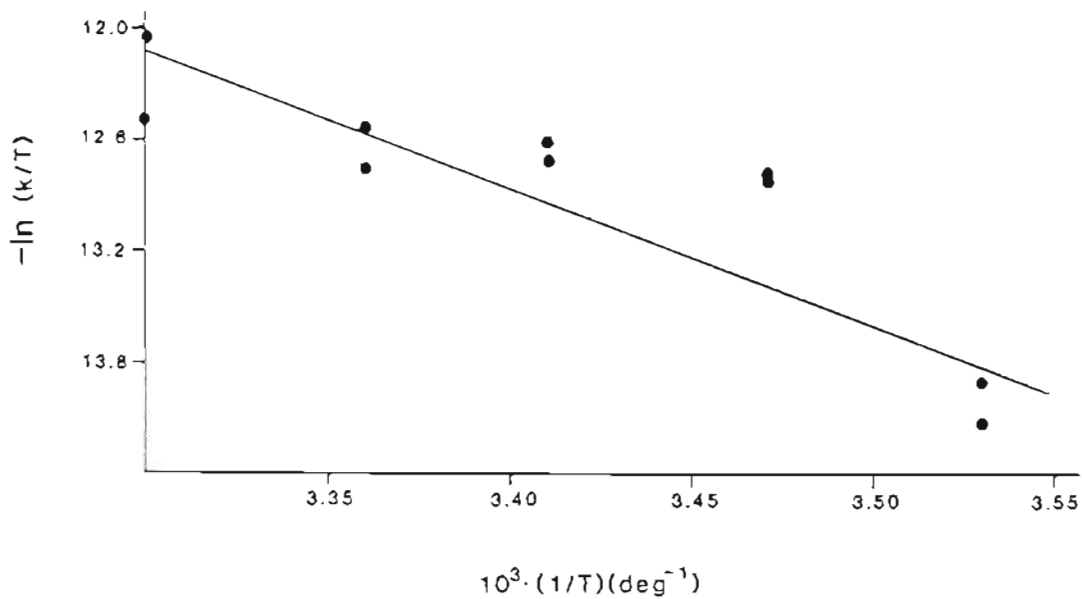
Figure 47. Eyring plot of kinetic data for slow reduction of PC-bound $(NH_3)_5Ru-4-(11'-dodecenyl)py^{3+}$ by Cr^{2+} ion. The line was drawn from linear regression analysis of the data points; experimental conditions are given in Table 15.
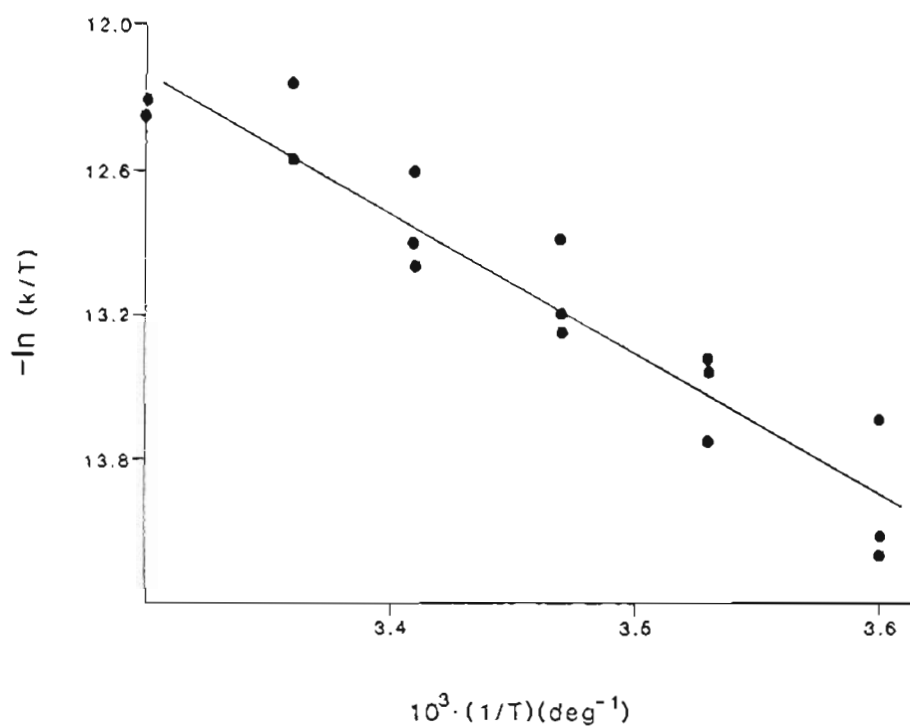
Figure 48. **Eyring plot of kinetic data for slow reduction of PC-bound $(NH_3)_5Ru-4-(11'-dodecenyl)py^{3+}$ by ascorbate ion.** The line was drawn from linear regression analysis of the data points; experimental conditions are given in Table 16.
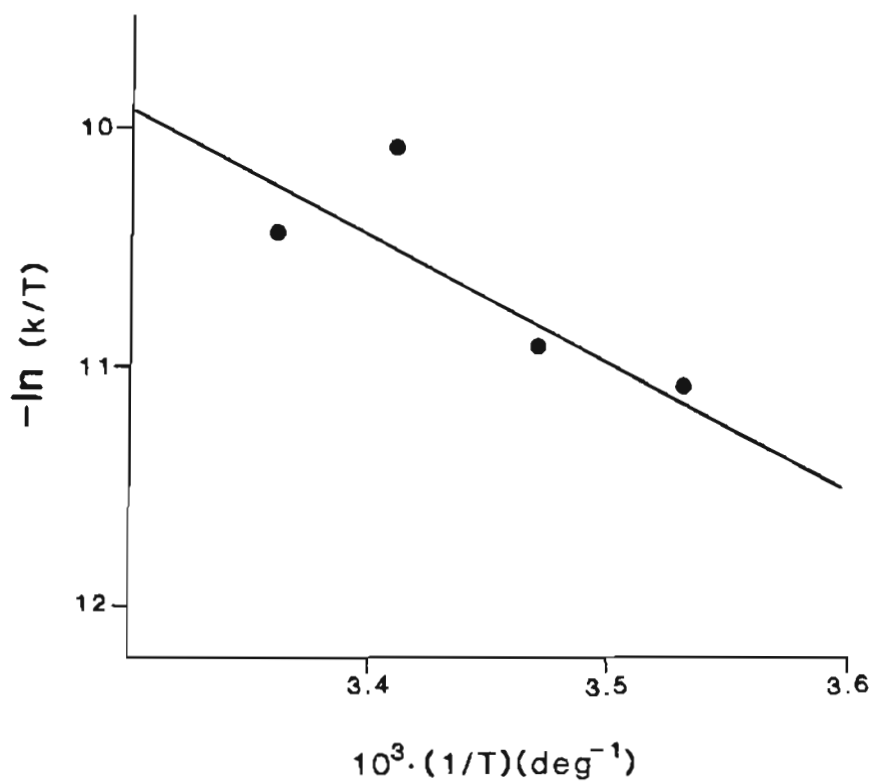
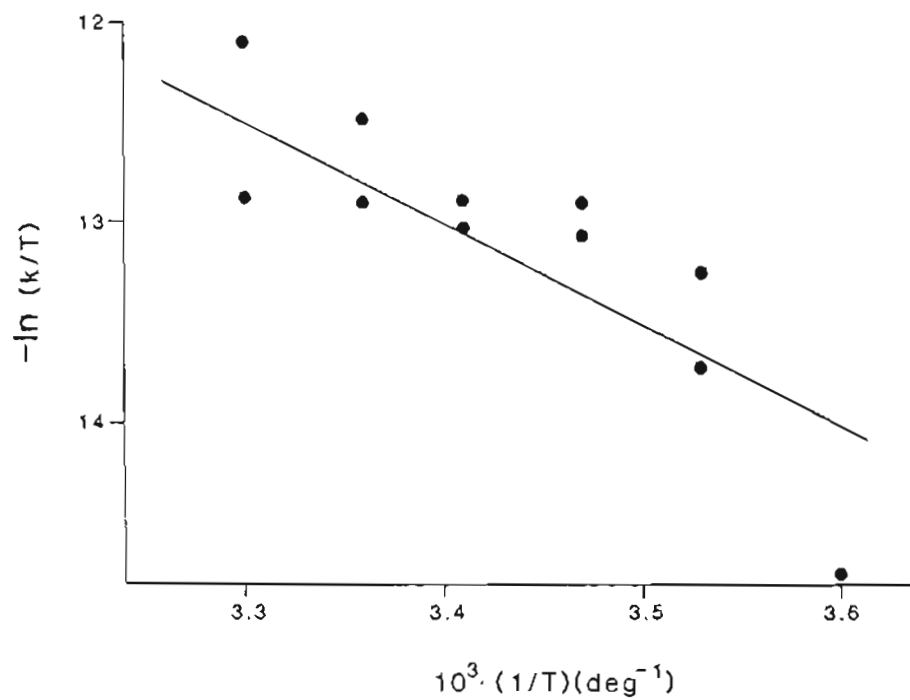Figure 49. **Eyring plot of kinetic data for slow reduction of** PC-bound $(NH_3)_5Ru\text{-}4\text{-}(11'\text{-}dodecenyl)py^{3+}$ by V^{2+} ion. Experimental conditions: 7.5 mM PC, 0.3 mM Ru(III) in 0.1 M sodium acetate, pH 4.0, with 0.5 mM V^{2+} added externally.
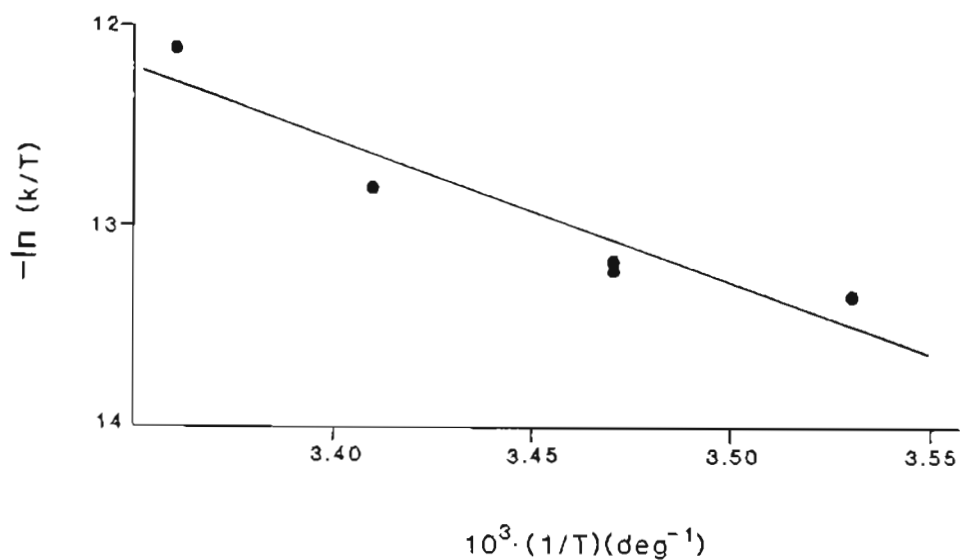
Figure 50. **Eyring plot of kinetic data for slow reduction of PC-bound** $(NH_3)_5Ru-4-(11'-dodecenyl)py^{3+}$ **by** Cr^{2+} **ion in CCCP-incorporated vesicles.** The line was drawn from linear regression analysis of the data points; experimental conditions are given in Table 18.
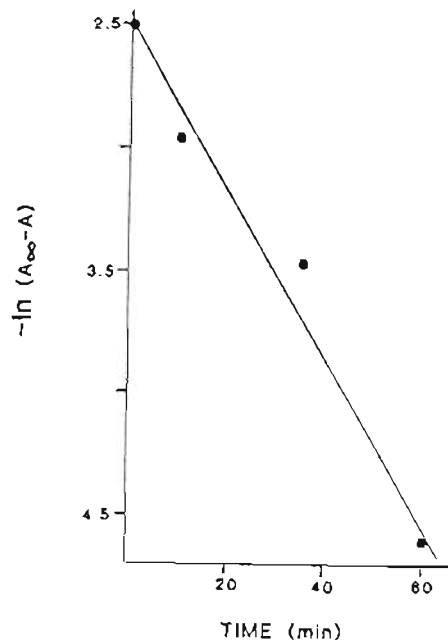
Figure 51. **Eyring plot of kinetic data for slow reduction of PC-bound $(NH_3)_5Ru-4-(11'-dodecenyl)py^{3+}$ by Cr^{3+} in valinomycin-incorporated vesicles.** The line was drawn from linear regression analysis of the data points; experimental conditions are given in Table 19.
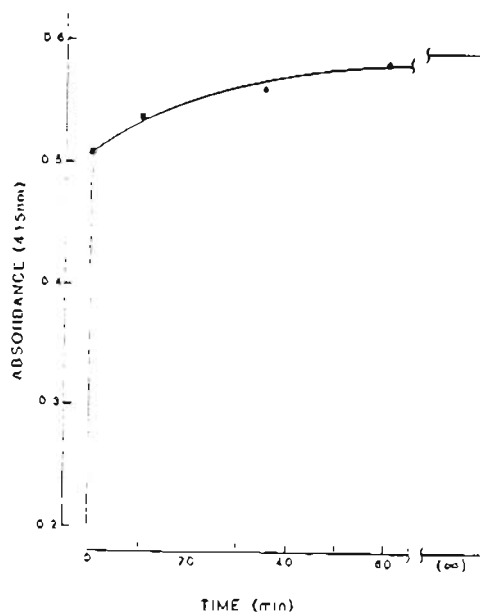
a

b

Figure 52. Slow reduction of PC-bound$(NH_3)_5$Ru-4-(6'-heptenyl)py^{3+}

ion by Cr^{2+} ion.

Graph a: 0.6 mM Cr^{2+} added to $(NH_3)_5$Ru-4-(6'-heptenyl)py^{3+}-

PC vesicles at 10°C. Initial concentrations: 7 mM PC,

0.1 mM Ru(III), in 0.1 M sodium acetate, pH 4.0.

Graph b: First-order kinetic plot of data points in graph a.

a
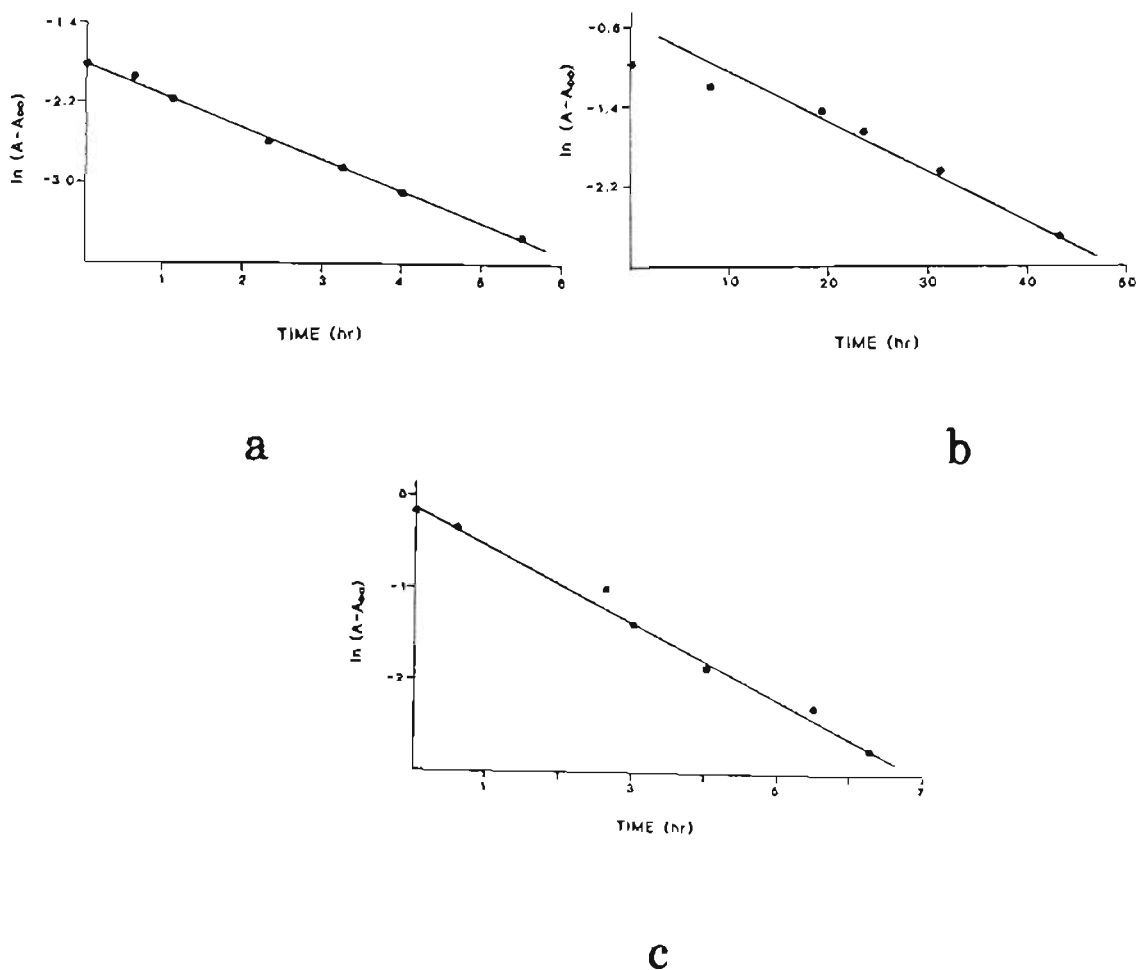
b

c

Figure 53. Bleaching of $(NH_3)_5Ru-4-(11'-dodecenyl)py^{2+}$ generated by reductants.

Graph a: 0.37 mM Ru(III), 90 µM ascorbate.

Graph b: 0.3 mM Ru(III), 40 µM Cr^{2+}.

Graph c: 0.27 mM Ru(III), 22 µM V^{2+}, in 0.1 M sodium acetate, pH 4.0, at 15°C. Absorbance changes detected at 400 nm.
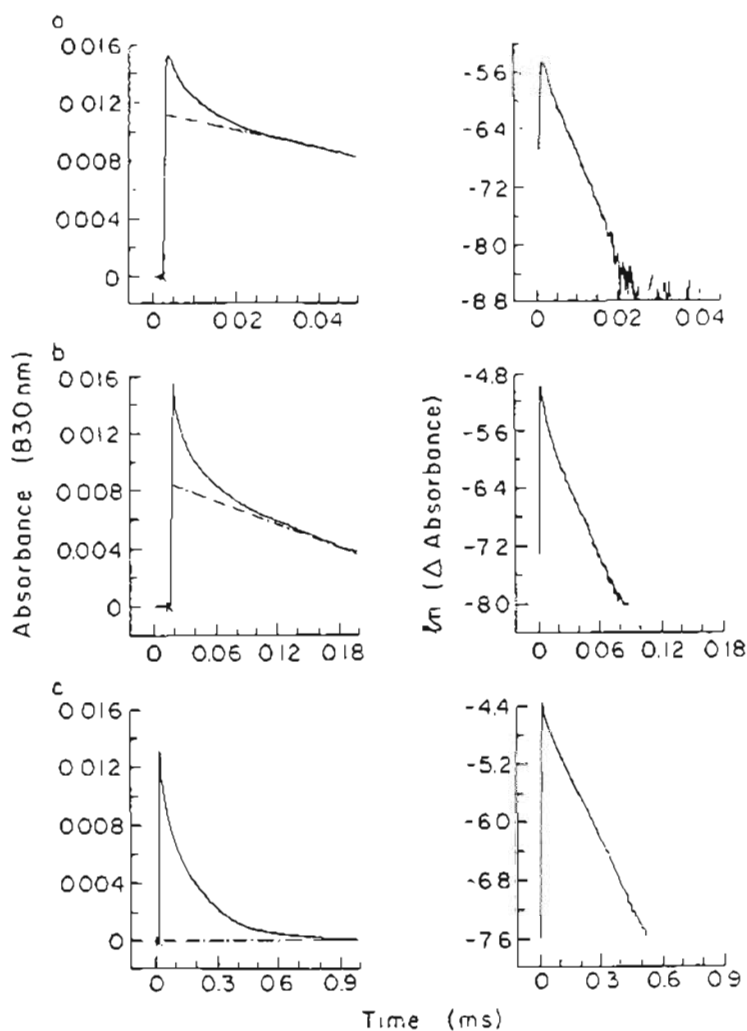
Figure 54. **Deactivation of photoexcited ZnTMPyP^{4+}-DHP vesicles.**

Left column, curves a-c: time course of absorbance changes

following 532 nm laser flash excitation.

Right column, curves a-c: kinetic analysis assuming three

concurrent first-order reactions, using estimated

baselines shown for curves a and b. Reaction conditions:
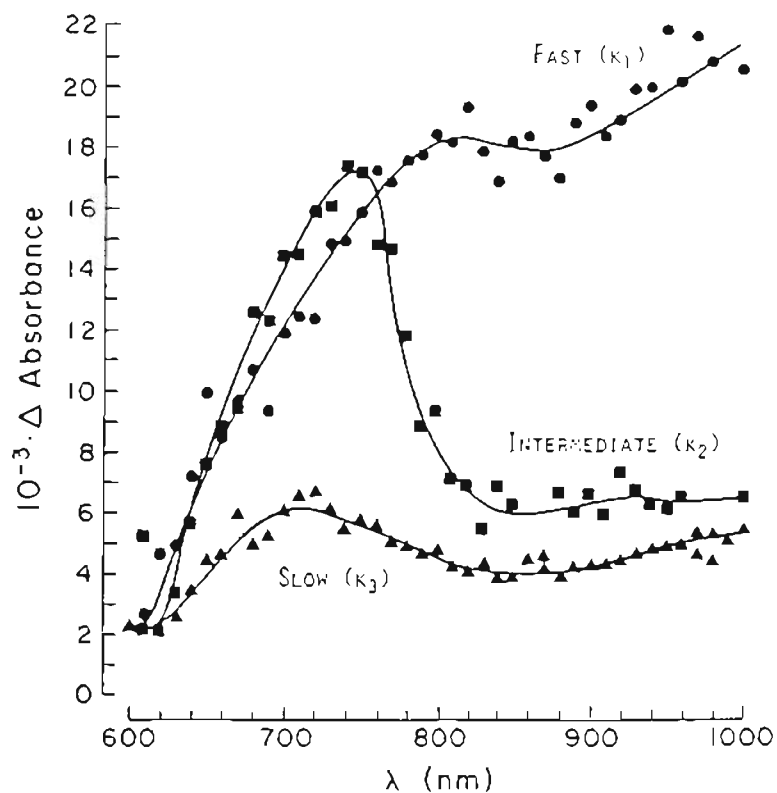
10 μM ZnTMPyP^{4+}, 6 mM DHP in 0.02 M Tris, pH 7.8, at 23°C.

Figure 55. Spectra of ZnTMPyP^{4+}-DHP photoexcitation intermediates. End-of-pulse spectra for rapid (circles), intermediate (squares), and slowly-decaying components (triangles) of triphasic deactivation curves calculated from transient spectra at 1.5, 4.8, 16, 50, and 230 μs after excitation. Reaction conditions: 20 μM ZnTMPyP^{4+}, 2.4 mM DHP in 0.02 M Tris, pH 7.8, at 23°C.
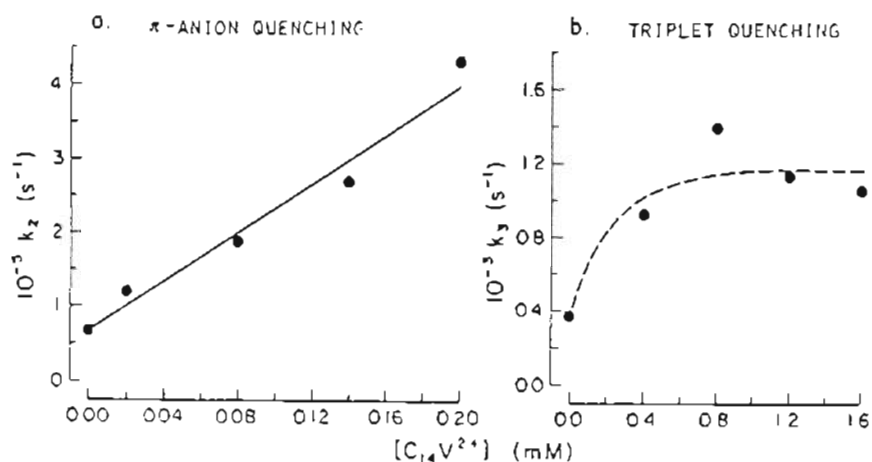
Figure 56. $C_{14}MV^{2+}$ quenching of $ZnTMPyP^{4+}$-DHP photoexcitation
intermediates.

> Graph a: viologen dependence for π-ion quenching, measured at
> 770 nm, with 20 µM $ZnTMPyP^{4+}$, 1.2 mM DHP in 0.02 M Tris,
> pH 7.8, at 23°C.

> Graph b: viologen dependence for triplet deactivation,
> measured at 830 nm, with 10 µM $ZnTMPyP^{4+}$, 6.1 mM DHP in
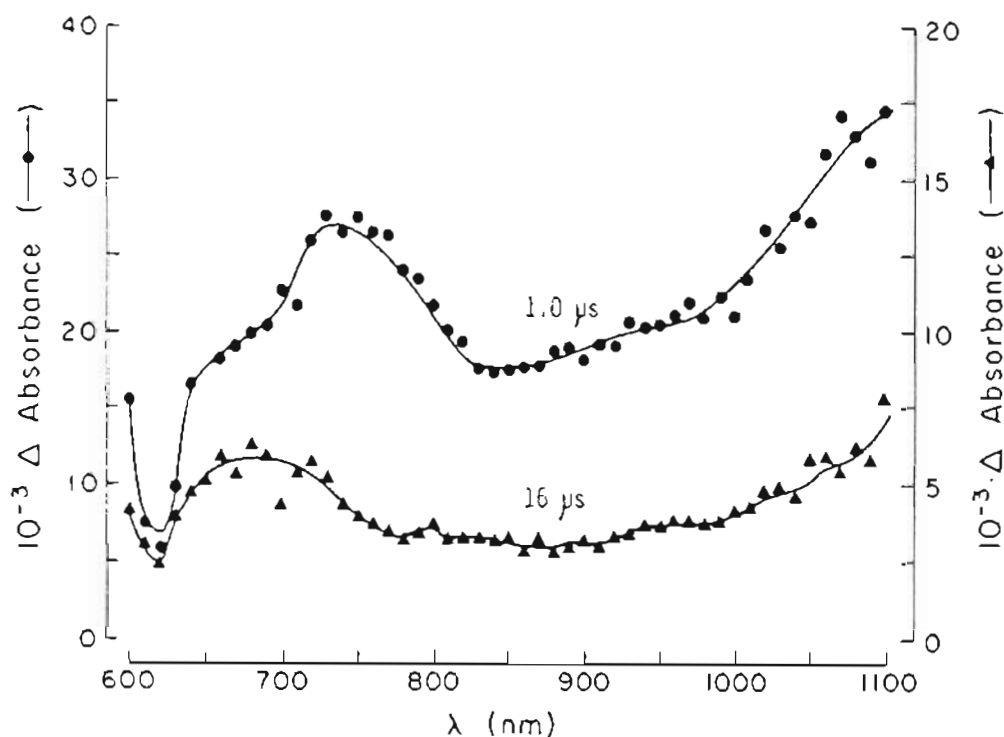> 0.05 M Tris, pH 7.8, at 23°C.

Figure 57. Spectra of $ZnTMPyP^{4+}-C_{16}MV^{2+}$-DHP photoexcitation

intermediates. End-of-pulse spectra for the composite of self-quenched $ZnTMPyP^{4+}$ triplet and $C_{14}MV^{2+}$ quenched π-ion (circles) and for the $C_{14}MV^{2+}$ quenched triplet (triangles) calculated from transient spectra at 1.0 and 16 μs after excitation. Reaction conditions: 20 μM $ZnTMPyP^{4+}$, 0.5 mM $C_{14}MV^{2+}$, 2.4 mM DHP in 0.02 M Tris, pH 7.8, at 23°C.
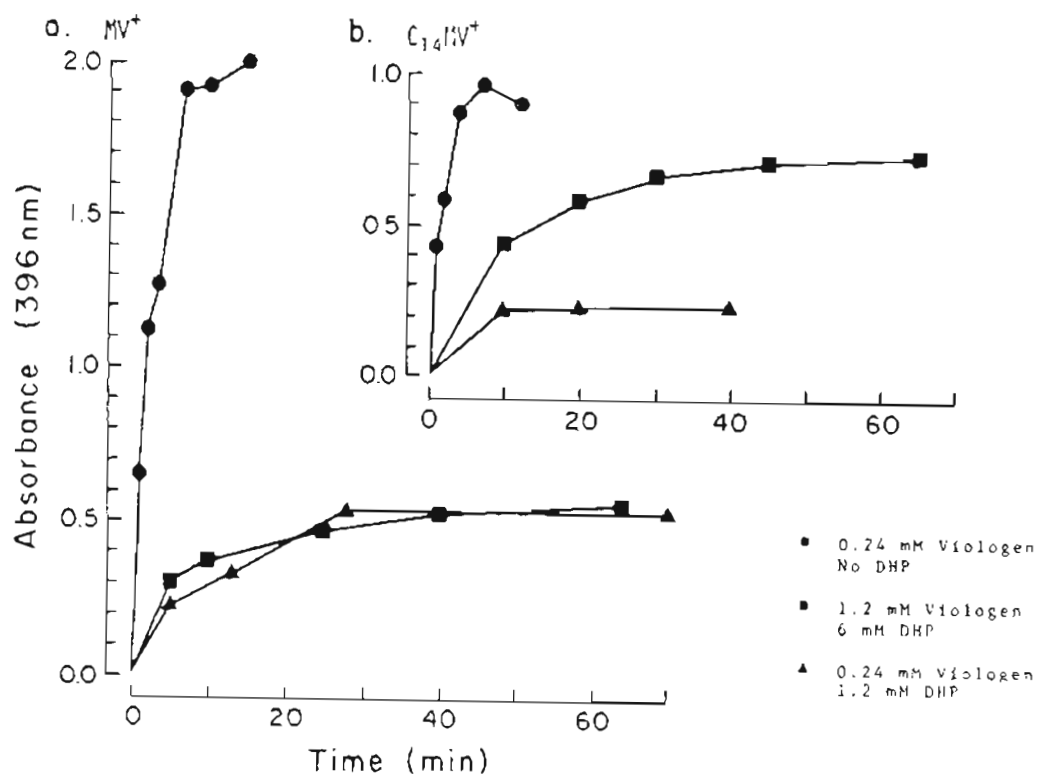
Figure 58. ZnTMPyP^{4+} photosensitized viologen reduction.

Graph a: MV$^+$ formation; circles: 10 μM ZnTMPyP^{4+}, 0.24 mM MV^{2+}, DHP absent; squares: 10 μM ZnTMPyP^{4+}, 1.2 mM MV^{2+}, 6 mM DHP; triangles: 20 μM ZnTMPyP^{4+}, 0.24 mM MV^{2+}, 1.2 mM DHP.

Graph b: C$_{14}$MV$^+$ formation; 10 μM ZnTMPyP^{4+}, 0.21 mM C$_{14}$MV^{2+}, DHP absent; squares: 10 μM ZnTMPyP^{4+}, 1.2 mM C$_{14}$MV^{2+}, 6 mM DHP; triangles: 20 μM ZnTMPyP^{4+}, 0.24 mM C$_{14}$MV^{2+}, 1.2 mM DHP. All reaction in 0.02 M TEOA, pH 7.8 at ambient temperature.
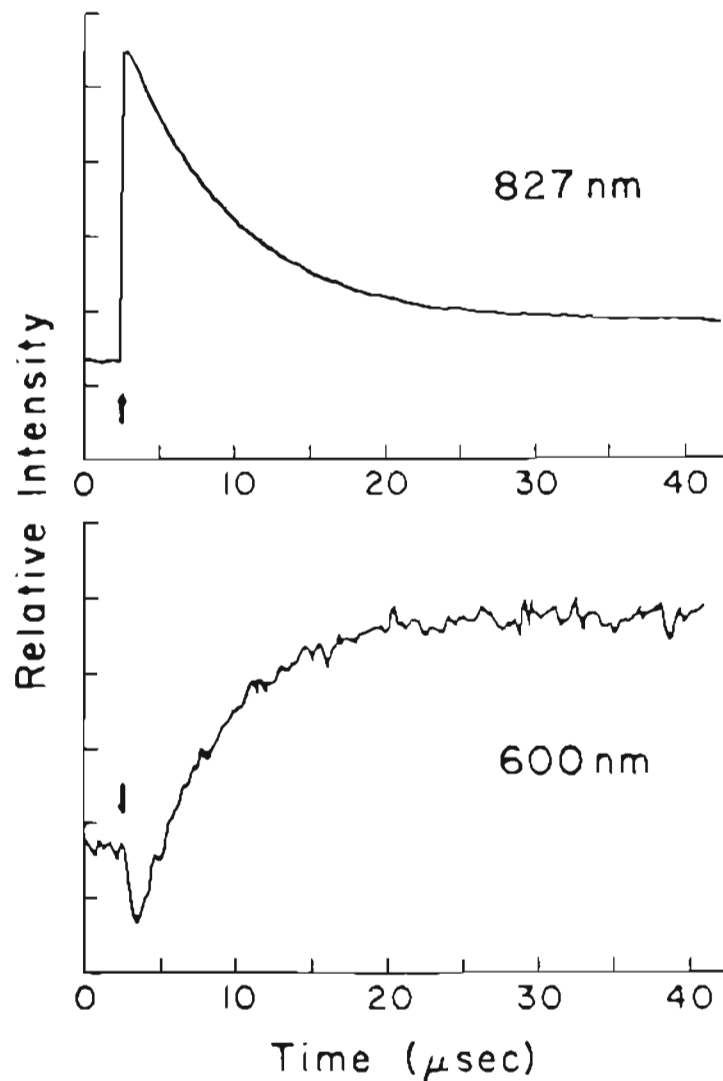
Figure 59. **Oxidative quenching of photoexcited ZnTPPS^{4-} by**
DHP-bound MV^{2+}.

Upper trace: triplet formation and deactivation.

Lower trace: viologen radical formation. The arrows indicate

the point of initiation of the laser pulse; amplitudes are

1 mV/division. Conditions: 20 μM ZnTPPS^{4-}, 70 μM MV^{2+},

3.6 mM DHP in 0.02 M Tris, pH 7.8, at 23°C.

APPENDICES

Appendix I

Derivation of the kinetic equation for slow-phase reduction of

symmetrically bound $(NH_3)_5Ru-4-(11'-dodecenyl)py^{3+}$ ion in PC vesicles

The rate expression for appearance of ruthenium(II) complex during

the slow reduction in Scheme IV, assuming the reactants are

statistically decorrelated, is:

$$(1) \quad \frac{d[Ru_i^{2+}]}{dt} = k_2[Ru_o^{2+}][Ru_i^{3+}] - k_3[Ru_i^{2+}]$$

The k_2 pathway represents the slow transmembrane exchange between

externally bound Ru^{2+} ion and internally bound Ru^{3+} ion and the k_3

pathway represents the slow pseudo-first order oxidation of internally

bound Ru^{2+} by perchlorate ion.

Since k_1, $k_1' \gg k_2$ and transmembrane diffusion of the bound

ruthenium species does not occur, $[Ru_o^{2+}]$ is constant:

$$(2) \quad k_2' = k_2[Ru_o^{2+}]$$

and since transmembrane diffusion does not occur:

$$(3) \quad [Ru_i]_T = [Ru_i^{2+}] + [Ru_i^{3+}]$$

where $[Ru_i]_T$ is the total internal ruthenium complexes. Hence,

(4) $d[Ru_i^{2+}]/dt = k_2' [Ru_i]_T - (k_2' + k_3)[Ru_i^{2+}]$

Since at $t = 0$, $[Ru_i^{2+}] = 0$, integration yields:

(5) $$\ln\left(\frac{k_2'[Ru_i]_T}{k_2'[Ru_i]_T - (k_2' + k_3)[Ru_i^{2+}]}\right) = (k_2' + k_3)t$$

At pseudoequilibrium, there is no net change in $[Ru_i^{2+}]$ and $[Ru_i^{3+}]$, i.e.,

(6) $$\frac{k_3}{k_2'} = \frac{[Ru_i^{3+}]_e}{[Ru_i^{2+}]_e}$$

Dividing both numerator and denominator in the logarithmic expression on the left hand side of equation 5 by k_2' gives:

(7) $$\ln\left(\frac{[Ru_i]_T}{[Ru_i]_T - (1 + k_3/k_2')[Ru_i^{2+}]}\right) = (k_2' + k_3)t$$

Substituting for k_3/k_2' (equation 6) and taking account of conservation of mass (equation 3), we obtain after rearranging terms:

(8) $$\ln\left(\frac{[Ru_i^{2+}]_e}{[Ru_i^{2+}]_e - [Ru_i^{2+}]}\right) = (k_2' + k_3)t$$

Since the absorbance at 415 nm, A, is proportional to the total Ru^{2+} concentration,

(9) $A_e = \varepsilon b \, ([Ru_o^{2+}] + [Ru_i^{2+}]_e)$

(10) $A_o = \varepsilon b \, [Ru_o^{2+}]$

(11) $A_t = \varepsilon b \, [Ru_o^{2+}] + [Ru_i^{2+}]$

where A_e, A_o, and A_t are the absorbance at pseudoequilibrium, initial time, and at time t, respectively. ε is the molar extinction coefficient of the bound Ru^{2+} complex ion, and b is the optical pathlength.

Substituting $(A_e - A_o)/\varepsilon b$ for $[Ru_i^{2+}]_e$, $(A_e - A_t)\varepsilon b$ for $[Ru_i^{2+}]_e - [Ru_i^{2+}]$, the final form of the integrated rate expression is

(12) $$\ln \left(\frac{A_e - A_o}{A_e - A_t} \right) = (k_2' + k_3)t$$

Plots of $\ln(A_e - A_t)$ vs. time should therefore be linear with negative slopes equal to the sum, $k_2' + k_3$, and y-intercepts equal to $|A_e - A_o|$.

Appendix II

Derivation of the Stern equation

The hydrophobic adsorption of a molecule to a bilayer membrane can be represented by the Langmuir adsorption isotherm, which is derived on the assumption that the adsorption sites are spatially fixed and non-interacting[1]:

$$(1) \quad \sigma_\ell = (\sigma_\ell{}^m - \sigma_\ell)[B]_{x=0}/K$$

where σ_ℓ is the number of molecules adsorbed per unit area (Å^2), $\sigma_\ell{}^m$ is the maximum number of adsorbed molecules (per unit area), K is the dissociation constant (M), and $[B]_{x=0}$ is the aqueous concentration of the adsorbing species B at the membrane-solution interface. This model also assumes that $[B]_{x=0}$ is equal to the B concentration in the bulk solution ($[B]$). However, if B is a positively charged molecule, its absorption to the vesicle surface produces a surface potential that would resist further adsorption of B, thereby reducing the B concentration at the interface. A more realistic approach is to relate the aqueous B concentration at the interface to its bulk concentration by the surface potential generated in terms of the Boltzmann distribution

$$(2) \quad [B^{n+}]_{x=0} = [B^{n+}]\exp(nF\psi_0/RT)$$

where $\psi_0 = \psi_{x=0} - \psi_{x=\infty}$ is the electrostatic potential in the aqueous phase immediately adjacent to the membrane-solution interface, and n is the number of charges of the adsorbing ion B^{n+}. If the membrane is

initially neutral, the charge density on the membrane surface due to adsorption of B^{n+}, σ_s, is equal to the surface concentration of adsorbed ions multiplied by n, the number of charges per ion, i.e., $\sigma_s = n\sigma_\ell$. The Gouy-Chapman equation from the theory of the diffuse double layer describes the surface membrane potential ψ_o (mV) in terms of the surface charge density σ_s, and the total concentration of monovalent electrolyte in the bulk aqueous solution C by the following equation[2]:

$$(3) \quad \sinh(F\psi_o/2RT) = A\sigma_s/C^{1/2}$$

where R, T, and F are the gas constant, temperature, and Faraday constant, respectively. A is a constant ($A = (8\varepsilon_r\varepsilon_o RT)^{-1/2}$) which depends on temperature and dielectric constant, where ε_r is the dielectric constant, and ε_o the permittivity of free space. At 25°C, $A = 136.6$ $M^{-1/2}$ $Å^2$/charge and $RT/F = 25.7$ mV[3].

Substituting equation 2 into equation 1 yields

$$(4) \quad \sigma_\ell = \frac{\sigma_\ell^m - \sigma_\ell}{K} \quad [B^{n+}]\exp\left(\frac{nF\psi_o}{RT}\right)$$

For n = 1, e.g., adsorption of monopositive ions to the membrane, equations 1-4 can be mathematically manipulated to generate an expression relating the binding density to the bulk concentration of B in terms of the binding parameters σ_ℓ^m and K; specifically, $\sinh x = (e^x - e^{-x})/2$,

$$(5) \quad \sinh(F\psi_o/2RT) = 1/2[\exp(F\psi_o/2RT) - \exp(-F\psi_o/2RT)]$$

$$= A\sigma_s/C^{1/2}$$

Squaring eq. 5 gives

$$(6) \quad 4A^2\sigma_s^2/C = [\exp(F\psi_o/2RT) - \exp(-F\psi_o/2RT)]^2$$

Substituting equation 4 for $\exp(F\psi_o/2RT)$ yields the Stern equation:

$$(4A^2\sigma_s^2/C) + 2 = \sigma_\ell K/(\sigma_\ell^m - \sigma_\ell)[B] + (\sigma_\ell^m - \sigma_\ell)[B]/\sigma_\ell K$$

References

(1) Aveyard, R.; Haydon, D. A. "An Introduction to the Principles of Surface Chemistry," London, Cambridge University Press, 1973, p. 25-27.

(2) Bockris, J. O'M.; Reddy, A. K. N. "Modern Electrochemistry," Vol. 2, Plenun, New York, 1970, p. 724-732.

(3) McLaughlin, S.; Harary, H. Biochemistry 1976, 15, 1941-1948.

Appendix III

Charging Energies in Reduction of PC-Bound $(NH_3)_5Ru-4-(11'-$
dodecenyl)py^{3+} Ion

A. **Charging energy in external reduction of PC-bound $(NH_3)_5Ru-4-(11'-$
dodecenyl)py^{3+} ions**

Reduction of external ruthenium(III) ions in PC vesicles containing
$(NH_3)_5Ru-4-(11'-dodecenyl)py^{3+}$ ions bound to inner and outer surfaces
decreases the overall positive charge on the outer vesicle surface.
Electroneutrality is maintained across the bilayer, however, since
ruthenium reduction is coincident with reductant oxidation on the same
side of the bilayer, and there is no net charge translocation across the
bilayer. This process is formally equivalent to charging a spherical
surface from the external medium i.e., a charge Q arising from oxidation
of the reductant in the external solution phase is deposited on the
vesicle surface. Assuming the vesicle surface is an isolated conducting
sphere of radius r, its potential is given by[1]

$$V = Q/4\pi\varepsilon r$$

and its capacitance,

$$C = Q/V = 4\pi\varepsilon r$$

where ε is the relative permittivity of the external medium (medium
dielectric constant x permittivity of free space). Hence, the
electrostatic energy in charging the external vesicle surface is

$$E_{charge} = V^2 C/2 = Q^2/2C$$

Assuming a maximum molar binding ratio of 1:12 for Ru:PC, and average molecular weight of 770 and 2×10^6 Daltons for PC monomer and vesicle, respectively, there are a total of

$$(1/12) \cdot (2 \times 10^6)(770) = 216$$

ruthenium ions per vesicle. Using an external to internal Ru ratio of 2:1, determined from the amplitude of fast and slow kinetic reduction steps, there are 144 external and 72 internal ruthenium ions.

Using n = 144, the total net charge Q on the external vesicle surface due to one-electron ruthenium reduction is given by

$$Q = ne$$

where e is the unit electrostatic charge, 1.6×10^{-19} coulombs,

$$Q = \frac{(144)(1.6 \times 10^{-19} \text{ coul})}{\text{vesicle}} = 2.3 \times 10^{-17} \text{ coul/vesicle}$$

Substituting 81 as dielectric constant for water, 8.85×10^{-14} Farad/cm for permittivity of free space, and using an external radius of 130 Å, the capacitance is calculated:

$$C = (4\pi)(81) \left(8.85 \times 10^{-14} \; \frac{\text{Farad}}{\text{cm}} \right) \left(\frac{130 \times 10^{-8} \; \text{cm}}{\text{vesicle}} \right)$$

$$= 1.17 \times 10^{-16} \; \text{Farad/vesicle}$$

The charging energy, therefore, is

$$E_{charge} = [(2.3 \times 10^{-17})^2 \; \text{coul}^2/\text{vesicle}^2]/(2)(1.17 \times 10^{-16} \; \text{Farad/vesicle})$$

$$= 2.25 \times 10^{-18} \; \text{Joule/vesicle}$$

Since there are 144 external Ru per vesicle, the charging energy per mole of external Ru is

$$E = \frac{(2.26 \times 10^{-18} \; \text{Joule/vesicle})(6 \times 10^{23} \; \text{mol}^{-1})}{144 \; \text{Ru/vesicle}} = 9420 \; \text{Joule/mol Ru}$$

This energy can be converted into an electrochemical potential by the appropriate conversion factors, 2.389×10^{-4} kcal/Joule and the Faraday constant, $F = 23.061 \; \text{kcal} \; v^{-1} \; \text{mol}^{-1}$.

$$E_{charge} = \frac{(9420 \; \text{Joule/mol Ru}) (2.389 \times 10^{-4} \; \text{kcal/Joule})}{(23.061 \; \text{kcal/v.mol})}$$

$$E_{charge} = 0.098 \; V$$

B. Charging energy in reduction of internally bound $(NH_3)_5Ru-4-(11'-$ dodecenyl$)py^{3+}$ ions.

Transmembrane reduction of internal Ru^{3+} by external Ru^{2+} is equivalent to the transfer of charge from the outer terminal to the inner terminal of a concentric plate capacitor. The capacitance of a

capacitor consisting of two concentric spheres of radii of a and b, where b > a, is given by[2]

$$C = 4\pi\varepsilon ab/(b - a)$$

Taking a = 80 Å, b = 130 Å, ε = (2.2)(8.85 x 10^{-12} Farad/cm) for lipid[3],

$$C = (4\pi)(2.2)(8.85 \times 10^{-12} \text{ Farad/cm})(80 \text{ Å})(130 \text{ Å})(10^{-10} \text{ cm/Å})/(50 \text{ Å})$$

$$= 5.1 \times 10^{-18} \text{ Farad/vesicle}$$

Since there are maximally 72 internal Ru per vesicle,

$$Q = (72) (1.6 \times 10^{-19} \text{ coul/vesicle}) = 1.5 \times 10^{-17} \text{ coul/vesicle}$$

Therefore,

$$E_{cap} = Q^2/2C = (1.15 \times 10^{-17} \text{ coul/vesicle})^2/(2)(5.1 \times 10^{-18} \text{ Farad/vesicle})$$

$$= 1.3 \times 10^{-17} \text{ Joule/vesicle}$$

Converting to energy per mole of internally bound Ru,

$$E_{cap} = \frac{(1.3 \times 10^{-17} \text{ Joule/vesicle})(6 \times 10^{23} \text{ mole}^{-1})}{(72 \text{ Ru/vesicle})}$$

$$= 1.08 \times 10^5 \text{ Joule/mol Ru}$$

Conversion to volts gives

$$E_{cap} = (1.08 \times 10^5 \text{ Joule/mol Ru})(2.389 \times 10^{-4} \text{ kcal/Joule})/(23.061$$

$$\text{kcal V}^{-1} \text{ mol}^{-1})$$

$$= 1.12 \text{ V}$$

References

(1) Corson, D.; Lorrain, P. "Introduction to Electromagnetic Fields and Waves," W. H. Freeman & Co., 1962, pp. 57-61.

(2) Halliday, D.; Resnick, R. "Physics Part II," 2nd ed., Wiley, New York, 1962, p. 765.

(3) Requina, J.; Haydon, D. A. Proc. Royal Soc. London A, 1975, 347, 161.

Appendix IV

Calculations of Vesicle Surface Area

The surface area of a sphere is given by $S = 4\pi r^2$, where r is the radius. A spherical bilayer vesicle having an inner radius r_1 and outer radius r_2 has the following surface areas, respectively:

$$S_1 = 4\pi r_1^2, \quad S_2 = 4\pi r_2^2$$

Hence the fraction of inner surface area to the total surface area of a spherical vesicle is

$$S_1/(S_1 + S_2) = r_1^2/(r_1^2 + r_2^2)$$

Assuming $r_2 = 250$ Å and a bilayer width of 50 Å, the percentage of inner surface area to total surface area of the vesicle is

$$\frac{(200)^2}{(200)^2 + (250)^2} = 39\%$$

BIOGRAPHICAL NOTE

Lester Y. C. Lee was born in Guangzhou, China in 1954.   He immigrated with his family to the U.S. in 1967 from Hong Kong and became a naturalized U.S. citizen in 1973.   He attended the University of Washington in Seattle and received a B.S. degree in Chemistry in 1977. Later that year he entered the graduate program at the Oregon Graduate Center and did his dissertation research under the direction of Dr. James K. Hurst.   In 1983 he joined the research group of Dr. David Whitten at the University of Rochester.   His current research interests include photoinitiated electron transfer involving radical ion formation, long range electron transfer in organized media, and photoredox behavior of indigo dyes.